NASA Contractor Report 181895

Techniques for Extreme Attitude Suspension of a Wind Tunnel Model in a Magnetic Suspension and Balance System

David Huw Parker

University of Southampton
Southampton, England

Grant NSG-7523

October 1989

National Aeronautics and
Space Administration

Langley Research Center
Hampton, Virginia 23665

NASA Contractor Report 181895

University of Southampton

Department of Aeronautics and Astronautics

Techniques for Extreme Attitude Suspension of a Wind Tunnel Model in a Magnetic Suspension and Balance System

by

David Huw Parker

October 1989

LIST OF CONTENTS

DISCLAIMER

Reference in this thesis to commercial manufacturers, products or trade names is essential to a complete understanding of the matters discussed but in no way constitutes any endorsement.

LIST OF SYMBOLS AND ABBREVIATIONS

a_{in}	matrix of force per unit current relationships for MSBS
A/D	analogue to digital (converter)
Alnico	type of permanent magnet (Aluminium-Nickel-Cobalt alloy)
AMC	augmented magnet configuration of model
AX-HE	axial to heave channel position sensing decoupling quantity
B	magnetic flux density (T)
C_1, C_2	axial to heave and heave to axial position sensing gain ratios
CPU	central processing unit
d	model diameter
D/A	digital to analogue (converter)
DDF	demand distribution factor
E/M	electromagnet
e_n	position/attitude error in degree of freedom n
F	force (N) - various subscripts to indicate direction
f	frequency (Hertz)
G_n	controller overall loop gain in degree of freedom n
H	magnetic field strength (A/m), with subscripts to indicate direction/gradient
H_n	demand distribution factor or overall loop gain
HE-AX	heave to axial position sensing decoupling quantity

He-Ne	helium neon (as in laser)
K	integrator gain
K_n	distributed force or moment product in degree of freedom n
l	model length
l_p	projected model length
LMSBS	large magnetic suspension and balance system
M	magnetisation (Tesla)
MOS	metal oxide semiconductor
MMI	Madison Magnetics Incorporated
MSBS	magnetic suspension and balance system
P_n	position or attitude in degree of freedom n
PACS	Photodiode Array Control System
PI-AX	pitch to axial channel position sensing decoupling quantity
r	position vector
S_k	output from position sensor k
T	magnetic torque
TTL	transitor-transitor logic
V	model core volume
x, y, z	MSBS axis system
x', y', z'	model axis system
x", y", z"	sensing system axis system

X	x-wise force per electromagnet group
Z	z-wise force per electromagnet group
α	coefficient of linear expansion
θ	pitch attitude
ϕ	roll attitude
ψ	yaw attitude
ρ	± 1
ω	angular velocity (radians/second)
μ_o	permeability of free space

DEMAT

FORCE

GAINER

MSHI

PIXEL computer program names

Terminology used only within the appendices are defined in context and not here.

ACKNOWLEDGEMENTS

The author is pleased to express his sincere thanks to the many people who have, in their various ways, contributed to the work reported here.

Principal amongst these has been my supervisor, Dr. M.J. Goodyer, Reader in Experimental Aerodynamics at Southampton University, for his valued support over several years, fund of ideas at times of difficulty and commitment and enthusiasm based on a wealth of experience.

Much gratitude is owed to Bob Halford for creating the Photodiode Array Control System, solving numerous technical difficulties along the way. I wish him well in the future. To John Hawkes, Mike Bartlett and their teams; many thanks for interpreting my drawings in building numerous assemblies for the MSBS.

Special thanks are due to Dr. Colin Britcher for accommodating me during an enjoyable and informative visit to NASA Langley Research Center, and to Dr. R.A. Kilgore and R.P. Boyden of that establishment for ensuring funding and monitoring the project.

During my time at Southampton, many friends and colleagues have provided much needed encouragement; if I do not name them, it is not to diminish their contribution. Thank you all.

Final thanks are due to my family for their steadfast support over several years.

This work was funded under NASA Grant NSG-7523, by the British Science and Engineering Research Council and the University of Southampton.

UNIVERSITY OF SOUTHAMPTON

ABSTRACT

FACULTY OF ENGINEERING AND APPLIED SCIENCE

DEPARTMENT OF AERONAUTICS AND ASTRONAUTICS

Doctor of Philosophy

TECHNIQUES FOR EXTREME ATTITUDE SUSPENSION OF A WIND TUNNEL MODEL IN A MAGNETIC SUSPENSION AND BALANCE SYSTEM

by David Huw Parker

Although small scale magnetic suspension and balance systems (MSBSs) for wind tunnel use have been in existence for many years, they have not found general application in the production testing of flight vehicles. One reason for this is thought to lie in the relatively limited range of attitudes over which a wind tunnel model may be suspended. This text reports on the modifications made to an existing small MSBS at Southampton University to permit the suspension and control of axisymmetric models over an angle of attack range from less than zero degrees to over ninety degrees. Previous work had shown that the existing arrangement of ten electromagnets was unable to generate one of the force components necessary for control at the extreme attitudes. Examination of possible solutions has resulted in a simple alteration which rectifies this deficiency. To generate the feedback signals essential to control the magnetically suspended model, an optical position sensing system using collimated beams of laser light illuminating photodiode arrays has been installed and tested. An analytical basis has been developed for distributing the demands for force and moment needed for model stabilisation amongst the electromagnets and over the full attitude range. This has been implemented by an MSBS control program able to continually adjust the distribution for the instantaneous incidence in accordance with pre-scheduled data. Results presented demonstrate rotations of models from nought to ninety degrees at rates of change up to ninety degrees per second, with pitching rates rising to several hundred degrees per second in response to step-change demands. A study of a design for a large MSBS suggests that such a system could be given the capability to control a model in six degrees of freedom over an unlimited angle of attack range.

CHAPTER 1

INTRODUCTION

1.1 The Potential of Magnetic Suspension and Balance Systems

An Englishman, Frank Wenham, is credited with construction of the first wind tunnel for aeronautical research in 1871. Earlier experimenters had used models of wings or complete aeroplane configurations, supported on an arm rotated by a falling weight, but had found that the technique was unreliable and inconclusive. The systematic use by the Wright Brothers of a small open return tunnel played a major part in their researches which led to the first manned, controlled and powered flight in 1903. Since those times the wind tunnel has been an essential tool of the aeronautical engineer, used in both fundamental research and in the development of any new type of aircraft or missile. Despite all the advances in algorithms capable of solving the equations of complex fluid flows, computational fluid dynamics is unlikely ever to entirely surplant the wind tunnel's essential role.

However, the technique of testing a scale model in a moving flowfield in order to simulate flight conditions has always been beset by drawbacks which limit the quality of data obtainable. The most fundamental of these is the failure in most facilities to achieve representative values of Reynolds' number (the non-dimensional parameter relating to the ratio of inertia and viscous forces in the flow). This problem has spurred the development of a variety of large and complex specialised wind tunnels, including those which operate at elevated pressures, and more recently at cryogenic temperatures.

The Magnetic Suspension and Balance System (MSBS) is intended to eliminate another problem in wind tunnel testing; that of support interference. This arises as a consequence of the need to mechanically hold the model under test in the air flow away from the tunnel walls. The flowfield is affected both by the altered geometry of the model as a result of the need to accommodate the mechanical support, and by the presence of the support itself. Reference 1 cites 176 publications which have analysed or

investigated this problem, illustrating the attention paid to it over many years. Further, the concentration on the transonic flight regime in much of the present production testing, coupled with the trend towards more integrated lift/propulsion configurations in the military area confirms the continuing significance of this problem, since it is in these situations where support interference can be at its most severe.

By removing all mechanical stings or struts, leaving a true representation of the flight vehicle supported by an array of electromagnets (E/Ms), the MSBS is intended to eliminate such difficulties. Further, through modulation of the electromagnet currents via a suitable control system, rapid changes in position and attitude are possible along with oscillatory motions. By monitoring E/M current data, information can be obtained relating to the aerodynamic loads on the model, thereby fulfilling the balance role implied in the MSBS abbreviation. Thus in principle, a wind tunnel equipped with an MSBS should be both more accurate and more productive than conventional facilities. Such prospects explain the wide interest in magnetic suspension technology following the reporting of the first wind tunnel MSBS, built at ONERA in the 1950s (2). Many of the ideas incorporated in this pioneering facility, including the use of optical position sensors to monitor model position and attitude, and the obtaining of calibrations of force against electromagnet current by applying known loads to a suspended model, were taken up by other researchers.

By the mid 1970s, 15 MSBSs of varying size and complexity had been built by institutions in France, Britain and the USA (4). The wind tunnels used varied from the subsonic range (e.g. early Southampton and second MIT system) through the transonic regime (ONERA) to hypersonic low density conditions (Princeton, RAE, UVA etc.). However, it was realised that these facilities generally gave low Reynolds number, and were not applicable to production wind tunnel testing (although much useful data of a more specialised nature was generated). The largest MSBS, that at AEDC, had a wind tunnel cross section of only thirteen inches. Investigations of scaling laws for MSBS technology showed that larger systems would be unattractive for reasons of high continuous power consumption (leading to excessive capital and running costs) and certain performance limitations (especially inadequate roll torque capability). As a consequence many of the systems

became inactive, and interest waned. However, by the end of the 1970s, the emergence of several new technologies, including superconductors, digital computers and advanced electro-optics, appeared to enhance the feasibility of a large magnetic suspension and balance system. In the intervening years, ways were sought of using a comparatively small MSBS to generate experimental data at useful Reynolds' numbers, leading to interest in wind tunnels operating at cryogenic temperatures and with self-streamlining walls (allowing the E/Ms to be as close as possible to the model core).

Spurred by these advances a new period of MSBS development began, principally fostered by NASA Langley Research Center. This period has seen detailed studies of possible large systems, along with the use of existing MSBSs to demonstrate applicable new technologies. In particular the 13 inch AEDC system and the MIT system with its unique electromagnetic position sensor have been transferred to Langley, whilst the Southampton MSBS has been progressively upgraded under grant. Thus the work reported here has been part of a continuing programme to extend the technological base required for the design of a large magnetic suspension and balance system to proceed in confidence. It has been suggested that such a system could be combined with adaptive wall techniques in an advanced cryogenic wind tunnel (3).

Recently a new small MSBS has been commissioned by the National Aeronautical Laboratory in Japan, with a symmetric array of 10 electromagnets and an ingenious digital sensing system (4). The small MSBS at Oxford University with its hypersonic low density tunnel remains in use (5). Also, an MSBS has been developed in the Soviet Union (6). With a 40 by 60 cm working section, and a low speed wind tunnel, this is the largest yet constructed. Thus, six wind tunnel MSBSs are known to be active at present. Plans also exist for construction of a new MSBS at the Royal Aerospace Establishment, Farnborough, England. This would operate with an existing low density hypersonic tunnel.

1.2 Application of MSBS Technology to Extreme Attitude Testing

Any large MSBS which may be built is certain to be a costly installation, and it would therefore seem appropriate that it should possess

the greatest possible flexibility in the capabilities which it offers the experimenter. One particular area of wind tunnel testing for which the MSBS appears to promise particular advantages lies in conditions where the attitude of the flight vehicle is strongly displaced from the wind axis, and in the case of extreme pitch attitudes, where it may be stalled. The work reported here investigates this possibility through an experimental demonstration of extreme attitude suspension. Specifically, by studying and implementing changes to the existing Southampton MSBS, it was intended that an axisymmetric model should be supported and controlled over a ninety degree positive angle of attack range.

It should be realised that this requirement was quite arbitrary, since it is neither related to any particular aerodynamic research application of the Southampton MSBS and its low speed wind tunnel, nor to any specification for a large MSBS. Instead it represented a challenging target, both for the design of hardware and the control system philosophy employed. In attempting to meet this goal, it was expected that most of the problems connected with an extreme attitude MSBS would be revealed. The particular solutions developed for the Southampton MSBS might also be applicable to a large MSBS, and further, it is possible to argue that a 90^{o} positive attitude range effectively represents a $\pm 90^{o}$ capability by simple inversion of the model, and that an extension to a full 360^{o} capability is feasible. Such issues are considered further in later sections.

Interest in high alpha capability for a large MSBS was confirmed by the usefulness study undertaken by the Sverdrup Company for NASA Langley in 1984 (7). Representatives of thirteen groups and companies performing wind tunnel testing were surveyed for their opinions as to the future needs for support interference-free data acquisition. High angle of attack capability emerged as the application of an MSBS viewed with the highest priority amongst the respondents. However, the existing design studies for large MSBS facilities have not emphasised high angle of attack capability, possibly because only limited demonstrations have been performed with any of the existing small magnetic suspension systems. Thus the work reported here is intended to prove the practicality of extreme attitude suspension.

Interest in extreme attitude - especially high alpha - flight has gained particular significance in the military arena in recent years as a result of the emphasis on close-in visual combat. The ability to maintain control of a manoeuvering aircraft beyond the stall permits rapid changes of direction at low forward speeds, bestowing tactical advantages. The X-31 program is intended to investigate such flight regimes, including conditions where engine thrust is a significant component opposing the aircraft's weight (8). Flight attitudes of up to 30^{o} are already common with the present generation of high performance combat aircraft. Missiles are also increasingly designed to cope with violent manoeuvers involving flight at extreme attitudes. Such performance is only possible with a thorough knowledge of the aerodynamics at these flight conditions. However, the complications of unsteady flow and asymmetric effects such as vortex shedding make the application of computational fluid dynamics at angles of attack greater than 20-30 degrees very difficult (9) forcing the use of experimental methods.

In the field of hypersonic aerodynamics, flight vehicles such as space shuttles and aerospace planes typically have re-entry angles of greater than twenty degrees, and studies have been conducted for designs with very extreme flight attitudes up to ninety degrees (10).

Thus in several practical areas of aeroydnamics there is a need to perform wind tunnel testing at extreme attitudes. However, it has been found that serious difficulties arise when conventional mechanical supports are used. At non-zero incidences or sideslip angles, a body crossflow over a cylindrical sting is established, destroying the axisymmetric nature of the wake behind the test body, often causing the shedding of separated vortices. These become stronger at higher angles of attack. A large mechanical support, as for example the curved strut commonly used for coning experiments on combat aircraft can affect the measured lateral characteristics of a model through the bursting of the vortices cast by slender wings. Accounting for such effects involves empirical correction factors obtained through repeat testing with alternate mounting systems. Stability characteristics measured in dynamic testing of models can be influenced particularly strongly by the necessarily large and complex support systems. See for example Reference 11.

To avoid the influence of sting support on the base flow of the test model, strut or arm supports may be used, but it is difficult or impossible to design these such that there is neither a shielding effect (with a support below the model) nor interference with cast vortices (with a leeward support). Reference 12 shows some comparative data for a sting and strut supported axisymmetric model at high angles of attack and a subsonic Mach number in which there is a discrepancy in measured normal force of up to 50 per cent. Mounting systems other than stings are required when propulsion simulation involving gas flows emerging from rear mounted engines is attempted, but with the trend towards more integrated engine/airframe configurations, locating the supports is becoming more difficult without significantly changing the lines of the airframe (13).

It is evident that all such problems arising from mechanical supports are eliminated through use of a magnetic suspension system, at the cost of a more expensive installation. However, it may be argued that an MSBS should be capable of suspending any shape of model, whereas support systems must be designed or modified for each new type of aircraft or missile tested, and alternate mounts tried to investigate the interference effects: the MSBS therefore could be more economic when both improved data accuracy and running costs are taken into account. The equipment used for dynamic testing in conventional tunnels often can itself be complicated, involving mechanical or electromagnetic drives to oscillate the model in the required senses (14).

1.3 Principles of Magnetic Suspension and Balance Systems

A bibliography has been compiled listing all known papers and reports relating to magnetic suspension work up to 1983 (15).

Several publictions (4,16) have reviewed the basic principles involved in MSBS technology, but these may usefully be repeated since they form the essential background to the alterations and additions made to SUMSBS in the work reported herein. Figure 1.1 illustrates the simplest conceivable MSBS, in which a North-South bar magnet is supported against gravity by a single monopolar electromagnet; such devices have been built in the past for demonstration purposes (17). As a consequence of Earnshaw's theorem, such

an arrangement is inherently unstable without some form of closed loop control. In this case an optical sensing technique is used to generate a feedback signal; the size of the shadow cast by the tail of the model in a light beam is measured by a photodetector. Typically the latter is a combination of focussing lens and light sensitive diode which produces an analogue voltage proportional to the incident irradiance. Alternative, non-optical sensing techniques have been used, including X-ray sensing (with self-evident practical drawbacks) and the electromagnetic sensor developed at MIT (18). The latter uses the model as the moving component of a variable transformer, measuring changes in the flux linkage.

However, it is not adequate to simply feed the position signal back via a constant gain in order to regulate the electromagnet power supply; the inductance of the E/M introduces a phase lag into the system which would mean that the adjusted force or moment on the model would arise far too late to control its position. Thus compensating circuits are required which commonly take the form of banks of resistors and capacitors to make up the 'phase advance' networks. These are effectively a combination of proportional plus differential controller and a low pass filter. More recently these have been replaced in some MSBSs (including that at Southampton University) by digital control computers, which nonetheless use the same stabilisation approach, albeit in difference equation form. Other approaches have also been reported for magnetic suspension systems in a non-wind tunnel environment (19, 20).

The arrangement shown in Figure 1.1 controls only the vertical position of the model; for wind tunnel applications it is necessary to control several model degrees of freedom simultaneously, ideally up to the six possible. A feedback loop is required for each degree of freedom controlled, resulting in an array of electromagnets together with position sensing and stabilisation sub-systems.

The model cores need not be permanent magnets; many magnetically soft materials exhibit saturation inductions of 2 Tesla or more, which may be compared with typical magnetisations of around 1 Tesla for permanent magnets, thus leading to higher forces and torques per unit applied field/field gradient. The (typically soft iron) core may be magnetised by the controlling

electromagnet coils, or by a dedicated 'Helmholtz' pair. However both approaches lead to larger and more complex electromagnet configurations, and possibly problems of highly non-linear force and moment calibrations as a consequence of the magnetisation being dependent on the applied loads. Thus, although many of the previous small MSBSs have employed iron cored models, current thinking does not favour this design feature for a possible large MSBS. Instead, the use of a superconducting solenoid as the model core is planned (21). As proposed, this features a rare-earth metal core contained within the epoxy impregnated solenoid, the whole being enclosed in a dewar or cryostat filled with liquid helium at 4.2 K. This would have a peak field magnetisation of 6.1 Tesla, representing a four fold increase in effective pole strength for a model of typical size and proportions compared to a permanent magnet core. Large savings in the size of the electromagnets necessary to support and control a model of arbitrary aerodynamic characteristics are then possible. A small prototype superconducting solenoid model was tested in the Southampton MSBS in 1984 (22). However for all of the experimental work reported here, conventional permanently magnetised model cores were used.

1.4 Scope of this Research

This report describes the Southampton MSBS at the outset of the work and reviews previous work on high angle of attack suspension, including the theoretical and experimental work undertaken. The principal problems needing to be solved in order to permit suspension over a ninety degree angle of attack range are introduced and the particular solutions adopted explained. These include major modifications to the hardware of SUMSBS, including the design and installation of an all digital position sensing system. The philosophy of the computer control program developed during the course of this work is described, along with important features of its implementation. A description of experience of operating the modified high angle of attack MSBS is given, along with data characterising its performance. Practical difficulties and shortcomings are pointed out as appropriate. The relevance of the work to a possible large MSBS with extreme attitude capability is considered, including an analysis of the likely capabilities of an existing

design proposal intended only for model suspension at moderate attitudes. Remaining difficulties requiring further study are also indicated.

CHAPTER 2

THE SOUTHAMPTON MSBS AND PREVIOUS WORK ON EXTREME ATTITUDE SUSPENSION

2.1 The Southampton MSBS circa 1984

The Southampton MSBS, originally commissioned in the early nineteen-sixties along the principles outlined in the introduction (23), with a non-symmetric arrangement of seven electromagnets and an analogue control system, was extensively rebuilt around 1980. A symmetric array of ten air cooled electromagnets was installed around an octagonal test section 7 inches across the flats. New power supplies based on DC servomotor controllers were added, permitting bipolar operation. Conventional optical sensors were used, comprising analogue detectors illuminated by either tungsten or (in the case of the axial motion channel) laser light beams. Depending on the particular model design, a number of roll motion sensing systems were used to permit six axis control.

The Southampton MSBS in this form was the starting point of the work described here, with all the changes made to it resulting from the demands of high angle of attack suspension. What follows, therefore, is a brief description of the system's operation. More detailed reviews of the electromagnet array, the position sensing system and the control algorithms may be found in Chapters 3 to 6 where the changes made for extreme attitude suspension are explained.

The control system was implemented digitally on a PDP 11/34 minicomputer, Figure 2.1. Outputs from the five or six position sensors were first made accessible to the computer via a 12 bit A/D system before being combined by summing or differencing to yield measures describing the model's position and attitude in each of the degrees of freedom controlled. For example, by adding the outputs of the four main sensors (Fig.4.1) a measure of vertical heave position could be obtained, whereas the difference between the sum of the front pair and the sum of the aft pair represented a

measure of pitch attitude. The dynamic stabilisation of the model was performed in the block described by its mathematical representation;

$$\left(\frac{1 + nTD}{1 + TD}\right)^2$$

This is the series pair of phase advance algorithms, implemented digitally according to the discretised equation thus;

for each step the output $z(k)$ is based on the input $y(k)$:

$$z(k) = y(k) + \frac{nT}{\Delta t}\Big(y(k) - y(k-1)\Big)$$

The derivation of this has been given elsewhere (24).

Demands for changes of model position and attitude by the user were input via the computer VDU in the next block, appearing as DC offsets to the feedback error signals. An additional term used was an integrator stage, which added on an integrated proportion of the error signal to give a constant output even with a zero error. This allowed the model to be correctly driven to a desired location and attitude. After multiplication by the overall channel gains, the resulting demands for electromagnet currents were output by a 16 bit D/A system to the power supply controllers. The frequency of the control system loop rate was principally constrained by the capacity of the computer to perform the necessary operations, and was originally set at 400 Hz. The influence of possible high frequency aerodynamic oscillations was not a consideration in selecting the loop rate for this demonstration facility. The control system was tied to a computer generated clock. This was ultimately derived from a binary number, and so for convenience in data acquisition involving this time information the program loop rate was subsequently altered to a power of two, specifically 256 Hz. Control parameters in the stability algorithms were adjusted in accordance.

Electromagnet current data was obtained via the A/D subsystem from shunts installed in the power supplies. Depending on the particular

control program used, data for up to a few hundred program loops could be stored during model suspension for subsequent processing.

During the development work of this sytem, no wind tunnel was available for use with the MSBS, but later a low speed (M = 0.2) wind tunnel was installed. Of the open return type, it allowed some testing of axisymmetric bodies to be performed (25). Extensive investigations of means of calibrating the system were carried out: that is relating the forces and moments on the suspended model to the electromagnet currents producing them. In particular the dynamic calibration technique was developed (26, 27). In this the model is deliberately forced in a known motion (e.g. a simple harmonic oscillation) and the calibration deduced from the corresponding stored current data.

The MSBS demonstrated outstanding reliability over several years of use. Notably the power supplies gave reliable service with no model fly-away ever being caused by power failure.

2.2 Distinguishing Features of Extreme Attitude MSBSs

Of the various magnetic suspension systems known to have been built, only a few have had any capability to control a model at an attitude significantly divergent from the wind tunnel axis. The second system built at MIT, by virtue of its complex and symmetrical array of electromagnets and its electromagnetic position sensing system, was capable of suspending a model at up to 30^{o} pitch or yaw angle, whilst the one commissioned at NAL in Japan undoubtedly has the potential for performance comparable with the Southampton system as it was at the outset of this project. The previous work carried out at Southampton (28) defined those problems requiring attention in designing an extreme attitude MSBS, and which distinguish it from more conventional MSBSs. The three most important are (quoting the reference):

1 - the identification of electromagnet array geometries and configurations capable of generating, via field and field gradient components, forces and torques upon the model

in the required senses and magnitudes over the full range of model attitudes;

2 - synthesis of control algorithms capable of accommodating large changes in model aerodynamic characteristics and magnetic couplings to the E/Ms;

3 - design of position, attitude and other sensors to monitor wide ranges of model motion.

These three problems are closely linked, and must be tackled simultaneously to achieve success. However, the analytic framework for the first was established in the previous work, and allowed trial suspension at attitudes up to 60^{o} angle of attack (although as 2 and 3 above were not addressed a continuous sweep from nought to sixty degrees was not possible). This work will now be reviewed.

2.3 Theoretical Background to Force and Moment Generation

As explained in (29), and using conventional Euler angles, the forces and moments upon an axially magnetised model may be expressed in terms of the field and field gradient components in the following way:

$$\mathbf{F}' = \mu_o \int_V \mathbf{M}'.\nabla'\mathbf{H}'\,dV \tag{1}$$

and

$$\mathbf{T}' = \mu_o \int_V \mathbf{M}' \times \mathbf{H}' + \mathbf{r}' \times (\mathbf{M}'.\nabla'\mathbf{H}')dV \tag{2}$$

where prime indicates model axes.

The question arises as to how many components must be generated by a given arrangement of electromagnets in order to permit suspension over an

arbitrary attitude range. Three field components (H_x, H_y, H_z) and nine field gradients (H_{xx}, H_{xy}, H_{xz}, H_{yx}, H_{yy}, H_{yz}, H_{zx}, H_{zy}, H_{zz}) exist, but from Maxwell's equations:

$$\nabla \cdot B = 0$$

and in free space where B is proportional to H;

$$\nabla \cdot H = 0$$

Thus

$$H_{xx} + H_{yy} + H_{zz} = 0$$

Also

$$\nabla \times H = 0$$

and

$$\left(\frac{\partial H_x}{\partial y} - \frac{\partial H_y}{\partial x}\right) + \left(\frac{\partial H_x}{\partial z} - \frac{\partial H_z}{\partial x}\right) - \left(\frac{\partial H_y}{\partial z} - \frac{\partial H_z}{\partial y}\right) = 0$$

So;

$$H_{xy} = H_{yx};\ H_{xz} = H_{zx};\ H_{yz} = H_{zy}$$

Thus we find that only eight independent field components exist.

It may be noted that for the special case of an axially magnetised model of fixed and uniform magnetisation for which the intergrands of equations 1 and 2 are constant, the force and torque vectors can be approximated as:

$$F' = \mu_o M' \cdot \nabla' H_o V$$

$$T = \mu_o M' \times H_o' V + \mu_o r' \times (M' \cdot \nabla' H) V$$

and if at the centroid of a rotating model the field is H_O:

$$T' = \mu_o M' \times H_o' V$$

These approximations are implicit in the conventional representation of the forces and moments generated by the fields and field gradient components from a group of n electromagnets thus:

$$\begin{pmatrix} F_x \\ F_y \\ F_z \\ T_x \\ T_y \\ T_z \end{pmatrix} = \begin{pmatrix} a_{11} & \cdots & a_{1n} \\ \vdots & & \vdots \\ a_{61} & \cdots & a_{6n} \end{pmatrix} \cdot \begin{pmatrix} I_1 \\ \vdots \\ I_n \end{pmatrix}$$

Several considerations conspire to make the number of electromagnets at least ten if several degrees of freedom are to be controlled. The use of symmetric groups of electromagnets ensures that the fields and gradients are reasonably uniform over a useful region in the centre of the MSBS. This results in modest linear excursions of the model away from the nominal datum producing only small changes in the magnetic couplings to the E/M array. The controller then does not need to adjust itself in some way to account for the altered translational position. It has been possible hitherto to follow a similar argument for angular rotations of small amplitude (a few degrees), but this is not possible for the case of extreme attitude suspension as considered here. Instead, the relationships expressed by the matrix equation above can be expected to vary strongly as a function of attitude, and in consequence the control system must be able to take account of such effects. This shows that a strong link exists between the first two of the problem areas introduced in 2.2.

2.4 Use of Simulation FORCE as a Predictive Tool

To investigate the force capability of an arbitrary group of electromagnets a computer based simulation was developed by Britcher (28),

based on a code developed by MIT (30). Called FORCE, this is a modular Fortran program which can calculate the fields produced by a set of electromagnets represented by straight line current carrying elements. This is accomplished through use of the Biot-Savart law (an integration technique). Further, by representing a magnetised model by an array of dipoles, the forces and torques which the fields and field gradients produce can be estimated. Model and electromagnet configuration can be stored in data files and recovered for repeated use, and data output in hard copy form.

However, FORCE is subject to a number of sources of error:

1) to reduce calculation time, both the model and the electromagnets are usually represented by relatively coarse grids and elements;

2) the model is assumed to have uniform magnetisation. This is justifiable in the case of materials with a high coercive force - such as rare earth - cobalts - but is not in the case of Alnico, used in many of the SUMSBS models;

3) the computations are only valid for the case of air cored electromagnets. In the case of SUMSBS, eight of the ten E/Ms have laminated iron cores which significantly increase the forces and moments which they can produce.

For these reasons FORCE was not expected to be reliable for calculations requiring high accuracy. However, there was no reason to suppose that its general predictions of trends in force and torque production were not accurate. By simulating the electromagnets of SUMSBS, Britcher was able to obtain performance curves indicating the system's capability as an axially magnetised model of typical proportions was rotated from zero degrees angle of attack up to ninety degrees. These showed that while large variations in the fields and gradients could be expected, all the necessary force and moment components were available over the full attitude range save one. This was a lack of the H_{yz} field gradient which manifested itself as a sideforce capability falling away from a maximum at zero degrees angle of attack to nothing at 90^{o}. The original data, which may be found in Reference 28, was calculated for a version of SUMSBS scaled up by a factor

of ten, so that the absolute values of the forces and moments obtained do not directly relate to the actual system.

2.5 Experimental Demonstration of Suspension at 60° Angle of Attack

To confirm these predictions, a trial demonstration of extreme attitude suspension was undertaken by Britcher. This involved the physical relocation of the existing optical sensing system so that its datum (null) incidence was at 50° degrees angle of attack. At this attitude the estimated sideforce capability was about half that of the maximum, which was judged adequate to control a model, after suitable adjustment of the overall loop gain. The MSBS control program was then altered according to the calculated couplings of the various electromagnets. For example, to generate a force approximately perpendicular to the model's longitudinal axis (a model sense heave force) the axial electromagnets were used in concert with the four laterals. This was the first time that the latter were called upon to generate a force other than a sideforce. The precise proportions in which the groups of electromagnets were used to generate the forces in the vertical plane were determined in a fairly arbitrary way, but this work presages the demand distribution principles developed in 6.2.

Having achieved initial suspension at 50° angle of attack the controller proved capable of control over the range forty to sixty degrees, a greater angle of attack than any previous MSBS. No refinement of the controller was attempted, and the force and moment capabilities were not confirmed by calibration work. The suspension quality was described as 'poor', owing to simplifications made in the electromagnet decouplings and deficiencies in the sensing system.

Considering the three problem areas outlined above, the need to design a large attitude range sensing system was avoided, since the usable range was not actually increased. Similarly a fixed parameter controller could be used, since the coupling changes over the twenty degree spread could be neglected. However the experimental work showed that by using suitable analytic techniques a controller could be designed to combine the capabilities of a group of electromagnets to perform a task other than that

for which they had been originally designed. The flexibility endowed by a digital control system was an essential feature in achieving this goal.

CHAPTER 3

ADAPTION OF ELECTROMAGNET ARRAY FOR 90° RANGE SUSPENSION

3.1 Introduction

The previous work showed that apart from a predicted lack of sideforce at around 90°, the existing symmetric array of ten electromagnets comprising SUMSBS was capable of generating all of the forces and moments necessary for suspension over the desired attitude range from zero to ninety degrees. Figure 3.1(a) shows how sideforce is generated by the action of the lateral electromagnets upon the model core at conventional suspension attitudes. Figure 3.1(b) shows the resulting sideforce capability. Changes caused by the first area of difficulty described in 2.2 centred upon finding a way of providing the missing force component at extreme attitudes. Two possible approaches exist. Either:

a) the sideforce is generated by the existing field gradients acting upon small magnets specially installed upon the model but not aligned with the normal axis of the core magnetisation (auxiliary magnet configurations),

or;

b) the electromagnet array is rearranged or augmented in some way so as to make the missing field gradient available, permiting a conventional model core to be used.

Both possibilities were considered by using the previously described computer simulation FORCE.

3.2 Auxiliary Model Magnet Configurations

To investigate the first approach, FORCE was amended by adding three extra subroutines to permit force and torque data to be obtained for model cores with the following auxiliary model magnets:

a) a set of cruciform 'fin' magnets located at the model centroid;

b) two sets of fin magnets aligned with the ends of the cylindrical core;

c) transverse magnetised wing magnets.

Figure 3.3 shows how the sideforce is generated by the symmetric use of the four lateral electromagnets when the model is at 90^{o} angle of attack. However, whilst producing the sideforce, the model core also interacts with these electromagnets to produce a pitching moment. In principle, this could be counteracted by the main source of this moment component, the four vertical electromagnets. These in turn produce a small sideforce component via the extra magnets.

Figures 3.4a to 3.4c show the two sideforce components and the corresponding pitching moment contributions for examples of models with the three aforementioned auxiliary magnet configurations, illustrated in Figure 3.2. The large discrepancy between the sideforce at zero degrees from the conventional arrangement of polarities, and that obtained through the use of the additional magnets at ninety degrees angle of attack is evident in all cases. The various shapes shown would be made up of square slabs of rare earth cobalt magnets, which exhibit high resistance to self demagnetisation.

Since these augmented magnet configurations must be maintained in the correct orientation to the electromagnet system to function, a means of controlling the roll attitude of the model is required. This could be effected using the same auxiliary magnets, but with a differing set of electromagnet polarities. Figure 3.5 illustrates how this could be accomplished using the four lateral electromagnets. However, a by-product of this roll torque is a model sense axial force, small at low incidences but becoming substantial as ninety degrees is approached. This component could be countered by axial forces generated by other electromagnets, at the cost of a reduction in the overall system force capability owing to the margin required for roll control.

Thus it can be seen that although auxiliary model magnets could be used to generate the missing sideforce component at high angles of attack, it results in a more complex control system. A roll motion sensing system would have to be designed commensurate with the ninety degree attitude

range, and although this is feasible, it has not been pursued in this project. A more fundamental problem is caused by the large increase in weight of the suspended model resulting from the auxiliary magnets. Taking the case of the transverse magnetised wing model of Figure 3.2, the auxiliary magnets add to the mass of the core by thirty per cent. Reference 28 suggested that the normal force capability of SUMSBS was likely to be severely limited in the thirty to forty five degree incidence range, and it seemed likely that the margins available for control in each of the degrees of freedom could be reduced owing to the need for large continuous currents to support the model's weight. For these reasons further study of the use of auxiliary model magnets was curtailed.

3.3 Amended Electromagnet Configurations

In addition to pointing out the inability of the existing '+' arrangement of the main electromagnets of SUMSBS to produce the H_{yz} field gradient needed for high angle of attack sideforce, Britcher suggested a possible solution in Reference 28. This lies in rotating or skewing the lateral electromagnets so that the existing force (and moment) capabilities become available at different attitudes. This would permit a conventional model core to be used, and roll control made unnecessary. Notionally, the simplest way of making sideforce available at high angle of attack would be to rotate the lateral electromagnets in the pitching motion sense by, for example, thirty degrees. This would result in the maximum sideforce being generated at 30^{o} angle of attack, and the sideforce shown to be adequate at 60^{o} in the earlier demonstration becoming available at 90^{o} (Figure 3.6). However the physical limitations of the MSBS structure makes such an arrangement of electromagnets impractical without complete redesign. A similar effect to rotating the lateral electromagnets is obtained by skewing them. This involves translating the vertical pair upwards and the rear pair downwards. Figure 3.7 shows the predicted sideforce for varying amounts of skew.

As a result of these studies, it was decided to modify SUMSBS by incorporating five inches of positive skew into the lateral electromagnets of SUMSBS; that is moving the front pair 2.5 inches upwards and the rear pair 2.5 inches down. A greater change would have resulted in large areas of

these E/Ms directly facing the vertical electromagnets, with only small separations. It was thought that this might produce unpredictable interactions between the fields which the E/Ms generate. A smaller amount of skew would not have resulted in sufficient improvement in the sideforce capability.

The modifications to SUMSBS involved removal of all eight iron cored electromagnets so that existing welded light alloy bracing struts could be removed. These would otherwise have prevented the lateral electromagnets being located in the required positions. New support beams for the lateral E/Ms were fabricated incorporating access holes for dummy model calibrators, model launching equipment etc. Care was taken to incorporate insulation to reduce large metal circuits which would permit eddy currents to be induced with alternating field components. The re-assembled arrangement of electromagnets is shown in Figure3.8.

3.4 Predicted Force and Moment Capabilities of Modified Southampton MSBS

The previous work on extreme attitude suspension showed that large changes in the forces and moments produced by the electromagnets would be expected as a model rotated from zero to ninety degrees angle of attack. To design a control system able to take account of such changes, both the trends and the absolute values of these effects must be known to within perhaps five to ten percent. Gross errors could not be accepted because the design of the controller would result in either excessive or inadequate forces and moments arising in response to error signals. In particular, an unforeseen component acting on the model as a result of inaccurate predictions could swamp the capabilities of the control system. Absolute precision is not necessary because of the inbuilt control margins: in the absence of large disturbing influences models can often be successfully suspended in an MSBS with a controller with too large or too small loop gains, with one of a group of electromagnets failed, or with various other deficiencies. Fine tuning can be undertaken by calibrating the suspended model and comparing the results with the predictions.

For these reasons a reasonably accurate model of the capabilities of SUMSBS with the modifications required for high angle of attack suspension was required. This was developed from the program FORCE but with empirical corrections to take account of measured discrepancies between its predictions and experimental data obtained through calibration work. Large errors were expected to be traceable to the iron cores of the eight main electromagnets of SUMSBS, which are not taken into account by FORCE.

Eskins performed extensive calibrations of SUMSBS before modification for extreme attitude suspension (27). Table 1 shows the measured performance of SUMSBS in three degrees of freedom for a model of known characteristics. This is compared with the predictions of a FORCE model of SUMSBS in its original form. The ratios between the measured and predicted values are also shown.

Component	Measured data	FORCE prediction	Error ratio
vertical heave	4.89N	2.258N	2.16
axial heave	1.60N	1.127N	1.41
pitching moment	0.373Nm	0.173Nm	2.16

model: 4 in long by $\frac{3}{4}$ inch diameter cylindrical core
assumed magnetisation: 1.0 Tesla

8 main E/Ms: single loop representation; 8000 Ampere turns
2 axial E/Ms: 8 element pseudo-solenoidal representation; 20000 ampere-turns

Table 1

The error for the pitching moment and vertical heave force is consistent, and much larger than for the (air-cored) axial electromagnets. The ratios 2.16 and 1.41 were applied to the predictions of FORCE with a model of the modified Southampton MSBS (i.e. with skewed lateral electromagnets) to produce the data of Figures 3.9 to 3.14. The same

corrections were used in the sideforce estimations for augmented configurations in 3.2 above.

The information is presented as the force and moment components generated by four groups of electromagnets, as indicated by the numbering system shown in Figure 3.9. These are in fact the groups used in creating the control system with de-coupled channels as explained in Section 6, and the data shown was used in this process. There remains a significant possibility of error in this data, as a consequence of the other limitations of FORCE outlined in 2.4, but it was hoped that these would not prevent suspension. Force calibration experiments with the modified Southampton MSBS are described in 9.3 to 9.7.

CHAPTER 4

POSITION SENSING SYSTEM

4.1 Introduction

This chapter reviews the requirements of an optical sensing system for an MSBS and discusses previous techniques. A description of the sensing system designed for the extreme attitude range requirement is given, including the electronics which interface the system with the control computer. Optical effects relevant to the correct functioning of the system are also outlined.

4.2 A Review of Optical Sensing Techniques

The statically unstable nature of the MSBS results in a need to continually monitor the position and attitude of the suspended model in order to close the control loop. An MSBS position sensing system, whether optically based or not, must possess a number of characteristics if it is to function successfully. Ideally it should:

1. have no mechanical contact with the suspended model;

2. suffer no interference from the magnetic field generated by the support system;

3. generate independent or separable electrical signals for each degree of freedom to be controlled;

4. have positional and angular resolution commensurate with the desired range of model motions and accuracy of data to be obtained with the wind tunnel system;

5. be readily accommodated outside the wind tunnel test section without unduly impacting on the electromagnet configuration or model launching technique;

6. be capable of accommodating any likely model geometry.

In practice many of the position sensing systems used have not fully met these specifications. In particular, they are frequently only capable of accommodating models composed of relatively simple axisymmetric shapes such as spheres, cones and cylinders. The most significant exception to this is the (non-optical) MIT electromagnetic sensing system, referred to in the Introduction. Its ability to suspend and control models of any arbitrary configuration remains one of its main attractions. However the calibration of this system is dependent on the size and shape of the magnetic core. Non-optical sensing techniques are not considered further here, although a large MSBS might well require at least two separate sensing systems to provide a measure of redundancy, and so alternatives to electro-optical sensors are needed.

In the pioneering ONERA MSBS, optical sensing techniques were employed, and the majority of the other MSBSs followed a similar approach. Typically, each degree of freedom of the model requiring to be controlled was sensed by a separate arrangement of light source and detector (Fig.1.1). A beam of light originating from a combination of tungsten filament, slit or pinhole and convex lens is passed across the test section of the MSBS to strike a focussing lens which concentrates the image onto a photodiode. The presence of model is sensed by the modulation of its shadow cast upon the detector. An analogue voltage is thus generated proportional to the model's position in the direction of the width of the beam. A signal relating to angular orientation may be obtained by using a pair of beams and sensors placed fore and aft of the centre of rotation, and differencing the resulting signals.

The Southampton MSBS at the outset of this work used an optical sensing system based on these principles. Figure 4.1 shows the arrangement of five light beams and sensors. Four were arranged in two cross shapes, and were used to measure the model's position in the vertical and horizontal heave senses, and also its pitch and yaw attitude through appropriate summing and differencing of the four output analogue signals. The fifth sensor, a long analogue detector without a focussing lens was illuminated by means of a low power (less than 1mW) helium neon (He-Ne) laser. This

configuration was used to allow the sensor unit to be accommodated directly below the wind tunnel test section, above the lower pair of electromagnets, and permitted relatively large axial excursions resulting from changes in pitch attiutde. To permit control of non-axisymmetric models, a variety of roll attitude monitoring systems were also fitted to SUMSBS at times, involving a further light beam and sensor pair.

The narrow beam/analogue sensor combination was found to suffer a number of drawbacks. Its inability to suspend very small models (for example in a hypersonic low density wind tunnel), and its lack of flexibility in the shape of models which may be suspended triggered experiments in the late nineteen sixties into alternative optical sensing techniques. At ONERA a novel approach was developed representative of broad class of optical sensors in which a target or tracking device placed on the model is illuminated either directly (e.g. by light emitting diode) or indirectly (e.g. by bright diffuse lighting). After evaluating a version of the MIT electromagnetic position sensor and such possibilities as articulated and translating sensors (31), the design shown in Figure 4.2 was developed. In this a checker pattern applied to the model is viewed by a photomulitplier tube which scans in a square path the transitions from light to dark of the target. By using an orthogonal pair of such targets and detectors all six degrees of model freedom could be monitored by suitable signal processing.

Loop rates between 500Hz and 10KHz were used, and a measured resolution of 4.7 thousandths of an inch achieved. The system was also capable of monitoring motions up to 40^{o} angle of attack, although there is no evidence that the associated control system was able to suspend a model at such incidences. However the vulnerability of the detectors to magnetic interference necessitated the use of extensive mu-metal shielding, and for the time they were excessively expensive (£500-£2000 at 1970 values). The ONERA MSBS work apparently petered out in the early nineteen-seventies.

At Oxford University, the desire to study the drag of very small spheres in a hypersonic tunnel led to an advanced control system based on a digital approach. The position information in two translational degrees of freedom was generated by an ingenious scanning optical system (Fig. 4.3). This involved a spot from a short persistence cathode ray tube rapidly

scanning across a photomultiplier in a TV-like raster. During the course of a scan the continuing presence of the spot allowed ramp voltages corresponding to the x and y sense of the system to be built up. These voltages would become fixed at their latest value when the presence of the suspended model interrupted the light beam. Thus over the course of a scan, signals corresponding to the x and y position of the model were generated.

Details of performance of the system are sparse, but problems were caused by the low light level of the scanning spot source, presumably manifest as interference from background lighting. Significantly, when the second Oxford MSBS was built, a conventional light beam and photodetector sensing system was employed, combined with analogue control circuitry (33).

At the time of renewed interest in MSBS technology in the late 1970s, one of the important areas requiring further study was seen to be the problem of position sensing.

Initial work at Southampton reviewed the possibilities (34) and noted in particular the potential of self-scanning photodiode arrays, one product of the rapid development in microelectronics in the preceeding years. These devices consist of linear or area arrays of small photodiodes each capable of individual analogue light measurement, but mounted on a single silicon component. They are now widely used in character recognition systems such as bar code readers, in spectroscopy, and as star trackers on satellites. The original attraction of these devices for MSBSs was believed to be their ability to continue generating a usable signal even in conditions of severe optical degradation due to smoke used in flow visualisation. Other advantages, particularly for the high angle of attack application considered here, have also been evinced.

The initial configuration proposed for the use of the self-scanning photodiode arrays (SSPDs) was to have linear arrays built into lens assemblies focussed onto diffusely illuminated black/white targets affixed to the model. This concept was refined in the General Electric design study for a large MSBS (35) and in other work (36) suggesting the use of analytic algorithms which would yield position signals to finer resolution than the diode spacing (so called 'sub-pixelisation').

The first actual use of a photodiode array with an MSBS was reported in 1981 (37). A single 512 element array with .001 in diode spacing was used with a halogen bulb and focussing lens source to monitor the vertical heave motion of a model in the Southampton MSBS. Circuitry was designed to monitor the location of the 'light' to 'dark' transition caused by the presence of the model in the light beam in a similar way to the existing photodiode/lens combinations. A comparator was used to threshold the output video signal so that at an arbitrary voltage between the light and dark signals a counter was stopped, thus generating a position related signal. This was then converted to a voltage for use in the analogue control system then in use. Much of the potential advantage of using a 'digital' sensor was thus not made available, but measurements suggested that the photodiode array was far less susceptible to optical degradation, as for example, caused by smoke used for flow visualisation. At the completion of the tests the array and electronics were removed from the MSBS.

Following the success of this work, a five component optical sensing system was installed with the 13 inch MSBS which had been moved from AEDC to NASA Langley in 1983. This uses five 1024 element photodiode arrays and laser light beams and has been extensively reported elsewhere (38). Some of its features are shared by the new sensing system designed for the Southampton MSBS.

4.3 Design Considerations for High Alpha Position Sensing System

The primary requirement for the new position sensing system planned for the Southampton MSBS was an ability to monitor the motion of an axisymmetric model of about 20mm diameter over an angle of attack range from less than zero degrees to over ninety degrees, so that a usable ninety degree range would be made available. Ideally motions in other degrees of freedom would be accommodated to a similar extent as with the existing sensing system. Initial work on augmented model magnet configurations to achieve high angle sideforce meant that the ability to monitor model rolling motions might also be needed. However, the decision to use a skewed arrangement of lateral electromagnets resulted in the deletion of the sixth sensing channel, at least for the time being.

For the existing analogue based position sensing system to function, one model edge had to be visible to each of the detectors at all times. If a second edge corresponding to the opposite side of the model became visible to any sensor its output would cease to change with continued motion, and the system would fail. Thus the maximum available translational motion was equal to the sensor field of view for a model of greater diameter than the beam width and equal to the model diameter for a model smaller than the beam width.

Rotational motion was detected by the difference in outputs from pairs of sensors fore and aft of the model centre of rotation, and so the sensitivity was dependent on the particular geometry of the system. In practice a pitch and yaw range of about $\pm 15^{o}$ about the datum (wind tunnel) axis was available. To monitor a ninety degree pitch angle range, much larger light beam/condensor lens units would have to be designed if a one-edge analogue based system was used. The resulting components could not be accommodated in the confined spaces around the MSBS electromagnets.

A further objection to the use of analogue detectors lay in the problem of system calibration. Since the location of the light beams and sensors of the existing sensing system was not precisely known, and the sensor outputs were non-linear, the optical system had to be calibrated for use in work requiring any precision. This was accomplished by traversing a non-magnetic outline of the model to be suspended - a 'dummy model' - across the field of view of the sensing system in all the required directions and rotational senses. Curves of output signal against position/attitude were thus obtained.

This is necessarily a difficult and time consuming process. Although high resolutions of position can be obtained - of the order of one thousandth of an inch or better - the non-linearities mean that it is difficult to incorporate them into the control program in such a way as to permit user demands of the form (for example) 'move in a heave direction by +2mm from the present position'. Information relating to the sensor outputs for every model position and orientation would have to be obtained and stored for access by the control program. Complete calibration in this way has never

been attempted. With the analogue photodiodes, the calibrations also vary over time with electrical drift and with dust build up on the optical elements, and so they must be performed at the same time as the experimental work. The use of digital sensors such as photodiode arrays should reduce such problems by having a fixed, predictable calibration which is less affected by optical degradation.

The simplest way of incorporating this technology into an MSBS is to use linear arrays in place of the analogue photodiodes, together with light beams and a traditional shadowing technique. A condensor lens is not necessary provided that the array length is comparable with the required model motion. Both linear and area arrays are available built in to cameras, but for reasons of cost and space limitation, the option of using these with SUMSBS was not investigated in detail. An imaging system, involving the generation of a focussed image of the target object at the face of the sensor via a suitable lens could have advantages, especially for a large MSBS, and this possibility is discussed in Section 11.4. However for a small scale system where diffraction effects can be accounted for the benefits of a focussing lens are small. Also the required depth of field of at least two inches is comparatively large compared to the feasible focal lengths which could be accommodated around the Southampton MSBS without impractically long beam path lengths. Hence the new sensing system uses five linear arrays illuminated directly by five light beams to monitor the position and attitude of an axisymmetric model.

4.4 Configuration and Capability of System

The detector device chosen for the large angle position sensor is the Reticon RL1024G self scanning photodiode array which consists of 1024 silicon photodiodes mounted on a single chip at an even spacing of 0.001" and protected by a glass window. Each device is illuminated by a collimated beam of Helium-Neon laser light. The magnetically suspended model intersects the light beams and its location is measured in terms of the light to dark transition of each array output. Provided that the model's diameter is less than the sensor length, the maximum linear motion of the model is equal to just less than the sum of the sensor length and the model diameter

provided that more than one model edge can be simultaneously viewed by a single detector array.

The arrangement of the five light beams and the detectors is shown in Figure 4.4. The four main beams are arranged in two pairs, which enter the octagonal wind tunnel test section from the lower diagonal faces. These form two right angle crosses, as seen from a point of view looking directly downstream of the test section, before leaving the test section at the upper diagonal faces. However, because the beams are inclined backwards by 45° to the y-z plane of the wind tunnel (i.e. as seen from the side), the shape of the intersection area of the pairs as viewed from an axis perpendicular to their plane is not a square but a rhomboid with a crossing angle of 70.53° (see Fig.4.5). If typical geometrical dimensions are specified, the translational and rotational capabilities of the system can be deduced. These are summarized below for a typical cylindrical model:

Perpendicular Separation of Double Beams	50mm
Cross Angle of Beam Pairs	70.5°
Pitch Angle Range at zero degrees yaw angle (datum heave, slip, and axial position)	-10°/+100°
Yaw Angle Range* at +45° pitch angle (datum heave, slip, and axial position)	±10°
Yaw Angle Range at -10°/+100° pitch angle (datum heave, slip, and axial position)	±6°
Yaw Angle Range* at 0°/+90° pitch angle	±10°
Slip Motion Range* at 0°/+90° pitch angle	±9mm
Slip Motion Range* at +45° pitch angle	±9mm
Heave Motion Range at 0°/+90° pitch angle	±13mm
Heave Motion Range at +45° pitch angle	±24mm

* denotes motion limited by tail of model moving out of axial light beam. Motions are relative to the model's axes.

It can be seen that, because of the diamond shape of the intersection areas of each of the two pairs of main beams, the maximum available motion in each of the degrees of freedom other than pitch occurs at the 45^{o} angle of attack.

To make full use of the potential for inherent calibration offered by digital sensors and the shadowing technique, it was decided at an early stage to use collimated light beams to illuminate the sensors. This means that a translation of (say) 10mm is interpreted by the sensing system as being of exactly this amount irrespective of the separation between the model and the detectors.

In principle this can be achieved to an accuracy dependent only on the resolution of the detector. For the RL1024G this implies a position keeping capability of one thousandth of an inch. The angular resolution depends on the model diameter, but for a typical three quarter of an inch model and a 110^{o} maximum attitude range the average value is given by 110/1750 or about $.06^{o}$. However, Figure 4.6 shows the relationship between the pitch measure and the angle of attack. Because this is a tan function, the angular resolution is closer to $.1^{o}$ at 45^{o} angle of attack, and $.05^{o}$ at 90^{o} angle of attack.

However one degree of model freedom is not measured by one individual sensor, but instead is obtained by combination of the outputs of the four main detectors. For example, pitch attitude information is obtained by adding the model position measured by the forward pair of sensors and subtracting the sum of the outputs of the aft pair. The consequence of this is that not only must the light beams be collimated, but also their separation and crossing angles must be known. If the complete geometry of the beams is determinate, then it is possible to predict the edge location of a given model for any position or attitude in terms of the number of illuminated or darkened photodiodes for each of the four arrays. The measure of the model's location in this form is termed its pixel count.

A simple Fortran program (PIXEL) was developed which calculates the edge location of a cylindrical model in terms of pixels for any chosen position or attitude. A full description of this program and the relevant geometry may be found in Appendix C. By incorporating this information into the MSBS control program in the form of look up tables it was intended that a user demand in literal form ('move in pitch attitude from 10 to 22 degrees') could be interpreted by the control program as a change in the pitch pixel count. In practice this ideal concept is complicated by considerations of optical distortion and edge diffraction effects. These are discussed in Section 4.8. Also since each sensor may see either one or two model edges, the pixel count for one position and orientation is not unique, but may exist in several forms. Computer logic is thus required to carefully distinguish incoming data from the sensing system, and relate it to the user input position demands. The necesary algorithms are explained in Section 5.

4.5 Illumination of Position Detectors

The requirement to produce highly collimated and precisely aligned light beams to illuminate the detector arrays dictated the selection of optical equipment for the new position sensing system. The four main beams originate in a single medium power He-Ne laser, whilst the axial sensor beam uses the low power laser from the existing analogue axial system. Lasers have been used since their beams can readily be expanded and collimated by lens systems and offered cost advantages over commercially available collimated tungsten or arc sources. However the use of coherent light can produce interference effects from two surface optical components (e.g. lenses). Use of suitable anti-reflection coatings can reduce these problems but their presence has been noted in experimental testing.

The laser beams are expanded and collimated by respectively short and long focal length cylindrical lenses, with fine control of separation and rotation. The main beam system uses an 8mw multimode laser to give a more even illumination than is possible with a Gaussian laser beam. The collimated beam is fed into a system of cube beam splitters and right angle prism mirrors to produce four separate beams with independent positional and angular control commensurate with the array resolution. Cube/prism type

optical components were chosen rather than the more common plane beam splitters and mirrors because they may be more rigidly mounted and with suitable anti-reflection coatings have better transmission characteristics. Fixed mirrors deflect the main beams across the test section to strike the sensors normally (Fig.4.8). The sensors are fitted to mounts which permit fine positioning in the two directions perpendicular to the beams, as well as rotation about the normal to the sensor face. As originally designed, the axial beam was incident at 45^{o} to the axial sensor, because there is insufficient room between the lower E/Ms and the wind tunnel test section to permit an inclined installation. Figure 4.7 shows an overall view of the Southampton MSBS modified for extreme attitude suspension. Appendix A contains the detail specifications of the optical system and Figures 4.8a to 4.8g illustrate aspects of it, including the diode arrays themselves and smoke visualisations of the laser beam paths.

4.6 Beam Alignment Unit

In order to carry out the beam alignment procedure outlined above, a target device must be installed in the test section. This is shown in Figure 4.8. It consists of an aluminium alloy block machined to tolerances of ±.001 inch with two end plates each with three $\frac{1}{4}$ inch diameter steel rods which ride in ball bushings fixed in the main block. The end plates are spring loaded, closing shut four pairs of knife edge slits on opposite sides of the block. These may be opened by means of lockable micrometer barrels acting on fixed quarter inch rods projecting from the centre of the main block, one on each side. Thus the slit widths may be precisely set and measured.

The block is mounted at 45^{o} in the system test section by supporting arms attached to the MSBS frame upstream and downstream of the test section. This allows the device to be used with the test section installed. By ensuring that the four main position sensors are correctly illuminated with the laser beams passing through the slits of the block, the separation and parallelism of the beams is assured. To set the crossing angle of the beams, the fixed central target rods referred to above are used, together with two more $\frac{1}{4}$ inch rods which may be inserted through the main block. The translational position of the four main sensors is first set so that the fixed

rods are seen as being in the centre of each of their respective fields of view. The removable rods are then inserted and angular adjustments of the beams made at the mirror gimbal units so that the shadows of the rods coincide, resulting in the setting of the beams to a crossing angle identical to that between the target rods. This angle is fixed and measured to be $70.5^{o} \pm .1^{o}$.

4.7 Photodiode Array Control System (PACS)

In 1985 the computer used with the MSBS was upgraded to a PDP 11/84, with considerable reduction in execution times. In operation with the Southampton MSBS in its existing form, it interrogated the position sensing system once per program loop, via the A/D system, in order to carry out the model stabilisation and determine E/M current output demands. To make full use of the data available from the digital sensors, new interface electronics were developed. Before discussing these, an explanation of the operation of the self-scanning photodiode arrays is appropriate.

Each cell of the arrays consists of a photodiode and a dummy diode both with an associated storage capacitance. The diodes are connected through MOS multiplex switches to video and dummy recharge lines which are common to all the cells. The scanning circuit is driven by a single-phase TTL clock with a periodic TTL start pulse introduced to initiate each scan. The cell-to-cell sampling rate is the clock frequency, and the total time between line scans is the interval between start pulses. During this line time, the charge stored on each photodiode is gradually removed by photocurrent. The photocurrent is the product of the diode sensitivity and the light intensity (irradiance). The total charge removed from each cell is the product of the photocurrent and the line time. This amount of charge must be replaced through the video line when the diode is sampled and reset, once each scan. Hence information as to the amount of light falling on each diode can be obtained. By differentially reading out the video and dummy cell lines, switching transients can be removed, improving the signal to noise ratio.

The output charge is proportional to the product of light intensity and the line scan time only up to a certain fixed level (the saturation exposure). The mode of operation used in this application is to saturate all the diodes of each array with an approximately uniform light source. The required

intensity of illumination thus increases as the integration time is reduced (scanning frequenty increased). Using data supplied by the manufacturers the saturation intensity for a given frequency can be calculated (see Appendix A).

Reticon supplied circuitry provides an integrated sample and hold type video signal from each array together with information as to:

1) the offset of a shadow edge from the datum of the first diode,

2) the state of illumination up to the edge (light or dark),

3) the width of the shadow (if a second edge is present).

In addition control logic can indicate:

4) the occurrence of a second edge,

5) the occurrence of an anomalous third edge, and

6) system errors that may invalidate values returned.

The purpose of the Photodiode Array Control System (PACS) interface electronics (Fig.4.9) is to transfer this data on demand to the controlling computer. PACS has been designed as a co-existent module with the current analogue sensing electronics. A microprocessor (Z80A CPU) is used to co-ordinate 16-bit counters, each of which stores the pixel count of one event (transition). Several additional operations are easily implemented. These include software control of photodiode clocking rates, video-binary threshold control, direct measurement of low frequency content (possibly for use in auto-setting thresholds and sensor problem detection), data buffering and basic data pre-processing. The microprocessor also undertakes a series of diagnostics on power-up.

Up to six diode arrays can be accommodated, although only five are used at present. One is designated the master drive board and provides a clock-derived synchronising signal to enable predictable scan status for all the arrays. Communication of data is achieved through a set of commands from the control computer which requests appropriate microprocessor activity.

In normal use, programs using PACS begin operation by initiating a reset command which scans from the lowest to the highest voltages on the video output signals of the sensors, and auto-sets the transition levels as half way in-between. The system clock begins counting at an overall loop rate of 242Hz. This is an arbitrary number which is not directly related to any exact control requirements, but instead arises as a consequence of the detail electronic design. Other loop rate frequencies may be used by sending specific commands to PACS from the main computer.

4.8 Diffraction of Edge Event

Prior to installation of the full five channel position sensing system, one prototype channel was installed (to sense axial motion) in the existing Southampton MSBS. Details of this exploratory work may be found in Reference 39. In investigating the characteristics of the beam and sensor, various real optical considerations were revealed which limit the achievable resolution of the complete optical system, although do not invalidate its general principles. The most significant of these relates to the characteristics of the shadow edge produced by a model placed in a sensing system light beam.

Ideally a transition event would produce a step change in sensor output, taking only two pixels to occur. In reality at any finite distance from the face of the sensor, an object will produce a transition edge ('modulation transfer function' - MTF) spread over several pixels, which may vary as the object is moved across the sensor. In particular, this type of sensor is quoted in manufacturer's data as having a non-uniformity of sensitivity between diodes of up to ±14%. Thus if the MTF is broadened by some other effect, and the threshold level is fixed, the apparent width of an object will vary for different locations, and the calibration of distance to the first event or the width of an object (if two edges are visible) will not be perfectly linear. The MTF is in fact broadened by diffraction effects.

For the situation of relevance here - that is, an edge in a beam of collimated light - near field or Fresnel diffraction theory is used. This is described in Appendix B, but the main results may be summarised as follows.

Moving from the full illumination into the shadow of the object, the irradiance distribution consists of a series of oscillations about the mean full value, which increase in amplitude before dropping monotonically to zero. The width of the MTF, measured in terms of the number of pixels, increases from zero when the object is directly in front of the sensor to tens of pixels at model/sensor separations representative of the full system. The true geometrical location of the object's edge corresponds to the pixel where the illumination is one quarter of the full value. Thus if the position sensing system is to be used as an absolute measuring device, the threshold should be set at the corresponding output voltage level.

However, the illumination of the sensor is such that it is completely saturated, and the diffraction fringes and the full illumination level are not directly seen, but are 'lost' in the even saturation output level. The one-quarter level cannot be deduced by examining the output profile unless some curve fitting procedure is used. This has not been pursued because a simpler solution is to measure the target object mechanically, and record the discrepancy with the measurement from the optical sensing system. It may be noted that this difference will only remain fixed if the model/sensor separation is constant, but it has been found that with care the threshold level may be set to give consistent measurements close to the true object size. Also, if the threshold level does not correspond to the one quarter illumination level, when the system is set up to give a constant object width measurement, the light rays are not parallel: hence the term 'collimated' light beam is always used. These effects can be mitigated by careful setting of the threshold levels for each channel of the sensing system.

Refinements such as this, made as a result of practical experience are discussed in Sections 7 and 8, along with certain hardware changes. Performance measurements of the sensing system are also given along with a description of remaining limitations. The relevance of this sensing system to the requirements of a large MSBS is considered in Section 11.4.

CHAPTER 5

CONTROL PROGRAM 1: POSITION SENSING ALGORITHMS

5.1 Introduction

In this chapter and the succeeding one, the real time computer program which has been developed to operate the high angle of attack MSBS is explained in relation to the previous control techniques used with SUMSBS. The basic loop structure of the digital controller has been carried over from the earlier work, as have many of the sub-routines which perform tasks which remain unchanged or required only slight amendment. The latter are outlined in Chapter 7. This chapter describes algorithms introduced as a result of the digital optical sensing system, whilst Chapter 6 discusses means of converting position and attitude signals into electromagnet current demands. For completeness, these sections include various refinements in the control system which were only added in the light of experience from the initial testing of the extreme attitude MSBS (which is discussed in 7.5).

Figure 5.1 shows a block diagram of the control system used for extreme attitude suspension.

5.2 Selection of Control System Axes

The original digital control system used with SUMSBS was designed to operate with a model suspended at an attitude close to the wind tunnel axis. With an axisymmetric model unconstrained in roll, the position sensing system generated five independent signals which were then fed into the control system. Demand signals were created from these, which, after being output to the electromagnet power supplies, resulted in five distinct force and moment components being exerted on the model. Four of the feedback signals were obtained by combining the output voltages of the four main sensing elements according to the following table:

Degree of Freedom	Forward Port	Forward Starboard	Aft Port	Aft Starboard
vertical heave	+	+	+	+
pitch	+	+	-	-
lateral heave	+	-	+	-
yaw	+	-	-	+

The information on the axial position of the model was taken directly from the output of the fifth position sensor. It is important to note that the use of the terms vertical heave, pitch etc. implies an axis system which is coincident with conventional wind tunnel axes (Fig.5.2). This system was used throughout the control program, so that by means of simple combinations of electromagnets relatively pure force and moment components were produced in the sensing system axes. Provided that the model's attitude was not strongly displaced from the wind tunnel axis, couplings of one component of motion to another as seen by the sensing system were second order and could be accommodated by the control system. For example, a pure pitch rotation about the model's magnetic centre would produce only a very small change in the model's apparent length, as seen by the axial sensor. Thus the error signal resulting from the discrepancy between the required and apparent axial position would be negligible.

However, the high angle of attack position sensing system has a datum which is inclined to the wind tunnel axes by 45^{o}, and with the large pitch excursions which may occur, it would be expected that the axial position signal would no longer be independent. Instead, combining it with the other feedback signals according to some geometrical law is necessary. From the MSBS user's point of view, it would be preferable to translate the model in wind tunnel axes (i.e. vertical heave is always normal to the air flow). Alternatively, since the inertial characteristics of each model sense degree of freedom are unique, it might be logical to maintain the distinction by controlling the model in a model based axis system. The third, and computationally simplest, approach is to preserve the sensing system data in its simplest form; that is, in the axis system in which it is created. No conversion to another axis system is then needed. Thus, from the point of

view of the controller, vertical heave is actually in a direction normal to a plane inclined at 45^{o} to the horizontal, whilst axial motion is normal to a plane but at -45^{o} to the horizontal.

In practice, because of the assumption that yaw and sideslip motions are only small perturbations from the datum position and attitude, the choice of control system axes only affects the degrees of freedom in the vertical plane. Further, it is clearly sensible for a pitch rotation to be about the model's y axis rather than some sensing system or wind tunnel datum, since the latter would also involve a translation of the model's centre of gravity at any position displaced from the datum. Thus the choice of axis system in the case of the extreme attitude controller reduces to selecting the senses of the two degrees of freedom in the vertical plane - loosely described as the heave and axial motions. Figures 5.3a to 5.3c illustrate the three possible definitions of the heave and axial senses.

If the sensing system is capable of generating unique information relating to the centreline of the model (as seen by the four main sensors) and the tail of the model (as seen by the axial sensor) then the following notation may be used to describe the position and attitude signals:

P_n = position/attitude in degree of freedom n

where;

$n = 1$ vertical heave position

2 pitch attitude

3 lateral slip position

4 yaw attitude

5 axial position

Note that this numbering sequence, which is also used in Section 6, differs from the sequence used in 2.3 and 10.7. It is derived from the order of signal processing in the original MSBS digital control program.

S_k = signal from position sensor k

where;

k = 1 forward starboard

2 forward port

3 aft starboard

4 aft port

5 axial

For all the axis systems:

$$P_2 = (S_1 + S_2) - (S_3 + S_4)$$

$$P_3 = (S_1 + S_3) - (S_2 + S_4)$$

$$P_4 = (S_1 + S_4) - (S_2 + S_3)$$

These expressions are the same as those implied by the table above.

Using the 'sensing system' axes, the other two degrees of freedom are given by:

$$P_1 = S_1 + S_2 + S_3 + S_4 - C_1(P_5 \cdot \tan\theta) \quad (1)$$

$$P_5 = S_5 \quad (2)$$

where;

θ is the model pitch attitude relative to the datum angle of attack (45^{O})

and C_1 is a constant relating to the relative sensitivity of the two channels, and fixed by the sensing system geometry. (See Appendix C).

If 'model axes' are employed, then the following equations hold:

$$P_1 = (S_1 + S_2 + S_3 + S_4) . C_2 \cos\theta \tag{3}$$

$$P_5 = S_5 \sec\theta - (P_1 C_2 \sin\theta) \tag{4}$$

where;

C_2 is a different geometry related constant. (See Appendix C).

The position data may be converted from the sensing system into the wind tunnel axes according to the fixed transformations as follows:

$$P_1 = (P_1 \cos 45 - P_5 \sin 45)_{\text{sensing system axes}}$$

$$P_5 = (P_5 \cos 45 + P_1 \sin 45)_{\text{sensing system axes}}$$

For the initial work with the high angle of attack MSBS it was decided to use the sensing system axes in the controller, since it is the simplest choice. One consideration in this decision was the amount of information required to be stored in the look up tables used to generate the control data for each angle of attack controlled. This is explained in 5.4 below. Subsequently, the control program was modified to operate in model axes, permitting a comparison to be made with the sensing system axes controller. Use of wind tunnel axes may also be practicable, but this has not been attempted. See Section 9 for further discussion.

Chapter 6 explains how the force components in the sensing system or model senses are generated from the ten electromagnets of SUMSBS.

As a consequence of the precise alignment of the sensing system elements, it is possible to impose an interpreter between the user inputs and the control loops so that a demand for a change in position in the wind tunnel axes may be split into components in the control system axes, be these sensing system or model based. Although this has not yet been done, it remains a possibility for the future and is another advantage of the predictable linear calibration of the SSPD sensors.

5.3 Generation of Attitude Offsets and Interpretation of Attitude Feedback Signals

Since the analogue photodiodes of the old sensing system produced single voltages as their outputs, the decoded position signals were unique descriptions of the model's position in space. In contrast the digital sensors can produce information relating to more than one model edge. The axial position sensor only ever sees one edge - the tail of the model - but the four remaining sensors may see edges corresponding to either side of the model, or both sides simultaneously. Therefore algorithms which can discriminate between the edges are required. On the system block diagram (Fig.5.1) these algorithms are collectively referred to as the edge interpreter. To explain its function a description of the data generated by PACS is required.

Information from PACS is requested by the PDP 11/84 by outputing a code via the host computer's output port corresponding to the particular sensor channel involved. After a delay of about 10 microseconds the data is made available at the computer's input port and may be loaded and used. In normal use two data types are needed. Firstly, there are the actual position sensor digital signals. PACS has two counters for each array. If two model edges are visible to a sensor, then the first counter contains the number of pixels to the first transition event ('offset') whilst the second contains the width of the object ('span'). If only one edge is present then the second counter simply contains the balance of pixels making up the total array length. Resetting operations at the end of a scan takes up a time period equivalent to nine pixels, so that when the arrays are fully illuminated or fully darkened a reading of 1033 rather than 1024 is found in the offset counter.

A different command to PACS produces a data word in return which contains information as to the nature of the transitions seen by the arrays. The setting of the various bits in the word indicates whether one or two edges are visible to each array, and also the nature of the transition (light-dark or dark-light).

Given this information, the host computer must generate five unique position and attitude signals for the feedback control system. In principle, they are obtained by summing and differencing of the individual sensor outputs in a way analogous to the previous controller, but with the added feature of relating the raw data to the approximate longitudinal centreline of the model.

Firstly, because the model centreline can be well beyond the physical edge of the array field of view, it is supposed that the pixels continue an arbitrary distance beyond each end of the array. If these imaginary pixels start at zero, whilst the first real one is at 513, then the real pixels continue to 1536, and the last imaginary pixel is number 2048 (see Fig.5.4). It is assumed that the model is of circular cross section and known diameter. The previously mentioned geometrical program PIXEL can then be used to generate the output data seen by the sensors for any position and attitude, given the light beam configuration. In particular, the program takes account of the apparent broadening of the model's diameter as it moves away from the datum attitude. This results from the model section cut by the light beams changing from a circle at the datum attitude to an ellipse at any other angle. Although the minor axis of the ellipse is the model's true diameter (assuming correct collimation), this is the length of the shadow cast upon the sensors only when the model is at zero degrees yaw angle and 45 degrees pitch angle.

Figure 4.6 shows the relationship between the pitch attitude measure, as defined in 5.2 above, and the angle of attack. It may be noted that the gradient varies from 38 per degree at 45 degrees angle of attack to 110 per degree as -10^{o} and 100^{o} a.o.a. are approached. Thus any assumption of a linear relationship, as has been possible previously, is clearly not tenable. Figure 5.5 shows the broadening effect of the model's apparent diameter with

angle of attack, taking into account the cross shape of the main beams of the sensing system and a cylindrical model of typical diameter.

It was decided that the absence of trigonometric functions in the assembly level language used for the MSBS control program made the real time calculation of the geometric data impractical. Thus PIXEL can output its results to a data file which is then opened and accessed by the control program MSHI. When the user inputs a demand for change in attitude, a vector is generated corresponding to the pitch and yaw combination. This causes the location of the model's centreline as seen by each of the four main sensors to be loaded. The apparent radius of the model at this attitude is also accessed. If the model is yawed, then two of the main sensors (front port and aft starboard) will see one value of the apparent radius whilst the other pair (front starboard and aft port) will see a different apparent radius. The pre-stored data loads both values and assigns them to the appropriate edge calculation. An algorithm then determines which of the two possible model edges found by adding and subtracting the radius would actually be visible to the sensor; that is, whether the pixel count is real or imaginary.

If only one edge is real, then this becomes the target pixel count used in the subsequent processing. If two edges are real, then the first one (that corresponding to a light to dark transition) is used. Thus four real edges are selected to base the attitude offsets upon. The true model radius is then subtracted or added as appropriate to the edge location to produce approximations to the model centreline. These are then summed and differenced according to the same laws used in generating the feedback signals (Table 1). Attitude offsets are thus created which are combined with the feedback pitch and yaw signals in the user demand offset block of Figure 5.1.

Data incoming from the sensing system via PACS is processed in the following way.

Because of the logic explained above, only the first counter of each array needs to be accessed for use in creating the feedback signals. However, an algorithm is used to determine whether the edge visible to each of the sensors corresponds to that used in generating the attitude offsets. If

it is, then the model physical radius is added or subtracted as appropriate to yield an approximate model centreline. Once this is repeated for all four sensors, the position and attitude measures are found according to the appropriate algorithms for the control axes being used, and described above. Thus, when the model's attitude has changed such that the approximation of the centreline found from the position sensor signals is the same as the approximate centreline used in generating the demand offsets, the true model centreline will be exactly in the correct location for the demanded attitude.

Figure 5.6 summarises the logic used in the edge interpreter.

If any of the position sensors do not yet see the correct model edge, then the alternate edge is used in producing the feedback signals. This introduces a discrepancy in the calibrated attitude implied by the user demand and that resulting from using the edges available. In general, however, as the model continues to move in response to the residual attitude error, the correct model edges become visible to the arrays and the correct location is achieved. Exceptions to this can occur where the target attitude results in an edge location close to the beginning of the sensor, producing a discontinuous change in apparent model attitude. See Section 8.7.

5.4 Heave/Axial Channel Coupling

The linear calibration of the position sensors means that, taking into account the geometry of the light beams, lateral and vertical heave together with axial motion is readily determined in an absolute manner. Thus the user may input demands for changes in these position measures in units of thousandths of an inch, provided the light beams are correctly collimated.

For the control system to work correctly, motions in the senses defined by the selected axis system must be countered by the corresponding force and moment component. For the case of forces in the vertical plane, it thus becomes necessary to link the error signals produced by the 'axial' position sensor channel. This is because at any pitch angle not equal to the datum (45^{o}) an axial position error will also generate a heave position error

signal, even though no such error exists. Figure 5.7 illustrates the situation when the controller uses sensing system axes.

This coupling heave error signal must be removed from the control channel. Fortunately, the known alignment of the sensing system components makes this possible. The magnitude of the axial to heave coupling component is implied by equation (1) above and is given by

$$AX - HE = C_1 \tan\theta . e_5$$

where e_5 is the axial position error, and C_1 is the function of the beam geometry introduced earlier. Its derivation is given in Appendix C. The tanget of the present pitch angle relative to the datum is stored in the program PIXEL and accessed along with the other sensor related data. The resulting axial-heave coupling signal is subtracted from the heave channel in the control loop. It should be noted that when pitch changes are being made, the tanget of the target angle of attack is used in the coupling equation, and so for large angle of attack changes the dynamic characteristics of the heave channel are affected by the initially erroneous coupling component. However, as the final angle of attack is approached the error in the tangent diminishes to zero.

If model axes are used in the controller, then a heave to axial coupling quantity must be taken into account. From (4) above, it is given by:

$$HE - AX = C_2 \sin\theta . e_1$$

where C_2 is a second geometry constant as above. Thus the sine of each available angle of attack is stored by a modified version of PIXEL and subsequently used in the control program. Note, however that in order to generate the heave position error in the model sense from the raw sensing system data, equation (3) above requires that the cosine of the present angle of attack is required, whilst equation (4) also involves the inverse quantity, sec θ. Hence this data is also calculated, stored and accessed, increasing the

total number of data items per angle of attack. However, this did not prove a problem, the PDP 11/84 having adequate storage capacity to accommodate all the information. Thus through comparatively simple changes to the program logic, it has proved possible to generate position sensing data in two different axis systems. However, it must be emphasised that the conversions are only valid if the physical elements of the sensing system are correctly arranged in the assumed configuration.

5.5 Pitch/Axial Channel Coupling

Pitching and yawing in the high angle of attack sensing system is intended to be sensed and controlled relative to the model's magnetic centre, which is usually close to its centre of gravity. This implies that the axial sensing channel sees the corresponding foreshortening of the model as it moves away from the datum, and responds by adjusting the demanded location of its tail. However, for small yaw attitude changes, and taking into account a model of typical diameter, the necessary coupling corrections are small. Thus they have not been included in the control system at present. This approach has been taken for the pitch and yaw channels in all previous MSBS control systems. However, in the case of the pitch channel of the high alpha sensing system, the tail of the model should move from the rear of the axial sensor field of view at 45° to almost the opposite end at 0° and 90° if pure rotations are to be produced. This must be accounted for in the control system (Figure 5.8).

The behaviour of the axial position is governed by the following equation;

$$l_p = [\tfrac{1}{2}l(1 - \cos\theta) - \tfrac{1}{2}(d \sin\theta)]/\cos 45 \qquad (5)$$

where l_p is the projected distance from the model's centre of rotation to the tail seen by the sensor, l and d its length and diameter respectively and θ the angle of attack relative to the datum (45°). The $\cos 45$ term arises from the inclined arrangement of the position sensor relative to the beam, as used in

the initial arrangement. As a result of the hardware changes permitting the axial sensing beam to strike the sensor normally, discussed in Chapter 7, this term becomes unity.

Figure 5.9 shows this function plotted for a typical model. As the angle of attack moves away from 45^{o}, in a positive or negative sense, there is an initial apparent lengthening of the model, followed by a rapidly increasing shortening. It was decided to ignore this effect for initial testing of the high angle of attack controller, and to cause the system to force the tail of model to lie at a fixed number of pixels along the field of view of the axial sensor. Thus, as the angle of attack was increased or decreased from the datum of the system (45 degrees), the model would be pulled backwards along its own length, producing an impure pitch rotation not about a spatially fixed axis. However, the dynamic behaviour of the model at the extremes of attitude proved unacceptable, and so it was both necessary and desirable to add proper decoupling of the axial and pitch channels. This involved two levels of refinement.

The first stage involved incorporating the data of Figure 5.9 into the pre-stored information of the control program. Thus when a new angle of attack is demanded, an offset to the demanded axial position in pixels is loaded and subtracted from the feedback data produced by the axial sensor. An effective axial position error then appears of the correct magnitude to oppose the signal resulting from the pitch attitude change. The integrator stage of the control loop ensures that the model is driven to the correct axial position such that the error falls to zero. Thus, if a series of attitude changes are demanded, each of small magnitude (e.g. one degree), the axial output should follow the curve of 5.9, implying that a pure pitch rotation about a fixed axis is occurring.

Much of the initial testing with the high angle of attack controller was carried out with this 'passive' pitch-axial decoupling. However, it was recognised that the approach was not completely adequate because it only operated in response to a demanded step change in angle of attack. Changes in pitch atittude may occur in other circumstances. Firstly, forced oscillations can be demanded by the MSBS user, in order to carry dynamic wind tunnel testing, and also in the dynamic calibration technique mentioned

in 2.1. Further, transient aerodynamic effects may cause sudden alteration in pitch attitude. In all these situations, where the nominal model attitude is away from the system datum, an apparent axial position error signal appears as a consequence of a pure pitch rotation. However, with the passive decoupler described above, the axial channel is programmed only to fix the tail of the model so that its position produces the sensor output corresponding to the nominal angle of attack. It therefore responds by producing an axial force change to maintain the axial position, even though the position has not actually changed. The consequence is that when a pure pitch oscillation is demanded, a combined rotation and translation occurs. Similarly, the response to a pitch attitude error involves an unnecessary axial force being applied, and in general, the dynamic behaviour of the suspended model could be expected to be affected by the cross coupling, especially at the extremes of the suspension range.

Thus it was decided to incorporate an 'active' pitch-axial decoupler as the second step in improving this aspect of the controller. This involves removing the apparent axial change resulting from the difference between the instantaneous pitch attitude and that requested by the user. This quantity can be written:

$$PI - AX = \frac{dP_5}{dP_2} e_2$$

where

$$\frac{dP_5}{dP_2}$$

is the rate of change of axial position measure with change in pitch attitude measure.

Now:

$$\frac{dP_5}{dP_2} = \frac{dP_5}{d\theta} / \frac{dP_2}{d\theta}$$

where

$$\frac{dP_5}{d\theta} = \tfrac{1}{2}l \,.\, \sin\theta - d/2 \,.\, \cos\theta \qquad (6)$$

for the modified axial sensor.

To incorporate the pitch-axial decoupling information into the controller so that it operates continuously on the present feedback information, a real-time calculation of the appropriate value of dP_5/dP_2 is necessary. This has been achieved by making use of the piece-wise linear fit technique already used for the demand translator stage of the controller, and explained later in 6.3. This involves the storage of calculated data for discrete attitude increments (every ten degrees), with the required information for intermediate angles being obtained by a linear interpolation.

Values of $dP_2/d\theta$ were obtained from Figure 5.4 for the ten degree increments, and for $dP_5/d\theta$ from equation 6 above. The resulting quotients representing dP_5/dP_2 were stored in a data file and made accessible to the control program. In each program loop, the controller uses the present pitch attitude measure, together with the stored values of dP_5/dP_2 to calculate the corresponding value at the model's angle of attack n:

$$\left.\frac{dP_5}{dP_2}\right|_{\theta=n} = \left.\frac{dP_5}{dP_2}\right|_{\theta=r} + \left\{\left(\frac{P_{2n} - P_{2r}}{P_{2s} - P_{2r}}\right) \cdot \left(\left.\frac{dP_5}{dP_2}\right|_{\theta=s} - \left.\frac{dP_s}{dP_2}\right|_{\theta=r}\right)\right\}$$

where;

$\theta = r$ is the nearest negative pitch measure threshold relative to $\theta = n$

$\theta = s$ is the nearest positive pitch measure threshold relative to $\theta = n$

The pitch-axial coupling quantity is subtracted from the axial feedback channel.

5.6 Summary

This chapter has explained how the data from the five photodiode array position sensors may be combined in various ways to represent independent measures of position and attitude and also how user offsets in the angular senses are generated from pre-stored data. This information may be summarised as follows.

For each pitch and yaw attitude combination, stored data exists for:

2 model centreline locations
2 model apparent radii
1 axial position offset.

In addition, depending on the axis system used, either the tangent or the cosine and sine of the angle of attack is also stored.

As initially configured, the data is stored for 110 angle of attack increments (-10^{o} to 100^{o}) and three yaw attitudes (usually -5^{o}, 0^{o} and $+5^{o}$). Thus, with the sensing system based controller 1998 data items are stored, whilst with the model axes controller 2331 items are needed. In addition, the active pitch-axial decoupler involves 12 values of dP_5/dP_2 corresponding to ten degree increments of angle of attack.

CHAPTER 6

CONTROL PROGRAM 2: FORCE/MOMENT DISTRIBUTION ALGORITHMS

6.1 Introduction

Section 3 showed that with the modified arrangement of ten electromagnets, the Southampton MSBS is capable of producing all the fields and field gradients necessary for controlled suspension over a nought to ninety degree positive incidence range. However to make use of such capabilities, the digital control program operating the MSBS must take account of the changing interaction between the electromagnets and the model as the latter is moved through the incidence range. These effects are of far greater magnitude than with a more conventional MSBS, where the force and moment capabilities have generally been assumed as constant for the limited attitude and position changes accommodated. Such assumptions are no longer valid in the case of extreme attitude suspension. In this section the ideas developed to meet these needs are explained, including the practical implementation.

6.2 Requirements of Force/Moment Translator

When correctly designed, the MSBS position sensing system should produce signals relating to the model's position and attitude. The control system should then manipulate the feedback signals, together with user offsets created by the algorithms explained in 5.5, to generate demands for currents in some or all of the ten MSBS electromagnets. These should combine to produce force and moment components acting on the model in senses which reduce the detected position/attitude errors.

In designing a conventional MSBS, in which the model's attitude remains close to the wind axis, the approach which has generally been adopted is use an electromagnet or group of electromagnets to generate one, two or perhaps three force/moment components. Thus, in the case of the previous Southampton MSBS controller, the four vertical electromagnets were used to generate a force in the z direction to balance the difference

between gravity and aerodynamic lift. The compensated (phase advanced) error signal in the heave sense, multiplied by a suitable gain, was simply output to each of the four E/Ms. Only sign differences to take account of the opposite polarities of the magnetised model differentiated the four output signals. With the model aligned with the wind axis, and ignoring imperfections in construction of the system and other second order effects, no other force or moment component was produced.

With a different set of polarities, the same four electromagnets could be used to generate a pure pitching moment about the magnetic centre of the model. To produce an axial force (F_x) to oppose aerodynamic drag, the two solenoidal magnets at either end of the system were employed. A sideforce and a yawing moment were obtained from the four lateral electromagnets in a way analogous to the use of the vertical E/Ms to give vertical force and pitching moment. Although the curves of predicted performance of Ref 28 show that other force and moment components could be generated by the electromagnets, these were small and of little benefit. Thus the design of the translator stage reduced to one of selecting the correct overall loop gains. These were in practice obtained through experimentation, and in any event had to be adjusted for models of significantly different inertial and magnetic characteristics.

However, at any general angle of attack between zero and ninety degrees the choice of how to combine the ten electromagnets to produce the five force and moment components is not self evident. The translator must be designed so as to generate relatively pure force and moment components at any given attitude, whilst taking account of the differing capabilities of each of the E/Ms, and also ensuring that the dynamic characteristics of the suspended model are consistent. To achieve these goals, the translator stage of the MSBS control program has been made considerably more complex than has been necessary hitherto.

6.3 Concept of Demand Distribution

The problem of designing the translator for the high alpha control system has led to the idea of demand distribution, in which the electromagnets are regarded as producing differing force and moment

components which are to be combined in varying proportions to generate discrete vectors in the directions corresponding to the data produced by the sensing system. The control system block which performs this demand distribution is now referred to as the demand multiplexer (Fig.5.1).

By extending the theory introduced in 2.3, and using the numbering sequence of 5.2 the generation of forces and moments may be represented in matrix form thus:

$$\begin{pmatrix} F_1 \\ F_2 \\ F_3 \\ F_4 \\ F_5 \end{pmatrix} = (G_1\ G_2\ G_3\ G_4\ G_5) \cdot \begin{pmatrix} K_{11} & K_{12} & K_{13} & K_{14} & K_{15} \\ K_{21} & K_{22} & K_{23} & K_{24} & K_{25} \\ K_{31} & K_{32} & K_{33} & K_{34} & K_{35} \\ K_{41} & K_{42} & K_{43} & K_{44} & K_{45} \\ K_{51} & K_{52} & K_{53} & K_{54} & K_{55} \end{pmatrix} \begin{pmatrix} e_1 \\ e_2 \\ e_3 \\ e_4 \\ e_5 \end{pmatrix}$$

where the phase advanced error signals in each channel are represented by e_1, e_2 etc, and G_1, G_2 etc are the corresponding overall loop gains. F_n here represents either force or torque. The product of the gains and the square matrix represents the force/moment per unit error signal. Together they imply a choice of routings of the error signals to particular electromagnets, and the force or moment produced by the resulting electromagnet current. However, if we require that each of the channels are independent, then the square matrix may be written:

$$\begin{pmatrix} K_{11} & 0 & 0 & 0 & 0 \\ 0 & K_{22} & 0 & 0 & 0 \\ 0 & 0 & K_{33} & 0 & 0 \\ 0 & 0 & 0 & K_{44} & 0 \\ 0 & 0 & 0 & 0 & K_{55} \end{pmatrix} \quad \text{and let } K_{11} \text{ be simply } K_1$$

$$K_{22} \quad K_2$$

$$K_{33} \quad K_3$$

$$K_{44} \quad K_4$$

$$K_{55} \quad K_5$$

We refer to the remaining non zero quantities as the distributed force/moment products. Their values are dependent on:

1) the choice of demand to electromagnet routing (demand distribution),

2) the force/moment per unit error of each E/M (the gain),

3) the maximum allowable current of each E/M.

In principle no a priori assumptions are made as to which E/Ms are used to produce which components. However, the symmetries of the electromagnet array may be used to simplify the problem considerably. Firstly, since the large attitude excursions are confined to the vertical plane, yaw motions are regarded as small perturbations from the datum (unyawed) attitude. No attempt to adjust the demand multiplexer in response to such motions has been made.

Thus at all attitudes a yaw torque is exerted upon the model by the four lateral electromagnets, and the same electromagnets may also be used to produce sideforce at any angle of attack. The following combinations of current polarities perform these functions:

Component	E/M 2	E/M 4	E/M 6	E/M 8
yaw	+	-	+	-
sideforce	+	-	-	+

Other electromagnets do not produce force or moment components in these senses at the datum yaw angle, so the demand distribution is fixed for all angles of attack. However, the magnitudes of the sideforce and yawing torque produced by the lateral electromagnets vary strongly with angle of attack, and so it is to be expected that the overall loop gains (which may be interpreted as representing electromagnet current per unit error signal) will have to be similarly adjusted.

6.4 Demand Distribution of Pitching Torque: A Comparison of Possible Approaches

In the case of pitch torque, the situation is more complicated. Over the full range of attitudes, a pure pitch torque is generated by the vertical electromagnets 3 and 5, operating with opposite polarities. At incidences close to zero degrees angle of attack, vertical E/Ms 1 and 7 produce a pure pitch torque when combined in the correct polarities. The four vertical electromagnets then have the following combination of signs:

Pitch Torque : less than 30^{o} incidence

E/M 1	E/M 3	E/M 5	E/M 7
+	-	+	-

This is in fact the means by which pitch torque was generated for the Southampton MSBS in its previous form.

At incidences around 90^{o}, the following combination of polarities are used:

Pitch Torque : greater than 60^{o} incidence

E/M 1	E/M 3	E/M 5	E/M 7
+	+	-	-

Thus if we consider the electromagnets to be in one of two groups - 1/7 and 3/5 - one group is always used with the same sign to generate positive torque, whilst the other requires a sign change. At some intermediate angle of attack between the extremes any attempt to use E/Ms 3 and 5 to generate a pitching torque would be futile, since their capability in this sense is exactly zero. The proportion of the demand to be distributed to each of the E/M pairs is determined in the control program by quantities known as 'demand distribution factors' (DDFs). Taking first the simple case at zero

degrees angle of attack, where each of the pairs of E/Ms have equal capability, we assign the following values:

DDF 1	DDF 3	DDF 5	DDF 7
+1	-1	+1	-1

where DDF 1, DDF 3 etc are the demand distribution factors in the pitch channel for E/Ms 1, 3 and so forth. Thus when the pitch attitude error signal is multiplied by each demand distribution factor and the overall loop gain G_2, a positive moment will be generated when the resulting signal is output to the corresponding E/M power supply.

At 90^{o} angle of attack the demand distribution factors have the following values:

DDF 1	DDF 3	DDF 5	DDF 7
+1	+1	-1	-1

Thus, with a still positive value of the overall gain, the signs of the electromagnet currents are adjusted such that all four still produce positive pitching moment contributions.

The question then arises as to how the error signal is distributed at any intermediate angle where the two groups of electromagnets have an unequal capability to generate a pitching torque: that is, how are values assigned to the demand distribution factors? Several approaches are possible, of which three will be considered here. These are:

1) to let the demand distribution factors always be of unity magnitude;

2) to let the demand distribution factors be proportional to the relative magnitude of the torque generated by the two E/M groups;

3) to let the demand distribution factors for the E/M group producing the most torque be unity magnitude, and for the other factors to be zero.

The first of these possibilities results in all the possible pitching torque capability being made available to the control system, and so is referred to as the maximum torque case. The third causes only the most effective torque component to be used, which means that for a given torque requirement within the system's capability, the least total current is demanded from the power supplies. Hence this is the minimum current case. The second possibility above is an intermediate choice which may represent a good compromise.

Two measures can be used to compare these design approaches. Firstly, the maximum possible torque which could be generated in each case may be calculated. Since this moment component is being considered in isolation from the other degrees of freedom, the torque calculated assumes that the electromagnets involved are not being used to produce another force/moment component. In reality, the vertical electromagnets are important force generators, and experience has shown that MSBSs tend to be force limited rather than torque limited. Nevertheless, the theoretical torque capability is a useful figure of merit.

For 1), the maximum torque is simply the sum of the components from the two E/M groups.

For 2), the maximum torque is produced when the more heavily used E/M group reaches its system limited cable current. If this is E/M set p, producing a torque T_p, with a demand distribution factor $DDFp$, whilst the second set r can produce T_r, and has a factor $DDFr$, then the resultant torque is given by:

$$T_{TOTAL} = T_p + (DDFr / DDFp) \cdot T_r$$

For 3), the maximum available torque is simply the torque generated by the one component used. It is supposed that although at 0^o and 90^o the two E/M groups have equal capabilities, only one of the groups is actually used to produce a pitching torque.

The second performance measure is the current required in the four electromagnets per unit torque generated (which is K_2 above). In the case of

SUMSBS, all the E/Ms have a maximum cable current of 20 Amperes. Considering the three demand distribution techniques in turn, K_2 may be calculated as follows.

For 1) $K_2 = 80/(T_p + T_r)$

For 2) $K_2 = 80/((DDF_p.T_p) + (DDF_r.T_r))$

For 3) $K_2 = 40/T_p$

Using the predicted capabilities of SUMSBS as calculated by FORCE and shown in Section 3.4, Figure 6.1 shows the values of the demand distribution factors, whilst Figures 6.2a and 6.2b show the maximum torque capability and current per unit torque estimates obtained for the three distribution techniques. Since the pitch torque produced by the demand distribution at angles of attack in between the design points is unknown without calculating the available pitch torque, a linear fit to the points has been shown.

Several conclusions emerge. Looking at the maximum torque distribution, the demand factor for the electromagnet group 3/5 is caused to abruptly change sign at about 53°. However, because of the error inherent in FORCE, the true angle of attack at which this group produces zero torque may be somewhat different. This would result in the sign of the resultant torque over some angle of attack range being opposite to that intended. Thus, the predicted full value of the maximum torque is unlikely to be available. In contrast, in the case of the proportional distribution, the distribution factor for this group is close to zero, so that a demand to it, although possibly of the wrong sign, will be of small magnitude; thus the predictions are more reliable. Such a problem does not arise in the case of the minimum current distribution, since only electromagnets 1 and 7 are being used to produce a pitching torque.

The maximum torque distribution has a high current per unit torque characteristic near to the E/M 3/5 sign reversal angle of attack, because a large amount of current is required to produce a small torque contribution from these electromagnets. At 53°, the 20 Amps in each of the two E/Ms produce no torque at all. In contrast, the proportional distribution has the

demand factors for these E/Ms smoothly passing through zero, greatly improving the predicted current per unit torque without seriously reducing the moment available at nearby angles of attack.

The minimum current distribution is not greatly superior in terms of current per unit torque performance, but at most angles of attack makes far less of the possible torque available than the other distributions. Also, on an intuitive basis, it seems appropriate that the demand distribution for a particular degree of freedom should be as evenly spread amongst the available E/Ms as is possible, to minimise the possibility of any one group being excessively used when all the degrees of freedom are taken together. For these reasons the minimum current approach is not adopted for the SUMSBS controller.

There is little to choose between the maximum torque and proportional distributions, so the technique which has been used is to have the demand factors for both groups as unity magnitude apart from in the 40 to 60 degree region where the proportional distribution is used. The algorithms used to perform this function are explained in 6.8.

6.5 Generation of Decoupled Forces in the Vertical Plane

To generate the forces in the vertical plane - that is in the vertical heave and axial directions - all ten E/Ms are needed at some incidences, and no simple combination of electromagnets producing pure force components exist. Hence an analytic technique is required to choose the best comhination of the ten E/Ms to produce each of the two forces.

It proves convenient to divide the ten electromagnets into four groups; within each group the currents differ only in sign (polarities). The groups are:

Group	Electromagnets
1	1, 7
2	3, 5
3	2, 4, 6, 8
4	9, 10

Each of these produces at any incidence an axial and heave force component in whatever axes system is employed. It is required that in response to an axial or x-wise position error signal, the multiplexer generates a pure axial restoring force, and similarly a heave or z-wise position error is countered by a pure heave force. It should be noted that in the theory which follows, no assumptions are made that imply which of the axis systems discussed in 5.2 is actually being used.

In matrix form;

$$\begin{pmatrix} F_1 \\ F_5 \end{pmatrix} = (G_1 \quad G_5) \cdot \begin{pmatrix} K_1 & 0 \\ 0 & K_5 \end{pmatrix} \cdot \begin{pmatrix} e_1 \\ e_5 \end{pmatrix}$$

where e_1 and e_5 are the phase advanced position error signals, and G_1 and G_5 are the overall current gains discussed in 6.7. The square matrix results from the distribution of the position errors to the four electromagnet groups thus;

$$\begin{pmatrix} K_1 & 0 \\ 0 & K_5 \end{pmatrix} = \begin{pmatrix} X1 & X2 & X3 & X4 \\ Z1 & Z2 & Z3 & Z4 \end{pmatrix} \cdot \begin{pmatrix} DDF1 & DDF5 \\ DDF2 & DDF6 \\ DDF3 & DDF7 \\ DDF4 & DDF8 \end{pmatrix}$$

X1, Z1 etc are the x and z force components produced by each of the electromagnet groups per unit current flow and DDF1-8 are the eight demand distribution factors making up the demand distribution matrix. Values of the force components may be estimated for any attitude using FORCE. Values for the demand factors must be assigned so as to satisfy the resulting equations;

$$K_1 = X1*DDF1 + X2*DDF2 + X3*DDF3 + X4*DDF4 \qquad (1)$$

$$K_5 = Z1*DDF5 + Z2*DDF6 + Z3*DDF7 + Z4*DDF8 \quad (2)$$

and

$$0 = X1*DDF5 + X2*DDF6 + X3*DDF7 + X4*DDF8 \quad (3)$$

$$0 = Z1*DDF1 + Z2*DDF2 + Z3*DDF3 + Z4*DDF4 \quad (4)$$

The problem is indeterminate without the addition of further constraints.

Firstly it is reasonable that in the equations 1 and 2 the demand factors should be the same sign as the corresponding force factor, so that the resultant contribution towards K_1 and K_5 is positive.

We also choose that;

$$|DDF1| + |DDF2| + |DDF3| + |DDF4| = 4 \quad (5)$$

$$|DDF5| + |DDF6| + |DDF7| + |DDF8| = 4 \quad (6)$$

This effectively separates the roles of the demand factors from the overall gains. Following on from the conclusions of 6.4, all the demand distribution factors would ideally have a magnitude of exactly one, since with increasing force demand the electromagnets would all reach their maximum currents simultaneously and the full force capability of the system would be realised. In general this condition will conflict with the coupling equations 1-4 above, but the optimum solution for these equations is regarded as one for which the demand distribution factors are as close to unity magnitude as possible. The need to obtain the maximum possible force distribution is seen as essential because the previous experimental work and the force predictions of 3.4 suggest that the currents needed to support a model's weight could otherwise approach the system limited cable current for certain electromagnets.

The available force per unit current flowing in each of the electromagnet sets is then given by:

$$F_1 = G_1 K_1 e_1$$

$$F_5 = G_5 K_5 e_5$$

These expressions are only valid up to the point where the first electromagnet set being used for each control channel reaches its system limited maximum current flow (20 Amperes in all cases). The maximum force is then:

$$F_{1_{max}} = 20\, G_1 K_1 / DDF_{1_{max}}$$

$$F_{5_{max}} = 20\, G_5 K_5 / DDF_{5_{max}}$$

where $DDF_{n_{max}}$ is the demand distribution factor of these groups. Hence by ensuring that the demand distribution factors are as close to one as possible, the force generating capability of the system in each of the two control channels is maximised.

Using equations 4 and 5 above an expression for DDF2 in terms of DDF3 and DDF4 can be obtained;

$$DDF2(1 - \rho1.\rho2.Z1/Z2) = -(Z1\,\rho1(4 - |DDF3| - |DDF4|) + (Z3.DDF3) + (Z4.DDF4))/Z2$$

where

$$\rho1 = 1 \quad \text{for} \quad X1 \geq 0 \;;\; \rho1 = -1 \quad \text{for} \quad X1 < 0$$

$$\rho2 = 1 \quad \text{for} \quad X2 \geq 0 \;;\; \rho2 = -1 \quad \text{for} \quad X2 < 0$$

and for DDF1;

$$DDF1 = \rho1(4 - (|DDF2| + |DDF3| + |DDF4|))$$

Thus if estimates of DDF3 and DDF4 are made, values of DDF2 and DDF1 may be calculated. Similarly for DDF5-8:

$$DDF6(1 - \rho5.\rho6.X1/X2) = -(X1\,\rho5(4 - |DDF7| - |DDF8|) + (X3.DDF7) + (X4.DDF8)/X2)$$

$$DDF5 = \rho 5(4 - (|DDF6| + |DDF7| + |DDF8|))$$

where:

$$\rho 5 = 1 \quad \text{for} \quad Z1 \geq 0 \; ; \; \rho 5 = -1 \quad \text{for} \quad Z1 < 0$$

$$\rho 6 = 1 \quad \text{for} \quad Z2 \geq 0 \; ; \; \rho 6 = -1 \quad \text{for} \quad Z2 < 0$$

6.6 Demand Distribution Estimator DEMAT

To make these equations useful a computer based grid search technique has been applied. This is the Fortran program DEMAT (Demand Matrix).

For a chosen angle of attack, the program uses a simplified version of FORCE as a subroutine to calculate in turn the axial and vertical force components produced by each of the four groups of electromagnets. As originally designed, these are then converted into sensing system axes by simple geometrical transformations:

$$F_x'' = F_x \cos 45 - F_z \sin 45$$

$$F_z'' = F_z \cos 45 + F_x \sin 45$$

where double prime indicates sensing system axes.

This ensures that the ensuing calculations produce decoupled force components in these senses. If demand distribution data in the model axes is required, then the transformations for an angle of attack θ are:

$$F_x' = F_x \cos\theta - F_z \sin\theta$$

$$F_z' = F_z \cos\theta + F_x \sin\theta$$

where prime indicates model axes.

The main part of the program then calculates values of the demand distribution factors from this data. In a series of loops dummy variables representing DDF3 and DDF4 or DDF7 and DDF8 are incremented in small intervals (typically 0.01) and the remaining demand factors calculated and checked against the constraints outlined above. Failure to meet any of the requirements results in the program jumping to the next trial values. The estimated force capability for the resultant set of demand factors is then calculated. At the end of the computation the demand distribution factors giving the maximum force components for the particular angle of attack are output.

6.7 Force Optimisation with DEMAT

The program maximises each of the two force components independently, as if they arose from separate origins. In practice, since the forces are produced by the same groups of electromagnets, the full capability of each cannot be realised simultaneously. Thus, for example, with the sensing system control axes, the available force in the wind tunnel vertical direction is *not* the vector sum of the maximised components in the heave and axial directions, but is determined instead by the group of electromagnets which is first driven to its maximum current capability as a result of being demanded by both control channels.

For a model in suspension with no wind, the (tunnel sense) vertical force required to oppose gravity predominates, but in actual aerodynamic testing, the direction in which force capability should be maximised is that in which the resultant of lift and drag acts, so that it may be opposed by the MSBS as effectively as possible.

This implies a knowledge of the likely aerodynamic characteristics of the vehicle under test. For example, for a fighter configuration, at normal flight incidences giving high L/D, the resultant is fairly close to the wind tunnel heave axis. Beyond the stall where lift falls but drag continues to rise, the resultant vector will be rotated (Fig.6.3). At 90^{o} angle of attack it will point almost along the length of the wind tunnel. If the model weight was

then regarded as secondary to the aerodynamic effects, the senses in which the forces in the vertical planes should be maximised would then be in the direction of the resultant ('heave'), and perpendicular to it ('axial'). The full value of this 'heave' force is then available since, in the absence of unsteady aerodynamic effects, the 'axial' component is not required at all.

To achieve this, it is not adequate to use one of the other axis systems (model axes, say) and attempt to optimise in turn the components produced in the resultant and perpendicular senses, because this is no different from optimisation in the model axes themselves, and has the drawback explained above. It *would* be possible to use one of the other axis systems, however, if the determination of the demand distribution factors for both degrees of freedom were combined into a single operation. Using a developed version of DEMAT, trial values for four DDFs at a time would be used to calculate the four unknown DDFs simultaneously. The resolved component in the direction of the desired resultant could then be obtained and optimised through repeat calculation with new trial values. Alternatively, the control system could use an axis system consisting of the resultant direction and the perpendicular to the resultant. The optimisation could then be carried out for each of the two channels independently. The axes would rotate along with the rotation of the resultant.

Generalising the problem to some extreme attitude MSBS being used for production wind tunnel testing of differing models, it would be better to use the former approach. A control system operating with one set of axes (whether they be model, tunnel or otherwise based) could then be installed. To accommodate the varying aerodynamic characteristics of the models, and assuming that they are fairly well known, the demand distributions could then be calculated simultaneously for both of the forces in the vertical plane so as to produce a maximised capability in the direction of the resultant for the particular model. At the same time, force data acquisition would be eased as it would be obtained in one consistent axis system for every model type.

Such an elaboration of DEMAT has not been pursued in relation to the work with SUMSBS, since there is no specified aerodynamic force envelope to design for. Instead, optimised force components in the axes systems specified in 5.2 were judged to be adequate for initial suspension. Figures

6.4a to 6.4d show the individual contributions to the heave and axial force components from each of the four electromagnet groups, and for both axes systems. These are the available forces from which DEMAT produces its optimised solutions.

It is to be expected also that with a 'good' demand distribution, that is, with the force demands spread as evenly as possible amongst the electromagnets, there will be in fact little diffference in the force capability in any particular direction resulting from using one axes system as opposed to another. This argument becomes more true as the number of electromagnets in a particular MSBS design increases. Further, optimisation in the model axes is likely to represent a reasonable choice for the case of an aircraft aerodynamic envelope, as described above, since the model sense heave force channel will tend to be close to the direction of the resultant aerodynamic force over much of the angle of attack range. The main exception to this will be around the stall, where the resultant will change direction considerably with only a small change in pitch attitude.

6.8 Overall Loop Gains

The system performance in all the degrees of freedom is strongly dependent on the model angle of attack. Hence it is reasonable to expect that the overall loop gains of the system will have to be adjusted in response to the measured pitch angle. If the position or attitude error in any of the five degrees of freedom is e_n, then the system will produce a restoring force or moment given by:

$$F_n = G_n K_n e_n$$

where G_n is the overall loop gain and K_n is the distributed force/torque product found as described above. Note that for the cases of sideforce and yawing moment the force/moment products are identical to the predicted capability in these senses, since the 'demand distribution factors' are simply one. In the belief that this will produce consistent suspension characteristics we choose that $G_n K_n$ is a constant. Accurate values for this produce for a model suspended at zero angle of attack in the un-modified Southampton

MSBS are available from previous calibration work. These have been used as a basis for calculating the loop gains for the high angle of attack control system.

Reference 27 provides data for a 15mm diameter, 100mm long cylindrical model of samarium cobalt magnetic material. This has a magnetisation of 0.88 Tesla. Scaling the data for a magnetisation of 1 Tesla, as used in the DEMAT calculations, gives;

Channel	Component	Capability	Gain
1	Vertical Heave	4.89 N	19000
2	Pitching Torque	0.373 Nm	22000
3	Lateral Heave	4.89 N	19000
4	Yawing Torque	0.373 Nm	26000*
5	Axial	1.60 N	16000

Thus for example, the maximum capability for the sideforce channel at zero angle of attack with the modified (skewed E/M configuration) is predicted to be 3.56 N, so that the required overall loop gain is given by:

$$G_3 = 19000.\,(4.89/3.56)$$

$$= 26098$$

In the case of the two forces in the vertical plane and the pitching torque the loop gain is based upon the force or torque per unit current before the most used electromagnet group (largest magnitude demand factor) reaches its maximum current. Once this current is reached the available increase of

* It is now believed that the higher value of gain used in the yaw channel compared to that in the pitch channel was a consequence of the lower, non-linear gain of the power supply's near zero current. In the yaw channel the E/Ms are usually close to zero current, whereas the vertical E/Ms are always used away from zero (to oppose the model's weight). Hence these E/Ms used for pitch control had an effectively higher gain than the lateral E/Ms. See also Section 9.

capability with increasing demand falls, requiring a larger gain to maintain the same suspension characteristics. Such a refinement has not been incorporated since it is not intended that the loads on the model should normally cause the maximum current to be continuously demanded from any of the electromagnets.

The gain calculations are carried out in a simple Fortran program GAINER, as indicated on the block diagram (Figure 5.1).

6.9 Implementation of Pre-scheduled Controller

It is impractical with the present Southampton MSBS control computer for the calculations of the demand distribution factors and of the overall loop gains to be performed in real time. Instead the control program accesses pre-calculated demand distribution data via look-up tables. Further it is not necessary for data to be stored for every angle of incidence; previous fixed parameter controllers have proved quite adequate for angle of attack ranges of at least 20^{o}. For the prototype high angle of attack control program twelve sets of distribution factors and gains are stored. These correspond to design incidences of -10^{o} to 100^{o} in ten degree increments. For intervening angles, as described by the pitch measure generated by the sensing system, a linear interpolation is performed on the stored information to produce a piece-wise fit to the data. This is intended to produce a relatively smooth rotation as different groups of electromagnets are called upon to generate the various forces and moments.

The interpolation of the distribution data and gains is performed in real time by a subroutine of the control program, based on the instantaneous pitch angle measure. To calculate the value of a demand factor or gain H_n where the pitch attitude measure has a value P_n based upon the stored data H_1 and H_2 at the attitude with pitch measures P_1 and P_2, the following expression is used:

$$H_n = H_1 + [(P_n - P_1)/(P_2 - P_1)] . (H_2 - H_1)$$

However as Figure 4.6 shows, the relationship between the pitch measure and the actual angle of attack is non-linear. Thus the value of the increment

$(P_2 - P_1)$ is not constant, but instead must be stored for each of the ten degree intervals. Thus as the model rotates through the threshold of each design angle of attack the demand factor, gain and interval data corresponding to the next design incidence is loaded. It should be noted that there is an implicit assumption that within each ten degree angle of attack span the relationship between the pitch attitude and its measure can be regarded as linear, which is not so. However, the error involved is small.

To summarise, the following data is stored for each ten degree increment:

Vertical Heave Channel	4 demand distribution factors, 1 loop gain
Axial Channel	4 demand distribution factors, 1 loop gain
Pitch Channel	2 demand distribution factors, 1 loop gain
Lateral Heave	1 loop gain
Yaw Channel	1 loop gain
Pitch attitude measure	1 interval value

Initial demonstration of controller pre-scheduling was carried out prior to the modification of the Southampton system for high angle capability. Using DEMAT, demand distribution matrices corresponding to -10^{o}, 0^{o} and $+10^{o}$ were calculated and made accessible by the MSBS control program.
In early experiments the control program did not use the linear interpolation algorithm, but instead a cruder technique in which the demand factors were abruptly loaded when the model passed through a pitch angle threshold, without interpolation. This produced an unacceptably jerky motion around the transition incidence, or even unstable oscillation between the controllers, as a result of the suddenly changed distribution of error signals to produce the same forces and moments.

6.10 Predicted Performance of System with Demand Distribution

Figures 6.5 and 6.6 show the demand distribution factors for the nought to ninety degree attitude range, calculated for the sensing system and model axes controllers, in ten degree increments. It may be noted that for certain angles of attack, no solutions have been found which satisfy all the equations. This does not mean that a model cannot be suspended at these

attitudes, but simply that it is not possible to generate two completely independent force components. This is not a major problem, since usable demand distributions may be found by interpolating between or extrapolating from the calculated data. The resulting force components are not independent, but by checking that the cross components are relatively small the controller can be made to function successfully. Since the demand distribution calculations are dependent entirely on the estimates of FORCE and are therefore subject to the errors inherent in that program, even supposedly pure force components may in fact generate cross coupled forces. These will tend to affect the dynamic characteristics of the suspended model, as well as causing differences between the predictions of DEMAT and data obtained in experimental calibrations. Empirical techniques were in fact used to improve the quality of suspension through adjustment of the demand distribution factors (see 9.1).

To investigate the use of the piece-wise linear interpolation technique for the demand distribution, Figures 6.5a to 6.5d for the sensing system axes controller also show optimised demand distributions found for the predicted forces mid-way between the design points used in the controller. In general, the discrepancy between the demand distribution used by the controller at these points, as implied by the straight line fits, is not very different from the optimised solutions. In many cases the optimised points lie on the interpolated lines.

Figures 6.7 and 6.8 show the predicted force capabilities in the two degrees of freedom, as calculated by DEMAT and with the empirical values of the demand factors for those angles of attack where the program was unable to produce a solution. The figure for the sensing system controller also shows an example of an empirically obtained demand distribution which offers a significantly improved force distribution with only a small cross coupling component. This demonstrates a limitation of attempting to produce completely pure components, in that the full force potential of the system may not be maximised. The points of the graphs are again linked by straight lines since the forces produced by the demand distribution are unknown without first calculating the individual force contributions from each electromagnet set.

The data of Figures 6.4 to 6.7 demonstrate abrupt changes in gradient and sign, as a consequence of the optimisation technique which in general does not lead to all the electromagnets being used in equal proportions (as was shown previously to be ideal). Comparing the overall force predictions, it can be seen that at 45^{o}, where the heave sense in model axes and sensing system axes coincide, the predicted capability of the two controllers is little different. The model axes controller shows its minimum heave force capability to be at 30^{o}, even though this might be the region of highest aerodynamic force for a high performance aircraft. This minimum appears to be related to the inability of the four lateral electromagnets to produce a component in this direction, whereas they make a significant contribution at other angles of attack.

Further discussion of the limitations of DEMAT may be found in Section 9.

CHAPTER 7

SYSTEM INTEGRATION

7.1 Introduction

This chapter discusses the assembly and initial testing of the extreme attitude MSBS controller. Software features carried over from the previous digital controller are mentioned, along with algorithms added in the light of practical experience. A description of normal operation is given, and the demonstrated capabilities of the system outlined.

7.2 Model Dynamic Stabilisation

As explained in Chapter 2, the need for dynamic stabilisation of a suspended model in an MSBS is met in the Southampton system by a digital simulation of earlier analogue control systems. The computer program block which performs this function has been retained for the extreme attitude MSBS. The only alterations required result from the altered program repetition rate and the differing overall loop gains used.

The upper value of possible loop rates is determined by the integration time necessary to ensure saturation of the sensing system arrays. Although the required irradiance level is small, there is an inevitably large loss resulting from the transverse spread of the laser beams at the point where they reach the sensors. The signal is also optically degraded by the presence of interference fringes. These prevent the light beam irradiance from having the uniform distribution assumed, limiting the practicable loop rate to below that of the sensor maximum scan rate (1 MHz).

When freed from the synchronising signal generated by PACS, the control program MSHI is capable of running at a loop rate over 400 cycles per second. Some degradation of suspension characteristics occurred when the previous control program repitition rate was reduced from 400 Hz to 256 Hz, and it is believed that although suspension is possible at much lower loop rates, this is not desirable. However using more modern digital controllers,

lower loop rates are thought to be practical. Section 11 discusses such possibilities.

For these reasons, the basic PACS loop rate of 242 Hz has been used throughout the work reported here. The corresponding loop period is used in calculating the values of the various constants in the dual phase advance algorithms. It has proved practical to use the same values for both the axial and vertical heave position channels, reducing the effect of one objection to the sensing system axis controller, which is that when the model is displaced by up to 45^{o} from the datum, the fixed axial and heave constants might result in altered dynamic behaviour from that at the design attitude.

Typical values used are as follows:

control loop period = 4.13 ms

n (high/low frequency gain ratio) = 10

T (time constant) = .0025 seconds.

An increase of loop rate to about 280 Hz without severe degradation of the optical signals has been demonstrated, although no attempt has been made to suspend models. A simple PACS command at the start of the control program permits the clock rate to be adjusted to a range of values. It should also be pointed out that the Reticon supplied pre-processor circuit boards appear to be limited to around 500 Hz. Optical modifications such as using a more powerful laser or adding cylindrical focussing lenses in front of the sensors to concentrate the light beams could permit loop rates up to the limit imposed by the computer's capability. The latter technique would, however, produce 'smearing' of the shadow edge signal owing to the integration effect of the cylindrical lenses.

7.3 Error Integrator

The error integration block is identical to that used in the previous digital controller and has the following difference equation:

$$y(k) = u(k) + K \sum_{n=-\infty}^{k} u(n)\Delta t$$

The proportion of the summed previous signal $\Sigma u(n)\Delta t$ which is added to the present sample is determined by the constant K. This has a strong influence on the dynamic characteristics of the suspended model owing to the destabilising effect of this block. Without the use of error integrators, a model can be suspended, but will tend to sit 'low' of the required attitude and position. A small proportion of error integration gradually drives the model to a demanded position or attitude, without significantly decreasing the damping. A larger integrated signal produces better position/attitude demand following for continuous motions, at the cost of poor damping for step changes.

7.4 Model Oscillation Generator

The previous digital control program incorporated a facility for exerting sinusoidal oscillations on the suspended model. A similar oscillator is included in the extreme attitude control program MSHI. A counter is included in the program loop which increments once per program loop up to 484 (twice 242). Corresponding to each increment is a non-dimensional amplitude value of a single sine wave, calculated in the Fortran preamble to the program and stored as a one dimensional array of data. The latest increment value then represents an offset from the array start address to the address containing the appropriate amplitude value. An oscillator with a fundamental frequency of half a Hertz is thus obtained. By sequentially adding the amplitude values to the error signal of a chosen degree of freedom, a sinusoidal motion in this degree of freedom may be generated. Multiples of the fundamental frequency may be obtained via scaling factors, and similar multiplying factors can be used to adjust the amplitude and phase of the oscillations.

The amplitude of the oscillations in all degrees of freedom are not calibrated in the same way as are demands for change in position or attitude because the response is a function of the oscillation frequency and the chosen

constants in the phase advance algorithms. However, determining the amplitude of oscillation from position sensing data acquired during a test is eased by the known calibration of the sensors.

7.5 Model Suspension and Initial Difficulties

After assembly of the various components of the new optical sensing system and extensive debugging of the control program MSHI, initial attempts at model suspension began. The optical alignment procedure outlined in Section 5 was performed successfully, although certain limitations were discovered, which are considered in 8.2. Figures 4.8 and 7.2 show the model used for initial testing. It consisted of a half-inch diameter Alnico core five inches in length surrounded by a 18.8 mm diameter Tufnol (resin impregnated cloth laminate) shell.

Use of a dummy model held in the system by a projecting arm and rotating mounts assisted in checking the correct functioning of the program, and the generation of meaningful sensing signals was confirmed. The need was shown also for a clamping algorithm to prevent the instantaneous pitch angle measurement which occurs during launch exceeding the values for which stored control data existed, resulting in the program crashing out. The algorithm involves checking the pitch measure against safe maximum and minimum values before allowing it to be used in subsequent processing.

Initial suspension of the test model was achieved at 45^{o} angle of attack, the null attitude of the sensing system. At first the correct active decoupling of the heave and axial channels described in 5.4 was not used so that suspension at the extreme high and low attitudes was affected by the resulting inadequate axial stiffness.

Two problems immediately revealed themselves.

The first was of irregular flicks in model position/attitude, often causing loss of control. Examination of data streams through the control program showed that corruption of position sensor information was occurring. This was apparently due to the PDP 11/84 host computer returning to PACS to remove data before it was ready.

The introduction of delay loops between the request to PACS and the recovery operation removed much of the problem. However a complete solution was not effected until position sensor 'clamps' were added to the control software. These are intended to remove the influence of transitory optical or electronic effects. In particular the sensors occasionally (i.e. a few times a minute) trigger the counters at the first pixel, producing an output of 1033, a measurement implying that no model is present. This is believed to be an electronic defect of the sensor pre-processing cards. The clamping algorithm involves comparing the latest sensor output with that which was produced in the previous program loop. If the change in terms of pixels is greater than a certain margin, then the new value is rejected and substituted by the previous measurement. Choosing the appropriate clamping margin involves making an estimate of the largest change in pixel count which might be expected as a result of the model being in motion from a user demand, such as a sinusoidal oscillation. For example, assume an oscillation of 5^{o} amplitude at 20 Hz represents an extreme upper limit of performance:

$$\text{then } \omega = 126 \text{ rad/sec}$$

For the sensing system as designed, the corresponding linear motion of the model centre line at the axial location of the main sensors = 2.2 mm

$$\text{maximum change in position} = 277 \text{ mm/sec}$$

$$\text{change over one program loop} = 1.1 \text{ mm}$$

$$= 45 \text{ pixels}$$

A clamping margin of 50 pixels has been used on all channels without any deleterious effects due to the action of the clamps being detected. However, even if the defect causing the clamp(s) to become operative lasts for only one program loop, this represents an effective halving of the program loop rate, probably resulting in some loss of control quality manifest as a reduction in steadiness.

The second problem which was evident at the start of testing was a generally poor station keeping characteristic, with an apparent limit cycle of 20 to 40 pixels on all the channels. This was much worse than hoped for, and

was eventually traced to digital quantisation errors as a result of a signal division step in the feedback loop of each channel. By altering the scaling of the signals, a finer control of electromagnet current was made available, with a consequent improvement in steadiness. Data on position/attitude keeping is given in 8.8.

A significant problem of signal degradation was also known to be present in the axial channel as a consequence of the location of the diode array. Firstly, because the array was mounted parallel to the wind direction, but the incident laser beam was at 45^{o}, optical interference fringes were produced on the diffracted edge signal as a result of reflections within the thin glass cover of the array. This effect was present in the earlier tests of the axial array with the un-modified low attitude MSBS (39) but was not found to noticeably affect the steadiness of the suspended model. However, in the fully developed extreme attitude MSBS the axial array was positioned closer to the adjacent lower forward electromagnet than in initial work. The consequence of this was an electrical pick-up on the array video signal of the 5 kHz switching transients of the electromagnet power supplies. Figure 7.1 is an output trace of the axial array output with a model in suspension. The oscillating signal levels when combined with the optical interference spikes simulated a random vibration of the model, causing the control system to respond by demanding a compensating oscillation.

To eliminate this problem, a brief investigation of some form of magnetic shielding of the array was made. A mild steel box produced an inadequate improvement in the signal quality, and the use of mu-metal was judged to be necessary. However, an alternative solution lay in entirely removing the array from the inside of the MSBS. A new mounting for the array was fabricated and fixed to the existing auxiliary equipment table on the port side of the MSBS. The laser beam from the unmodified axial optical system is deflected to the array by means of a small mirror attached to a mount positioned in the location previously occupied by the axial sensor mount.

In addition to eliminating the problem of optical and electrical interference on the axial array, the modified arrangement has other advantages. Adjustment of the array position is more easily accomplished

when the wind tunnel test section is installed, whilst the array is no longer vulnerable to damage during work with the test section removed. In early work, the ribbon cable connecting the array circuit board to the mother card was sliced on several occasions when a model fell out of suspension. Also, because the axial channel beam strikes the array normally in the improved system, the maximum possible motion of the model in the axial direction is increased from one inch times (cos 45) to about one inch (i.e. the array length).

7.6 Normal Operation of MSBS

Use of the MSBS involves a number of routine procedures which begin with turning on the sensing system and He-Ne lasers. A ten minute warm-up time is required to ensure even and full saturation of the sensors. There is evidence that initially the pointing of the laser beams changes during this period, so that one end of one or more sensors may not be illuminated at first. With the beam alignment procedure correctly carried out, adjustment of the sensor's position to give full illumination is not normally required. A visual check of this is made by examining the video outputs of the sensor pre-processor cards as displayed on an oscilloscope. The sensor output program PACS is run to produce a real-time output of all the arrays. Correct functioning is indicated by the generation of five 1033-0 measurements, showing that the sensors are correctly illuminated with no edge event (object) present. This program is halted and the control program MSHI activated.

MSHI begins with a Fortran preamble which prepares an array for storage of data acquired during the run, calculates the oscillator fundamental sine wave and opens data files containing the pixel count information, the pitch attitude increments, and all the demand distribution factors and gains. An additional file can be used to store a series of commands making up a demonstration routine. This feature is carried over from the previous digital controller. The items in the data files, several thousand in total, are moved into one dimensional arrays. The main assembly level control program is then called, which immediately jumps to a startup sub-routine. This records the address locations of the arrays containing all the control data, so that they may be used as the base for subsequent access via suitable offsets. The

subroutine also activates the photodiode array control system, setting up the edge event thresholds as outlined in 4.8. After 5 seconds, light emitting diodes on the PACS boards confirm that the self-checks have been successfully completed and the system clock begins cycling. The subroutine returns control to the core of MSHI, which awaits a synchronising pulse from PACS before proceeding. A frequency meter operated via the D/A subsystem by a pulse output from the control program indicates the program loop rate. A model launch angle of attack must be input, and the power supplies activated before the model is manually inserted into the test section at the approximate required position. The error integrators are set 'on' by default, but may be switched 'off' if desired.

Normal model launch incidence is 45^{o} as certain variables in the control program have initial values which correspond to this incidence. For example, the position sensor error clamping algorithms require use of the previous sensor output pixel counts. Thus the initial values must be 512 rather than zero, since the centreline of the model should lie half-way along the array length at 45^{o} angle of attack. Launch at other incidences is possible, but becomes more difficult at the extremes of the attitude range. The reason for this appears to be a consequence of wildly unsuitable demand distributions being loaded during the manual launch of the model. This would result from the pitch measure, calculated when some but not all of the four main edge shadows are visible, being very different from that corresponding to the required angle of attack.

When in suspension, the model's position and attitude may be adjusted using an amplitude and code letter system. To the user, this appears identical in operation to the technique used with the previous digital controller, except for the fact that the amplitudes of the offset signals are calibrated. Thus for example 50 z means translate the model by 50 thousandths of an inch in the z direction in whatever controller axis system is presently in use. A command of 4-m means move to minus four degrees angle of attack. The code aide-memoire kept on the computer terminal is reproduced here:

Degree of Freedom	Translation			Rotation		
	x	y	z	roll	pitch	yaw
offset	x	y	z	l	m	n
oscillation amplitude	a	b	c	d	e	f
oscillation frequency	i	j	k	o	p	q
oscillation phase	r	s	t	u	v	w

The pre-programmed routine is activated by lg, the integrators by lh, and data acquired by n {(where n is the number of program cycles). The data which may be stored is determined by inclusion at the appropriate point in the control program of an operation to push the value of a quantity of interest onto a data stack. If data storage is not requested by the user, the stack is emptied at the end of each program loop. During program development, data items such as the raw value of the sensor outputs, the value of the edge flag word from PACS and intermediate values in loop calculations were recorded. Versions of the control program in routine use are designed to record de-coded position and attitude measures, or the instantaneous values of electromagnet currents. The latter are obtained via the A/D sub-system from current shunts.

Facility is provided for the introduction of offsets in the roll degree of freedom, should the roll attitude be controlled. Alternatively, the code letters involved are available for the user input of other quantities during suspension, if required.

The model is manually removed from the MSBS at the completion of tests, with the electromagnets automatically returning to a zero current condition.

7.7 Demonstrated Capability of Extreme Attitude MSBS

Following its initial test period, including the refinement of the position sensing algorithms, the MSBS has shown itself capable of operation

over most of the planned range of possible positions and attitudes. These include suspension from -7° to 97° angle of attack. Attempts to achieve the full -10° to 100° range of stored attitude data have not met with success because during the rotation to these extremes the instantaneous pitch measure exceeds that of the required value. This causes the pitch measure limiting algorithm mentioned earlier to be activated. Thus, even if the model attitude continues to diverge, the pitch attitude signal becomes fixed. However, this is not seen as a major failure since a true 100° attitude range is available, and if required the control program could be amended to give a 110° range. This would involve the calculation and storage of demand distribution data for -20° and 110° angles of attack and various other detail changes to the control program.

The yaw attitude range is primarily limited with the models used by the tail moving out of the axial sensing beam at the extremes of the angle of attack range. This is because of the large transient axial sensor output changes produced as a consequence of the circular cross section of the model being obliquely viewed by the axial sensor/beam at these attitudes. Thus only a +/- 5° range is normally used, although much more is potentially available around the 45° angle of attack datum.

Figure 7.2b shows the original Tufnol-shell model suspended at 90° angle of attack, with the laser beams of the sensing system visualised by means of smoke. The reduced width of the beams as they leave the MSBS at the top of the picture indicates the shadowing effect of the model. During early experiments this model was damaged beyond repair, and subsequent experimental work on the controller was carried out using an existing aluminium alloy shell model of 22mm diameter. Figures 7.3a and 7.4b show a demonstration model of the HOTOL aerospace-plane suspended at a range of attitudes. This model has a magnetic core with two flat faces which has a preferred roll attitude, thus endowing the shell with passive roll stabilisation. A 10mm diameter model has also been suspended over the full attitude range; smaller diameter models are also practicable, although the angle of attack range is progressively reduced at the extremes. As the inertial characteristics of different models can vary considerably, the overall loop

C-2

gains in the controller generally require adjustment to maintain the quality of suspension (damping and stiffness).

7.8 Displacement-Time Histories for Large Motions

Using the data storage feature of the control program, the behaviour of the suspended model during large changes in position and attitude may be examined. By loading a series of small attitude changes as the pre-programmed routine, the model can be made to rotate in a pseudo-continuous fashion over a large attitude range. Figure 7.5 shows the pitch attitude recorded during a rotation from nought to ninety degrees in response to a pre-programmed routine consisting of ninety steps of one degree magnitude. Each angle of attack is demanded for 25 program loops before being succeeded by 25 loops of the next increment. The rate of change of angle of attack is thus slightly less than ten degrees a second. The measured pitch attitude value plotted is that at the twenty-fifth loop of each increment. It can be seen that the attitude following is generally very good, with a tendency for the actual attitude to be slightly greater than the required value, with some overshoot resulting when ninety degrees angle of attack is reached. Note that because of the non-linear relationship between the pitch measure and angle of attack, the plots are not straight lines. A further example of a nought to ninety degree sweep is shown in 8.7, where defects in the motion are discussed.

Figures 7.6 and 7.7 show the pitch attitude response of the model to very large step demands of twenty degrees and forty degrees respectively. In both cases, agravated by the error integrators, large initial overshoots occur, followed by almost monotonic decay to the correct angle of attack. It may be noted that the period to complete the rotation in both cases is the same (about half a second). The angular rates during the almost linear portions of the responses are very large: about seven hundred degrees per second in the case of the forty degree rotation. The damping in the case of the 20 degree rotation is noticeably poorer, suggesting that the pitch channel gain around 45^{o} angle of attack is set slightly too low.

Figure 7.8 shows a time history for a model undertaking a motion in response to a sinusoidal demand at half a Hertz frequency, with a 45 degree

amplitude about the 45 degree datum of the sensing system. The rotation of the model from nought to ninety degrees angle of attack thus takes one second. It should be noted that as the demand is for a sinusoidal motion in terms of the pitch attitude measure, the actual motion is a distorted sinusoid. This is a consequence of the non-linear relationship between the controller pitch measure and the angle of attack.

Figure 7.9 illustrates a large oscillation at 45 degrees angle of attack in the model heave sense. The amplitude is about 0.6 inches and the frequency is 1 Hertz. The motion appears pure, although the maximum positive displacement is slightly more than the negative displacement. This may be associated with a small pitch attitude deviation which is seen to occur at the upper extreme of the motion. In turn, this probably results from defects in the information generated by the optical model position sensing system. These and other unsatisfactory aspects of the suspension characteristics are discussed in Section 8. The largest heave oscillations demonstrated at 45^{o} angle of attack were of 1.1 inch amplitude at $\frac{1}{2}$ Hz frequency.

It may be noted that all of the large amplitude motions shown involve the first edge seen each of the four main arrays - and therefore used in the subsequent processing - changing from one side of the model to the other. Hence the edge interpreter algorithms are fulfilling their purpose of generating a continuous signal for each of the degrees of freedom.

7.9 Exploratory Operation of MSBS with Low Speed Wind Tunnel

All of the initial experimentation with the extreme attitude MSBS was performed with the fibreglass wind tunnel test section not installed. Subsequently the modification of the test section to incorporate the high-grade windows for the sensing system light beams was carried out. This involved the fitting of four removable perspex inserts each fitted with a pair of anti-reflection coated glass windows, to permit the four main beams to enter and leave the test section. In addition, three similarly coated windows were added to allow the axial sensor beam to enter the test section at the rear of the system, cross to the top of the test section and re-cross to leave at the bottom on its way to the axial array. With the windows installed, some

degradation of the array video signals was noted, owing to the reduced mean illumination levels.

To permit initial demonstration of wind tunnel operation with the extreme attitude MSBS, an axisymmetric model of 18 mm diameter was constructed from aluminium alloy. This had a 110 mm cylindrical body with a circular radius ogive nose giving an overall model length of 145 mm. A core made up of twenty 12.5 mm diameter by 5 mm thick discs of neodymium-iron-boron magnetic material was used. This material has excellent resistance to de-magnetisation and a high remanent magnetisation of around 1.2 Tesla.

The model was successfully suspended from nought degrees to ninety degrees angle of attack in the MSBS, wind-off. Some initial operation of the atmospheric wind tunnel was carried out at Mach numbers up to 0.1 and angles of attack up to sixty degrees. The maximum Reynolds Number based on model diameter was thus around 4×10^4. At higher angles of attack, the similarity in model length with test-section internal diameter means that care is needed in adjusting model position to prevent the nose touching the top wall. Clearly, in such circumstances, the unacceptably high blockage factor of a typical model makes the acquisition of aerodynamic data in the Southampton MSBS a pointless exercise. Useful work could be performed at lower incidences, perhaps below forty five degrees. In summary, no fundamental problem in the use of the extreme attitude MSBS with the wind tunnel has been revealed by the limited testing performed.

CHAPTER 8

ASPECTS OF PERFORMANCE OF THE

EXTREME ATTITUDE POSITION SENSING SYSTEM

8.1 Introduction

The previous sections have described the hardware and software modifications made to SUMSBS to permit extreme attitude suspension. The data presented in 7.4 showed that the central goal of suspension over an angle of attack range greater than 90^{o} has been achieved. In this chapter and the one which follows a more detailed discussion of the performance of certain aspects of the MSBS is given. This involves the presentation of data characterising the position sensing system and a discussion of some difficulties encountered in its use. Force/current calibrations in the lateral heave degree of freedom have also been carried out over a ninety degree angle of attack range, and these are compared with the predictions of Section 3.4 in Chapter 9. A discussion of a vertical force calibration at ninety degrees angle of attack may also be found there.

8.2 Limitations of Position Sensing System

The behaviour of a suspended model is crucially dependent on the quality of data input from the position sensing system. This is especially so for constant conditions or small rates of change of position and attitude (near D.C.). The sensing system of this MSBS is unusual in permitting large motions compared to the size of the model. It is therefore important to examine its detail performance and how this affects the MSBS as a whole.

The correct functioning of the control system has been shown to rely on a known physical configuration and on linear sensor response. However it is difficult to independently verify these characteristics. For example, the previous sensing system was calibrated by means of the dummy model technique (4.3). It has not been possible to carry out a check calibration of the digital sensing system with the existing dummy model traversing

equipment because the translation required to move an object across the complete field of view of an array is too large; only portions of a calibration line can be obtained.

Figure 8.1 shows a partial calibration of one of the main sensors (the forward starboard). As the direction of the traverse is approximately in the vertical direction with the dummy model at about zero degrees angle of attack, the position data does not relate to a motion parallel to the face of the array. Figure 8.2 reproduces a calibration of the axial sensor made during the preliminary tests with this installation and reported in Reference 39 The trend of a linear calibration is demonstrated in both instances.

However, a variety of defects in the optical sensing system and the associated computer control algorithms are present in the extreme attitude MSBS and these determine the accuracy (as opposed to the resolution) with which a model may be held steady in suspension. The ultimate resolution of the sensing system is determined by the inter-diode spacing of the sensor arrays, which in the case of the RL1024G units used is 0.001 inch. The usable accuracy is more than this as a result of the influence of several factors, both optical and non-optical in origin. These include:

1) thermal distortion

2) mechanical vibration and creep

3) resolution of control computer

4) resolution and response of electromagnet power supplies

5) uniformity of illuminating laser beams

6) quality and surface condition of optical components

7) uniformity of response of diode arrays.

It is difficult to apply meaningful values to all of these, but their likely influence can be assessed with available data and the evidence of the suspension system behaviour. In addition, the interaction between some of

the control algorithms and the sensing system can produce undesirable effects at particular angles of attack. These are discussed below.

A comparison of the all-digital sensing system with the previous analogue (single diode) sensors is also useful.

A complete assessment of the accuracy of the analogue sensing system used in combination with the digital control system was never made. The practical limit on resolution was set by the A/D system used to make data available to the control computer: this was one part in 2047. The data of Reference 27 suggests that this translated into a resolution of about 0.001 inches for the four main sensors, and about 0.0003 inches for the axial sensor. However, as with the digital sensing system, the outputs of the four main sensors were summed and differenced, so that the effective resolution for the four degrees of freedom measured by these units was four times better than that of a single sensor. The analogue axial sensor had a significantly poorer accuracy owing to the influence of the fluctuating output of the illuminating helium-neon laser.

The performance of the analogue sensing system was primarily affected by a gradual change of calibration owing to the build up of dust on the light sources and receivers. The resulting decrease in overall loop gains would produce less well damped suspension characteristics, and ultimately loss of control. Drifts in the datum position and attitude of the model of unknown magnitude were also caused. Mis-alignment of optical elements was less of a problem than with the digital sensing system owing to the shorter path lengths and simpler design.

8.3 Thermal and Vibrational Distortion

As a consequence of the long optical path lengths in the extreme attitude sensing system - up to 2.0m - one possible effect of any mechanical distortion will be to produce angular changes to the positioning of the plane mirrors. These will cause the illuminating beams to be translated across the face of the sensors. If the translation is sufficient, the sensors may cease to be fully saturated, and the sensing system will fail.

However, as the laser beams are 7mm by 30mm in cross-section when they strike the 1.024 inch by 0.001 inch array aperture, there is a considerable margin for mis-alignment not to cause failure. This does not mean that any beam drift produces no change in the suspended model's position and attitude. Although the model may continue to be suspended, the change in angle of the beam will cause its edge location seen by the sensor as a fixed measurement to correspond to an altered position in space. Figure 8.3 illustrates the problem, which can equally apply whether the cause of the angular deviation is through thermal or vibrational causes, or mis-alignment in the optical set-up procedure. It should be noted that if a simple translation of the beam occurs, but the array remains fixed and fully saturated, no change in model position occurs, although of course if the array is translated, the model moves in sympathy.

The mirror gimbal units used to deflect the four main beams up to the MSBS test section have a specified angular deviation with temperature of 2 micro radians per degree Celsius. Over the approximately one metre between the mirrors and the sensors, this implies a linear translation rate of 0.08 thousandths of an inch per degree. For any likely temperature variation (say 5-10 degrees) therefore, the thermal drift will be less than the equivalent of one pixel spacing. However the thermal stability of the somewhat cruder custom-made optical mounts fitted to the MSBS will be poorer than for the bought-in units, and thermally induced angular drifts of the order of one pixel spacing appear likely.

In considering linear position changes, the major source of temperature variation is likely to result from expansion of the aluminium alloy framework of the MSBS. The arrays are mounted near the top of these supports, on brackets directly attached to the vertical members. If it is assumed that any change in height is directly conveyed to the sensors, the linear variation x relative to the location of the gimbal mirror mounts can be estimated as follows:

$$x/h = \alpha t$$

where h = 1.5m, for aluminium alloys $\alpha = 23 \times 10^{-6}/K$, and let t = 5 K

Thus: $x = 0.17mm$, or about 7 pixel spacings

Although this is a crude calculation, it demonstrates that thermal variations are likely to cause measurable variations in model position and attitude.

By monitoring the outputs of the sensing system with the beam alignment unit jig installed over a seven hour period, drifts of up to six thousandths of an inch have been recorded in the location of an object edge. On turning the equipment on and allowing for a warm-up period the following day, the outputs were seen to be closer to the original values (measurements in pixels):

Time	channel 1	channel 2	channel 3	channel 4
Day 1: 11.00 hrs	381	383	376	378
Day 1: 18.00 hrs	383	376	381	372
Day 2: 10.00 hrs	379	380	376	378

It may be noted that the two sensors of channel 2 and 4 are located on the same side of the MSBS, facing the windows of the laboratory, suggesting the influence of direct sunshine on the thermal expansion during the course of a day. The data is quite inadequate to confirm this, however.

Vibrational influences on the suspension system originate from two sources:

(1) the forces and moments produced by the interactions between the electromagnets acting upon the model, and

(2) random impulses from the MSBS surroundings.

Of these, the first is more important. Extreme jolts caused to the MSBS frame or from movements around the MSBS laboratory can be seen to cause slight changes to the video signals from the digital sensors, but no model fly-aways have occurred from these causes.

Electromagnet induced vibrations could occur as a consequence of the mutual attractions and repulsions between the E/Ms producing sufficiently large distortions of the frame for components in the sensing system to be moved. To determine whether the forces involved are sufficiently large, consider the case of the two solenoidal axial E/Ms. An approximation to the force between them can be given by Reference 40.

$$F = -\frac{3}{2}\frac{\pi\mu_o N^2 R^2 I^2 x}{(R^2 + x^2)^{5/2}}$$

where N is the number of turns in each electromagnet (1000)
R is the average radius of the electromagnets (0.15m)
I is the current in each of the electromagnets (up to 20 A)
x is the separation between the electromagnets (0.6m)
μ_o is the permeability of free space ($4\pi \times 10^{-7}$ H/m).

(This equation is strictly valid only for the action of a large electromagnet on one of much smaller radius).

This gives a force of approximately 100N when the electromagnets are full on. The forces between the eight main electromagnets and the axials will be significantly larger owing to the greater fields produced by the iron cored electromagnets and the reduced separations. However, the electromagnets are firmly mounted to heavy frames and well supported, so that these forces are unlikely to produce large deflections. The single exception to this is the mounting of the two axial electromagnets. These are effectively hung from the top of the MSBS frame, permitting bending about a transverse axis above the centreline of the E/Ms.

It is difficult to model the structure of these components of the MSBS, especially as the weight of the axial electromagnets is unknown, but it is believed that an effective bending moment made up of 50N acting at over a twenty centimetre moment arm will produce measurable deflections of the rig, in a resonant manner.

In certain circumstances, with the overall loop gains in the controller poorly adjusted, coupled oscillations between the axial electromagnets, the axial optical system support frame and the suspended model have been induced. Occurring at a few Hertz frequency, visible motions of several millimetres were noted. Further evidence of magnetically induced distortions has been noted when a model is launched. As the electromagnets turn on to take the weight of the model, slight changes in the video signals from the diode array sensors can be seen. This is especially so on channel 4, which has the lowest illumination level, and therefore more clearly shows a signal change causing loss of saturation of any of the dioades. It has not been possible to isolate the cause of this movement as relating to a particular optical component, but probably is a consequence of the flexing of the whole support structure. It is concluded that an interaction between the sensing system and the E/Ms does alter the effective calibration of the former, and that this will be more severe during oscillatory motions. Such effects may also have been present in earlier position sensors.

8.4 Computer Digitisation Effects

The influence of digital quantisation errors on the position keeping characteristic of the suspended model was noted in 7.5. The resolution of calculations in the computer is in principle determined by the number of bits per word (16 in the case of the PDP 11/84). However the D/A units through which demands to the electromagnets are routed have a resolution of only 12 bits, reducing the fineness of control which can be achieved. Further, the output signals when examined on an oscilloscope are seen to have large transients imposed on the mean level. The control program also makes extensive use of the computer's floating point processor, with many conversions of data from floating point form to integer form, introducing rounding errors. These effects cannot explain any reduction in the quality of model station-keeping, however, as the hardware is identical to that used with the previous form of SUMSBS.

An important effect on the closed-loop behaviour of the MSBS is the non-linearity of response of the power supplies close to zero current. Characterised by Thomas (41), this is discussed in Section 9.6.

8.5 Optical Limitations to Collimation

The self-calibration feature of the MSBS sensing system is dependent on the collimation of the four laser beams which cross the test section on their way to the four main sensors. A discussion of the precision of collimation which has been achieved is therefore appropriate.

Approximate collimation of the beams is achieved through adjusting the separation between the expansion and collimation lenses to be equal to the sum of the respective focal lengths, which is followed by the use of the finely adjustable collimation lens mount. An object of known width, such as the target rods of the alignment unit, will produce a sensing system estimate of its width to within 1 thousandth of an inch when positioned directly in front of an array.

As the object is moved away from the sensor to a distance corresponding to the location of a suspended model, the measured width increases. This is because the default threshold level voltage of the sensing system edge detector is set half-way between the 'dark' and 'light' levels. The implication is that the threshold level is closer to the light level than the one-quarter level which the edge diffraction theory (Appendix B) predicts is the actual location of the model edge. Also, if the process is repeated for each sensor, the discrepancy between the physical size of the object and the sensing system estimate is not consistent. For example, the following is typical data obtained during the initial set-up of the sensing system (all measurements are in pixels, i.e. one thousandth of an inch):

Object true width	sensor 1 estimate	sensor 2 estimate	sensor 3 estimate	sensor 4 estimate
255	263	266	262	269

There are two causes for this variation. Firstly, even if the beams are perfectly uniform and the edge transitions match the theory exactly, the digital method of measurement will inevitably produce an error of ± one pixel. However, the laser beams are not uniform owing to a range of optical defects which produce a random variation in the width measurement if the object is translated along the length of the array. These are discussed further below.

The second, systematic source of error is the variation in the mean irradiance of each of the laser beams as a consequence of the varying number of optical components through which they pass in the beam splitter unit (Section 4.5). By reference to Figure 8.4, it can be seen how a lower irradiance level causes an over-estimate of an object width compared to that obtained with a higher irradiance, if the threshold level is constant. In order of ascending number of optical components in their respective light paths, the four channels may be listed in the following manner: 3, 1 and 2 (equal), 4. This has been found to relate consistently to the variation in width estimates from each channel.

A solution to this problem lies in setting the threshold levels of the four channels individually so that they generate more nearly equal estimates of a target object width. This is readily accomplished using one of the available library of commands to PACS. The threshold levels of chanels 1, 2 and 4 are reduced so that they give measurements within ±1 pixel of that from channel 3. It is then possible to take account of the constant discrepancy between the physical size of an object (such as a suspended model) and the measurement of the sensing system. Thus, for example, in the program which generates the position sensing data, PIXEL, the model radius input as the basis of the calculations is larger than the actual model size.

8.6 Optical Limitations to Linearity of Response of Sensor Arrays

Although calibration of the photodiode arrays as installed shows a linear relationship with position when examined over increments of a millimetre or so, the response for very small motions equivalent to a few

pixels is not as good. In addition, evidence of larger irregularities in response have been found at the ends of the arrays if precautions are not taken in the optical set-up procedure.

The small scale irregularities have several contributory factors. Firstly, the individual photodiodes have a random variation of responsivity of up to ±14 per cent. This will affect the slope of the edge transitions, and, with a fixed threshold voltage level, can be expected to cause small variations in the width measurement of an object - perhaps up to four pixels with the model to sensor separation of the Southampton MSBS.

An important cause of signal variation is one of optical interference caused by the combination of refraction and partial reflection at two surface optical components such as the expansion and collimation lenses. The laser light is particularly suited to causing interference as a consequence of its coherent, nearly mono-chromatic nature. If a sensor array is slightly displaced, bringing it out of saturation, the large variations in irradiance can be seen as many small interference fringes superimposed on the approximately uniform mean level.

These fringes can also be seen as individual spikes on the transition edges of model-in-suspension video signals. Figures 8.5a to 8.5e show traces of the video signals of the five sensors with the model suspended at 45 degrees angle of attack. Note that the 'light' signal is a negative voltage with respect to the 'dark' level.

Some of the edge are of the pure form predicted by diffraction theory, whilst others show interference spikes of up to 4 pixels wide. These are fixed in their position along the video image, and so are superimposed on the diffracted transition of a model in motion. Thus, depending on whether the peak of a spike is just below or just above the threshold level, the edge detection algorithms will produce measurements which can suddenly change by the width of a spike for an actual position change of only one pixel. The control system will respond to these sudden changes, producing an oscillatory motion, especially if the required position/attitude implies an edge location lying between the two achievable values.

This is a near-random effect which cannot be taken account of in the processing of input data to the control system unless far more sophisticated curve-fitting algorithms can be incorporated. This interference, therefore, places a further limit on the achievable accuracy of measurement. However, as the position attitude signals are composites of the individual sensor outputs, an averaging effect will help reduce the influence of this effect. Taking a worst case, a unidirectional error of four pixels on all four main sensors would imply a discrepancy between apparent and actual angle of attack of 0.4 degrees at 45 degrees angle of attack.

The video outputs show evidence of pick-up of the power supply switching frequency in the form of a small oscillatory wave at 5kHz.

Figure 8.6 shows a portion of the output of one of the sensors, expanded to show the transition edge as made up of individual pixel analogue voltages. In this case the signal is a monotonic curve as predicted by theory. The transition from 'light' to 'dark' occurs over about 25 pixels, which is in accordance with the estimates of Appendix B.

8.7 Non-Uniformity of Illuminating Beams

A further difficulty noted during the optical set-up was the influence of so-called 'marginal' rays on the uniformity of the illuminating laser beams. If that part of the laser beam which is used to illuminate the arrays is too large in comparison with the total width at the point of collimation, a uniform illumination cannot be assumed. This is because although simple optical theory assumes that the laser beam expansion lens focusses through a single point this is in fact not the case. The focussing occurs over a measurable distance so that a spot of finite size is produced, with the consequence that when collimation is attempted on the light close to the central axis, light close to the edge of the beam is slightly convergent.

The effect of this in the case of the extreme attitude sensing system is that as a model approaches the end of one of the beams used to illuminate the four main sensors its apparent diameter decreases by an amount up to the equivalent of ten pixels. This is primarily a problem where the edge interpreter algorithms are expecting a change in the model edge to be used

for generating the feedback position/attitude signals. Depending on the direction of motion, the edge corresponding to a light to dark transition either remains in view when it should not, or appears unexpectedly early. This produces a discontinuity in the position attitude signals, most noticeable in the pitch measure during a large rotation. Because of the arrangement of the sensors and their direction of scan, this discontinuity occurs at an angle of attack less than 45^{o} for the two port arrays, and at an angle greater than 45^{o} for the starboard arrays. The exact values depend on the model diameter: for a typical 22mm diameter model, they are 36 degrees and 54 degrees angle of attack.

A partial solution to this problem has been found in arranging the illuminating laser beams not to be positioned centrally on the arrays, but instead in an asymmetric arrangement. The centre of each beam is positioned closer to the start of the array (pixel 1) so that the more uneven, less well collimated portion is beyond this end of the array. The other non-uniform portion of the beam is then illuminating pixels towards the end of the array. This does not cause a problem, since no edge swap-over occurs at these values, and even at 0 degrees or 90 degrees angles of attack the model edges are over 300 pixels from the end of the array for a model of typical diameter. However the non-linearity remains and is evident in the behaviour of the model during very large heave oscillations, when to maintain a constant pitch attitude measure the controller forces a slight waver in the actual pitch attitude at the extremes of the motion. A complete solution would lie in the use of a longer focal length collimation lens producing a wider collimated beam. The influence of the marginal rays would then be reduced. An increase in laser beam power might then also be needed.

With care, the optical system can be set-up so that the edge swap-over process produces a minimal discontinuity, (see for example Figure 7.5). Any minor mis-alignment of the optical components, or the use of incorrect data in the stored position information file can cause defects in motion. These can take the form of a step change (Figure 8.7) or an oscillation depending on whether the edge swap-over occurs too late or too early during a position or attitude change.

8.8 Model Station Keeping Characteristics

The foregoing has pointed out reasons why the accuracy of the position sensing system is poorer than the resolution implied by the inter-diode spacing of the linear arrays. One measure of the quality of model suspension is how closely the measured position and attitude follows the demanded values. This takes account of both the resolution of the sensing system and the ability of the controller, translator and power supplies to respond to the feedback data. It does not show how the optical and other defects affect the accuracy of the sensing system. Nevertheless, the station keeping characteristic is of importance in judging the performance of the MSBS as a whole.

The position and attitude signals generated by the four main sensors have theoretical resolutions which are better than the inter-diode spacing because of the averaging effect of the summing and differing by which they are calculated. Thus for example one unit of the heave attitude measure at 45 degrees angle of attack is equivalent to 0.36 thousandths of an inch in either the sensing system or model based axis systems. This will tend to ameliorate the non-linear effects outlined above, since the latter may be of either sign in direction.

Figures 8.8a to 8.8c show examples of position and attitude traces obtained by recording the decoded position information over a one second period. Three angles of attack are shown: zero degrees, forty five degrees and ninety degrees. In all cases the model is not yawed and is at the datum heave position. The controller in use is model axes based and the theoretical resolution of the position/attitude measure is indicated: note that for the three degrees of freedom in the vertical plane these are dependent on the angle of attack. The data shown are the values of the composite, de-coded signals found as explained in Section 5. Arbitrary offsets have been added to separate the traces as the signals represent the error in each channel, and should, therefore, all be zero. The calibration of these measures in terms of physical units is also indicated.

When a linear regression curve is fitted to each set of data (not shown) the average model position and attitude is found to be with zero error,

as expected, since the integrator stages in the control loops are active. However, almost all the traces show a continuous noise which appears to have both random and cyclical content. The magnitude of the noise on the five channels in terms of units of the position measures is comparable, meaning that in physical units of distance and angle, the actual motions are significantly different. Thus, the motions in the axial direction on Figure 8.8b are of ±5 units, which corresponds to ±5 thousandths of an inch, whilst in the heave direction the same noise of ±5 units corresponds to a variation of ±2.2 thousandths of an inch. The typical deviation on the pitch signal is also about ±5 units, which corresponds at this angle of attack to a deviation of ±0.125 degrees. At nought degrees angle of attack (Figure 8.8a) the pitch attitude signal varies by ±6 units, but this corresponds to an angular change of only ±0.075 degrees.

It is evident that at each angle of attack all the traces with the exception of those generated by the axial sensor show a relationship with peaks and troughs corresponding to the same instant in time. This is to be expected as although the position/attitude signals are independent, in general the same electromagnets are used to respond to any error signal, whether it be real or created through defects in the control system, power supplies etc. Thus noise originating in one control channel will produce changes in electromagnet current which will act on the model in all the degrees of freedom. The noise will feedback and be detected by all the sensors. It appears, however, that this does not happen with the axial channel as the physical magnitude of the error signals in this channel largely swamp the influence of the smaller noise-induced errors on the other control channels.

The ultimate limit of accuracy of position and attitude is that of a single pixel change in signal producing a limit cycle of ±1 pixel. This will only arise with a monotonic shadow edge being viewed by the sensor. For all the reasons outlined previously, and most especially the occurrence of interference fringes of a few pixels width crossing the threshold level of the edge detector, step changes larger than one pixel can be expected over a single program loop. Nevertheless, the trace for the axial channel with the model at ninety degrees shows a deviation of only ± two pixels of the target value over the one second period. The remaining traces show poorer accuracy, but the random content of the signals is very small. The yaw

attitude measure and the lateral slip measure at 45^{o} angle of attack, for example, would be near constant were it not for slight cyclical components which can be seen to echo larger oscillations in the pitch and vertical heave signals.

The frequency of the oscillations in the various degrees of freedom are believed to correspond to the resonant frequencies of the model. In some cases - the 12 Hz oscillation in the axial channel at forty-five degrees angle of attack, for example - the oscillation is sustained and of constant amplitude. In others - for example the four lower traces of Figure 8.8a - the vibration is sometimes excited, but subsequently dies away. These characteristics have been observed in all the degrees of freedom over the full attitude range. The oscillations at ninety degrees angle of attack have the largest magnitude of the three traces, and occur in all the degrees of freedom to a varying extent.

When viewing a model in suspension, however, the vibrations are most noticeable in the pitch and axial control channels. This may be correlated with the poorer resolution of these two positions and attitude measures compared with the remainder: that is, the physical amplitude of the oscillations is a direct function of the sensing system resolution.

However, it is not known whether such vibrations have been present in the previous form of the Southampton MSBS, but were not seen owing to the finer resolution of position and, especially, pitch attitude, or whether instead they are a consequence of the new control algorithms. In particular, the inappropriate selection of values in the stabilisation routines is known to affect suspension characteristics through producing an inadequate phase advance angle at the model's natural frequency. The fact that the recorded oscillations in lateral heave and yaw attitude are not discernable to the naked eye appears to lend credence to the former argument, but against this it may be pointed out that the amplitudes of these oscillations in terms of units of the position measures are generally smaller than the amplitudes of the pitch, axial and vertical heave oscillations. A definitive explanation for the observed vibrations has not, therefore, been found.

8.9 Summary

The optical position sensing system developed for the extreme attitude MSBS has fulfilled its primary role of permitting suspension over a large attitude range. Its accuracy is affected by systematic (vibrational) and random errors which are up to ten times the resolution. Repeatability of position and attitude setting and the display of sensing system information are much improved over the earlier analogue sensing system. Further optimisation of both the physical components and the software is possible. A discussion of the extreme attitude sensing problem in relation to a large magnetic suspension and balance system may be found in Section 11.

CHAPTER 9

ASPECTS OF CONTROL SYSTEM PERFORMANCE

9.1 Empirical Changes to Demand Distribution

Th essential features of the extreme attitude MSBS control system explained in earlier sections have not had to be altered in the light of practical experience apart from the additional algorithms outlined in 7.5. The major features of the demand translator, including the recall of pre-stored data and the linear interpolation to obtain demand distribution and overall loop gain values, have functioned as expected.

However, in order to obtain satisfactory suspension quality - subjectively determined in the form of stiffness and damping - many empirical adjustments of the overall loop gains at particular angles of attack were made. These were to be expected given the approximate nature of the predictive method used to obtain the initial values, as outlined in Section 6.8. In general, alterations to the demand distribution factors have not been required. Exceptions to this have been confined to the forty degree data set for the heave channel in the sensing system axes controller, and in the 70 to 80 degree range for the axial channel for the model axes controller.

In the first of these two cases, the rapid decline in use of the aft upper and forward lower electromagnets in the heave sense shown by Figure 6.5a to occur as a model is rotated from forty to thirty degrees turned out to produce unacceptable transient motions in the axial direction. Although small angle of attack changes of 1 degree could be accomplished, a step change of five degrees or more in this region caused the model to move too far backwards, completely obscuring the axial motion sensor and resulting in a loss of control. A solution was found in putting the demand distribution factor of these two electromagnets to almost zero at forty degrees, and redistributing the heave force demand amongst the remaining electromagnets so that the axial units were more heavily used. The quality of suspension in the forty to fifty degree angle of attack range was not affected.

The problem with the model axes controller at the higher angles of attack was also traced to the demand distribution of the forward lower and aft upper pair of electromagnets. In this case, the values used in the axial channel were found to produce transient couplings to the heave channel in the region where the axial demand factors underwent a sign reversal. A linear interpolation had been performed on the data used at fifty degrees and eighty degrees to obtain the values to be used at sixty and seventy degrees, because as shown by Figure 6.6a, DEMAT was unable to find fully decoupled axial force components at these angles of attack. The distribution thus obtained for sixty degrees proved adequate, but between seventy and eighty degrees, the model appeared neutrally stable in its vertical heave sense, with a slow oscillation occurring. By reducing the proportion of the axial demand output to the forward lower and aft upper electromagnets, and increasing the demand distribution factor for the four lateral electromagnets, acceptable suspension behaviour was obtained. Slight adjustments to the demand factors for ninety degrees angle of attack so as to produce less dramatic changes in demand distribution between 80 degrees and 90 degrees were also made.

It is instructive to note that in both of the problem areas cited, the effect of poor demand distribution in one of the degrees of freedom involved was to worsen the quality of suspension in the other control channel. Examination of the relevant estimates of the force components of the electromagnet group produced by the program FORCE, and shown in Figure 6.4a and 6.4d, shows that in both cases the observed difficulties can be correlated with angles of attack where the force produced by the forward lower/after upper E/M group undergoes a sign change in the particular axis system used. With the original demand distributions used, small changes in angle of attack will have produced large changes in the force produced by the electromagnet group in terms of both magnitude and sign.

The coupling to the other degree of freedom can thus be explained if it is accepted that the decoupled components estimated by DEMAT are unlikely to be exactly mirrored in reality, because of the inherent errors of FORCE mentioned in 2.4. Instead, small cross-couplings between the axial and vertical heave components are always likely to be present in the controller, be it sensing system or model axes based. Normally these are supressed by the corresponding primary components, but where large changes

in demand distribution are occurring, with abrupt changes in electromagnet current, their transient influence will be greater. It is clear that care must be taken in interpreting the predictions of the program DEMAT in such circumstances.

9.2 Behaviour of Position/Attitude Decoupling Algorithms

When compared with existing magnetic suspension systems, the extreme attitude MSBS controller has required careful processing of the input data from the position sensing sub-system to produce separate streams of information for each degree of freedom over the full attitude range. The distinction between sensing system axes, model axes and wind axes has not previously been drawn, as a consequence of the limited attitude range of earlier systems. Two axis systems have been successfully implemented. The initial sensing system based controller was computationally the simplest, but the somewhat artificial definitions of the vertical heave and axial directions are inconvenient from the MSBS user's point of view. The use of model axes is simpler to understand, and the modified control program was readily implemented in place of the original controller.

The two controllers exhibited very similar general suspension characteristics. At the extremes of the attitude range, the purity of motion for step changes in angle of attack appeared better for the model axes controller, but no data has been acquired to confirm this.

The response of the model to forced oscillations in the vertical plane - that is, pitching, vertical heaving and fore-aft motion - is dependent on the angle of attack and the frequency of the oscillation. At low frequencies, relatively pure sinusoidal oscillations may be produced at any angle of attack in either of the axis systems used.

For example, Figure 9.1 shows the recorded response of the model to a user demand for a vertical heave oscillation. The model is at a nominal angle of attack of zero degrees, which is -45 degrees relative to the datum of the sensing system. The model axes based controller is being used, so that a conventional motion in the vertical sense relative to the wind direction should be produced. However, this will be seen by the axial sensor as an

apparent fore-aft motion. If the sensing system axes were used, the controller would not remove this apparent error, so that the model would be forced into a compound motion. This would ensure that the axial sensor would produce a constant output. The model axes controller however, subtracts the deviation of the model in the heave direction from the axial control channel, so that the required model sense heaving results.

Figure 9.1 compares the recorded axial sensor output - as distinct from the axial position measure - with the required output found by multiplying the instantaneous heave position by the appropriate trigonometric function given in Section 5.4. The deviation in angle of attack is also shown.

The axial output can be seen to follow the required trace with acceptable accuracy, although the amplitude of the oscillation is slightly too small, and a systematic defect of unknown origin is visible around the maxima of the oscillations. The pitch attitude measure shows no systematic form: the maximum deviation of ± 0.2 degrees is slightly poorer than for a static model at the same attitude. Similar behaviour has been noted at the other extreme of the attitude range.

The response shown is not repeated as the frequency of oscillation is increased. Instead, the achieved axial deviation becomes progressively less than that required, and at frequencies beyond 10 Hertz the motion decays into the heave motion which would be produced by the sensing system axes controller. Such behaviour is also noted with pitching oscillations, so that at high frequencies, the rotations are coupled with fore-aft translations.

An explanation for this characteristic can be deduced by noting that the resultant amplitude of oscillation in response to a constant magnitude user input is not constant if the frequency is altered. As the frequency of oscillation is increased, the action of the stabilisation algorithms progressively reduces the amplitude, so that motions of several millimetres at 1 Hertz or so will be barely perceptible at 10 Hertz if the user does not increase the value of the input amplitude. The decoupling quantities which are subtracted from the axial channel in the model axes controller are very similar to the sinusoidal offsets used by the model oscillator, and will be subject to the same frequency response. Thus, the phase advanced error

signal in the axial channel is progressively less affected by the decoupling signal emanating from the pitch and heave channels as the frequency of oscillation in these degrees of freedom is increased.

To overcome this difficulty, the amplitude - frequency relationship for sinusoidal oscillations would have to be determined over the range of interest. The information thus obtained could then be stored in the control program, and used to adjust the decoupling factors by which the pitch attitude and heave errors are multiplied before being subtracted from the axial channel data stream. The effect of inadequate decoupling with increasing frequency could then be compensated for. The by-product of also having calibrated amplitudes for user-demanded oscillations would be beneficial.

The relative ease with which two axis systems for the extreme attitude MSBS controller were used raises the possibility that the third option outlined in Section 5.2, that of using wind tunnel axes, could be implemented successfully. This has not been attempted, but it is felt that the advantage to the MSBS of having fixed definitions of the vertical heave ('lift') and axial ('drag') senses makes this an attractive option.

9.3 Force Calibrations: an Introduction

Force and moment calibrations are performed with an MSBS for the primary reason of determining the relationship between the aerodynamic forces acting on a model in suspension and the electromagnet currents which produce magnetic forces to oppose them. For such calibrations to be of value, they must be performed to a high accuracy and repeatability: better than one per cent error would be desirable. The large attitude range of the modified Southampton MSBS results in a multiplicity of possible test conditions for which such measurements could be performed. In the absence to date of a specific application for the system, high precision calibrations have not been carried out.

However, the selection of demand distribution factors through the program DEMAT was shown in Section 6.5 to be dependent on the predictions of the program FORCE. These predictions were adjusted by multiplying

factors to take account of the measured capability of the earlier form of the MSBS at a limited number of specific points. A second reason for carrying out force calibrations with the extreme attitude MSBS is therefore to confirm the validity of these correction factors. A greater error can be accepted for these measurements; a confirmation of the trend of the predictions is adequate.

In the next section calibrations of sideforce over a ninety degree attitude range are reported, whilst the one which follows describes a vertical force calibration of a model in suspension at ninety degrees angle of attack.

9.4 A Calibration of Sideforce

As outlined in 3.1, the only obstacle to using the previous arrangement of the ten electromagnets of the Southampton MSBS lay in its inability to generate sideforce at the upper end of the desired extreme attitude range. It is valuable, therefore, to determine whether the simple modification made - that of skewing the four lateral electromagnets - produced the anticipated effect of altering the sideforce capability as suggested by Figure 3.7. The fact that suspension to ninety degrees angle of attack and beyond was achieved confirms that some sideforce is available at these extreme attitudes, but does not provide information as to the form of the sideforce distribution over the full attitude range. Thus a sideforce calibration was performed at ten degree intervals from nought to ninety degrees angle of attack.

The model used had an Alnico core four inches in length with a 15mm diameter; that is, the same dimensions assumed in the estimates of Section 3. The core was surrounded by a non-magnetic shell giving a total mass of 199g. Loads were applied to the model by adding weights to a loading pan attached to the mid-point of the magnetised portion by a lightweight thread, and hung over a low friction pulley. The pulley was mounted outside of the MSBS between the two starboard lateral electromagnets. Figure 9.2 illustrates the arrangement.

As this 'static calibration' technique is known through previous experience to achieve acceptable accuracy with only a limited number of

increments in weight, a four point calibration was used, incuding a tare measurement with the unloaded pan and thread.

The MSBS control program was modified to record the instantaneous currents in the four lateral electromagnets; that is, the units employed to produce a sideforce. Reference 27 suggests that 50 samples of current are adequate for such calibrations, but the storage of 100 samples, corresponding to a 0.41 second period, was felt to improve the quality of data.

Figures 9.3a to 9.3j show plots of the averaged current data for each electromagnet at the four test points over the ten increments in angle of attack. In each case a least squares straight line fit had been applied to the data, and for electromagnets four and six the sign of the currents has been reversed so that the gradients are all positive. The sum of the four electromagnet currents has been added and the gradient of this line is indicated. Note that, because at zero applied load the lateral electromagnets are opposing the weight of the pan and thread, the summed current lines do not pass through the origin.

9.5 Sources of Variation in Lateral Electromagnet Response to Sideforce Loading

The data shows good linearity with the limited number of test points. Some of the plots - for example those for ten and twenty degrees angle of attack show a significant difference between the gradients for the two diagonal pairs of lateral electromagnets. Two contributory reasons are suggested for this. Firstly the four lateral electromagnets are used to produce vertical heave and axial forces upon the model, but with the same polarity for each unit, unlike the differing polarities used for sideforce generation. Thus, if owing to mis-alignment of the thread and pulley, some of the applied load acts in one of these other directions, the control system will respond by adjusting the currents in the lateral electromagnets for this component in addition to the desired sideforce. Greater care in repeat calibrations could eliminate this.

The second cause of the differing gradients is thought to lie in the lower gain of the electromagnet power supplies close to zero current. This

was described in Reference 41 and would result in the pair of electromagnets operating in this range producing less than the desired current, and therefore force. The remaining pair of electromagnets compensate by producing more force, requiring greater current and giving rise to a steeper gradient.

The influence of the non-linear power supply response close to zero current is believed to be a significant factor reducing the quality of suspension with the extreme attitude MSBS. This is because the electromagnets are being used simultaneously to produce several force and moment components, resulting in widely differing current levels, even within one of the groups used in the demand distribution calculations. Thus, unexpected cross couplings may arise owing to the inadequate response of those electromagnets operating near zero current.

Evidence of these effects was provided during the conversion of the MSBS controller from operation in sensing system axes to model axes. In the former case, the demand distribution of the forces in the vertical plane was such that the lateral electromagnets were contributing a significant proportion of the force opposing the model's weight around zero degrees angle of attack, with current levels of around two Amperes. When the model axes controller was introduced, the lateral electromagnets were no longer called upon to fulfil this role at zero degrees, and so had mean current levels of zero Amperes.

However, in both controllers, the four lateral electromagnets were employed for sideforce and yawing torque generation, with a fixed demand distribution. It was found that the stiffness in these degrees of freedom was less for the model axes controller than for the original system, necessitating an increase in the overall loop gains to compensate. This was presumed to be a consequence of the lower power supply gains around the zero current level. The influence of the power supply non-linearity is discussed further below.

9.6 Overall Sideforce Capability

By dividing the gradients of the summed current lines into the available current in the four lateral electromagnets, the maximum sideforce capability at each angle of attack may be estimated. Figure 9.4 shows the

resulting plot of sideforce against angle of attack and compares it with the predictions of Section 3.3. It is again emphasised that both sets of data assume that the lateral electromagnets are not being used in generating any of the other force or moment components. Thus for example, at ninety degrees angle of attack, and using the model axis controller, the model used requires about ten Amperes in each of the lateral E/Ms to oppose its 2 Newton weight: thus only about one Newton of sideforce is actually available.

The experimental data shows remarkable agreement with the values produced by FORCE with allowance for the empirical corrections of 3.4. This can only be regarded as fortuitous given that FORCE assumes a constant model magnetisation of 1 Tesla, whereas the Alnico core used will have an uneven distribution of magnetisation which may on average be up to about 1.2 Tesla. It is known that in the demagnetising fields of the MSBS, Alnico magnetisation tends to fall, so that a lower value of around 1 Tesla is likely after a period in suspension.

More significant than the absolute values of the sideforce measured is the confirmation of the sideforce distribution with angle of attack predicted by FORCE. This gives encouragement that the force and moment relationships with angle of attack assumed for the other degrees of freedom may be correct. In turn, greater reliance may be placed on the demand distributions produced by the program DEMAT.

9.7 Vertical Force Calibration at Ninety Degrees Angle of Attack

The calibration of forces in the vertical plane of the modified Southampton MSBS is considerably more complicated than with earlier conventional MSBSs, because at various angles of attack all the electromagnets are employed in generating the two force components. Thus a series of force - current relationships exists with differing gradients which are characteristic of the demand distribution in use at the particular angle of attack. In addition, choosing the directions in which the calibrations are to be performed is as much a problem as is deciding on the axis system used by the controller. The sensing system axes used in the original controller are

certainly of no interest to the aerodynamicist, whilst the model axes are probably less useful than wind axes.

Thus, if the primary purpose of the calibrations is in the MSBS's intended role of aerodynamic data acquisition, then whatever axis system is used in the controller, the force calibrations should be performed in the conventional lift and drag senses. However, to investigate the operation of the demand distribution process, it is more informative to perform the calibrations in the axes in which the controller is (intended to be) decoupled.

As an example of this, a calibration of the vertical force capability of the extreme attitude MSBS was performed with the model suspended at ninety degrees angle of attack. The model axes based controller was used, so that the forces measured were in the axial sense. This angle of attack was used as it is simple to apply forces to the model without recourse to complex loading rigs used in high precision work (e.g. 27). In addition it demonstrates the unique capability of the Southampton MSBS. The model used was the same as for the sideforce measurements.

The method used to add loads to the model consisted of fixing aluminium and brass rings of various weights to the mid-point of its length. The MSBS control program was modified to store on command the currents in all ten electromagnets. As in the sideforce calibration, 100 samples (that is, 100 program loops) of data were acquired for each loading point. The resulting averaged currents are plotted in Figures 9.5a to 9.5d. The gradients of the summed current lines for each electromagnet group are also shown.

In evaluating this data, it is useful to note the values of the demand distribution factors in use at this angle of attack, as they are slightly different from those plotted in Figure 6.6, owing to the empirical changes mentioned above. They are:

E/M group 1	
(Forward lower/aft upper)	0.502
E/M group 2	
(forward upper/aft lower)	1.388

E/M group 3 (laterals)	-1.78
E/M group 4 (axials)	0.33

It would be anticipated that the summed current gradients of the four electromagnet groups would be in the proportions implied by the above factors. Consider first the four lateral electromagnets and the two axial electromagnets. The relevant demand distribution factors above are in the ratio 5.4. The summed current gradients are 20.6 A/N and 1.61 A/N respectively. However, the fact that the one group has twice as many electromagnets as the other means that an additional multiplying factor of two must be taken account of, so that the experimental ratios in demand distribution is 6.4.

It should be noted that the current ratios demanded by the control program are completely independent of the actual force capabilities of the electromagnet groups and the assumptions made by the programe FORCE. Thus, even if one electromagnet group actually produced none of the expected force, the ratio of its summed current gradient to that of the other groups would be in accordance with the ratios of the demand distribution factors, although the remaining electromagnet groups would have to be used to a greater extent to make up the missing force, and cross couplings to other degrees of freedom might exist. The fact that this is not the case can only be explained by the fact that the power supplies do not convert the demands output by the controller into electromagnet current correctly. Once again, therefore, the errors are believed to be related to the non-linearity of the power supplies close to zero current.

Figure 9.6 reproduces Figure 5.2 of Reference 41 in order to show that in the region where the axial electromagnets are operating at about one Ampere, the demanded current will be perhaps fifty per cent greater. The approximately ten Ampere current in the lateral electromagnets will not, however, be very different from that requested by the controller. Thus the effective demand distribution factor of the axial electromagnets is less than

intended. To compensate, the other electromagnet groups will be used to a greater extent than anticipated.

The situation with the four vertical electromagnets is even more complex. It might be expected that the electromagnets within each of the two diagonal groups would have approximately the same current, and that the resulting pair of summed current gradients would be in the same proportion as the corresponding demand distribution factors. Examination of the graphs shows that this is not the case. Instead, there is a noticeable difference in both gradient and magnitude of the four lines.

The discrepancy in the currents within each of the electromagnet groups is a consequence of the constant demand for a pitching torque output to the four vertical electromagnets. This arises through the action of the error integration step of the control loop, without which the model would not suspend correctly at ninety degrees angle of attack. Examination of the data streams within the control program confirms that, with no user input offset to the axial or vertical heave position, the current demand signal output to the electromagnets within each of the two groups is identical. Offsets appear only as a consequence of the integrated pitch attitude demand. The difference between the currents in the forward upper E/M and the aft lower E/M and that between the forward lower E/M and the aft upper E/M is comparable over the range of vertical force loadings.

The effect of such large integrated error signals will not have been noted with previous MSBSs owing to their far smaller attitude ranges.

Taking into account the current offsets for the pitching moment, the form of the vertical electromagnet current traces should therefore be of pairs of lines with a constant separation, provided that the loads do not change the moment of inertia and thus give an unchanged integrated pitch signal) and that constant gain power supply response can be assumed. As both conditions are not met, because of the added mass of the loading rings and because the aft upper electromagnet is operating in the reduced-gain region close to zero current the divergence of the current lines results.

An attempt to determine the relative significance of the two influences on the calibration is not considered worthwhile, as means of

eliminating both difficulties exist, at least in principle. The technique of applying loads to a model via a mass-spring system does not alter the model's mass, and with the aid of a suitable rig, it could eliminate changes to its radius of gyration also. A means has been proposed and, to a limited extent, tested to eliminate the irregularity in the power supply response (41). This involves using a correction algorithm in the output stage of the computer control program to linearise the gain. The exploratory work described here suggests that both refinements would be valuable.

Despite its faults, the calibration described is useful in indicating the techniques required in demand distributed MSBS where the various electromagnets have differing relationships with applied load. The maximum possible force or torque in a particular degree of freedom, for example, is detrmined by the electromagnet group with the steepest current versus load characteristic. In the case of the axial force at ninety degrees angle of attack, the relevant electromagnet group is number three; the laterals. With a gradient of 20.6 A/N, and a total of 80 Amperes available in the four units, the maximum force available is 3.88 Newtons. Using the demand distribution factors as above, and the force component predictions of Figure 6.6, the predicted maximum (model sense) axial force is 3.55 N; that is, 5 per cent less than the measured value. Given the poor quality of the experimental technique, and the likely error in the prediction program FORCE, including the unknown magnetisation of the model, this is felt to be an acceptable result.

The force per unit current characteristic of the axial channel at any attitude determines the selection of the overall loop gains in the controller. This quantity is the change in total force produced by the MSBS in response to a unit change in current in each of the electromagnet groups, and is only valid up to the point where the most used electromagnet group reaches its system limited value. It may be deduced from the experimental data by summing the reciprocal of the gradients of all the current against force relationships and dividing by the number of electromagnet groups (four).

For the experimental data, this is found to be 0.358 N/A at ninety degrees angle of attack.

9.8 Use of an Extreme Attitude Magnetic Suspension System as a Force Balance

The conventional calibration of an MSBS involves the application of known loads to a suspended model in various clearly defined directions. With good experimental technique, cross couplings to other degrees of freedom may be minimised and a high degree of accuracy has been demonstrated (27). Much of the practical use of MSBSs to date has involved axisymmetric models at zero degrees angle of attack and yaw. In these circumstances, the aerodynamic forces can be easily deduced from measured electromagnet current data.

However, in considering the use of an MSBS capable of suspending models of arbitrary aerodynamic characteristics over large attitude ranges, the calibration problem becomes more complicated. Firstly, a calibration must be performed in the senses required at every attitude of interest, because of the changing demand distributions. Thus, in the case of the Southampton system, calibrations would be needed for every angle of attack. These could be obtained via a static loading technique, requiring a complex rig, especially if a model axis controller is in use. Alternatively, the use of the potentially quicker dynamic calibration technique would be advantageous and the use of a strain gauge balance has also been investgated (42).

During aerodynamic testing, current data for all the electromagnets would be required, and subsequently analysis would have to separate the various force and moment components called upon to oppose the aerodynamic forces. This would rely on knowledge of the demand distribution.

If several electromagnet groups are used to generate a component of interest, it is not essential to then analyse the data for each group; data from one set is sufficient to relate the currents used to the force or moment which was produced. However, all the currents within the particular group selected must be known, in order that, through summing and differencing in accordance with the demand distribution factors in use at the particular attitude, the force and moment component of interest may be isolated from the other components which the electromagnet group may have been generating.

The foregoing assumes that all the electromagnets have identical linear responses to demand so that the generation of one force or moment component by a particular electromagnet is not affected by the generation of different components by the same electromagnet. This would be an essential feature of a large MSBS, but has been shown above not to apply with the Southampton MSBS because of the non-linearity of response of the power supplies to demand.

However, if the power supplies have the ideal characteristics required, it is not necessary to measure the electromagnet currents directly, either in the calibration process or in aerodynamic testing. This is because the currents produced would be proportional to the demand signals within the control computer. If a force/moment calibration is performed in the axis system in which the controller operates, the demand signals produced by the stabilisation algorithms (including the integrator stage) for each degree of freedom will be proportional to the resulting force or moment. Thus the demand rather than the current itself can be measured and related to the applied calibration loads.

During experimental testing, the same demand signals for each degree of freedom may be recorded and easily related to the separate force and moment components: there is no need to take account of the demand distributions because the information recorded is prior to the demand translator stage of the control program. This would ease the task of the experimental aerodynamicist, since knowledge of the demand distribution process would not be required. The need for input/output data exchange from current shunts in the electromagnets to the control computer - presently used with the Southampton MSBS - would in principle be eliminated, although confirmation of the assumed power supply characteristics would be needed. Further evaluation of this calibration technique is required to be sure of its validity. Notice that this approach should apply equally well to the dynamic calibration technique, which has the great potential benefit of being more rapidly performed than static calibration. This is particularly important given the large number of possible model position and attitudes with an extreme attitude MSBS.

9.9 Summary

The principle of using linear interpolation on data pre-stored in the MSBS control program has proven an adequate way of taking account of the changing relationship between the electromagnets and the magnetically suspended model. In static or near D.C. conditions, the decoupling algorithms, intended to ensure that separated position and attitude signals are produced, function correctly. As the rate of motion is increased, the decoupling becomes ineffective, but the behaviour is (in principle) analytic and could be improved.

The sideforce calibration confirms that the trend of force capability predicted by Section 3.3, implying that FORCE may be used over large attitude ranges to estimate the force/moment capabilities of an MSBS. The vertical force calibration has shown that if the demand distribution algorithms are to be relied on, the irregularity in power supply response of the Southampton MSBS should be removed. A vertical force capability approximately equal to twice the weight of a typical model has been demonstrated at ninety degrees angle of attack.

CHAPTER 10

A STUDY OF THE EXTREME ATTITUDE CAPABILITY OF A DESIGN FOR A LARGE MAGNETIC SUSPENSION AND BALANCE SYSTEM

10.1 Introduction

The work in this thesis has shown how, with certain modifications, an existing MSBS could be used for extreme attitude suspension. It is beyond the scope of this report to suggest an optimum arrangement of electromagnets for any given attitude range requirement. This chapter, however, applies some of the principles which have been introduced to an existing design study for a large magnetic suspension and balance systems (LMSBS) in order to investigate its potential for extreme attitude suspension. References 21 and 51 report the results of a study by Madison Magnetics Incorporated (MMI) into the design of a large MSBS capable of controlling a wind tunnel model in six degrees of freedom (i.e. including roll) over an attitude range of $\pm 30^{o}$ in pitch, and $\pm 10^{o}$ in yaw. The resulting arrangement of fourteeen electromagnets meets a specified force and moment requirement based on the use of an advanced superconducting solenoid model core, and neodymium-iron-boron wing magnets for roll torque generation.

Examination of the electromagnet arrangement (Figure 10.1) suggests that it is capable of producing all the forces and moments needed for control of a model over a far larger range of attitudes than assumed in the specification. Its arrangement of eight symmetrically disposed main electromagnets plus two axial E/Ms is similar to SUMSBS at the outset of the work reported here. In addition it has four large 'saddle' electromagnets for roll torque generation. It should therefore be capable of suspending an axisymmetric model up to 60^{o}, in the positive or negative sense (as was SUMSBS), although the force and moment capabilities at the extremes may of course be significantly reduced compared with those at the design attitudes. Fortuitously, however, the four roll control electromagnets are ideally arranged to produce an H_{yz} field gradient around 90^{o} angle of attack, thus removing the obstacle to suspension and control of an axisymmetric model at

these attitudes. Further, the four lateral E/Ms are in principle able to produce a rolling torque on the magnetised wings of the baseline model.

It thus appears worth determining whether the electromagnet system is capable of suspending and controlling a model in six degrees of freedom over a ninety degree attitude range. Since the electromagnet configuration is fully symmetric - unlike the modified version of SUMSBS - it should then be capable not only of a $\pm 90^{o}$ angle of attack range, but of allowing a full 360^{o} rotation in the vertical plane.

This statement is subject to several conditions which include that:

1) all E/Ms are capable of independent bipolar operation

2) suitable demand distributions can be generated

3) evidence can be found that the resulting force/moment capability is adequate when compared with the likely aerodynamic loads

4) a position sensing system commensurate with such extreme motions can be designed.

Using the programs FORCE and DEMAT, together with published data on the MSBS design, the second of these areas is considered here.

10.2 Modelling of MMI Large MSBS Design

In order to investigate the extreme attitude capability of the Madison Magnetics MSBS design, a suitable computer model of the electromagnet configuration is required.

Three distinct electromagnet types are used in the design. These were simulated using the existing options of FORCE (Reference 28). For completeness, the detailed input values are listed in Appendix D. The eight main solenoidal E/Ms, along with the two axial solenoidal E/Ms were represented using the 'pseudo-circular' option, in which the overall dimensions and location of the electromagnets are input. Each E/M is then split into segments, twelve in number, each being replaced by a single straight line

wire element. The four saddle electromagnets are modelled by single wire loops made up of eight straight line elements.

The proposed model core is a superconducting solenoid with a holmium core. This has a far higher magnetisation than either a permanent magnet or magnetised soft iron. Its internal dimensions are 0.75m long by 0.0635m diameter. To simulate it using FORCE, in which the model is a 1 Tesla permanent magnet, it is necessary to use a scaling factor by which the actual number of Ampere-turns for each electromagnet is multiplied. Using the model pole-strength data of Table III-1 of Reference 51 for a 2.5 inch diameter model, and allowing for the use of a holmium core (21), this scaling factor is 4.12.

The baseline model also features an F16 planform wing with a neodymium-iron-boron wing material. This has an average magnetisation of 1.15 Tesla in the applicable demagnetising field, and is assumed to fill 85% of the wing volume, the rest being support structure. This wing can be modelled by FORCE with certain approximations. In particular, as FORCE assumes a constant thickness wing, we replace the tapered wing of the F16 with an equivalent wing with a reduced span and fixed thickness.

This has the following specification:

semi-span	0.36m
centreline to root distance	0.0635m
magnet root chord	0.242m
taper ratio	0.26
average thickness	0.009m
sweep at mid-chord	20^{o}

wing centred on datum axes of core.

The following table lists the resulting scaled Ampere turns:

E/M set	Ampere-Turns/1000 (actual)	Ampere-Turns/1000 (scaled for correct magnetisation)
8 Main E/Ms	3146	12961
2 Axial E/Ms	5456	22478
4 Roll E/Ms	2640	3036/10877*

10.3 Check Calculations with FORCE

To confirm the accuracy of the FORCE model of the MMI design, the results of calculations are shown below on the force capabilities at the extreme of the design envelope: 30^{o} angle of attack, 10^{o} yaw attitude and 20^{o} roll angle.

Electromagnet group	F_X (N)	F_Y (N)	F_Z (N)
Lift	-5708	12	10626
Drag	12073	1245	3532
Roll	-29	-8980	-3169
Lateral	-1782	9175	111

The projected roll torque is 146 Nm compared to the reference figure of 140 Nm. It should be noted that the MMI data assumes that no cross-coupling occurs between the lift, axial and lateral electromagnets and the magnetised wing. This is not the case for a swept planform, but the force couplings have not been included in the data above.

For each force component, the usable capability is limited by the need to provide torque components and a control margin with the same electromagnets.

---

* for wing and core calculations respectively

Using the data of Table II-5 of Reference 21, these margins are equivalent to force components thus:

F_x (N)	F_y (N)	F_z (N)
-98	-445	-1602

Taking account of the appropriate signs of the cross coupling components, the net force capability in each channel is compared to the data of Reference 21 thus:

Force Component	F_x (N)	F_y (N)	F_z (N)
FORCE prediction	4485	995	9387
Reference data	4180	1380	9091
Ratio	1.07	0.72	1.03

The FORCE predictions thus compare tolerably well with the MMI Reference data, except in the case of the lateral force. This component is, however, dominated by the roll coupling component, and therefore depends on how well the roll electromagnets are modelled by FORCE. Since they are a complex shape but have been represented by only eight straight line elements, the accuracy of the modelling is not expected to be very high. Nevertheless, the FORCE model is considered adequate enough for further use.

One point not immediately evident from the MMI report is that the full lift and drag force component are not available independently: that is, the assumption has been made that the two force components arise simultaneously. Thus the lift force alone at the extreme of the suspension range is less than 6000 N when no contribution arises from the axial electromagnets. By the same token, the possible drag force in the absence of the full lift force is much greater than that specified above. It is felt that

specifying the force and moment capability of an MSBS in terms of independent components is preferable to a description based on the net result of combined loadings.

10.4 Sideforce and Roll Torque Capability of the MMI LMSBS

To investigate the potential of the use of the large MSBS design for extreme attitude suspension, certain simplifying assumptions have been made. First, calculations are only performed for the nought to ninety degree quadrant, since symmetry implies that the results are applicable for 90^{o} - 360^{o}. Further, we do not investigate cross couplings when the model is yawed over the baseline ±10 degree range during extreme angle of attack suspension. It is assumed that as the angle of attack is increased at some incidence between thirty and sixty degrees the electromagnet group used to produce a roll torque (initially the saddle coils) and that used to produce sideforce (the laterals) exchange roles. To determine whether this is possible, consider Figure 10.2, which shows the FORCE-estimated sideforce and roll torque for the two electromagnet groups.

The data shows that the points of equal capability for the two electromagnet groups do not occur at the same angle of attack for the sideforce and roll torque components. This implies that the saddle electromagnets are generally more powerful than the lateral E/Ms. The question then arises as to whether the two force and moment components can be generated independently over the full attitude range by the two groups of electromagnets.

A simple form of demand distribution theory can be applied to determine the correct proportions in which to use the two electromagnet groups to produce the sideforce and rolling moment. Following the notation of Sections 2.3 and 6.4 rationalised to include rolling torque:

$$\begin{pmatrix} F_y' \\ T_x' \end{pmatrix} = (G_2\ G_4) \cdot \begin{pmatrix} K_2 & 0 \\ 0 & K_4 \end{pmatrix} \cdot \begin{pmatrix} e_2 \\ e_4 \end{pmatrix}$$

where subscript 2 is lateral heave; subscript 4 is roll attitude.

and

$$\begin{pmatrix} K_2 & 0 \\ 0 & K_4 \end{pmatrix} = \begin{pmatrix} Y_1' & Y_2' \\ T_{x1}' & T_{x2}' \end{pmatrix} \cdot \begin{pmatrix} DDF1 & DDF3 \\ DDF2 & DDF4 \end{pmatrix}$$

where Y_1', Y_2' and T_{x1}', T_{x2}' are the sideforce and roll torque (model axes) of the two electromagnet groups.

Thus
$$K_2 = Y_1' DDF1 + Y_2' DDF2$$
$$K_4 = T_{x1}' DDF3 + T_{x3}' DDF4$$
$$0 = T_{x1}' DDF1 + T_{x2}' DDF2$$
$$0 = Y_1' DDF3 + Y_2' DDF4$$
$$\rightarrow DDF1 = -(T_{x2}'/T_{x1}')\, DDF2$$
$$\rightarrow DDF3 = -(Y_2'/Y_1')\, DDF4$$

The simple conclusion is that the demand distribution factors of the sideforce channel must be in inverse proportion to the torque capability of the electromagnet groups, and that the DDFs for the roll channel are in inverse proportion to the force capability. By analogy to the demand distribution theory for the forces in the vertical plane, we assume that:

$$|DDF1| + |DDF2| = 2$$

$$|DDF3| + |DDF4| = 2$$

As the two electromagnet groups produce a force and torque component with consistent signs, it is necessary to assume that the demand distribution factors in each degree of freedom for the two groups have opposite signs, to ensure that the couplings are correctly opposed. The problem is then determinate, and values may be assigned to the demand distribution factors and the uncoupled values of K_3 and K_6 calculated. From these, the maximum

force and torque capabilities may be obtained. This process was carried out for ten degree increments, as with the SUMSBS extreme attitude controller. The results are shown in Figures 10.3a to 10.3c.

The not unsurprising conclusion is that at one angle of attack, the force and moment capabilities fall to zero: this occurs at an incidence of 45^{o}. It is thus impossible to suspend a model at this attitude, and at attitudes nearby. Adequate sideforce and rolling torque does exist at 60^{o} and beyond to 120^{o}, but an MSBS with such limited extreme attitude capabilities is not desirable. It should be noted that none of the other electromagnet groups are able to produce either of the two force and moment components without cross-couplings of equally large magnitude. The MSBS design is, however, entirely capable of controlling an axisymmetric model - that is, one unrestrained in roll - over a full 360^{o} degree range, but this would be of far less use than even a 90^{o} degree capability with a roll controlled model.

10.5 Modified Madison Magnetics MSBS Design

It is apparent that to allow the roles of two electromagnets to exchange, without their net capabilities falling to zero at some point, an additional group of E/Ms are needed to offload the first pair. A relatively simple means of adapting the Madison Magnetics design to achieve this is illustrated by Figure 10.4. Each of the saddle electromagnets is split and re-joined at the y-z plane to form a pair of symmetrical electromagnets, eight in total. The argument used is that these can carry out an identical function to the original four saddle E/Ms around nought degrees and (as proposed above) around ninety degrees angle of attack, but that at intermediate angles they can have differing demand distributions so as to minimise the cross couplings.

The options and dimensions used to model these new electromagnets may be found in Appendix D.

For this modified MMI design, the eight saddle E/Ms are split into two groups in order to carry out the demand distributions. Referring to Figure 10.4:

Group 5 nos. 11, 12, 17, 18

Group 6 nos. 13, 14, 15, 16

The estimated sideforce and rolling torque for the two groups is shown in Figures 10.5a and 10.5b. The manner in which one group produces a sideforce of consistent sign and a roll torque which reverses sign, whilst the other group generates a roll torque of consistent sign and a sideforce which reverses sign indicates that it should be possible to independently generate the two components at intermediate angles of attack.

The extra group of electromagnets means that the demand distribution problem is indeterminate, so a simplified version of DEMAT was used to generate demand distribution factors for the two degrees of freedom. As three groups of electromagnets are used, the sum of the magnitudes of the factors is three. The values are shown in Figures 10.6a and 10.6b, whilst Figure 10.7 shows the resulting sideforce and roll torque capability. As was found with the predictions of the vertical forces with SUMSBS, large and abrupt variations in the predicted capabilities of the modified Madison Magnetics design result from the calculations. Empirical changes to determine the sensitivity of the results to slight changes in the assumed force and torque components and the angle of attack at which the calculations are performed might be expected to produce more continuous distributions whose validity at intermediate angles is known. However the important result is obtained that the capability in each degree of freedom does not fall to zero at any angle of attack between zero and ninety degrees (and, by implication, over a full 360^{o} range).

Both the sideforce and roll torque capabilities over the incidence range are as good as or better than those at zero degrees angle of attack. It should be noted that the saddle electromagnets are used for generating both components in the ninety degree range, implying that the full value of the roll torque and sideforce cannot be obtained simultaneously. Nevertheless, the predicted performance is comparable with the LMSBS specifications.

To determine the force capabilities in the vertical plane, DEMAT was used to generate demand distribution data for the forces in the vertical plane using the model of the MSBS design and for the nought to ninety degree

quadrant. To make the data more readily understandable, the decoupling has been carried out in the wind tunnel axes. As discussed in Section 9, it should prove possible to suspend a model using such an axis system if desired. The electromagnet numbering scheme employed is an extension of that used with SUMSBS and is as follows:

Electromagnet Group	Type	E/M numbers in group
1	vertical	1, 7
2	vertical	3, 5
3	lateral	2, 4, 6, 8
4	axial	9, 10
5	saddle	11, 12, 17, 18
6	saddle	13, 14, 15, 16

However, as the lateral and saddle electromagnets are required for sideforce, roll and yaw torque generation, it is assumed that these electromagnets are not available for use in generating any of the components in the vertical plane. Thus once again the sum of the magnitudes of the demand distribution factors is three, instead of four in the case of SUMSBS.

The demand distribution calculations were carried out for ten degree increments, and the resulting data is presented in Figures 10.8a to 10.8c. From this data, the force capability in the two degrees of freedom was calculated and is shown in Figure 10.9. The data suggests a remarkably uniform force capability over the full attitude range, which markedly contrasts with the seemingly similar arrangement of electromagnets of SUMSBS. The reason for this lies in the design of the axial E/Ms, which are much more powerful relative to the other E/Ms in the Madison Magnetics design than are the axial E/Ms of SUMSBS when compared with the iron cored vertical and lateral units.

When comparing these predictions with the point estimates of Reference 21, it is important to note that the decouplings have been carried

out separately (as with SUMSBS) so that, for example, the full values of heave and axial force are not available simultaneously. Also current margins for pitch control or model oscillation are not included.

10.6 Summary

It has been shown that the Madison Magnetics design for a large MSBS is capable of suspending an axisymmetric model over a 360° angle of attack range. It is unable to generate independent sideforce and rolling torque on a non-axisymmetric model at angles of attack around 45° (and 135°, 225° and 315°). However by splitting the four saddle roll electromagnets into eight, it becomes possible to obtain demand distributions which ensure that finite values of the components are available over the full range of attitudes. It remains to be shown whether the resulting capability in the presence of simultaneous sideforce and rolling torque is adequate. With a specification for a high-alpha MSBS the design could be optimised by altering the shape of the saddle electromagnets or the number of Ampere-turns.

The force capabilities in the vertical plane do appear comparable with the stated requirements for the large MSBS. An optimisation process as outlined in Section 6.7, in which a direction for a required resultant of axial and vertical heave forces is specified, would be valuable.

10.7 Extension of Demand Distribution to Arbitrary Attitudes

A further point which can be deduced from the foregoing is that with the symmetrical arrangement of eighteen electromagnets in the modified Madison Magnetics MSBS there is no difference between a 360 degree angle of attack range and a 360° yaw attitude range, at least when considering an axisymmetric model. Although no calculations have been carried out to show that demand distributions can be found, a capability to generate forces and moments at any arbitrary attitude in a full sphere about the system centre exists.

It would no longer be possible to simplify the demand distribution problem for any of the degrees of freedom as has been done for SUMSBS. Instead the process must be performed by taking into account the capability

of each electromagnet to produce a component in each degree of freedom. The only symmetry which exists is for pairs of electromagnets diametrically opposed to each other (as with, for example, with the forward upper and aft lower, the forward lower and aft upper, and the axial electromagnets of SUMSBS and the MMI design). If the eighteen electromagnets of the modified Madison Magnetics MSBS configuration is thus grouped into nine pairs, the demand distribution problem for six degrees of freedom and an arbitrary attitude capability may be presented thus:

$$\begin{pmatrix} F_1 \\ F_2 \\ F_3 \\ T_x \\ T_y \\ T_z \end{pmatrix} = (G_1, G_2 \ldots G_6) \begin{pmatrix} K_1 & & & & & 0 \\ & K_2 & & & & \\ & & K_3 & & & \\ & & & K_4 & & \\ & & & & K_5 & \\ 0 & & & & & K_6 \end{pmatrix} \cdot \begin{pmatrix} e_1 \\ e_2 \\ e_3 \\ e_4 \\ e_5 \\ e_6 \end{pmatrix}$$

where

$$\begin{pmatrix} K_1 & & & & & 0 \\ & K_2 & & & & \\ & & K_3 & & & \\ & & & K_4 & & \\ & & & & K_5 & \\ 0 & & & & & K_6 \end{pmatrix} = \begin{pmatrix} X_1 & X_2 & \ldots & X_6 \\ Y_1 & Y_2 & \ldots & Y_6 \\ Z_1 & Z_2 & \ldots & Z_6 \\ T_{x1} & T_{x2} & \ldots & T_{x6} \\ T_{y1} & T_{y2} & \ldots & T_{y6} \\ T_{z1} & T_{z2} & \ldots & T_{z6} \end{pmatrix} \cdot \begin{pmatrix} DDF1 & DDF10 & \ldots & DDF46 \\ DDF2 & & & \\ DDF3 & & & \\ & & & \\ & & & \\ & & & \\ DDF8 & & & DDF53 \\ DDF9 & DDF18 & \ldots & DDF54 \end{pmatrix}$$

with

$$|DDF1| + |DDF2| + |DDF3| + |DDF4| + |DDF5| + |DDF6|$$

$$+ |DDF7| + |DDF8| + |DDF9| = 9$$

and similarly for the other demand distribution factors.

(Note the rationalisation of the numbering sequence compared to that used in Chapter 6).

The problem of selecting the fifty four demand distribution factors so as to obtain maximised force and moment components is only likely to be solved through numerical methods unless additional constraints are added. If ten degree increments in angle of attack and yaw attitude were to be used in a pre-scheduled translator as with SUMSBS (with no account of roll attitude effects), the calculations would have to be performed in the 0 to 90 degree range of each of the two degree of freedom. The demand distributions for all remaining attitudes could be obtained by symmetry. Nevertheless, 100 sets of the fifty four demand factors would be required, to which must be added the six hundred corresponding overall loop gains. At any general angle of attack or yaw angle within the spherical region of possible attitudes, the values of the demand distribution factors and gains could be obtained by averaging the values obtained by linear interpolation between the four sets of stored data corresponding to the four adjacent pitch/yaw attitude combinations. This represents a formidable but not impossible level of complexity.

CHAPTER 11

DISCUSSION

11.1 Introduction

This chapter attempts to summarise the work reported in earlier sections and to place it into a context of magnetic suspension system technology broader than the specific aim of achieving a ninety degree angle of attack range. Those technical features of relevance only to the particular case of the Southampton MSBS are contrasted with ideas of more general application. Possible improvements to the Southampton system which have not previously been discussed are introduced, along with some concepts that might be applied to a large MSBS.

11.2 Design of Electromagnet Array

The requirement to produce five independent force and moment components on an axially magnetised model over an attitude range from nought to ninety degrees angle of attack led to a simple modification of the Southampton MSBS. However the skewing of the four lateral electromagnets so as to bias the existing sideforce capability in the sense of a positive angle of attack rotation, can only be regarded as an approach of limited application elsewhere. Instead, it is an expedient way of ensuring adequate sideforce over the desired range, without the complexity of using additional electromagnets. The evidence that, by carefully employing an existing electromagnet force prediction program, the effect of a modification to an MSBS can be predicted to an accuracy sufficient for designing a control system is, however, encouraging.

It may be noted that the incorporation of symmetrical skew does not exhaust the possible arrangements of the ten electromagnets of the Southampton MSBS. By asymmetrically skewing the four lateral electromagnets, so that the pair on one side are rotated in the sense of a negative angle of attack, an unlimited angle of attack range with an

axisymmetric model would be made available. If the vertical electromagnets were skewed, an unlimited yaw angle capability could be provided.

In general, an MSBS should be designed from the outset to take account of the full range of attitudes and positions required for aerodynamic testing. For a large scale magnetic suspension and balance system to be useful for the production testing of flight vehicles, the incorporation of full six degree of freedom control is felt to be essential. If extreme attitude suspension is required, whether it be in the yawing or pitching sense, it is highly desirable that roll control should also be included in the control system. A rolling torque could be exerted on a model in the Southampton MSBS over the ninety degree attitude if it were equipped with transversely magnetised wings, as suggested in Section 3.3. However, it is believed that when the cross couplings of the required roll control electromagnet currents acting on the model core are taken into account, the net torque capability would be small. The increase in model dead-weight of perhaps a third would also be significant. No formal calculations have been performed to confirm these suppositions.

The need to minimise cross couplings over a range of attitudes leads to an increasing number of electromagnets in an MSBS design, so that the demand distribution can always be correctly adjusted. Thus in adapting the Madison Magnetics MSBS design for extreme attitude suspension as described in Chapter 10, the number of electromagnets required increased from fourteen to eighteen. This electromagnet array would be very complex from a practical engineering standpoint, but it is extremely flexible in the range of force and moment components which it is able to generate.

It is an important point, however, that if six degree of control of a magnetically suspended model at conventional attitudes is assumed for a large MSBS, then the resulting electromagnet array is already much more complex than those used for any of the previous magnetic suspension systems. The extension to extreme attitude suspension appears to require only a limited further investment. This, of course, assumes that the position sensing system is capable of monitoring the large model motions.

11.3 Position Sensing System

The position sensing system used with the modified Southampton MSBS represents a significant departure from that used previously. Although it is based on the traditional technique of shadow edge detection, the 'digital' nature of the photodiode arrays has been exploited to permit extreme attitude suspension through the use of computer algorithms which permit diametrically opposed model edges to be used for signal generation. This in turn has led to the use of collimated illuminating light beams, permitting the linear calibration of the arrays to be used to create an absolute position measurement system. In practice, the limits to the accuracy of the arrays have been set by the real optical effects of marginal rays, diffraction and interference. Therefore the theoretical accuracy implied by the resolution of the inter-diode spacing has not been achieved.

The range of attitudes and positions which have been demonstrated with the modified Southampton MSBS are larger than for any previous MSBS. These are summarised below:

demonstrated range of model diameters	10 to 22 mm
angle of attack range	-7^{o} to 97^{o}
yaw angle range	$\pm 5^{o}$ over full angle of attack range
model sense heave oscillation amplitude	up to 28 mm for a 22mm diameter model
period for rotation 0 - 90 degrees	1 second
maximum angular rotation rate	over 600 degrees per second

11.4 Possible Features of an Optical Sensing System for a Large MSBS

The optical position sensing system has been shown to suffer from certain limitations, and these have significance in considering the techniques which might be applied to a large MSBS.

Although the present sensing system is only able to suspend models of cylindrical or near-cylindrical shape, the main limitation to suspending models of arbitrary shape is the absence of a roll motion sensor (roll motion sensors have extensively been used with earlier versions of the Southampton MSBS). If it is supposed that such a sensor existed, and that the dimensions of a particular model could be fully described, then in principle it would be possible to predict the sensor outputs for any model position and attitude. Such information could be obtained using modern computer-aided design packages which could carry out far more complex calculations than those performed by the program PIXEL. Thus the effect of wings, fins etc. coming into view of the sensors could be taken into account by the pre-stored sensing system data.

The Photodiode Array Control System is only capable of storing two shadow edge transitions, but it would be possible to design an electronics processing system to cope with any number of transitions. This might allow a particular part of a model (the fuselage, say) to be tracked whilst ignoring edges corresponding to other parts of the model. For simple cylindrical models it is probably possible to calculate the position sensing information in real-time in the control program (in the case of the PDP11/84 used with SUMSBS, by means of truncated series for the geometrical data). However, this would be cumbersome or impossible for models of arbitrary shape.

The foregoing is based on the use of collimated light beams to illuminate the sensors. An improvement to the edge transition signal of such a system could be obtained if an imaging lens were placed in front of the diode array sensors in order to create an image of the shadow at the point where it is created, rather than the diffracted transition at the sensor used at present. This is especially attractive in considering the larger dimensions of relevance to a large MSBS because the sharper edge signals of an imaging

system would suffer less from the problems of non-uniformity mentioned in Section 8.

Alternative means of illuminating diode array sensors have been proposed. These include affixing target shapes on a model and illuminating them with diffuse light (a progression of the ONERA sensing system referred to in Section 4.2). A simple form of this has been used with the NAL MSBS (43). To cope with large attitude excursions, such an approach would require complex signal processing and maintaining the correct illumination could prove difficult. A commercial wind tunnel position measurement system based on the use of self-illuminated targets has been available (44), but the data processing rate is not known.

It would be useful to add a roll motion sensor to the modified version of the Southampton MSBS, even if a roll torque capability were only available over a limited range. To investigate the use of the imaging technique, it is suggested that this should comprise a linear array and lens combination viewing a longitudinal strip on the underside of a magnetically suspended model. Figure 11.1 illustrates the possible arrangement which in principle is capable of operating over the full attitude range of the MSBS.

In considering the arrays themselves, several points may be noted. Two dimensional or area arrays have been proposed for a large MSBS (35). As the particular General Electric CIDs (charge injection devices) suggested are no longer commercially available or manufactured, they cannot be included in a future MSBS design. However, sensor arrays of up to 1024 by 1024 elements at a 11 micrometer spacing are now available, but a major objection to their use in comparison with linear arrays is that for a given level of technology, the frame rate of data from the area arrays will always be several orders of magnitude less than an equivalent system using linear arrays. Most of the pixel data produced by area arrays is superfluous as the model edge or target object will only cover the image over a small portion of the array area. It is felt that the use of area arrays should be unnecessary for the MSBS application.

The technology available for linear arrays has advanced considerably since the Reticon G-series used for the SUMSBS system were introduced.

Inter-diode spacings of 10 m or less are not uncommon, implying a potential for better position and attitude resolution than the 25 μm spacing of the earlier arrays. By improving the dynamic range of the sensors, repititon rates (scanning frequencies) at least ten times faster for a given illumination level have been made available. The longest commercially available array, manufactured by Fairchild Weston, has 6000 pixels at 10 μm spacing. Linear arrays with 10000 pixels or more are foreseen.

Considering the special needs of an extreme attitude sensing system, a simple scale-up of the Southampton system is possible but not attractive. In the absence of focussing lenses - i.e. using a one-to-one ratio of model motion to motion in terms of pixels - the use of 2.4 inch sensors would imply a sensing system, and an MSBS, only slightly larger than the 13 inch system at NASA Langley. Focussing lenses could be employed to allow a larger field of view, at the cost of reduced resolution. This illustrates the fundamental point that with a given maximum length of array and a known angular requirement, the achievable angular resolution is fixed irrespective of the optical installation. The use of sophisticated curve fitting algorithms intended to determine model position to sub-pixel resolution has been investigated (36). However, the increased computation involved and the influence of real optical effects - especially the non-uniformity of diode response - may limit the usefulness of such an approach, although the potential benefits are great.

The maximum possible angular range of a sensing system based on measuring translations of an edge or target relative to the centre of rotation is much less than 180 degrees, because the output signal is a tangent function of angle of attack. An angular sensor based on a target image placed near the centre of rotation could permit unlimited attitude excursions.

Alternative means of improving resolution incude cascading a number of arrays electronically to form a simulation of a much longer array, or to have the arrays physically move along with the model. The former possibility would involve optically splitting the complete field of view of the sensing system, perhaps using optical fibre light guides. It is thought that this has been attempted elsewhere. (Optical fibres have already been employed in an MSBS optical sensing system - 45). The second approach leads to greater

mechanical complexity, with articulated arms rotating the arrays for large changes of attitude, whilst small attitude changes and oscillations could be accommodated by the array length in the usual way. It is suggested that through the advances in robotic technology, such a system may now be feasible. In the long term, the ultimate solution to position sensing for a large MSBS may well lie in miniaturised inertial sensors with telemetry links to the outside of the system. A major potential problem with optical sensors in the transonic regime is deviation in beams and images through changes in the refractive index of air across shock waves (46). Deviations of fractions of a degree would represent significant model position uncertainties with the type of sensing system used with the Southampton MSBS.

The technique of using an alignment fixture placed within the large MSBS test section will certainly be required by an optical sensing system in order to ensure a known frame of reference. This, in fact was proposed in the General Electric design study (35). The use of such a device with the Southampton extreme attitude MSBS has demonstrated the principle. The use of an absolute position sensing system requiring no calibration following set-up is an essential feature of a large MSBS.

11.5 Computer Algorithms for Extreme Attitude Suspension

The modifications made to the existing MSBS control program to permit extreme attitude suspension were in two areas:

(a) position sensing algorithms, and

(b) demand translator algorithms.

Those algorithms which were developed as a consequence of the design of the optical sensing system are largely specific to the Southampton MSBS. However, the importance of defining the axis system in which an extreme attitude controller operates is strongly emphasised. The generation of unique position and attitude signals for an MSBS capable of unlimited attitude suspension would require algorithms capable of accommodating the change over in sign of the attitude error signal at ±180 degrees.

The ineffectiveness of the decoupling algorithms used with the Southampton MSBS at anything other than near D.C. conditions noted in Section 9 could be overcome in a more sophisticated controller. The incorporation of algorithms to linearise the power supply characteristics would also be beneficial.

The demand translator algorithms, designed to take account of the varying interaction between the model and the electromagnets, involve real-time linear interpolation between sets of pre-stored data in order to obtain the correct demand distribution for a given attitude. By carefully defining the problem, a practical means of obtaining the values of the pre-stored data has been obtained which, although only applied to the two forces in the vertical plane of SUMSBS, could be extended to an arbitrary array of electromagnets and any number of degrees of freedom. Knowledge of the force and moment capabilities of the electromagnet array through use of a computer simulation is required to implement this approach.

If a numerical technique is used to generate the demand distribution data, such as the program DEMAT, care must be exercised in using the results, because of the effect of sign changes in electromagnet currents producing transient forces and moments noted in 9.1. Check calculations to assess the sensitivity of the results to small changes in position and attitude and in the force and moment components assumed should be performed. It might be possible to calculate demand distributions for every possible attitude and position and install them in the control system. However, it is felt that the benefit of the slightly improved maximum capabilities which might result when compared with the interpolation approach used with SUMSBS would be outweighed by the added complexity.

11.6 Future MSBS Control Techniques

The work reported here, although involving important changes to the computer control program used to operate the Southampton MSBS, has not altered in any significant way the dynamic stabilisation algorithms used. It is testament to the robust nature of the digitally-simulated phase advance algorithms that they have proved adequate to the task of controlling a wind tunnel model over a ninety degree angle of attack range. They cannot,

however, be regarded as representing the optimum digital control technique for the future (or the present). It is possible that the discontinuities in the traces obtained during large attitude changes (Figures 7.5 and 7.6) may be caused by the controller output saturating, indicating that it is at the limit of its performance. Further experimentation is required to investigate this thoroughly.

Several alternatives have been considered (47, 48), of which the one based on optimal control theory has recently been investigated at Southampton (41). This uses a controller which attempts to minimise a suitable criterion of performance when the system is described in state space form. However, as the states of the system generally cannot be measured directly, it is necessary to obtain them via a simulation of the system: the 'observer'. To take account of possible errors in the modelling, the difference between the estimated system behaviour and the actual system feedback is fed back to the observer to adjust its output.

A simulation of such a controller intended for regulating the vertical heave sense of a model in the Southampton MSBS was created by Thomas (41). A comparison with a model of the existing control system suggested that the new controller would respond at least twice as rapidly to a step change in position, and would offer improved resistance to noise, at the cost of a more complex program. The experimental installation of such a controller with SUMSBS is desirable.

Having been designed and implemented in a control program, the characteristics of such a new controller would be fixed. However, controllers are now being designed and used (49, 50) which are capable of self-tuning (that is, adjusting the parameters in a fixed control law) and of self-adapting (altering the control law itself). Such control technology applied to an MSBS could offer great flexibility in safely accommodating changes in model dynamic characteristics and aerodynamic loads. The increased computational complexity would certainly require parallel processing technology, which may soon be readily available. It seems likely that a large MSBS controller using modern techniques could operate at a lower loop rate than has been used

hitherto, making the design of the sensing system somewhat easier through permitting longer diode integration times.

11.7 Concluding Remarks

The unprecedented attitude range of the modified Southampton MSBS has been achieved through an inter-connected series of modifications, which have followed from the chosen aim of demonstrating a ninety degree angle of attack capability. Although the particular solutions adopted may not all be directly relevant to a large MSBS with extreme attitude capability, the problem areas addressed are. The need to carefully select and implement the axis systems used, the use of an absolute position and attitude sensing system, and the systematic adjustment of the force/moment translator would all be essential features in the design of such a facility. Although the small size of the Southampton MSBS limits the quality of aerodynamic data which can be obtained with this extreme attitude MSBS when operated with the existing low speed wind tunnel, it is felt that the experience gained has proved that an MSBS may be designed and built to meet any chosen attitude range requirement.

CHAPTER 12

PRINCIPAL CONCLUSIONS

An existing magnetic suspension and balance system (MSBS) has been modified to permit suspension of a wind tunel model over an angle of attack range from less than zero degrees angle of attack to over ninety degrees, together with yaw attitude excursions and changes in position comparable with or better than those previously achieved. Axisymmetric models of circular cross-section and arbitrary diameter less than one inch may be accommodated. Models have been suspended up to sixty degrees angle of attack with the MSBS wind tunnel operating at modest speeds (up to Mach 0.1).

The generation of sideforce upon the model using a skewed arrangement of the four lateral electromagnets and over the full attitude range has been verified. This component was absent in the previous arrangement of the ten electromagnets of SUMSBS and prevented suspension close to ninety degrees angle of attack.

An analytical framework has been developed which allows the force and moment components generated by the various electromagnets of the Southampton MSBS to be combined so that the axisymmetric wind tunnel model may be controlled in five separate degrees of freedom over the full angle of attack range. This approach is reliant upon predictions of the force and moment components generated by an existing computer simulation, with attendant sources of error. The technique may be extended to an arbitrary number of electromagnets.

The computer control program which regulates the electromagnet currents of the MSBS has been modified so as to take account of the predicted relationship between the model and the force and moment components, through pre-scheduling the appropriate information to be used at each angle of attack. This permits continuous motions over the full position and attitude range.

Traditional stabilisation algorithms involving the digital simulation of analogue phase-advance networks have proved adequate for the extreme attitude MSBS, with no major changes having been made to those previously used with the Southampton MSBS. The model has been suspended over the full attitude range specified at the outset of the work using controllers operating in either of two differing axis systems. The frequency response characteristics of the stabilistion algorithms have limited the correct decoupling of the position and attitude signals to near direct current conditions.

An optical model position sensing system has been developed commensurate with the desired extreme attitude range, and therefore offering a larger range of possible position and attitudes than any previous MSBS optical sensor. This permits the MSBS user to request known and repeatable changes in position and attitude. The sensing system is subject to optical limitations which prevent the measurement accuracy being equal to the resolution of the sensing system elements.

It is believed that a large magnetic suspension and balance system could be designed capable of generating the independent force and moment components necessary for suspending a roll-controlled model over an unlimited angle of attack range.

LIST OF REFERENCES

1. Tuttle, M.H. and Gloss, B.B.: *SUPPORT INTERFERENCE OF WIND TUNNEL MODELS - A SELECTIVE ANNOTATED BIBLIOGRAPHY*, NASA TM-81909, 1981.

2. Tournier, M. and Laurenceau, P.: *SUSPENSION MAGNETIQUE D'UNE MAQUETTE EN SOUFFLERIE.* La Recherche Aeronautique, no.59, July - August 1957, pp 21-27.

3. Barnwell, R.W., Edwards, C.L.W., Kilgore, R.A. and Dress, D.A.: *OPTIMUM TRANSONIC WIND TUNNEL.* Presented at 14th AIAA Aerodynamic Testing Conference, March 5-7 1986.

4. Boyden, R.P.: *A REVIEW OF MAGNETIC SUSPENSION AND BALANCE SYSTEMS*, AIAA 15th Aerodynamic Testing Conference, May 1988.

5. Dahlen, G.A.: *CONE DRAG IN THE TRANSITION FROM CONTINUUM TO FREE MOLECULAR FLOW.* University of Oxford, Department of Engineering Science Report 1538/84, March 1984.

6. Vyshkov, Iu. D., Koval'nogov, S.A., Usachev, V.N. and Shapovalov, G.K.: *A SYSTEM FOR THE ELECTROMAGNETIC LEVITATION OF MODELS IN A SUBSONIC WIND TUNNEL.* TsAGI, Uchenye Zapiski, vol.17, no.4, 1986, pp 94-97.

7. Martindale, W.R., Butler, R.W. and Starr, R.F.: *STUDY ON NEEDS FOR A MAGNETIC SUSPENSION AND BALANCE SYSTEM OPERATING WITH A TRANSONIC WIND TUNNEL.* NASA CR-3900, 1985.

8. Lynn, N.: *X-31 - BREAKING THE STALL BARRIER.* Flight International, vol. 132, 11th July 1987, pp 27-28.

9. Almosino. D.: *HIGH ANGLE OF ATTACK CALCULATIONS OF THE SUBSONIC VORTEX FLOW ON SLENDER BODIES.* Presented at 21st AIAA Aerospace Sciences Meeting, June 10-13, 1983.

10. Spearman, M.L.: *SUPERSONIC AERODYNAMIC CHARACTERISTICS OF SOME RE-ENTRY CONCEPTS FOR ANGLES OF ATTACK OF UP TO NINETY DEGREES.* Presented at 12th AIAA Atmospheric Flight Mechanics Conference, August 19-21, 1985.

11. Ericsson, L.E. and Reding, J.P.: *DYNAMIC SUPPORT INTERFERENCE IN HIGH ALPHA TESTING.* Journal of Aircraft, Volume 23, December 1986, pp 889-895.

12. Dietz, W.E. and Alstatt, M.C.: *EXPERIMENTAL INVESTIGATION OF SUPPORT INTERFERENCE ON AN OGIVE-CYLINDER AT HIGH INCIDENCE.* Journal of Spacecraft and Rockets, Vol.16, Jan-Feb 1979, pp 67-68.

13. Price, E.A. Jr.: *AN INVESTIGATION OF F-16 NOZZLE AFTERBODY FORCES WITH EMPHASIS ON SUPPORT SYSTEM INTERFERENCE.* AEDC-TR-79-56, AFAPL-TR-2099, Dec. 1979.

14. Seungki Ahn, Kwang-Yoon Choi and Simpson, R.L.: *THE DESIGN AND DEVELOPMENT OF A DYNAMIC PLUNGE-PITCH-ROLL MODEL MOUNT.* Presented at AIAA 27th Aerospace Sciences Meeting, January 9-12, 1989.

15. Tuttle, M.H., Kilgore, R.A., Boyden, R.P.: *MAGNETIC SUSPENSION AND BALANCE SYSTEMS - A SELECTED, ANNOTATED BIBLIOGRAPHY.* NASA TM-84661, July 1983.

16. Covert, E.: *MAGNETIC SUSPENSION AND BALANCE SYSTEMS FOR USE WITH WIND TUNNELS.* Presented at 12th International Congress on Instrumentation in Aerospace Simulation Facilities, June 22-25, 1987.

17. Hamlet, I.L. and Kilgore, R.A.: *SOME ASPECTS OF AN AIR-CORE SINGLE-COIL MAGNETIC SUSPENSION SYSTEM.* In: Summary of ARL Symposium on Magnetic Suspension and Balance Systems. ARL 66-0135, April 1966, pp 109-135.

18. Stephens, T.: *DESIGN, CONSTRUCTION AND EVALUATION OF A MAGNETIC SUSPENSION AND BALANCE SYSTEM FOR WIND TUNNELS.* NASA CR-66903, November 1969.

19. Scudiere, M.B., Willems, R.A. and Gillies, G.T.: *DIGITAL CONTROLLER FOR A MAGNETIC SUSPENSION SYSTEM.* Review of Scientific Instruments, August 1986.

20. Carmichael, A.T., Hinchcliffe, S. and Murgatroyd, P.N.: *MAGNETIC SUSPENSION SYSTEMS WITH DIGITAL CONTROLLERS.* Review of Scientific Instruments, August 1986.

21. Boom, R.W., Eyssa, Y.M., McIntosh, G.E. and Abdelsalam, M.K.: *MAGNETIC SUSPENSION AND BALANCE SYSTEM ADVANCED STUDY.* NASA CR-3937, 1985.

22. Britcher, C.P., Goodyer, M.J., Scurlock, R.G., Wu, Y.Y.: *A FLYING SUPERCONDUCTING MAGNET AND CRYOSTAT FOR MAGNETIC SUSPENSION OF WIND TUNNEL MODELS.* Cryogenics, Vol.24, no.4, April 1984, pp 185-189.

23. Goodyer, M.J.: *THE MAGNETIC SUSPENSION OF WIND TUNNEL MODELS FOR DYNAMIC TESTING.* University of Southampton PhD Thesis, April 1968.

24. Britcher, C.P., Goodyer, M.J., Eskins, J., Parker, D. and Halford, R.J.: *DIGITAL CONTROL OF WIND TUNEL MAGNETIC SUSPENSION AND BALANCE SYSTEMS.* Presented at 12th International Congress on Instrumentation in Aerospace Simulation Facilities, June 22-25, 1987.

25. Newcomb, A.W.: *THE EFFECT OF STING INTERFERENCE AT LOW SPEEDS ON THE DRAG COEFFICIENT OF AN ELLIPDOIDAL BODY USING A MAGNETIC SUSPENSION AND BALANCE SYSTEM.* NASA CR-181611, February 1988.

26. Goodyer, M.J.: *A PRELIMINARY INVESTIGATION OF THE DYNAMIC FORCE CALIBRATION OF A MAGNETIC SUSPENSION AND BALANCE SYSTEM.* NASA CR-172580, May 1985.

27. Eskins, J.: *AN INVESTIGATION INTO FORCE/MOMENT CALIBRATION TECHNIQUES APPLICABLE TO A MAGNETIC SUSPENSION AND BALANCE SYSTEM.* NASA CR-187695, August 1988.

28. Britcher, C.P.: *SOME ASPECTS OF WIND TUNNEL MAGNETIC SUSPENSION SYSTEMS WITH PARTICULAR APPLICATION TO LARGE PHYSICAL SCALES.* University of Southampton PhD Thesis, July 1982. Also NASA CR-172154, September 1983.

29. Parker, D.H. and Britcher, C.P.: *PROGRESS TOWARDS EXTREME ATTITUDE TESTING WITH MAGNETIC SUSPENSION AND BALANCE SYSTEMS.* Presented at AIAA 15th Aerodynamic Testing Confernece, May 18-20, 1988.

30. Stephens, T. and Adams, R.: *WIND TUNNEL SIMULATION OF STORE JETTISON WITH THE AID OF ARTIFICIAL GRAVITY.* MIT TR-174, March 1971. Also NASA CR-1955.

31. Moreau, R., Besson, J., Hoarau, R.: *ELECTRO-OPTICAL DETECTORS FOR MAGNETIC SUSPENSION AND THE STUDY OF FREE MOTION OF MODELS.* Presented at the Second International Symposium on Electro-Magnetic Suspension, University of Southampton, July 12-14, 1971.

32. Altmann, H.: *AN OPTICAL SCANNING DETECTION SYSTEM AND ITS USE WITH A MAGNETIC SUSPENSION SYSTEM FOR LOW DENSITY SPHERE DRAG MEASUREMENTS.* Presented at the Second International Symposium on Electro-Magnetic Suspension, University of Southampton, July 12-14, 1971.

33. Haslam-Jones, T.F. *MEASUREMENTS OF THE DRAG OF SLENDER CONES IN HYPERSONIC FLOW AT LOW REYNOLDS NUMBERS USING A MAGNETIC SUSPENSION AND BALANCE.* Department of Engineering Science Report no.1235/78, University of Oxford, March 1978.

34. Britcher, C.P., Fortescue, P.W., Allcock, G.A. and Goodyer, M.J.: *INVESTIGATION OF THE DESIGN PHILOSOPHIES AND FEATURES APPLICABLE TO LARGE MAGNETIC SUSPENSION AND BALANCE SYSTEMS.* NASA CR-162433, November 1979.

35. Bloom, H.L. et al: *DESIGN CONCEPTS AND COST STUDIES FOR MAGNETIC SUSPENSION AND BALANCE SYSTEMS.* NASA CR-165917, 1982.

36. LaFleur, S.S.: *ADVANCED OPTICAL POSITION SENSORS FOR MAGNETICALLY SUSPENDED WIND TUNNEL MODELS.* Presented at 11th International Congress on Instrumentation in Aeronautical Simulation Facilities, August 1985.

37. Moore, R.H.: *PHOTODIODE ARRAY POSITION SENSING OFA MODEL IN A MAGNETIC SUSPENSION WIND TUNNEL.* University of Southampton, Department of Electronics BSc Project Report, May 1981.

38. Tcheng, P. and Schott, T.D.: *A FIVE COMPONENT ELECTRO-OPTICAL POSITIONING SYSTEM.* Presented at 12th International Congress on Instrumentation in Aerospace Simulation Facilities, June 22-25, 1987.

39. Parker, D.H.: *HIGH ANGLE OF ATTACK POSITION SENSING FOR THE SOUTHAMPTON UNIVERSITY MAGNETIC SUSPENSION AND BALANCE SYSTEM.* NASA CR-178358, August 1987.

40. Ferrari, R.L.: *AN INTRODUCTION TO ELECTROMAGNETIC FIELDS.* Van Nostrand Reinhold, 1975.

41. Thomas, M.J.: *AN OPTIMAL CONTROLLER FOR THE VERTICAL HEAVE CHANNEL OF A MAGNETIC SUSPENSION SYSTEM.* University of Southampton, Department of Aeronautics and Astronautics BSc Project Report, May 1988.

42. Roberts, P.W. and Tcheng, P.: *STRAIN-GAGE BALANCE CALIBRATION OF A MAGNETIC SUSPENSION AND BALANCE SYSTEM.* Presented at 12th IEEE International Congress on Instrumentation in Aerospace Simulation Facilities, 22-25 June 1987.

43. Hideo Sawada, Hiroshi Kanda, Hisashi Suenga: *A POSITION AND ATTITUDE SENSING CAMERA IN NAL'S MSBS.* Magnetic Suspension and Balance Systems Newsletter, Experimental Techniques Branch, NASA Langley, January 1988.

44. Eloptopos: Manufacturers notes, Eloptricon AB, Sweden.

45. Jacobson, I.D., Junkins, J.L. and Jancaitis, J.R.: *DATA ACQUISITION AND REDUCTION FOR THE UVa SUPERCONDUCTING MAGNETIC SUSPENSION AND BALANCE FACILITY.* Presented at the Second International Symposium on Electro-magnetic Suspension, University of Southampton, July 12-14, 1971.

46. Green, J.E.: *OPTICAL MEASUREMENTS OF MODEL ATTITUDE: COMMENT ON EFFECT OF REFRACTION BY DENSITY GRADIENTS IN TUNNEL FLOW.* Contained in European Transonic Windtunnel 2nd Cryogenic Technology Review Meeting, DFVLR, 28-30 June 1988.

47. Baheti, R.S.: *MULTIVARIABLE FREQUENCY DOMAIN CONTROLLER FOR A MAGNETIC SUSPENSION AND BALANCE SYSTEM.* Presented at 21st Conference on Decision and Control, December 8-10, 1982.

48. Masterman, M.J.: *THE DESIGN OF A DIGITAL CONTROLLER FOR A MAGNETIC SUSPENSION SYSTEM USING DIRECT Z-PLANE TECHNIQUES.* University of Southampton, Department of Aeronautics and Astronautics BSc Project Report, April 1983.

49. Saridis, G.N.: *SELF ORGANISING CONTROL OF STOCHASTIC SYSTEMS* - lecture series in control and systems theory, vol.4. Marcel Dekker, 1979.

50. Landau, Y.D.: *ADAPTIVE CONTROL - A MODEL REFERENCE APPROACH* - lecture series in control and systems theory, Vol.8. Marcel Dekker, 1979.

51. Boom, R.W., Eyssa, Y.m., McIntosh, G.E. and Abdelsalam, M.K.: *MAGNETIC SUSPENSION AND BALANCE SYSTEM STUDY.* NASA CR-3802, July 1984.

52. Manufacturers Notes; Image Sensing Products, EG & G Reticon.

53. Hecht, E. and Zajac, A.: *OPTICS.* Addison-Wesley.

LIST OF FIGURES

4.2 principle of ONERA scanning optical sensor

4.3 scanning optical sensing system used with the first Oxford University hypersonic MSBS

4.4 illustrating the arrangement of light beams of the optical sensing system designed for extreme attitude suspension

4.5 illustrating the diamond shaped intersection area of each pair of laser beams illuminating the four main arrays

4.6 relationship between the pitch attitude measure and angle of attack

4.7 an overall view of the Southampton MSBS modified for extreme attitude suspension

4.8 various features of the optical sensing system

4.9 PACS

5.1 a block diagram illustrating the control system used for extreme attitude suspension

5.2 conventional axes used with Southampton MSBS

5.3 possible definitions of vertical heave and axial directions

5.4 showing real and imaginary pixels

5.5 showing change of apparent diameter of model with angle of attack

5.6 edge interpreter logic

5.7 generation of apparent heave position change with pure axial motion in sensing system axes

5.8 generation of apparent axial position signal with change in pitch attitude

5.9 relationship between axial position change and angle of attack

6.1a various pitching torque demand distributions for E/Ms 1 and 7

6.1b various pitching torque demand distributions for E/Ms 3 and 5

6.2a current per unit torque for various demand distributions

6.3 showing effect of change of angle of attack on resultant of lift and drag

6.4 forces in sensing system and model axes

6.5 demand distributions for sensing system axes controller

6.6 demand distributions for model axes controller

6.7 predicted force capability in vertical plane: sensing system axes controller

6.8 predicted force capability in vertical plane: model axes controller

7.1 showing electrical interference on axial sensor output

7.2a early demonstration of suspension at 70^{o} angle of attack

7.2b model at ninety degrees angle of attack

7.3 demonstration model at various angles of attack

7.4 attitude demand-following for a 0 to 90 degrees sweep

7.5 25 to 45 degrees step change in attitude

7.6 25 to 65 degrees step change in attitude

7.7 time history for large amplitude pitching oscillation

7.8 time history for large amplitude heaving oscillation

8.1 partial calibration of channel one photodiode array

8.2 calibration of axial array

8.3 showing how a change in a mirror angle can result in an error in model position and attitude

8.4 illustrating how the irradiance level of an illuminating laser beam can affect the measured width of an object with a fixed transition detector threshold

8.5a video output on channel 1

8.5b video output on channel 2

8.5c video output on channel 3

8.5d video output on channel 4

8.5e video output on channel 5

8.6 video output on channel one expanded to show one edge transition

8.7 attitude demand-following for a 0-90 degree sweep showing a discontinuity caused by sensing system

8.8a position and attitude station keeping - 0^{o}

8.8b position and attitude station keeping - 45^{o}

8.8c position and attitude station keeping - 90^{o}

9.1 position and attitude in response to a demand for a vertical heave oscillation at nought degrees angle of attack

9.2 showing the technique used for sideforce calibration

9.3 sideforce calibration - 0^{o} to 90^{o} angle of attack

9.4 a comparison of predicted and measured amounts of sideforce from the lateral electromagnets

9.5 vertical force calibration

9.6 non-linearity of response of power supplies

10.1 Madison Magnetics Inc. Large MSBS design

10.2a sideforce from lateral electromagnets

10.2b rolling torque from lateral electromagnets

10.3a demand distribution factors for sideforce generation

10.3b demand distribution factors for roll torque generation

10.3c sideforce and roll torque capability of MMI large MSBS design

10.4 suggested modification of MMI large MSBS design

10.5a sources of sideforce - modified design

10.5b sources of roll torque - modified design

10.6a DDFs for sideforce generation - modified design

10.6b DDFs for roll torque generation - modified design

10.7 predicted sideforce and rolling torque of modified design

10.8a DDFs E/Ms 1 and 7

10.8b DDFs E/Ms 3 and 5

10.8c DDFs E/Ms 9 and 10

10.9 predicted axial and heave force capability of modified MMI design

11.1 a possible roll motion sensor for the Southampton MSBS

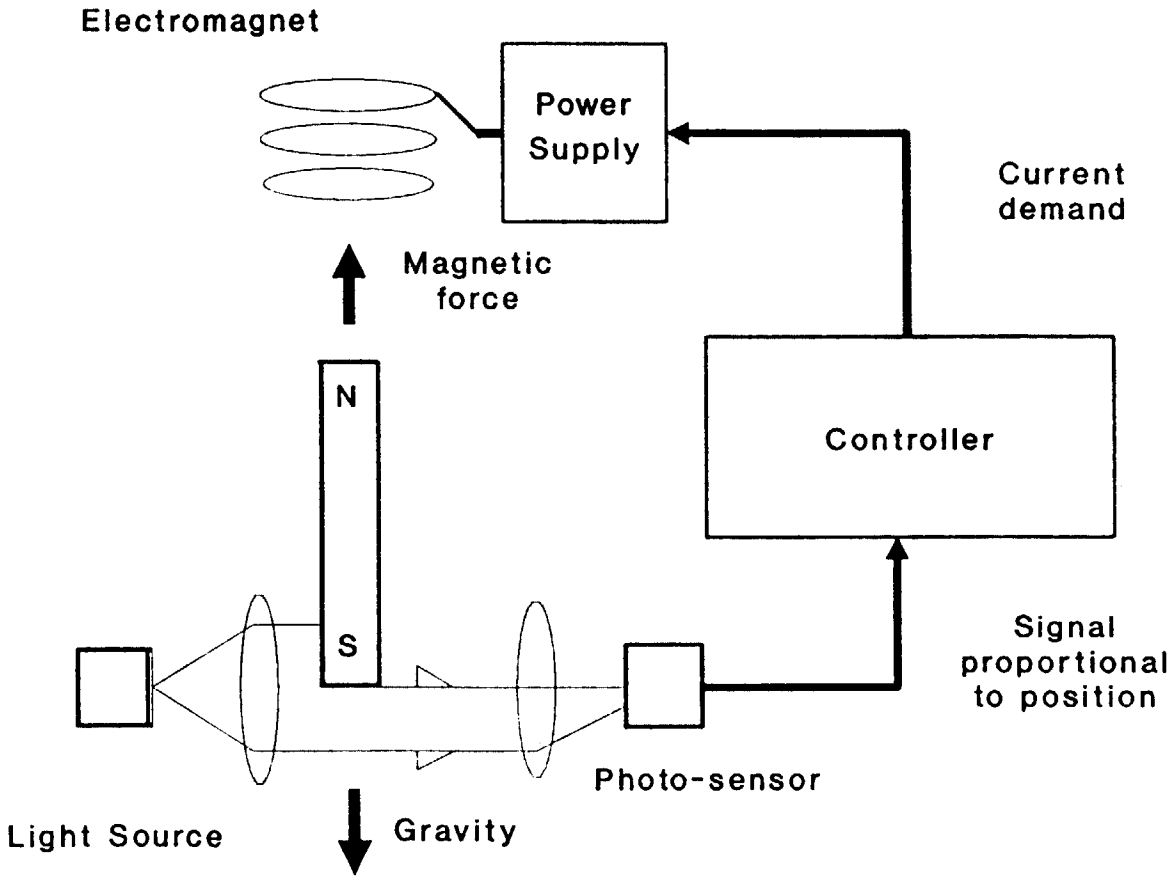

Figure 1.1: one degree-of-freedom MSBS

system uses a traditional optical sensor based on
a beam of light focussed onto a single photo-detector

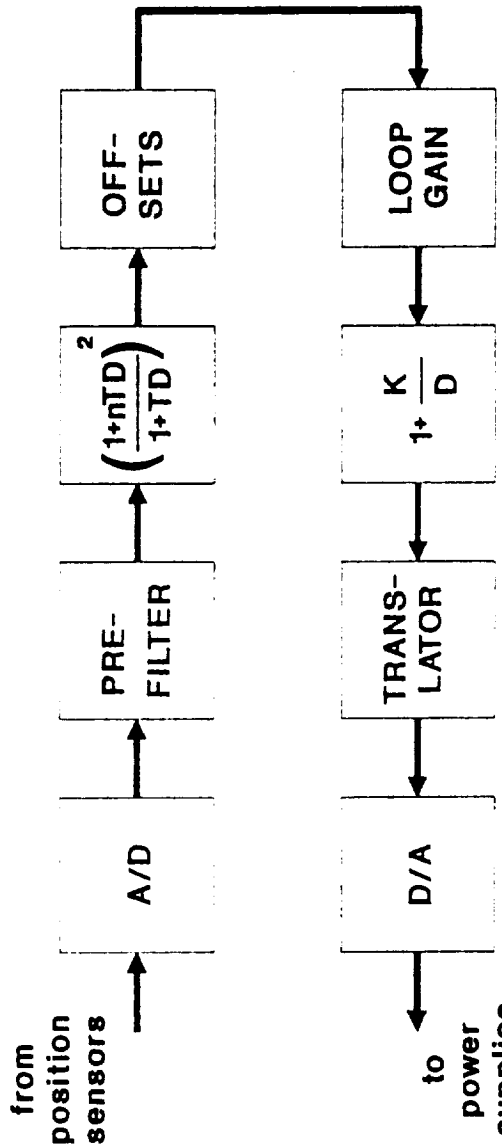

Figure 2.1: a block diagram of the digital controller used with the Southampton MSBS

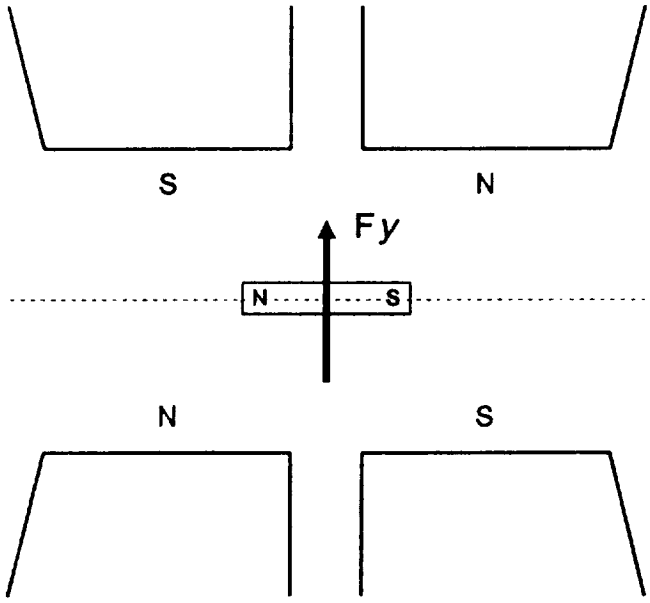

Figure 3.1a: a plan view of the Southampton MSBS showing the generation of sideforce from the action of the four lateral electromagnets on an axially magnetised model at conventional attitudes

model and current assumptions as of section 3.4 in main text

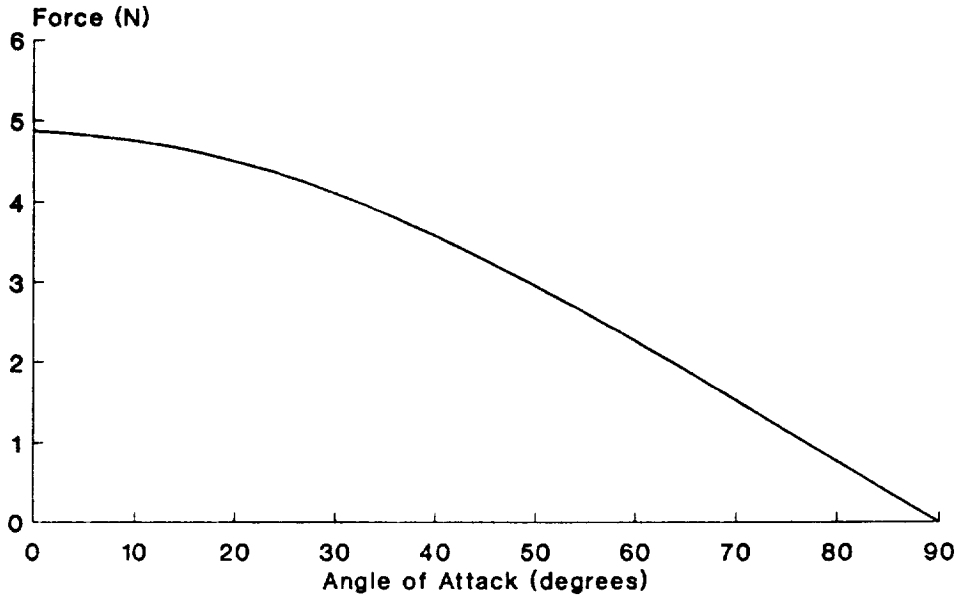

Figure 3.1b: estimated sideforce - un-modified Southampton MSBS

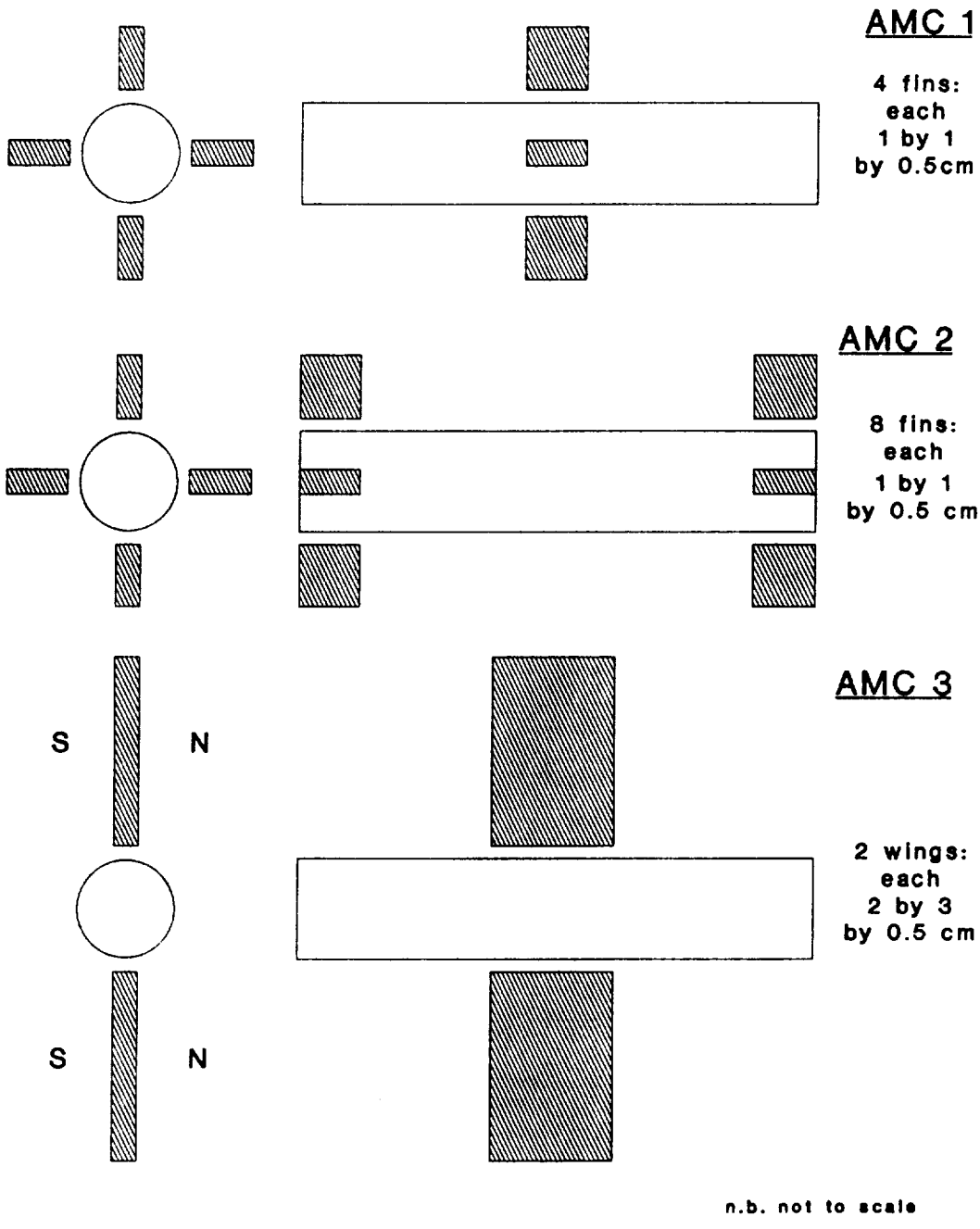

Figure 3.2: Examples of Auxiliary Magnet Configurations
all cores are 4 in long by 16mm diameter

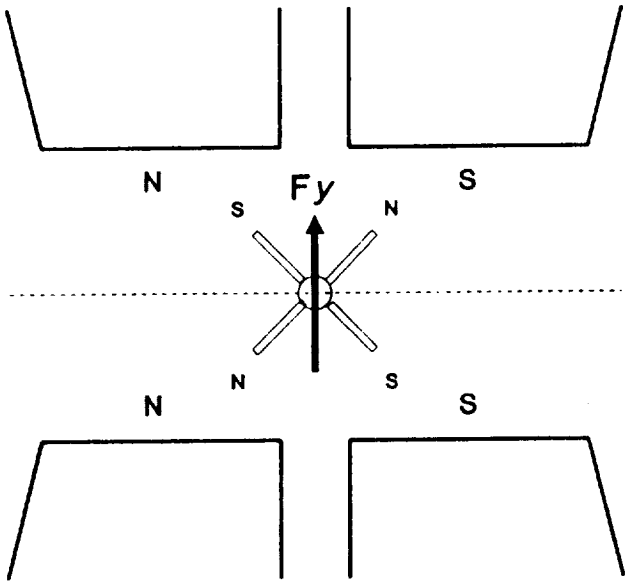

Figure 3.3:

Showing how sideforce may be generated on a model at 90 degrees angle of attack by the action of the lateral electromagnets upon auxiliary model magnets Cruciform fin magnets shown: magnetised wings are similar

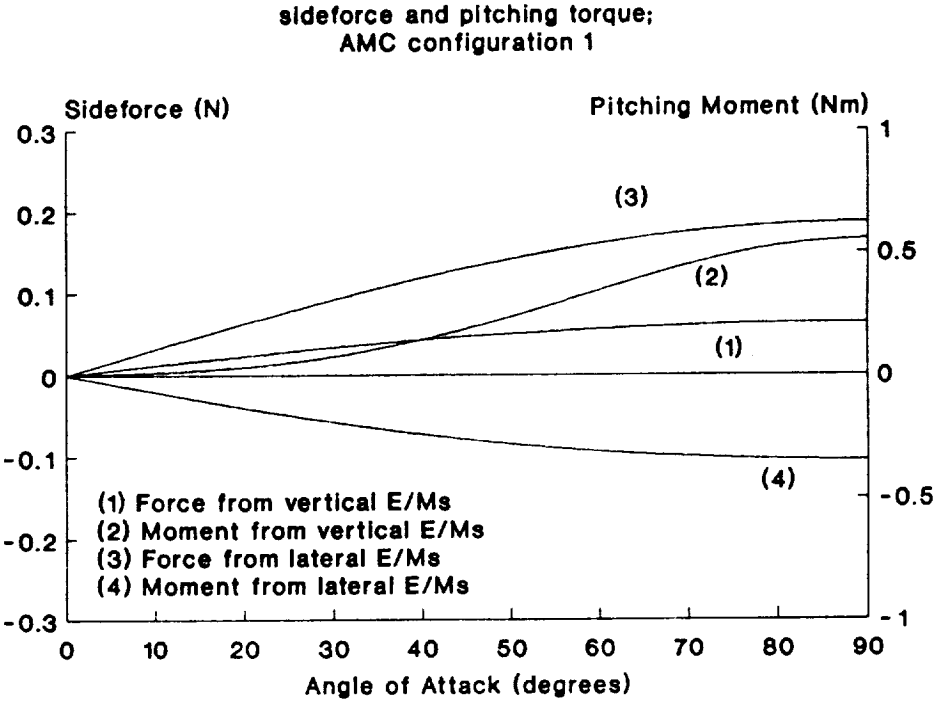

Figure 3.4a

sideforce and pitching torque;
AMC configuration 2

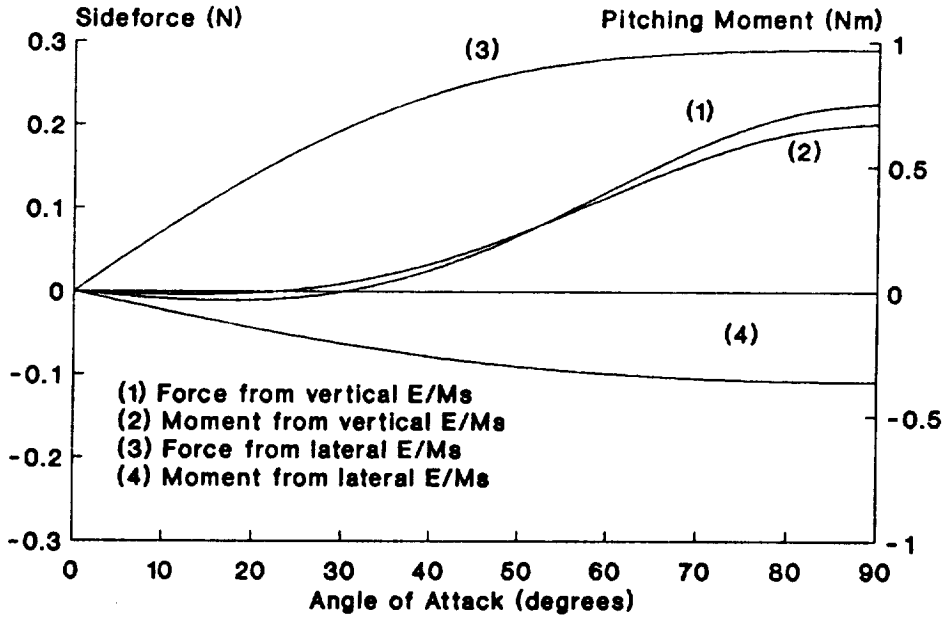

Figure 3.4b

sideforce and pitching torque
AMC configuration 3

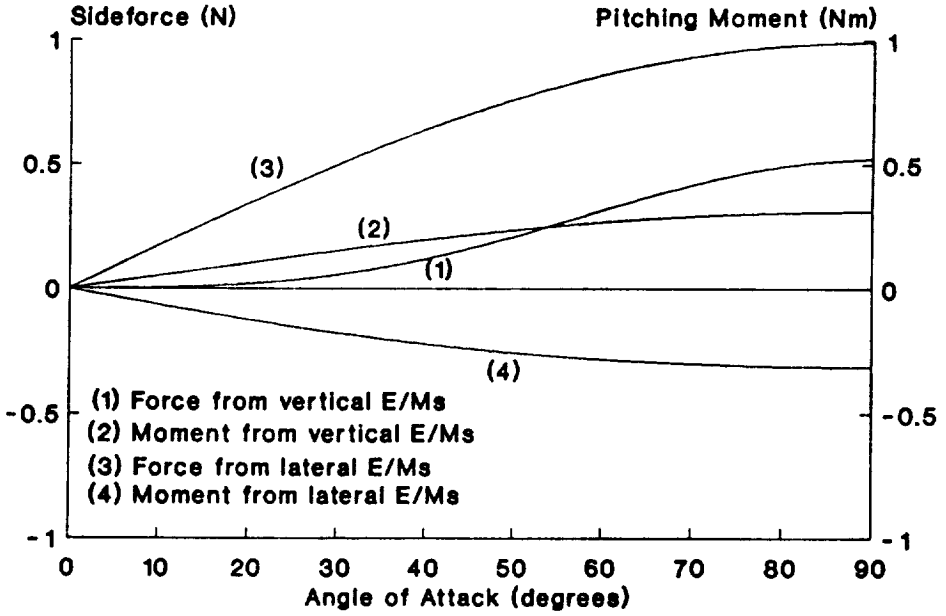

Figure 3.4c

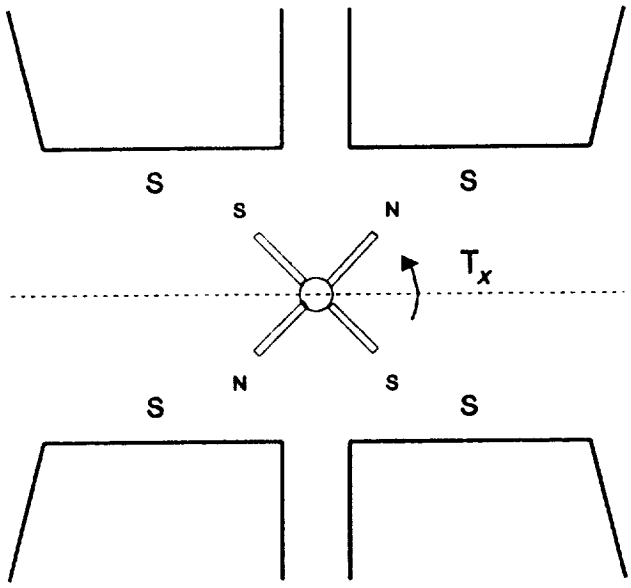

Figure 3.5: Showing how a rolling torque may be exerted at extreme attitudes upon a model equipped with auxiliary magnets: Example is of cruciform fins - transverse magnetised wings are similar

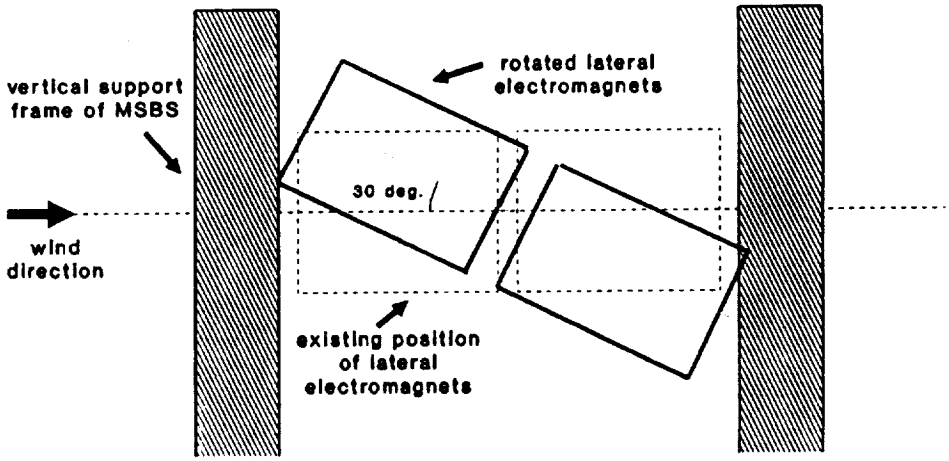

Figure 3.6: Showing the possible rotation of the lateral electromagnets to provide sideforce at 90 degrees angle of attack.

View from side of MSBS with all other E/Ms deleted for clarity

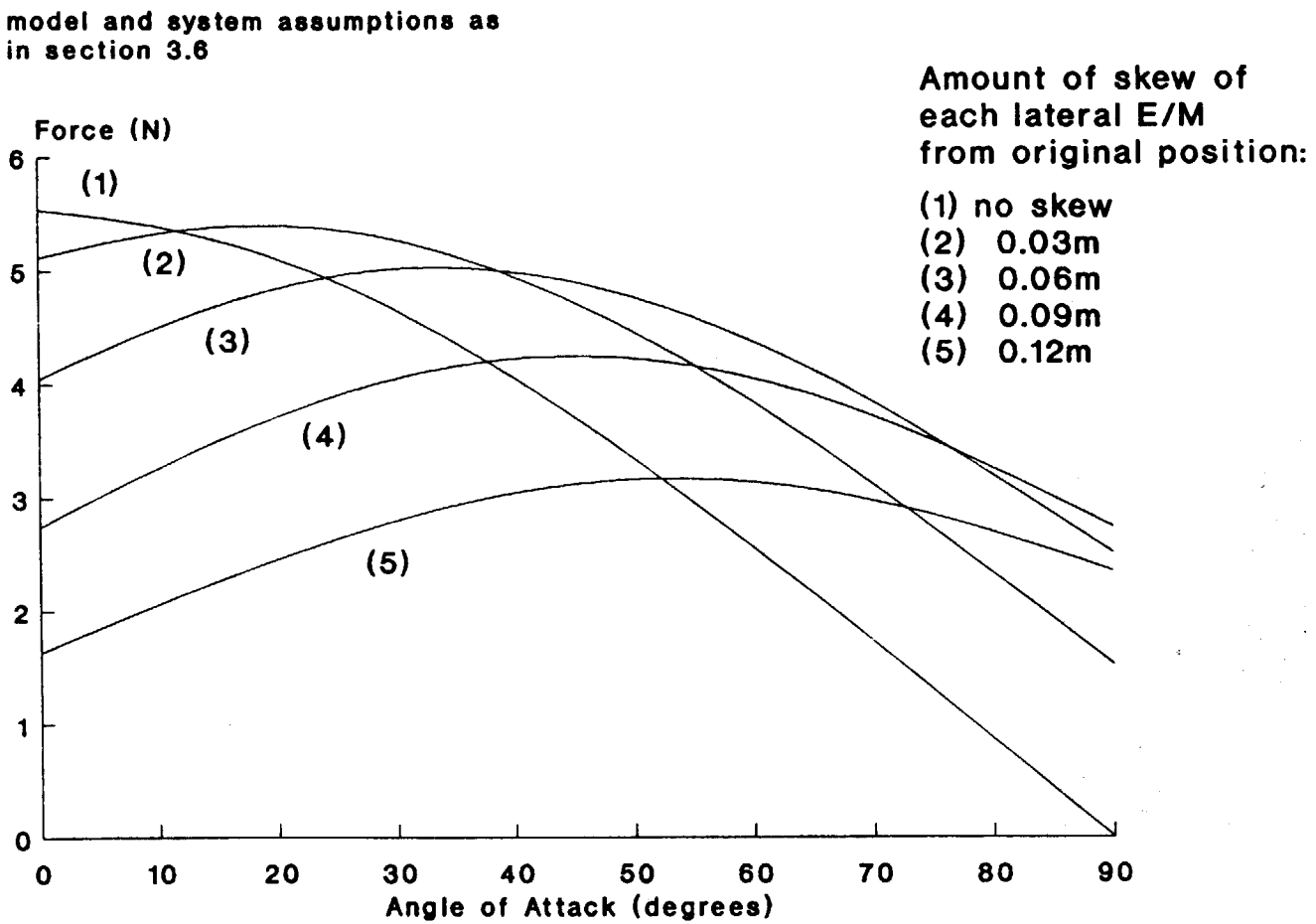

Figure 3.7: Predicted sideforce with varying amounts of skew in lateral electromagnets

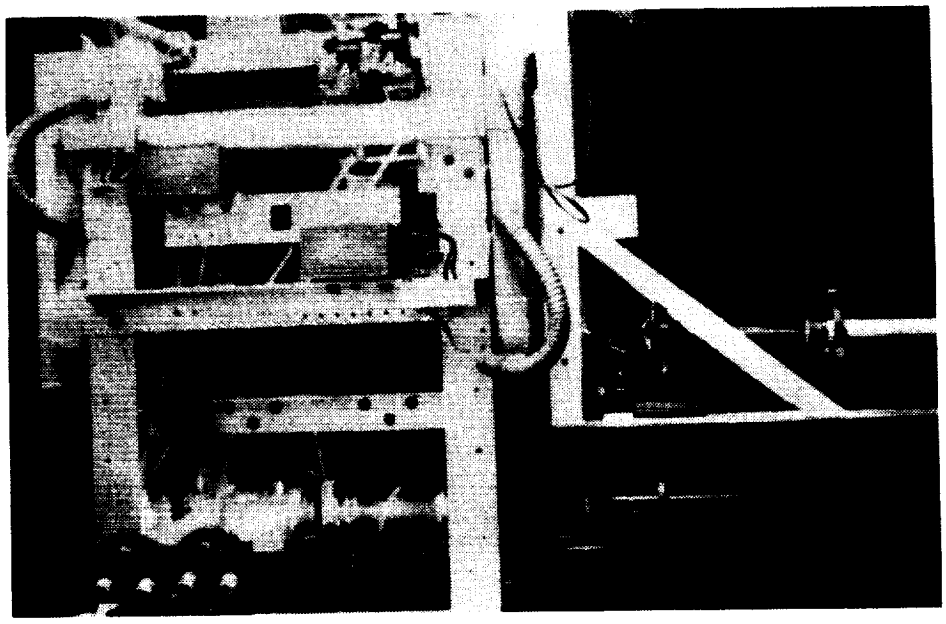

Figure 3.8: the Southampton University MSBS modified to incorporate skew into the arrangement of the four lateral electromagnets

Notice the laser beams of the sensing system which have been visualised using smoke

the rectangular laminated cores indicate the location of the skewed lateral electromagnets

ORIGINAL PAGE
BLACK AND WHITE PHOTOGRAPH

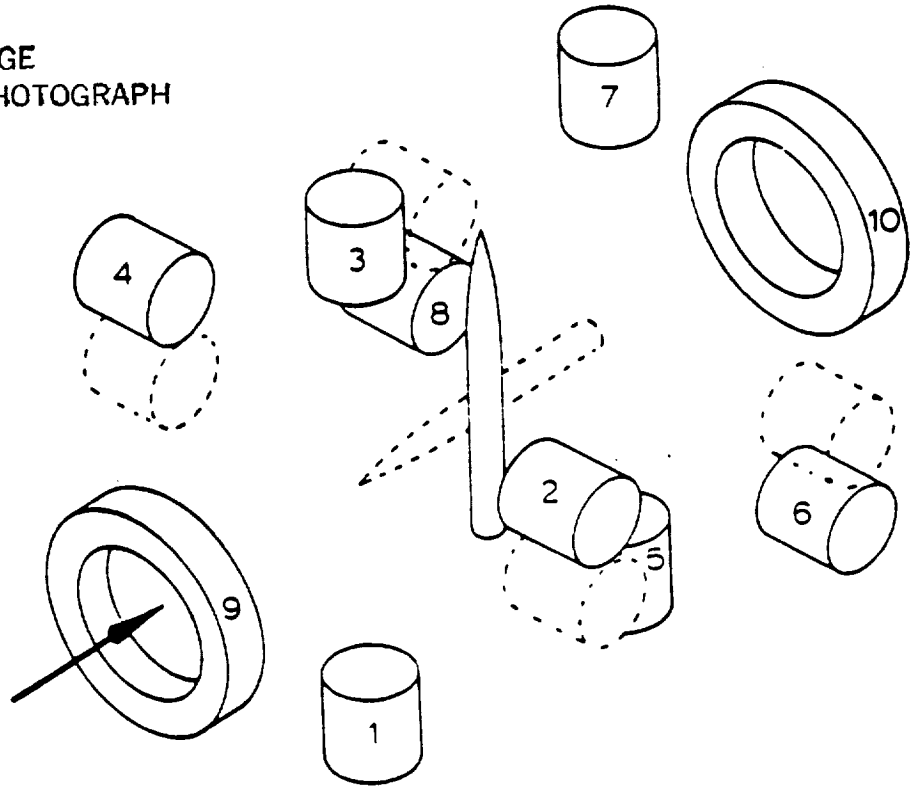

Figure 3.9: the coil numbering scheme used with the Southampton MSBS

The original location of the lateral electromagnets is indicated by the dashed lines

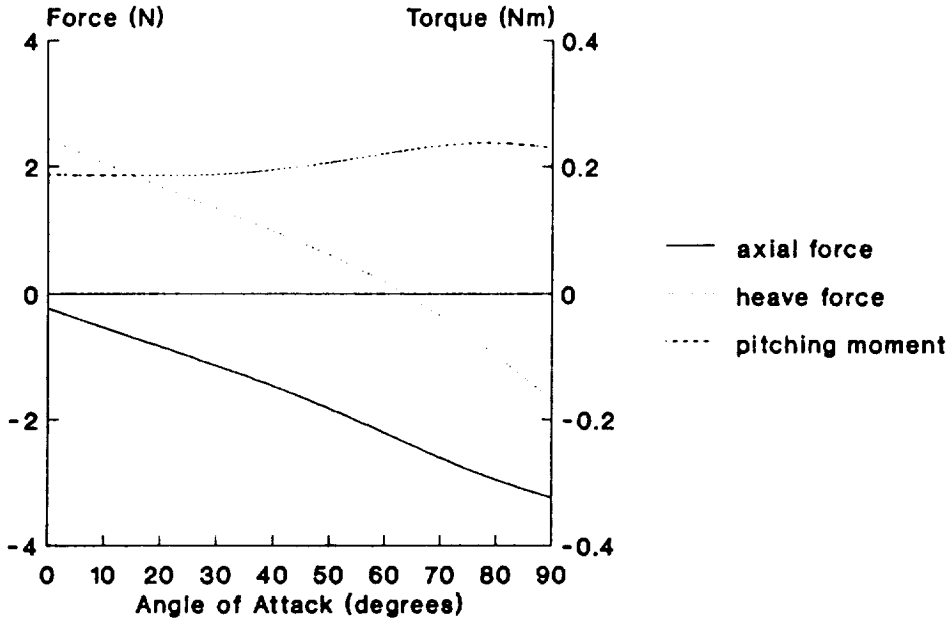

Figure 3.10: force and moment components from the aft upper and forward lower vertical electromagnets

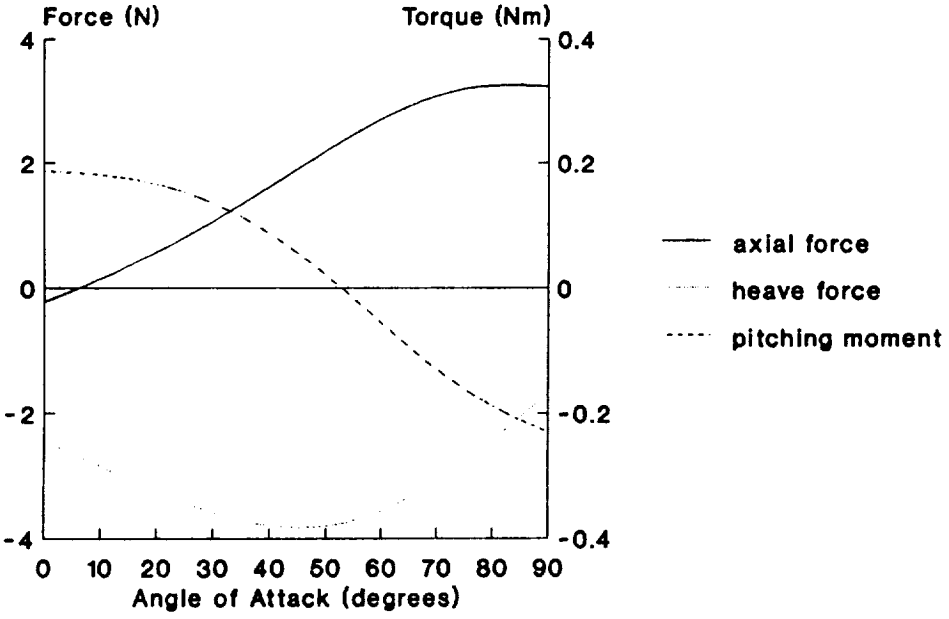

Figure 3.11: force and moment components from the forward upper and aft lower vertical electromagnets

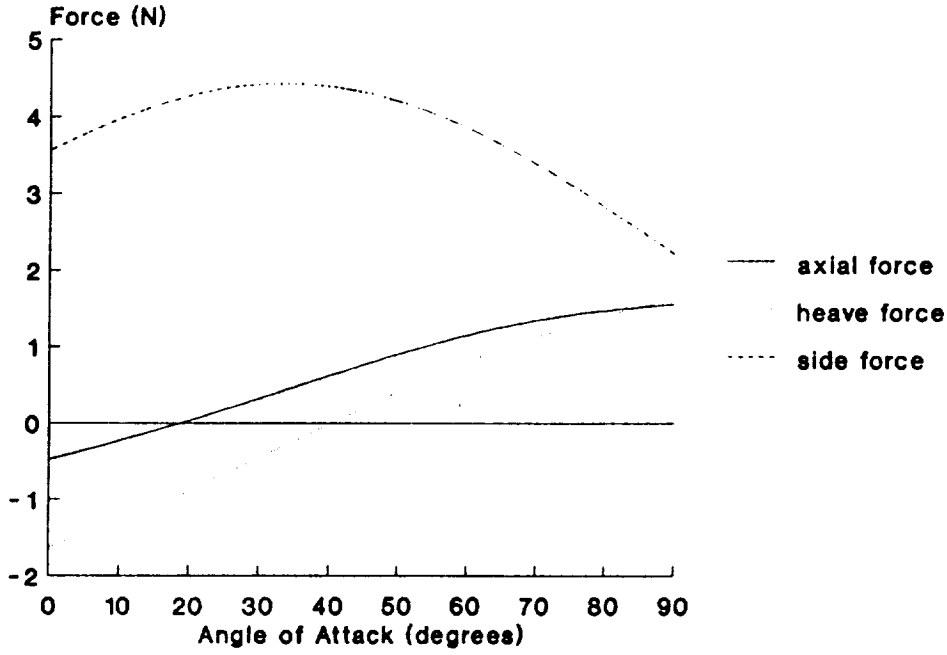

Figure 3.12: force components from the lateral electromagnets

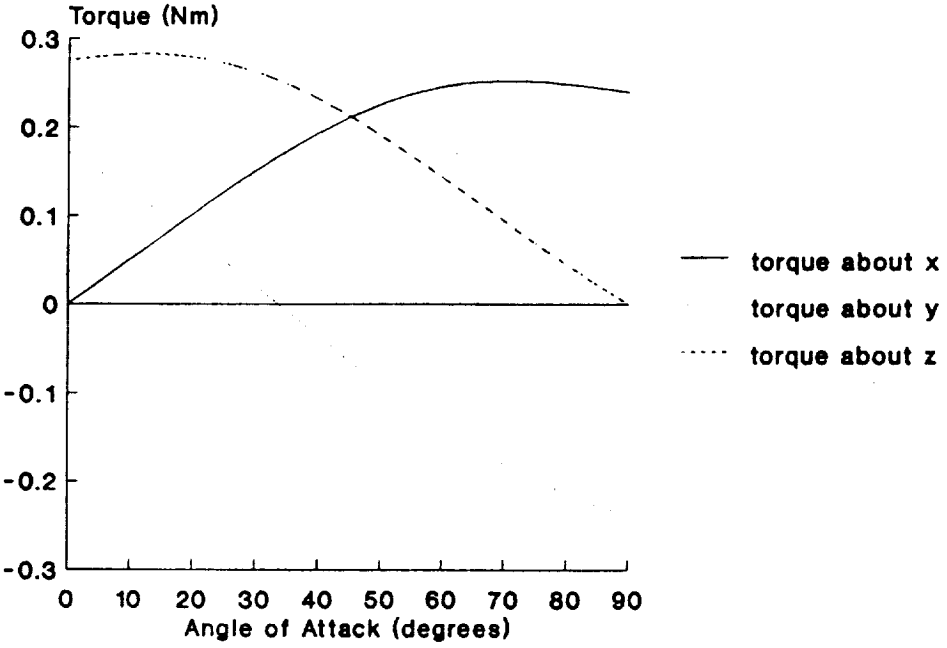

Figure 3.13: torque components from the lateral electromagnets

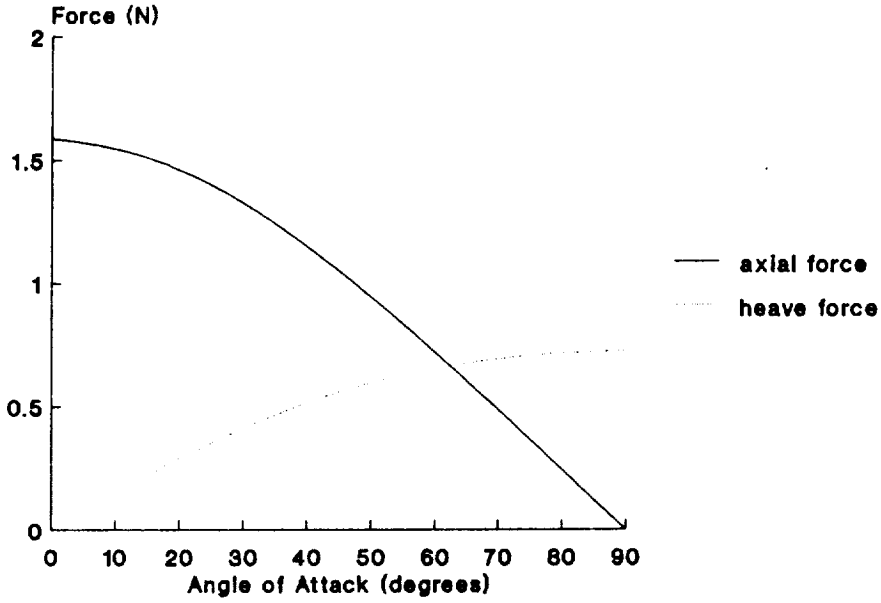

Figure 3.14: force components from the axial electromagnets

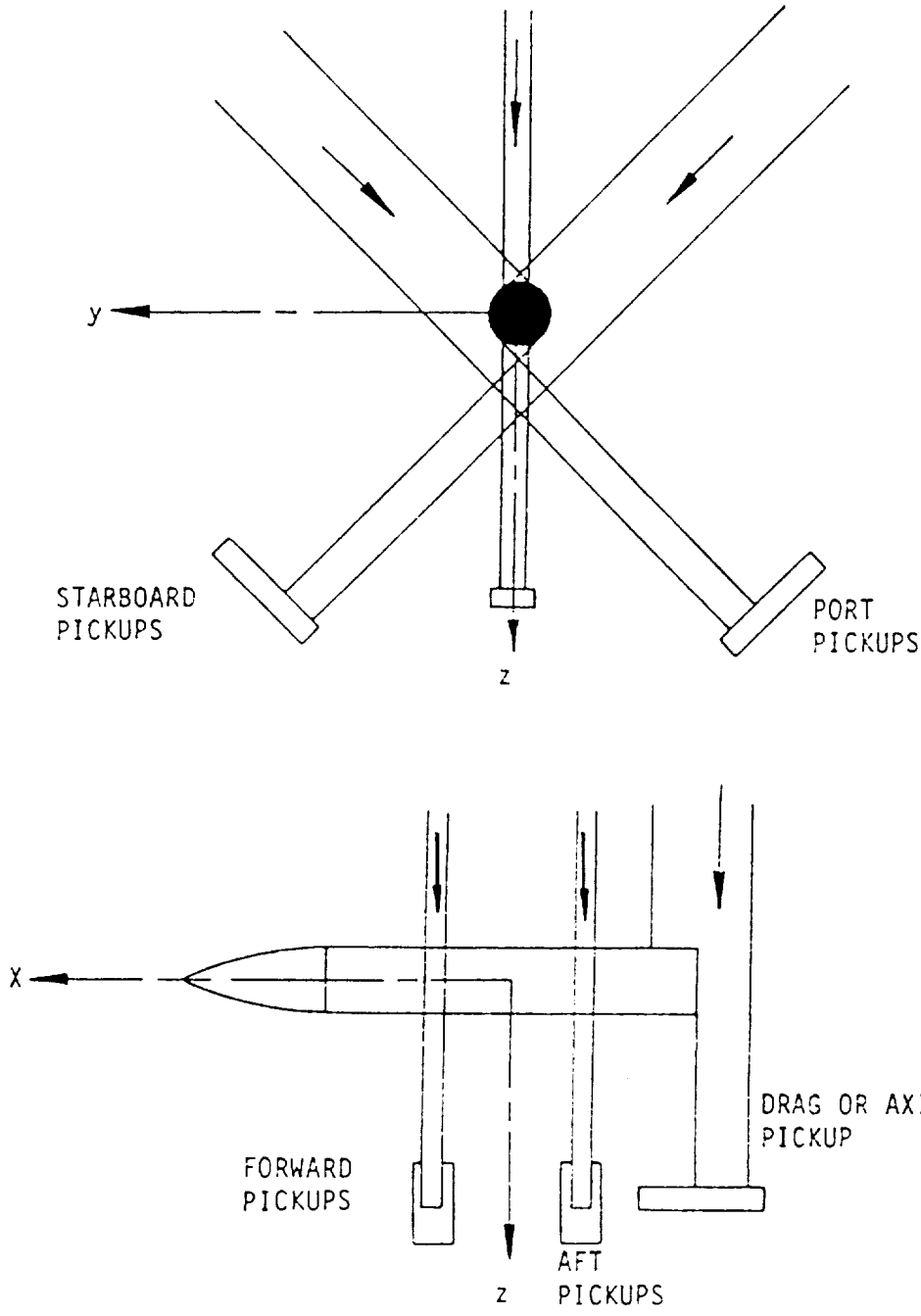

Figure 4.1: analogue position sensing system used with Southampton MSBS and based on shadow detection

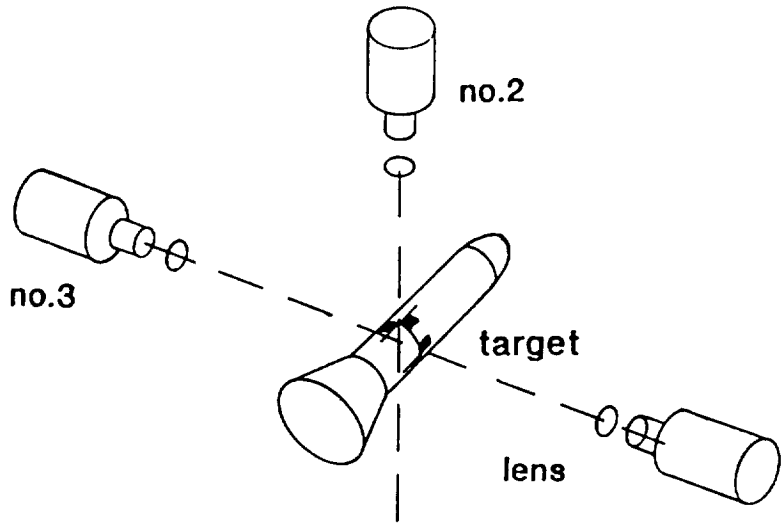

six-degree of freedom measurement

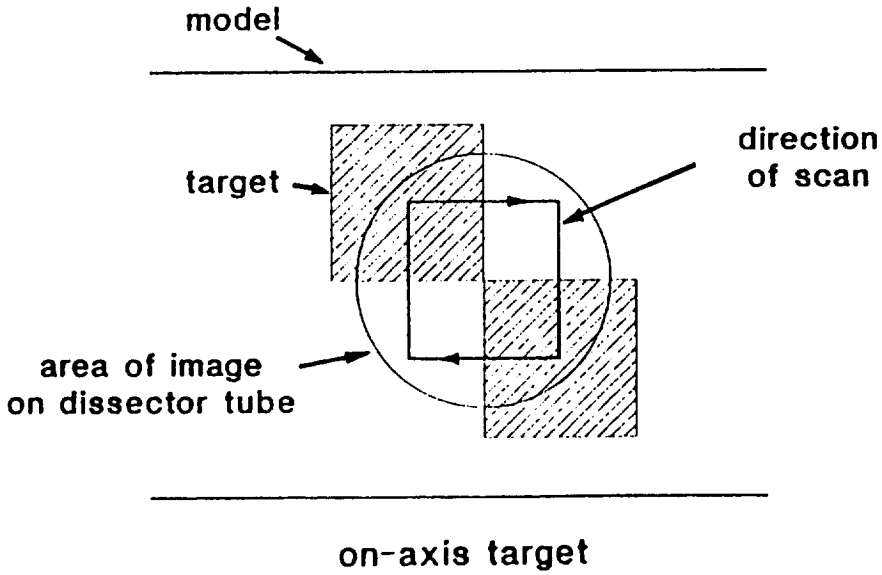

on-axis target

Figure 4.2 principle of ONERA scanning optical position sensing system

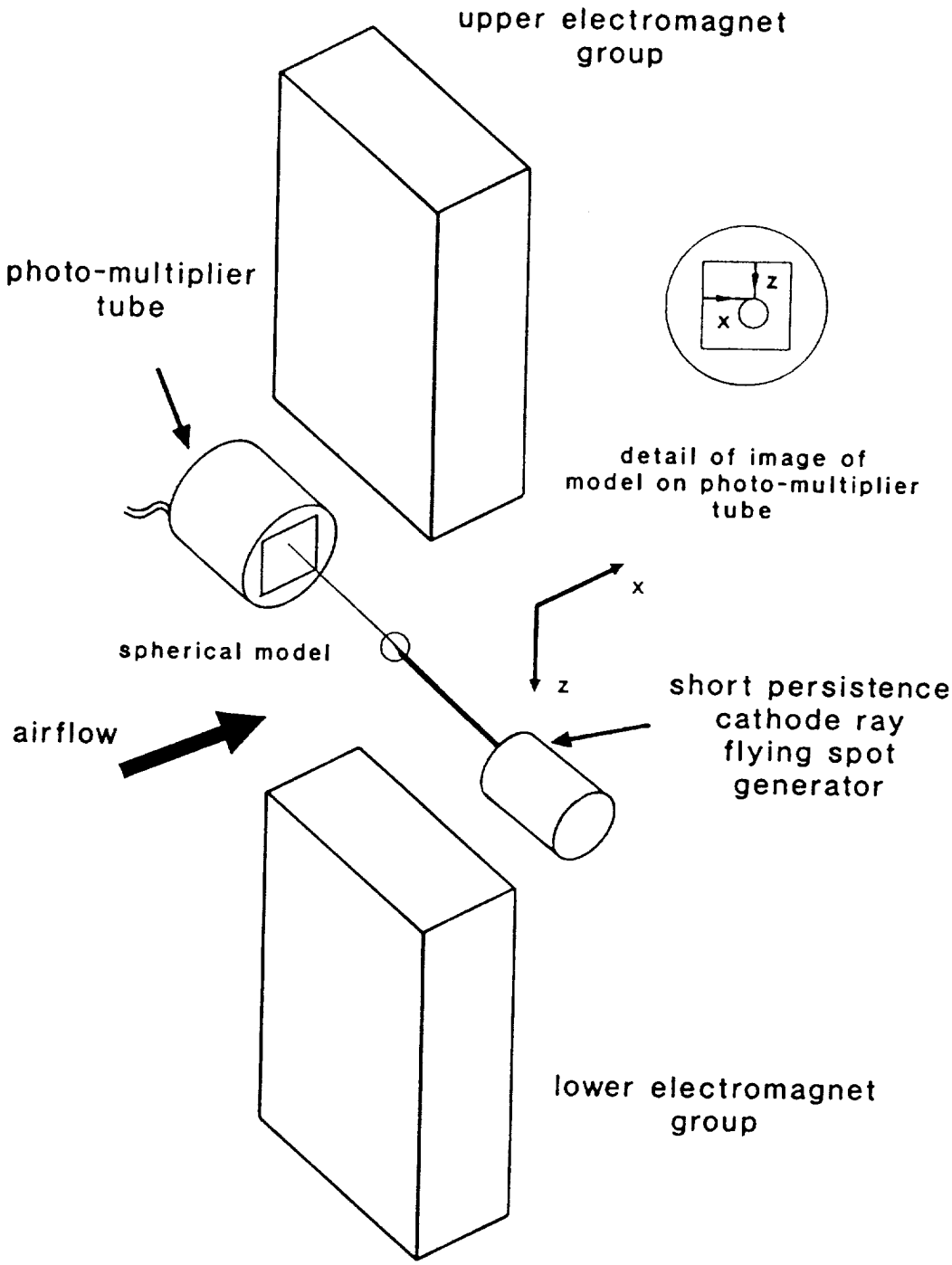

Figure 4.3: scanning optical sensing system used with the first Oxford University hypersonic MSBS
schematic reconstruction from available information

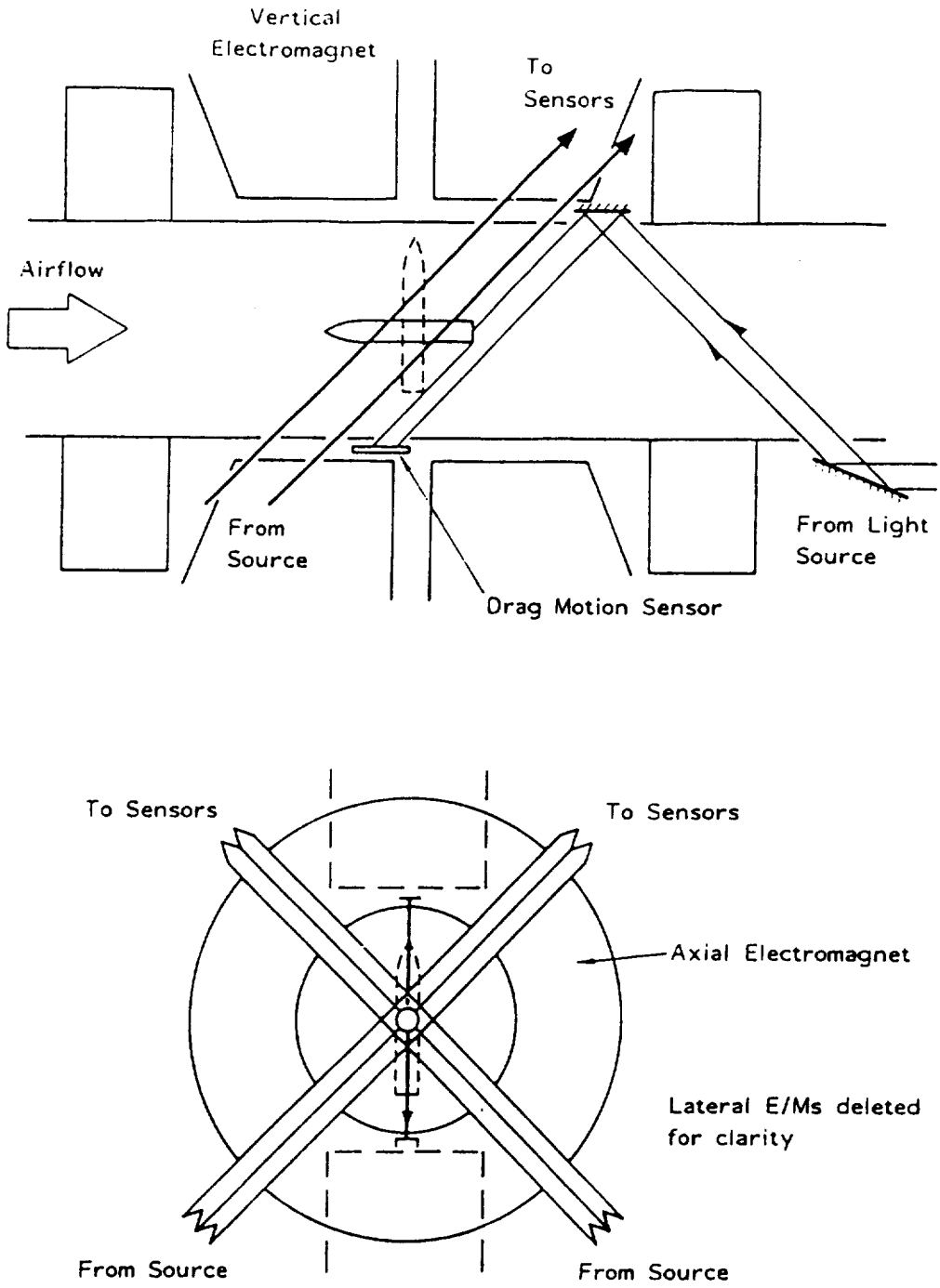

Figure 4.4: illustrating the arrangement of light beams of the optical sensing system designed for extreme attitude suspension

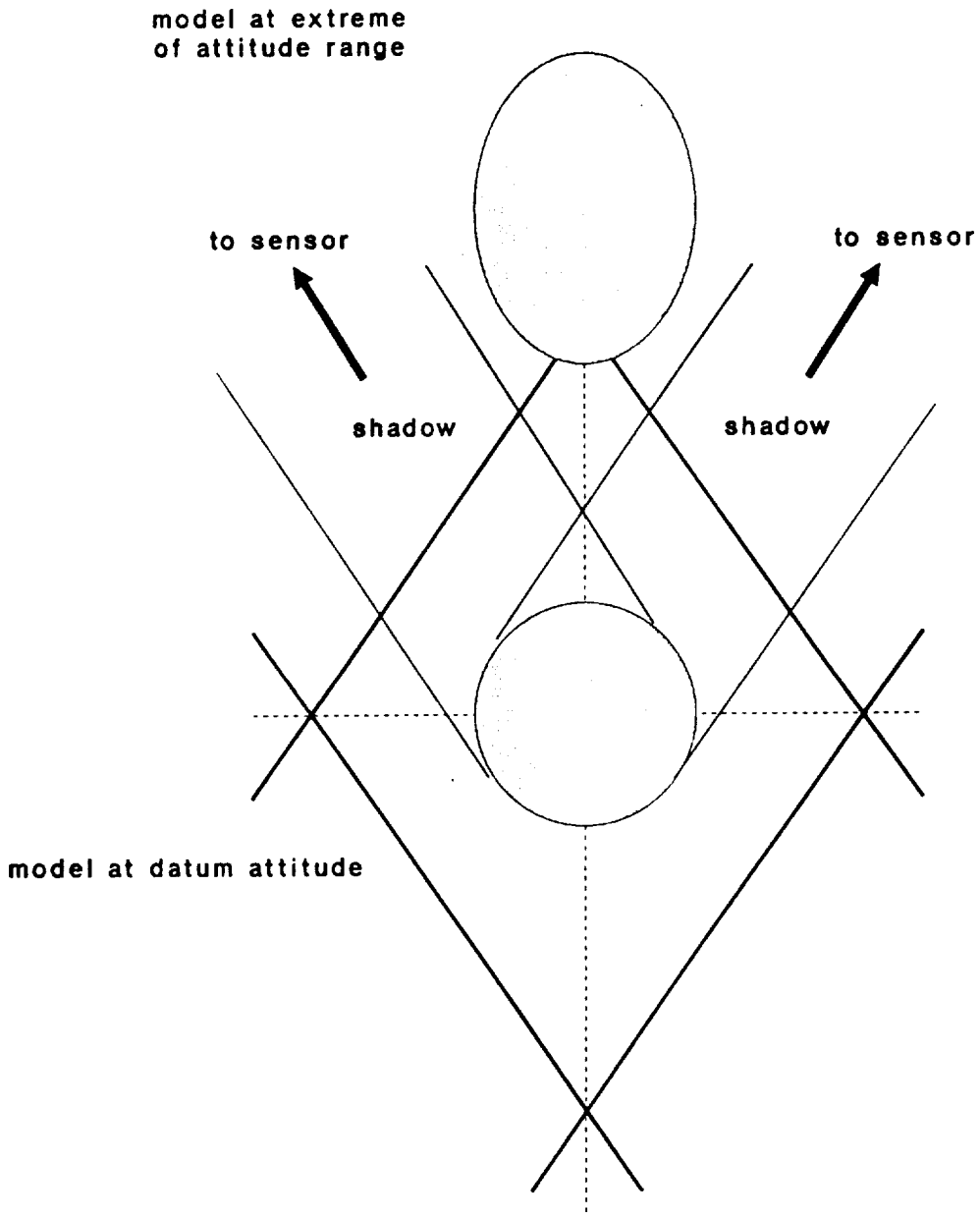

Figure 4.5: illustrating the diamond shaped intersection of each pair of laser beams illuminating the photodiode arrays

The diagram shows the beams being cut by a circular section model at datum attitude (45 degrees), and by the same model at the extreme of the attitude range, where the intersection shape is an ellipse. In the former case two edges are visibe to each of the sensor arrays; in the latter case, only one edge is visible.

applicable to a circular section model
of any diameter

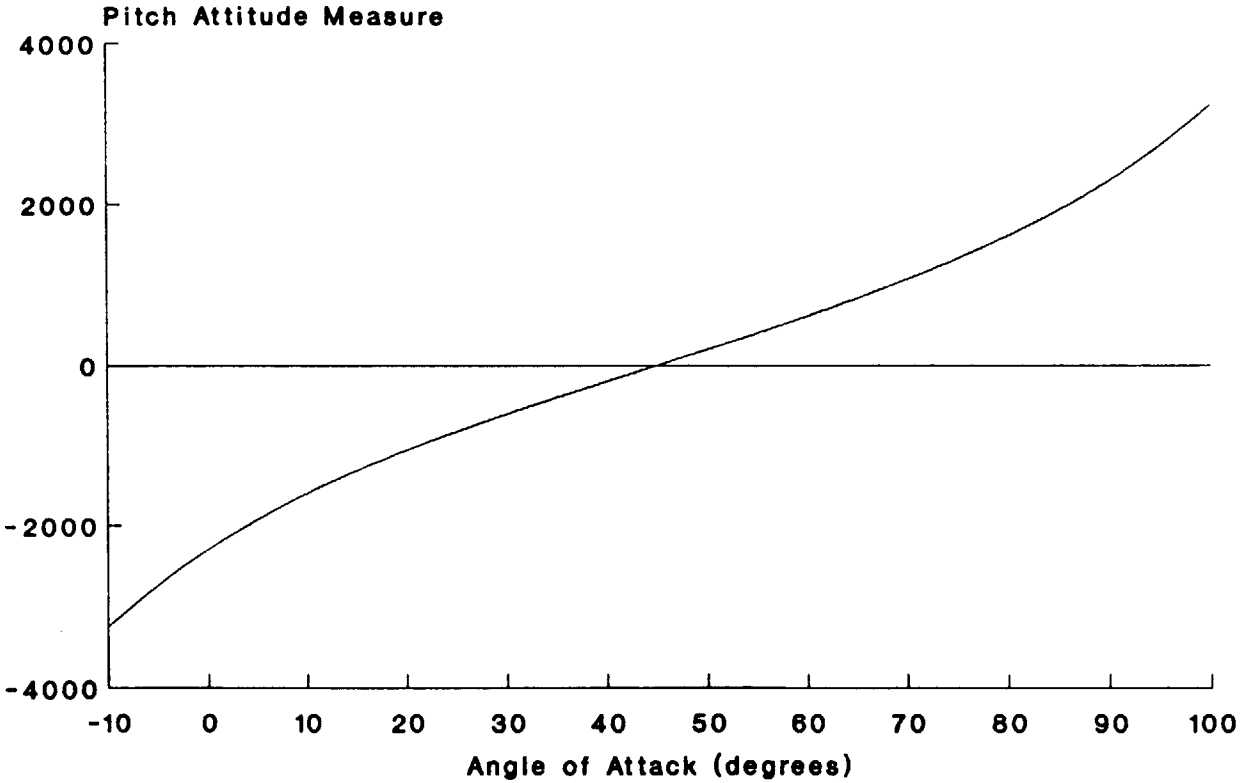

Figure 4.6: Relationship of pitch attitude measure with angle of attack

Figure 4.7 (following page):

an overall view of the Southampton MSBS modified for extreme attitude suspension.

Illustrating from left to right:
MSBS/computer interface electronics box
including Photodiode Array Control System;
power supply electronics cabinet;
MSBS operator's computer terminal;
wind tunnel fan-housing and diffuser;
MSBS rig with photodiode array pre-processing
electronics at top left;
wind tunnel intake and contraction.

PDP 11/84 control computer is
remotely located from wind tunnel facility.

ORIGINAL PAGE
BLACK AND WHITE PHOTOGRAPH

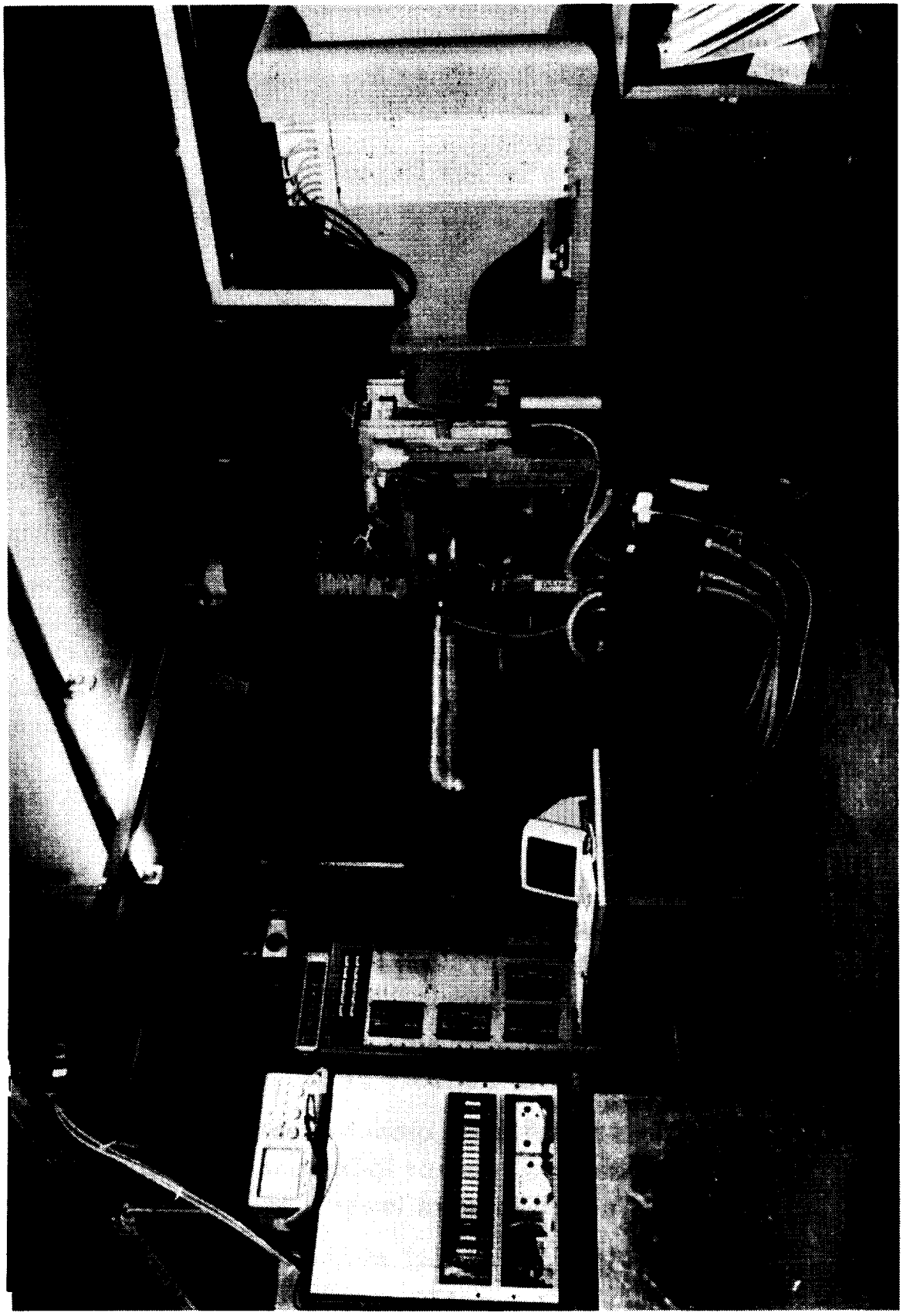

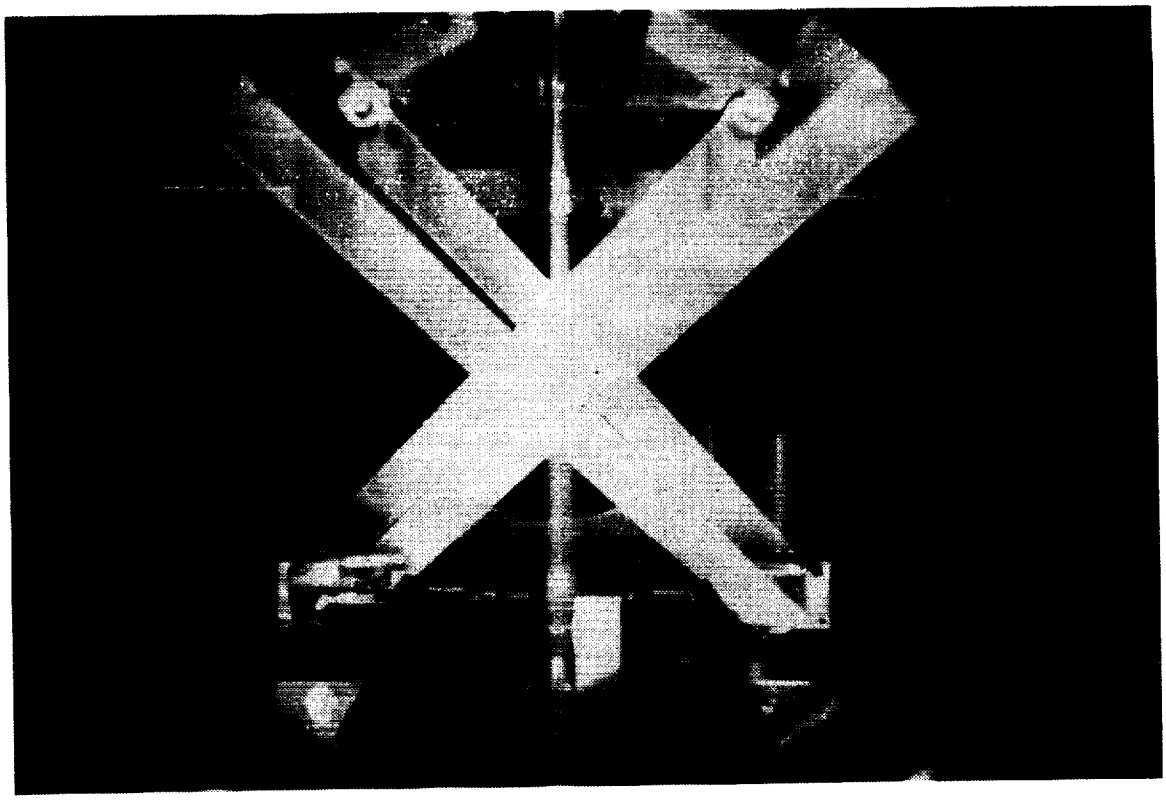

Figure 4.8a: view upstream of MSBS showing higlighted sensing system laser beams.

Four main beams enter system at bottom left and bottom right, crossing system to form two crosses, and depart to sensors at top right and top left.

Vertical laser beam crosses test volume vertically to strike axial sensor located in original position above forward lower electromagnet.

Wind tunnel test section not installed.

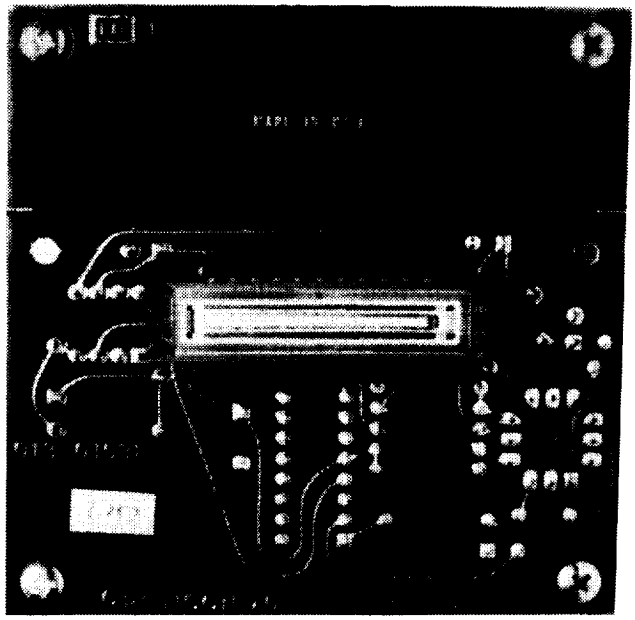

Figure 4.8b: Reticon RL1024G photodiode array and electronics card

ORIGINAL PAGE
BLACK AND WHITE PHOTOGRAPH

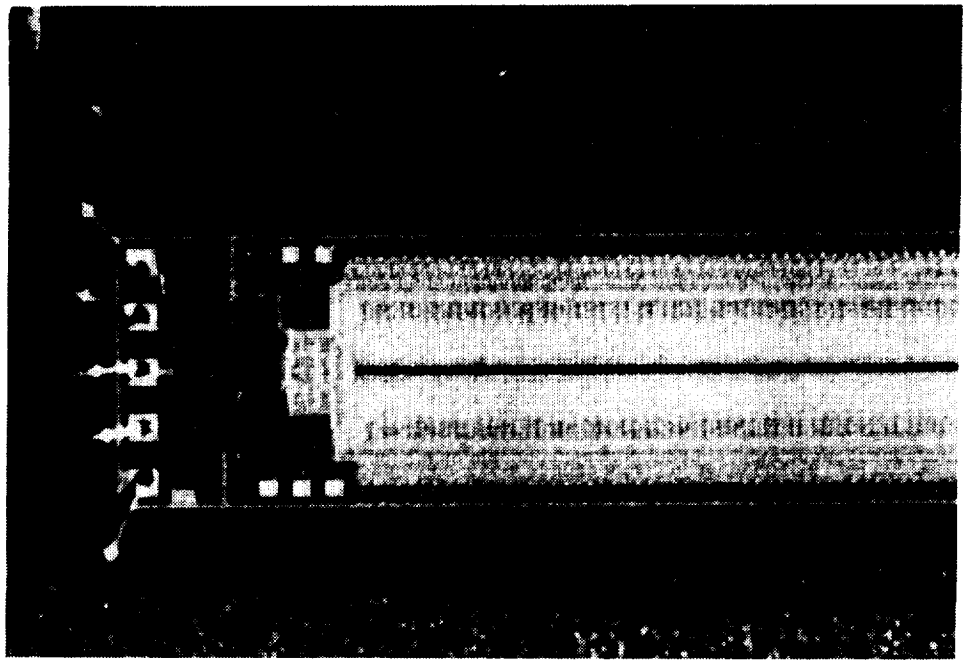

Figure 4.8c: close-up of one end of a diode array showing 0.001 inch aperture and micro-circuitry

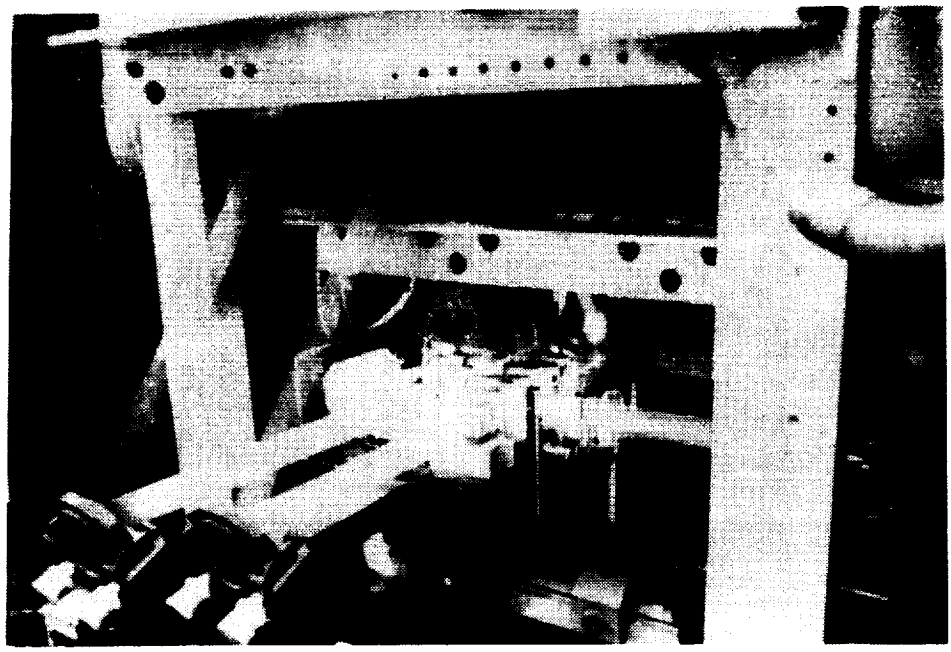

Figure 4.8d: optical beam splitter assembly and mirror gimbal units located below MSBS electromagnets.

ORIGINAL PAGE
BLACK AND WHITE PHOTOGRAPH

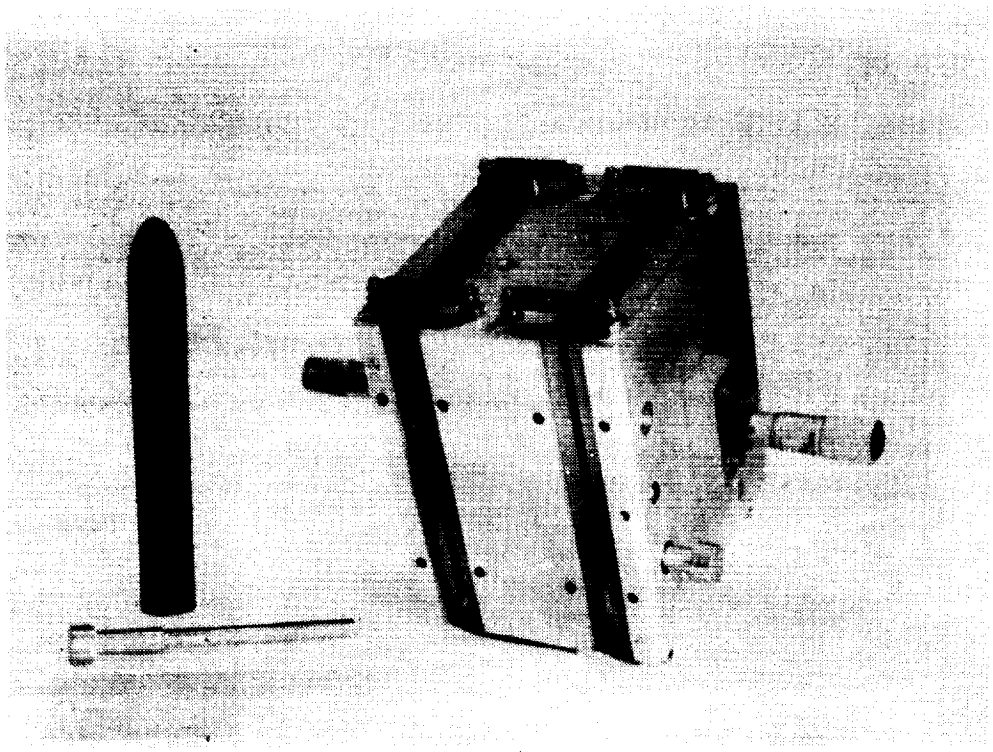

Figure 4.8e: original axisymmetric model and optical alignment jig.

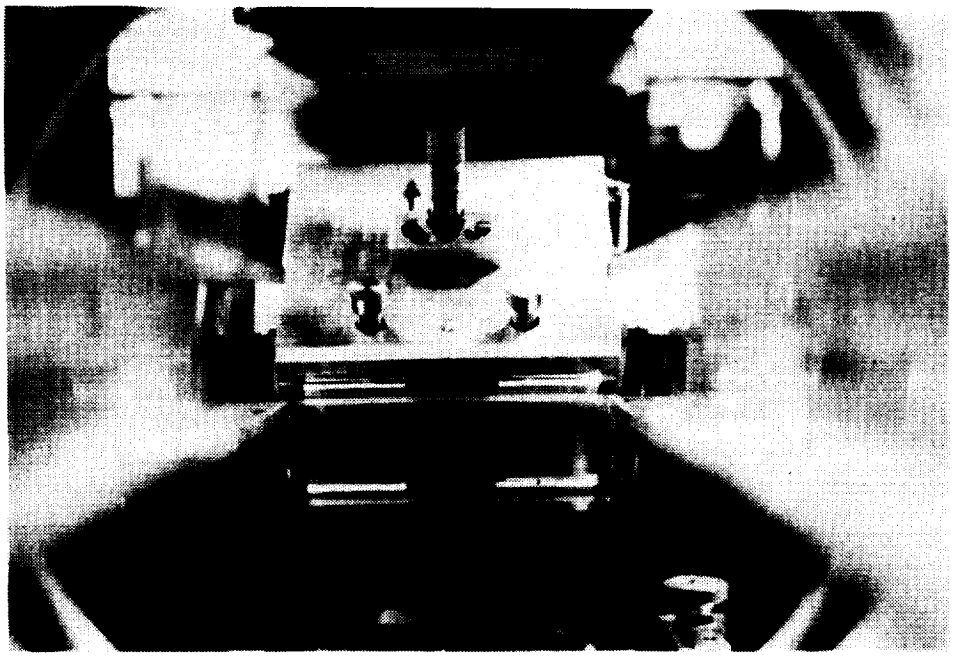

Figure 4.8f: optical alignment jig installed in MSBS by supporting members. Four streaks of light indicate paths of laser beams. View looking downstream.

ORIGINAL PAGE
BLACK AND WHITE PHOTOGRAPH

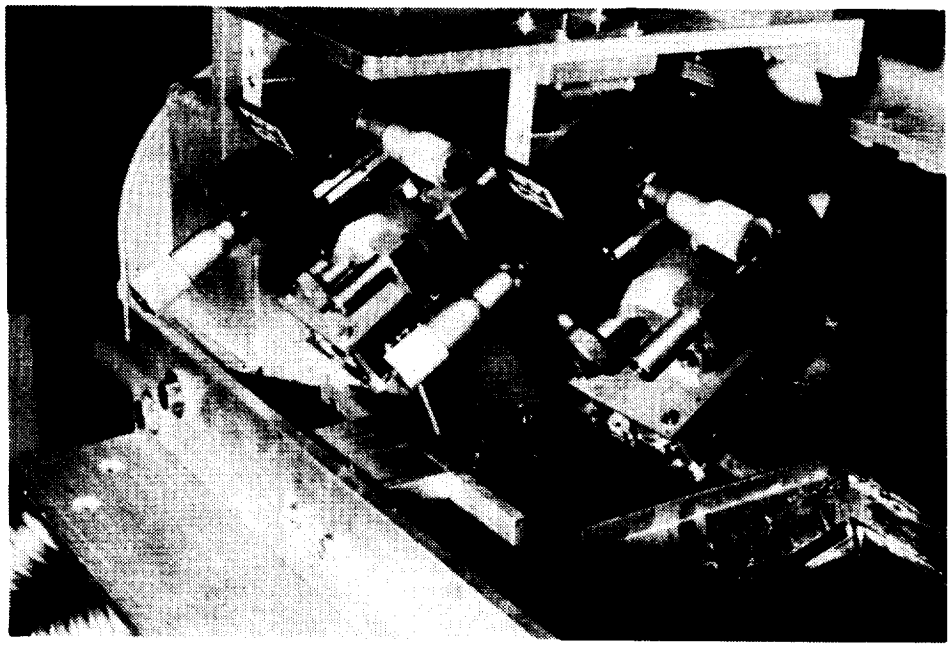

Figure 4.8g: pair of adjustable mountings for diode array sensors. Fixed deflector mirrors are also visible.

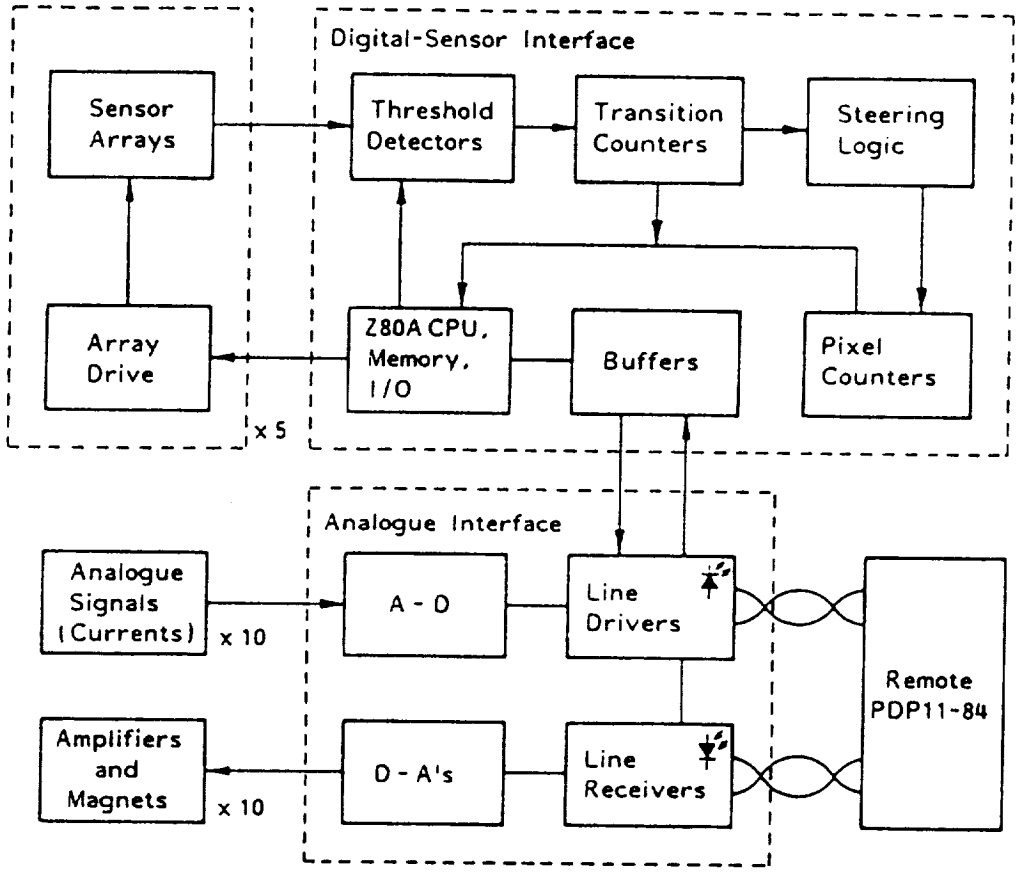

Figure 4.9: a block diagram of the Photodiode Array Control System

C-3

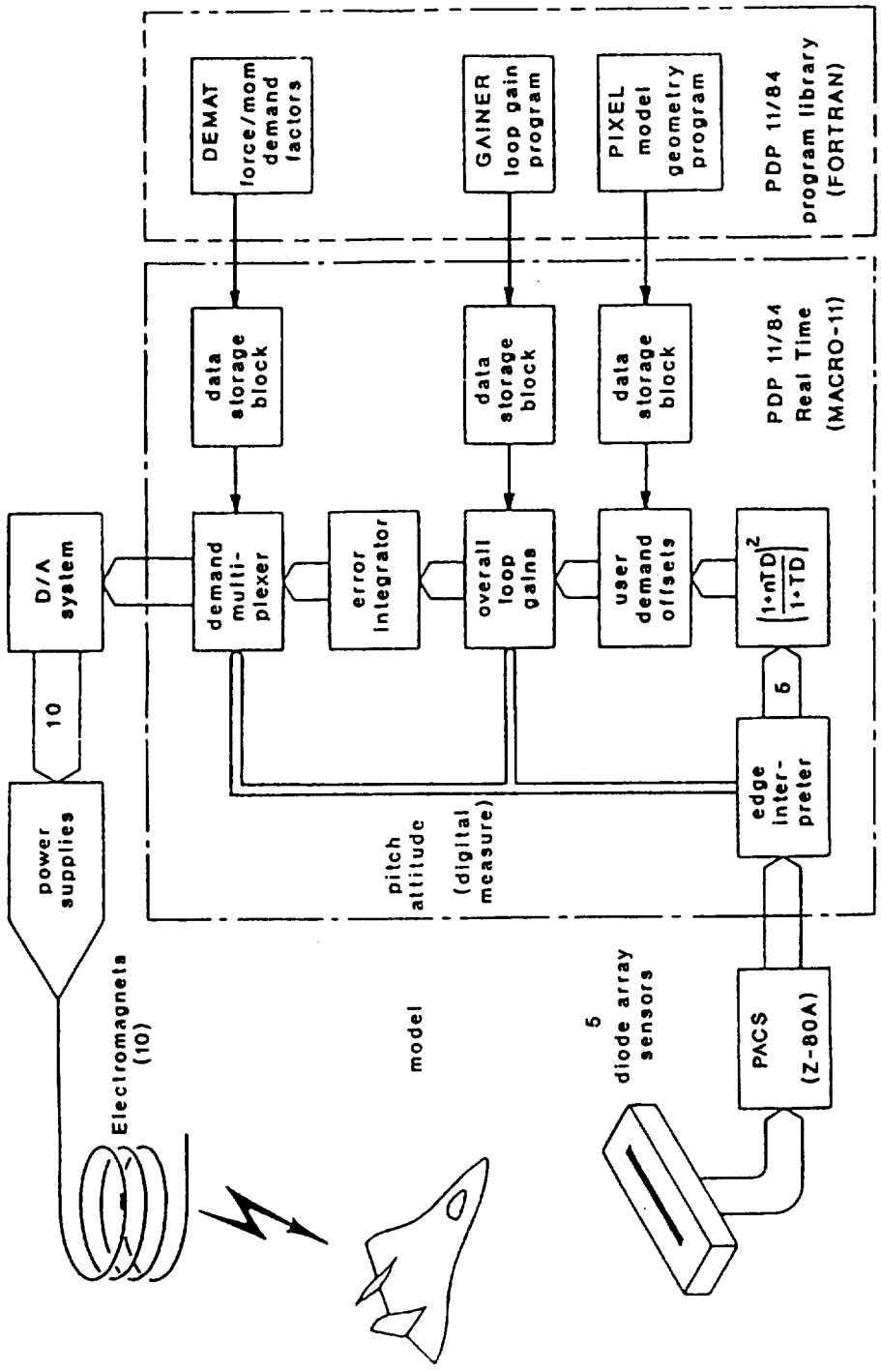

Figure 5.1: a block diagram of the Southampton MSBS showing extreme attitude control system

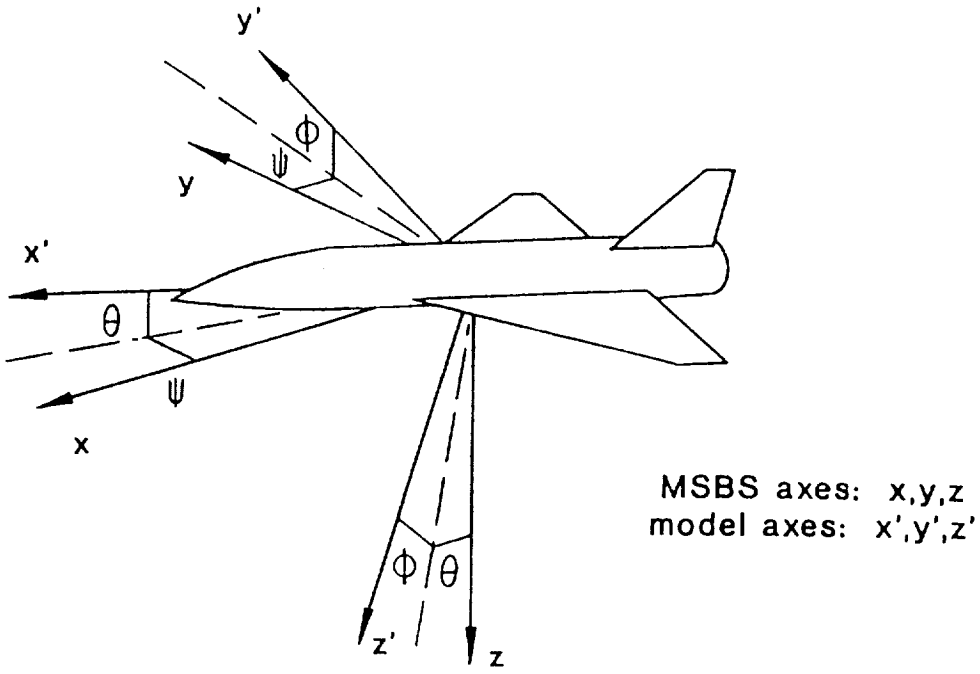

Figure 5.2: Conventional Axis Systems
used with Southampton MSBS

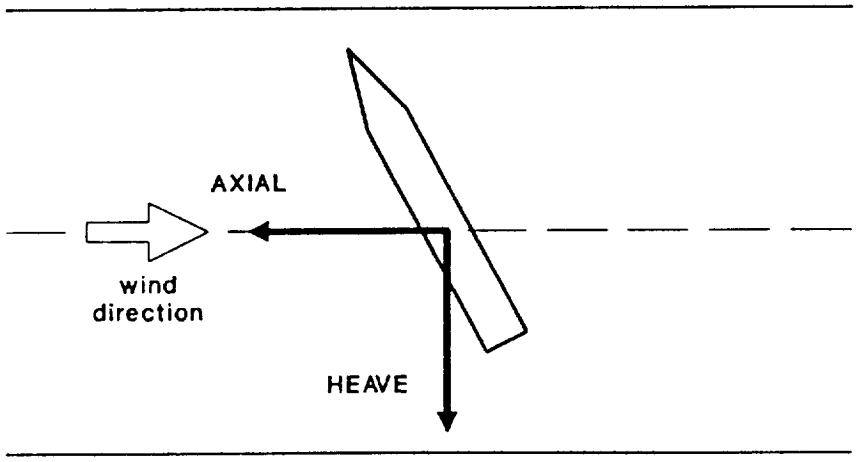

Figure 5.3a: wind tunnel axes

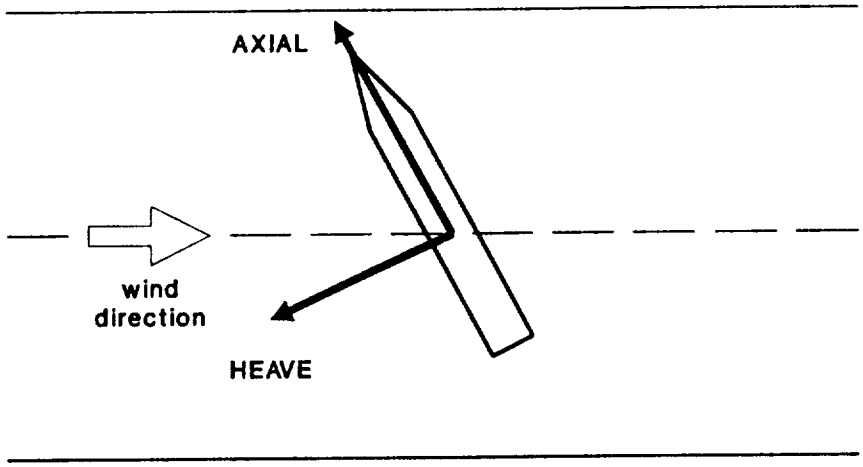

Figure 5.3b: model axes

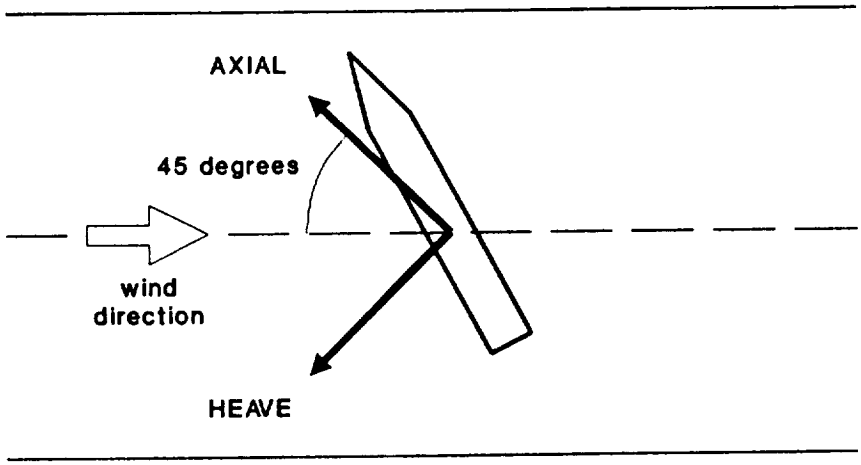

Figure 5.3c: sensing system axes

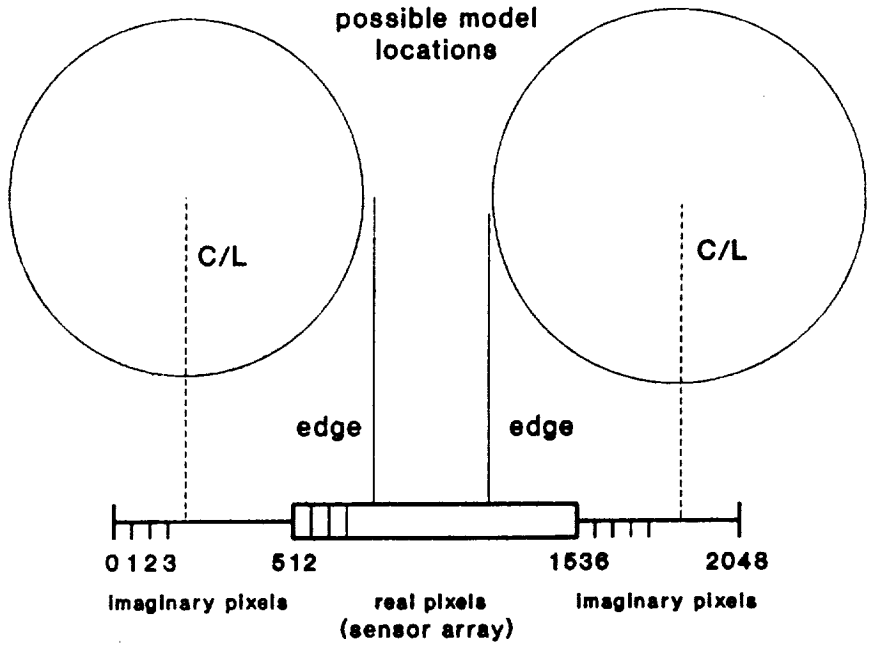

Figure 5.4: showing the definition of real and imaginary pixels

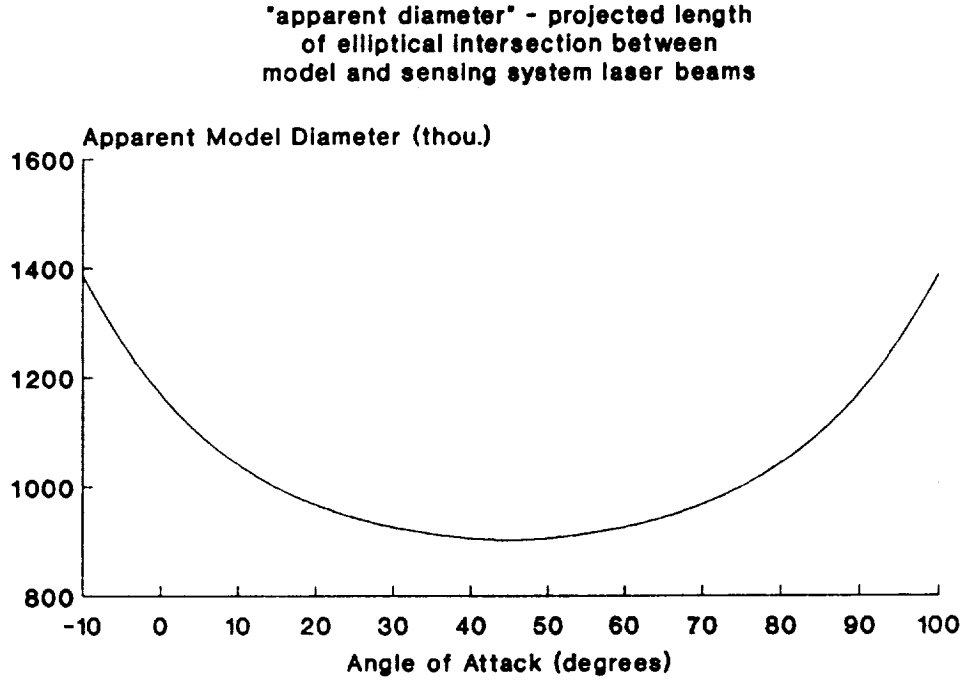

Figure 5.5: relationship between apparent diameter and angle of attack for 22mm diameter model

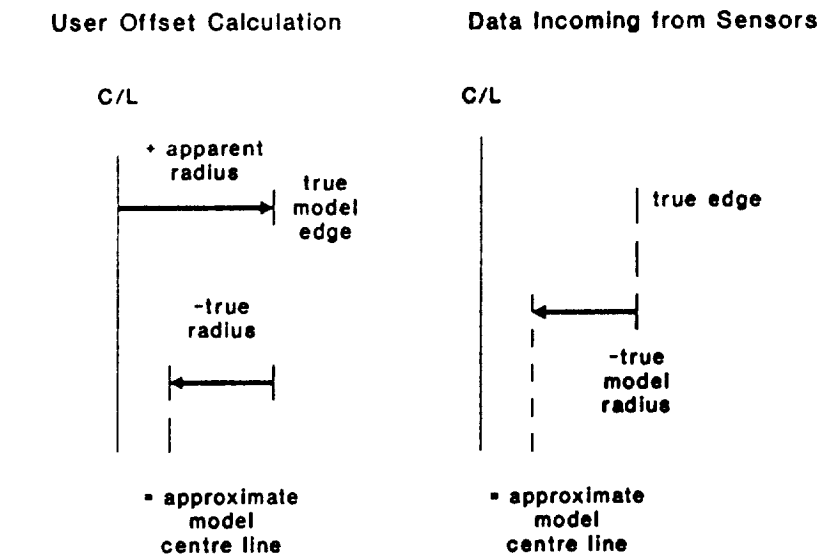

Figure 5.6: edge interpreter logic

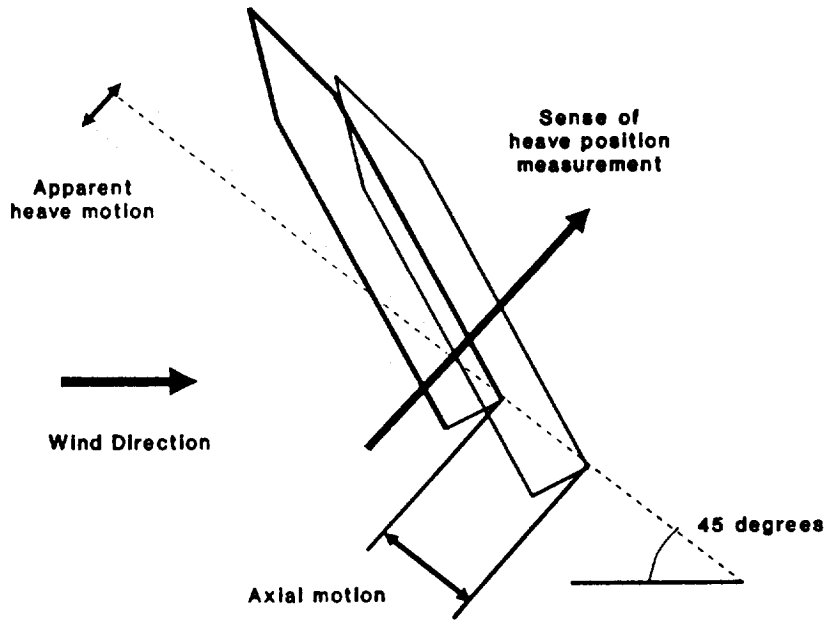

Figure 5.7: generation of apparent position change with pure axial motion in sensing system axes

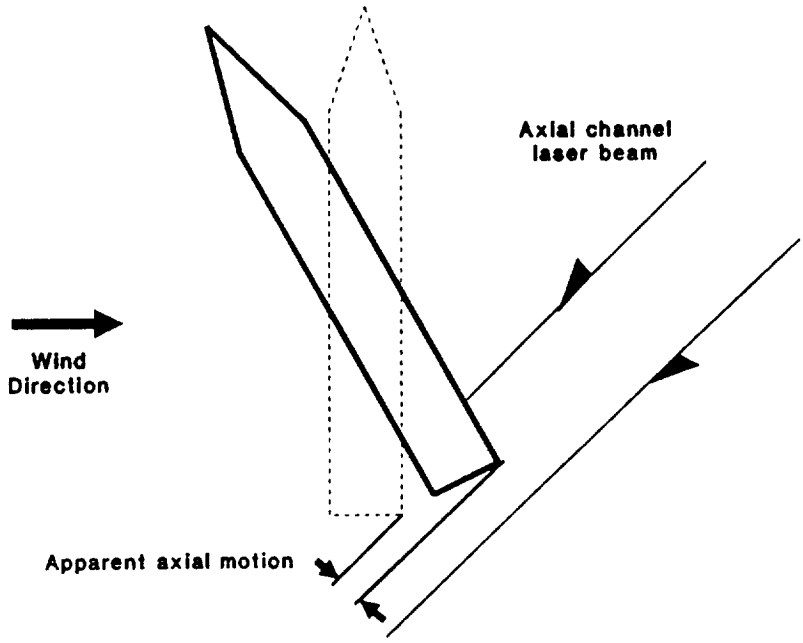

Figure 5.8: generation of apparent axial position signal with change in pitch attitude

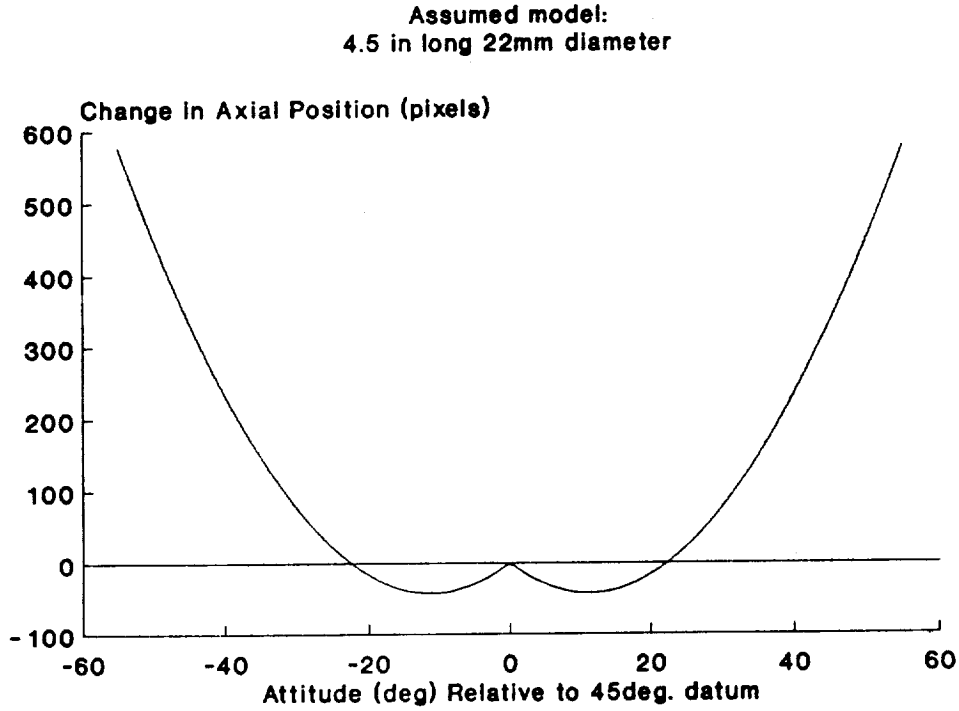

Figure 5.9: relationship between axial position and pitch attitude

MSBS Controller Pitch Channel

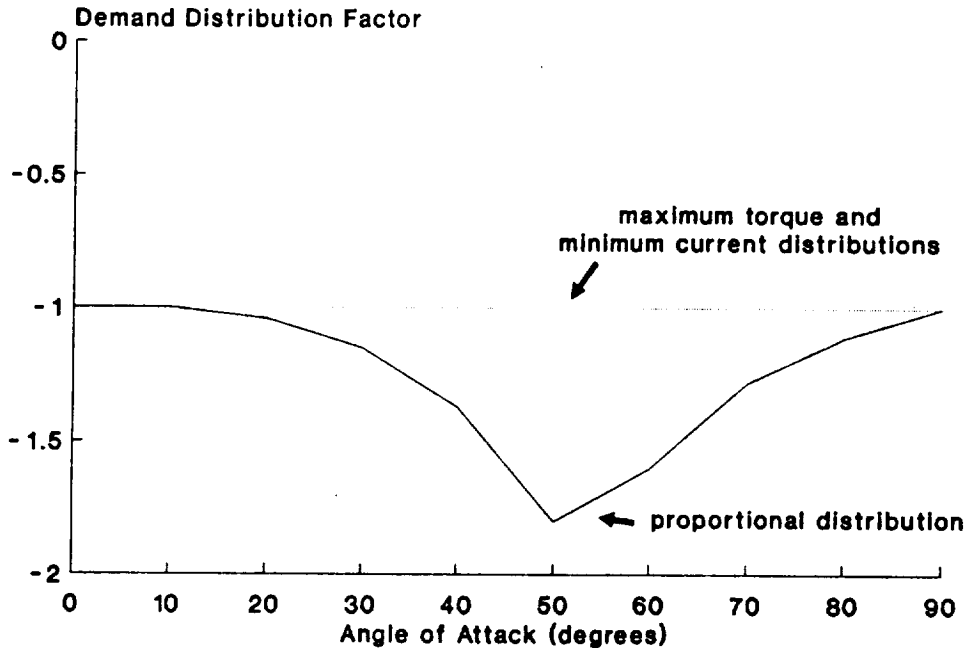

Figure 6.1a: pitch torque
demand distributions for E/Ms 1 & 7

MSBS Controller Pitch Channel

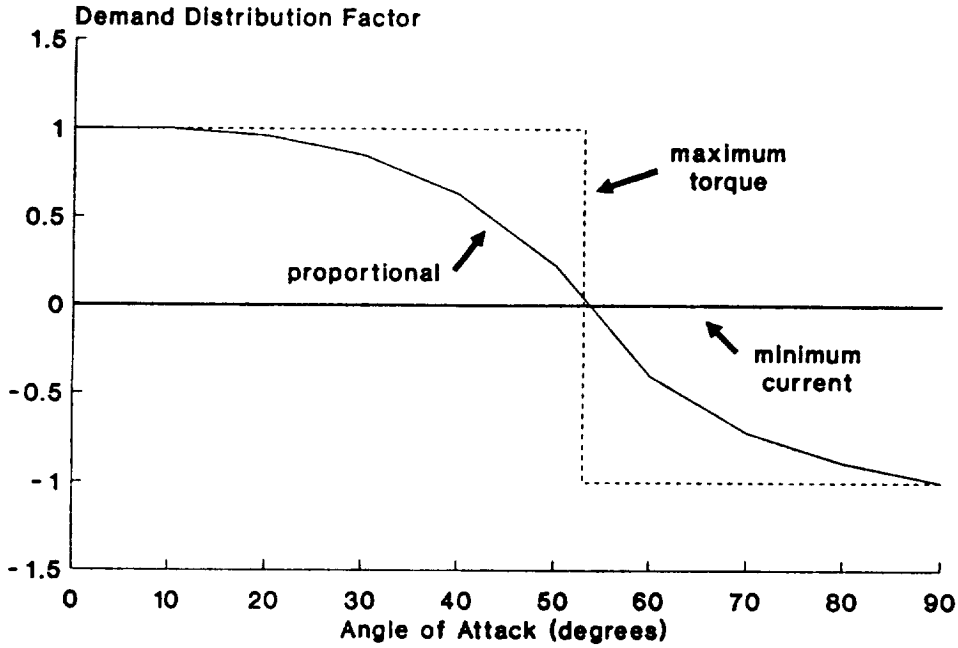

Figure 6.1b: pitch torque
demand distributions for E/Ms 3 & 5

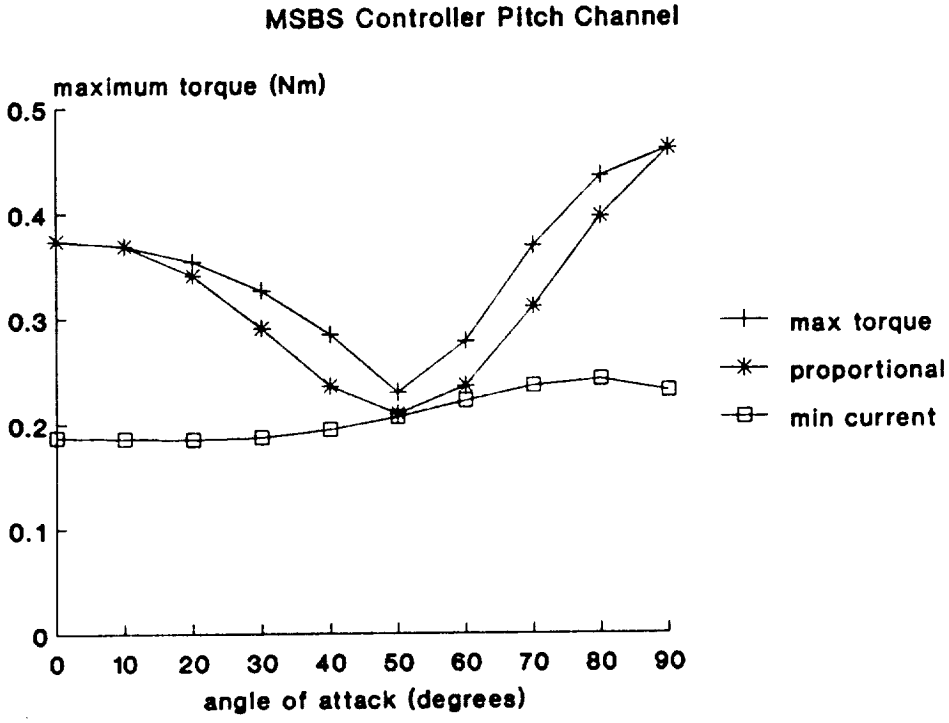

Figure 6.2a: maximum torque resulting from various demand distributions

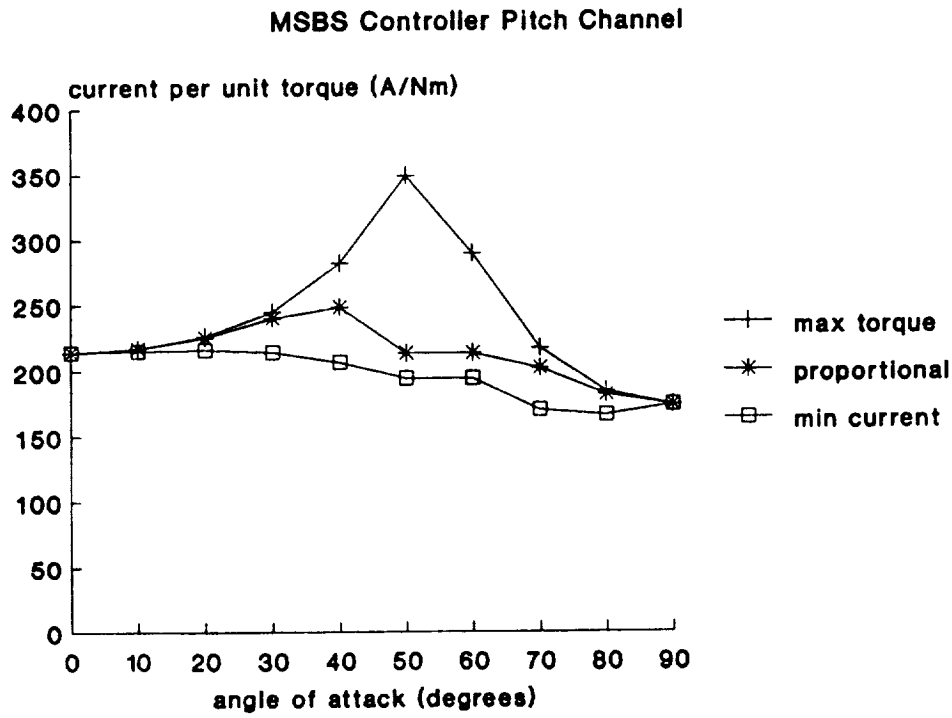

Figure 6.2b: current required per unit torque for various demand distributions

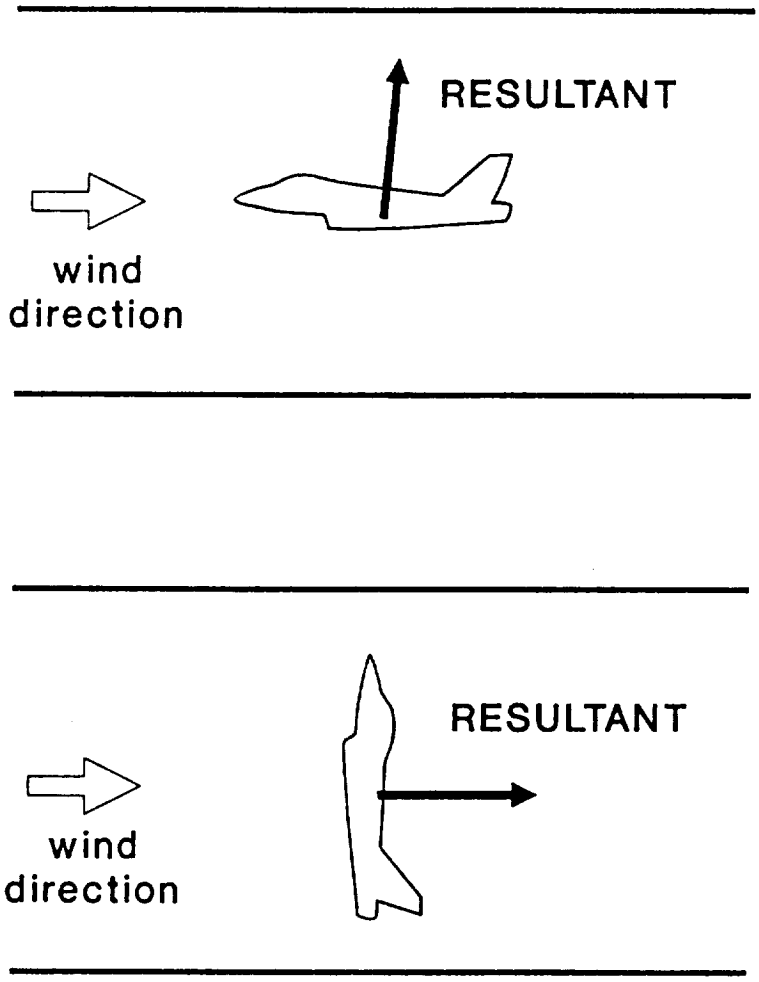

Figure 6.3 Showing Effect of Change of Angle of Attack on Direction of Resultant of Lift and Drag

The MSBS must generate a force to oppose the component shown

Heave Forces
Sensing System Axes

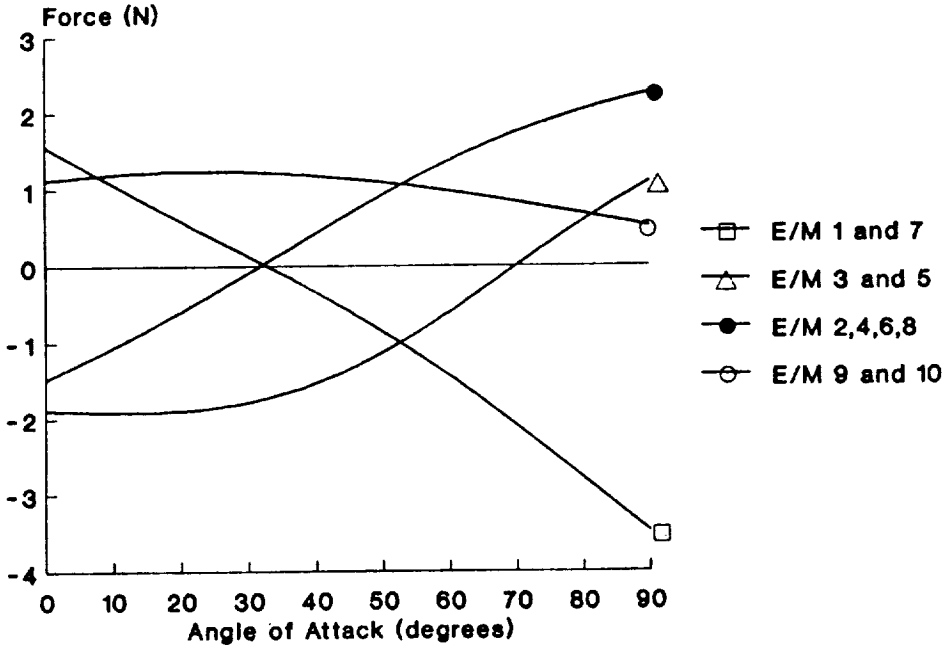

Figure 6.4a Forces in Vertical Plane

Axial Forces
Sensing System Axes

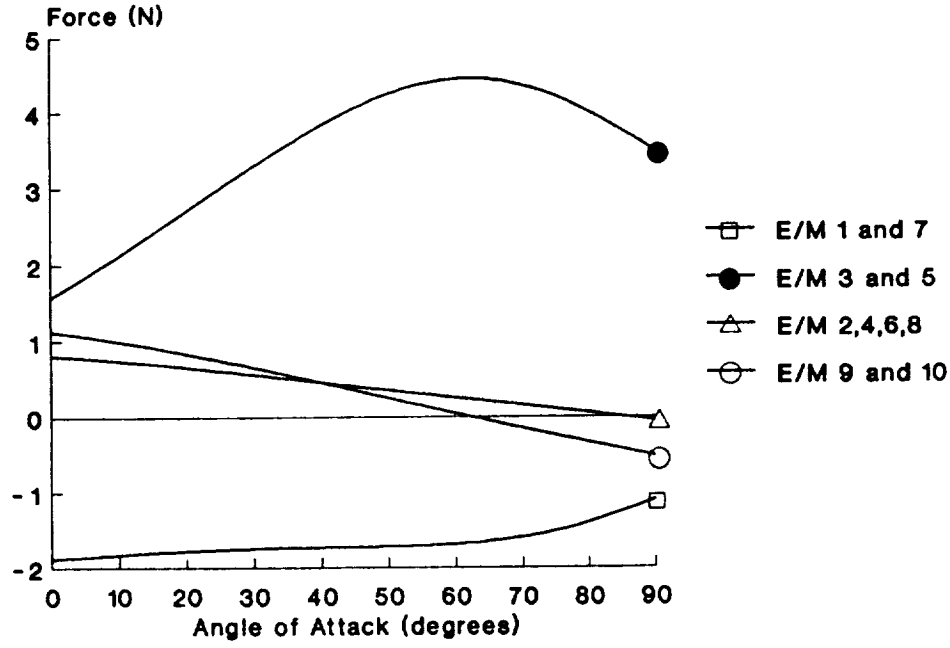

Figure 6.4b Forces in Vertical Plane

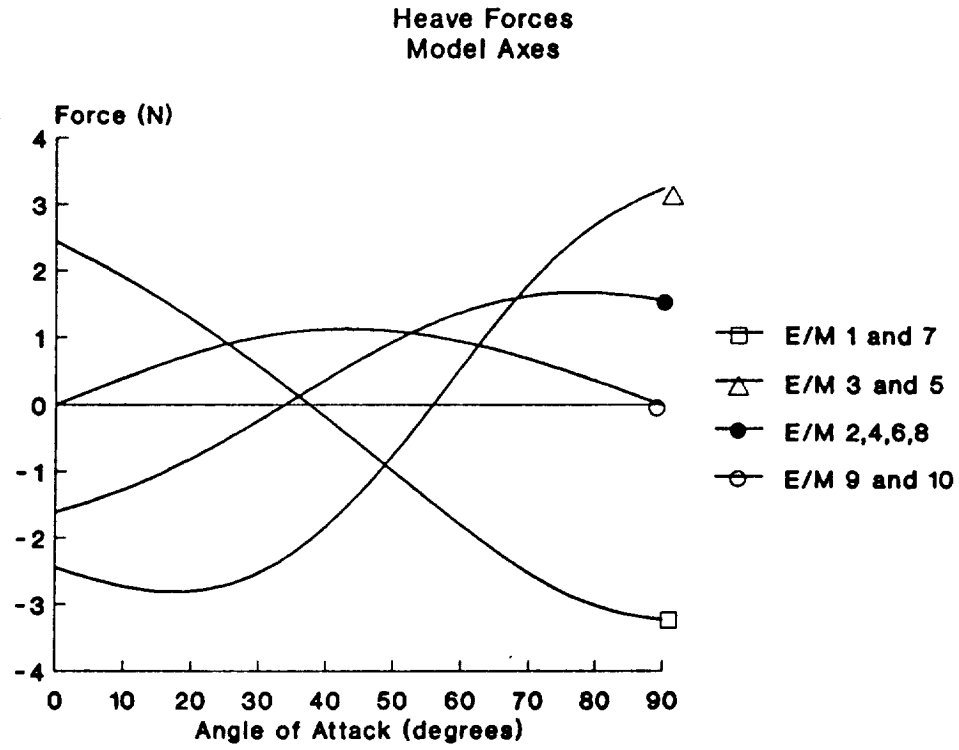

Figure 6.4c: forces in vertical plane

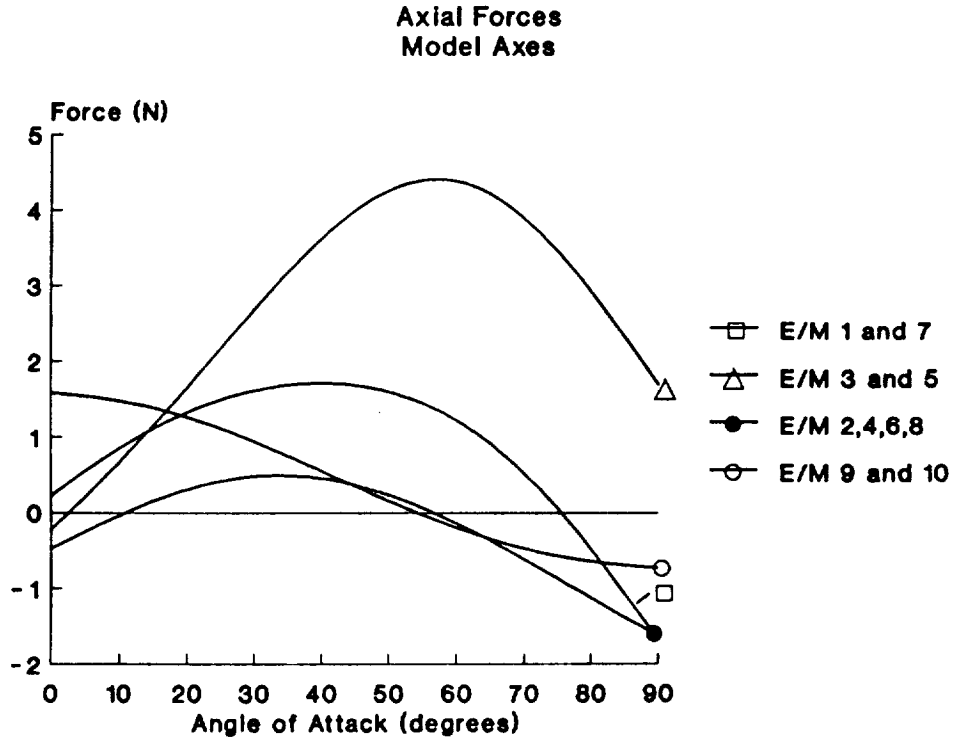

Figure 6.4d: forces in vertical plane

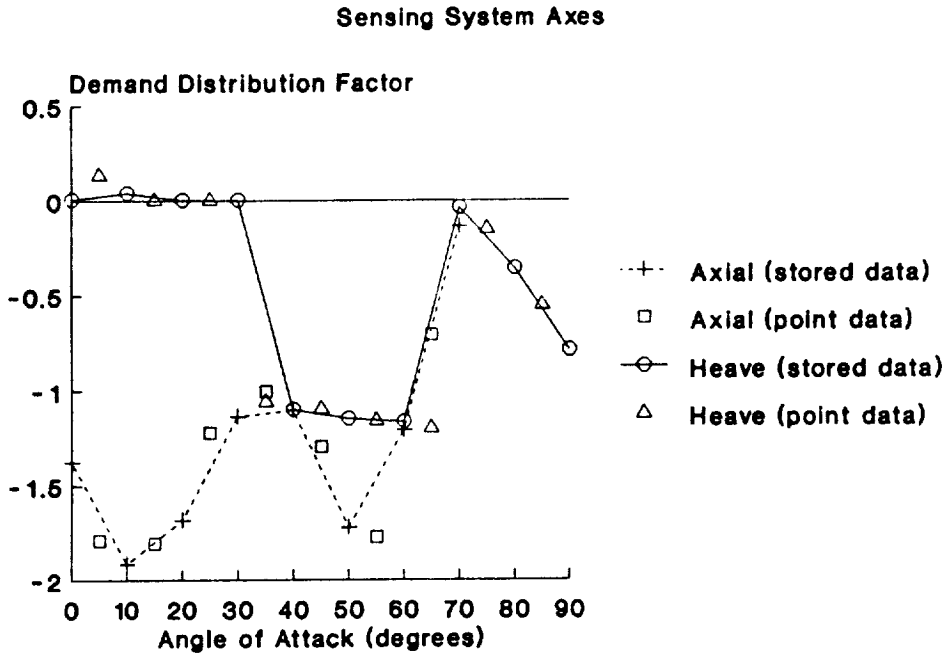

Figure 6.5a: demand distribution
for Electromagnet Group 1

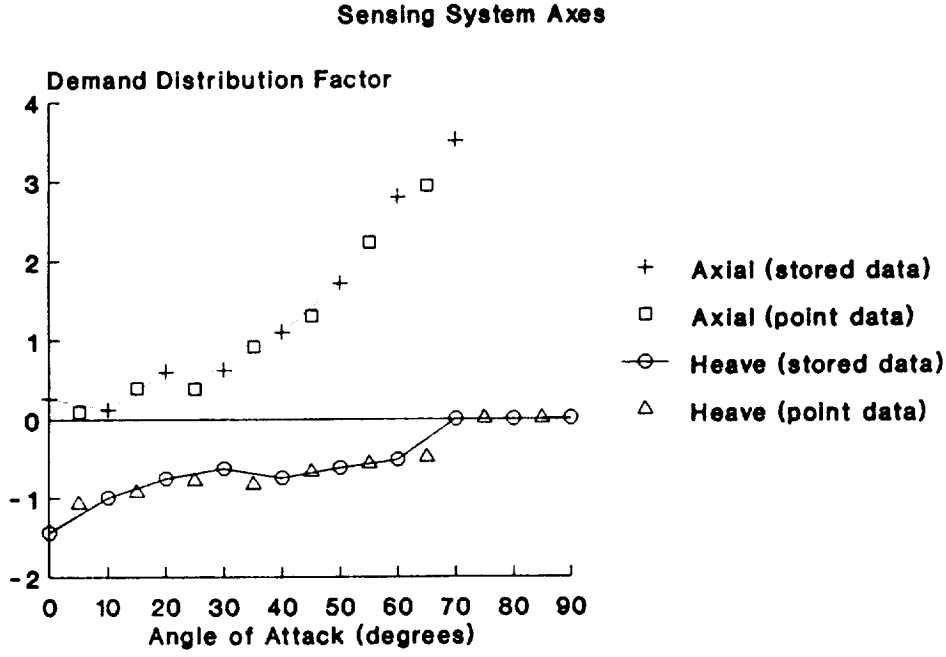

Figure 6.5b: demand distribution
for Electromagnet Group 2

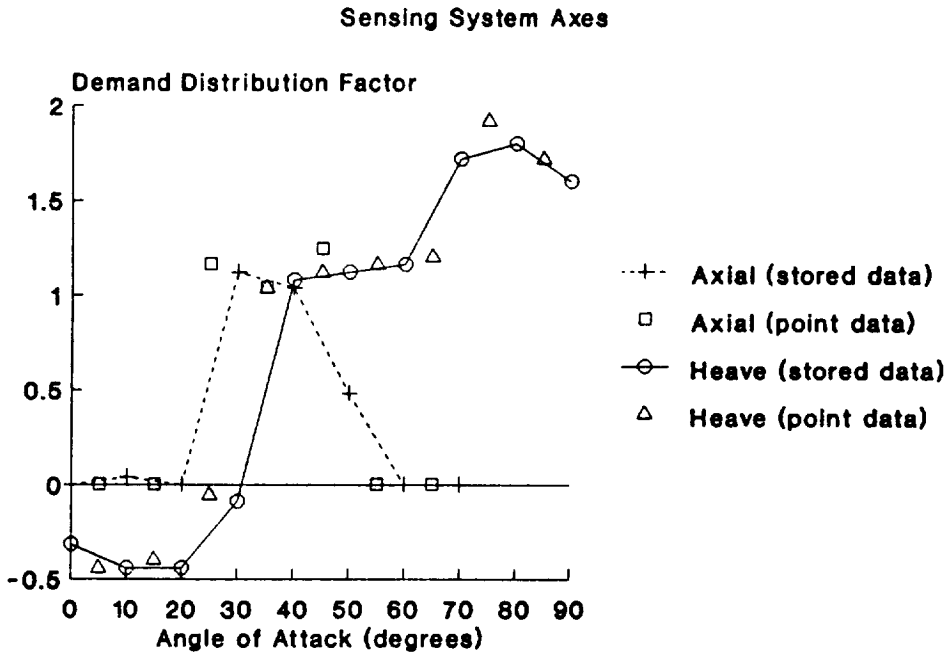

Figure 6.5c: demand distribution for electromagnet group 3

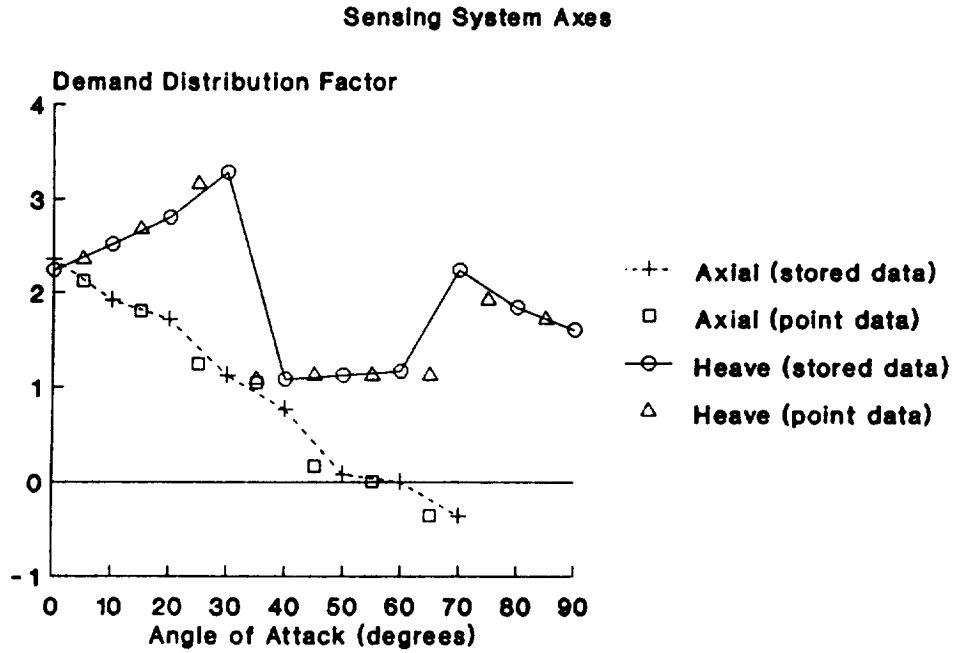

Figure 6.5d: demand distribution for Electromagnet Group 4

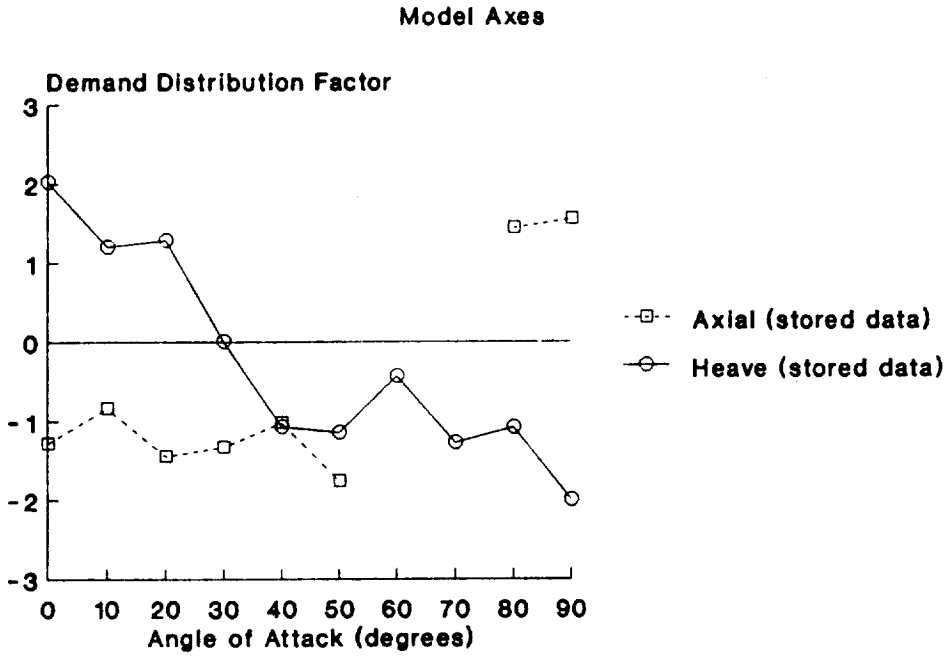

Figure 6.6a: demand distribution for Electromagnet Group 1

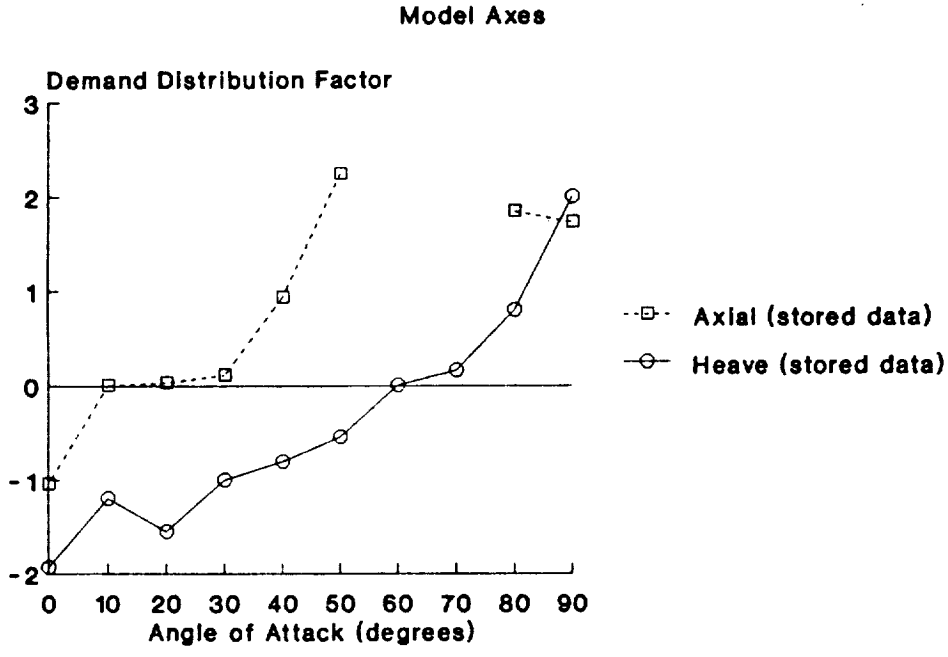

Figure 6.6b: demand distribution for Electromagnet Group 2

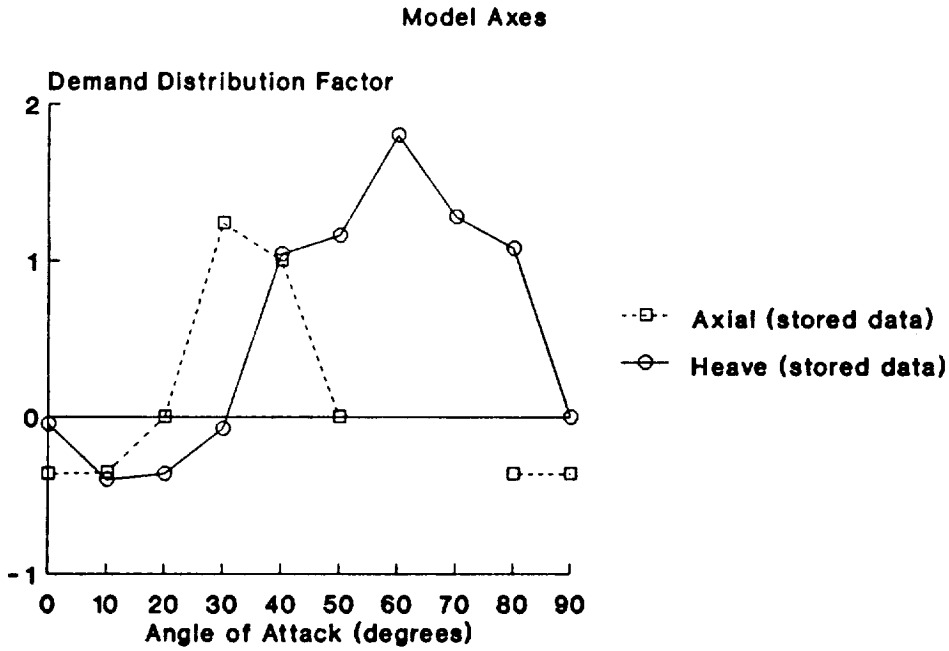

Figure 6.6c: demand distribution
for Electromagnet Group 3

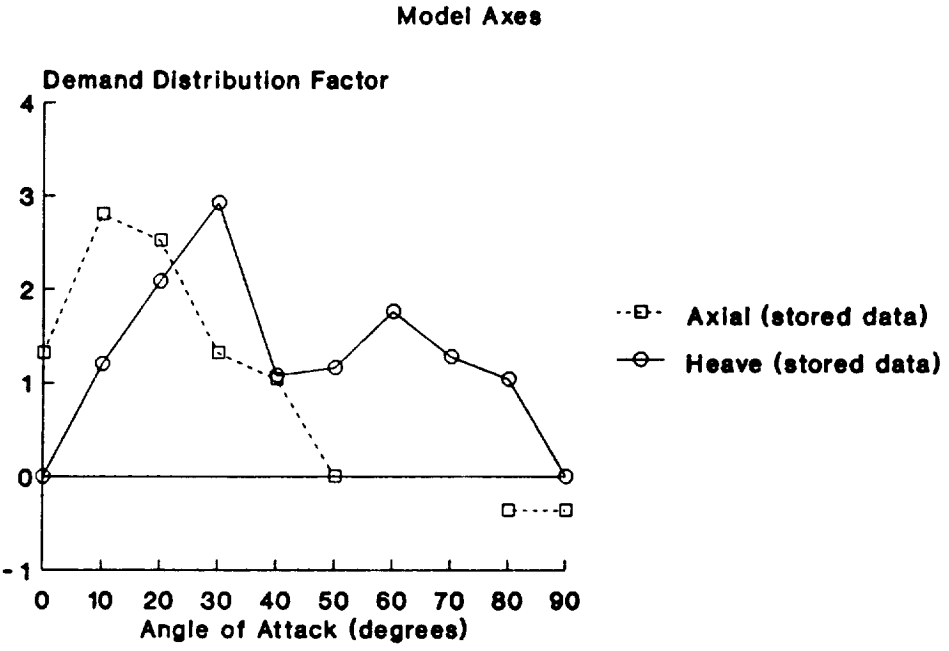

Figure 6.6d: demand distribution
for Electromagnet Group 4

Force Capability in Vertical Plane
Sensing System Axes Controller

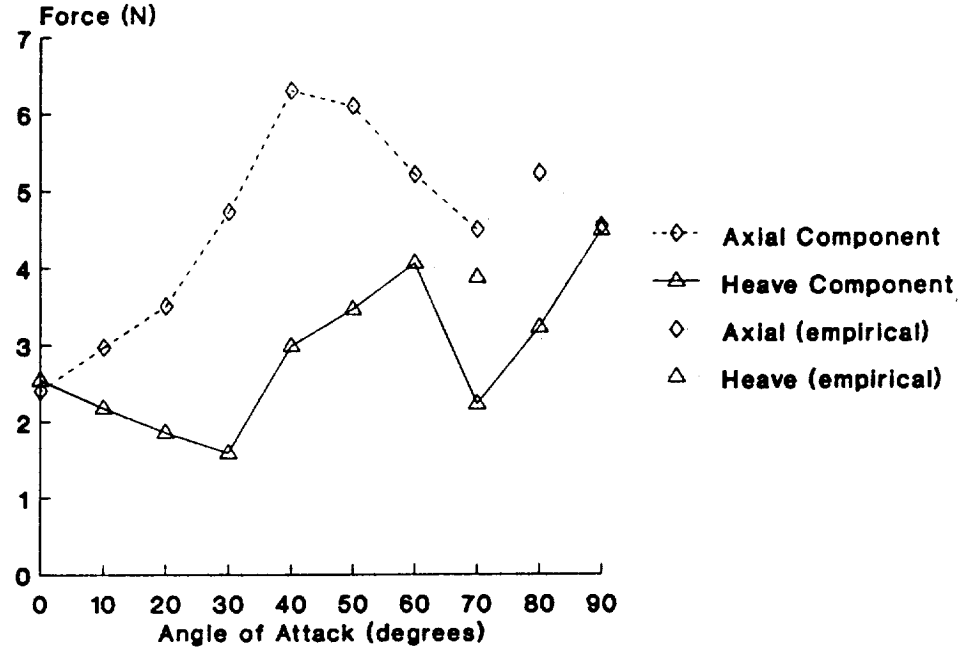

Figure 6.7

Force Capability in Vertical Plane
Model Axes Controller

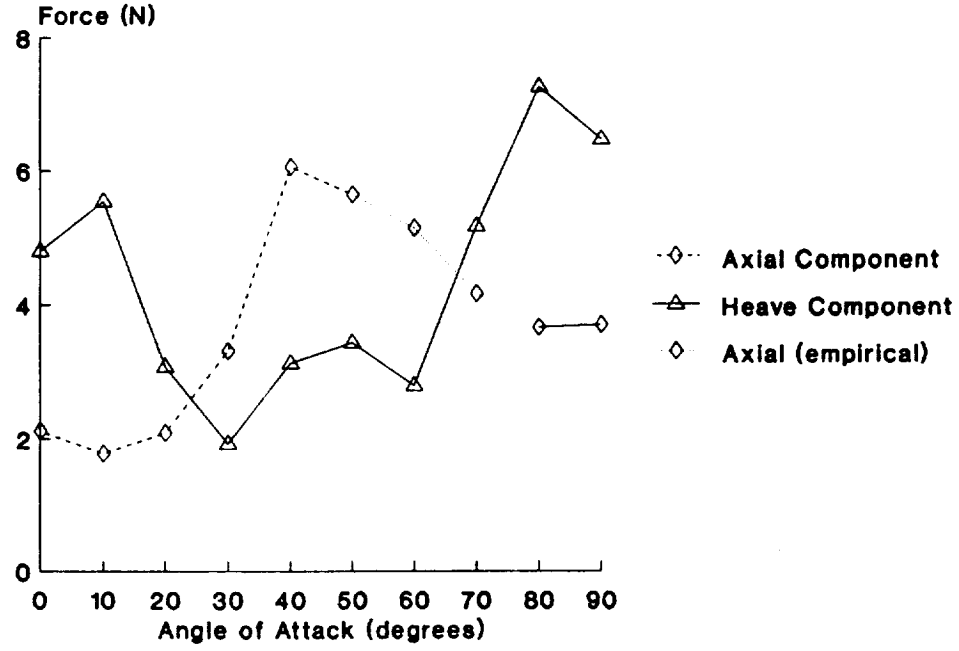

Figure 6.8

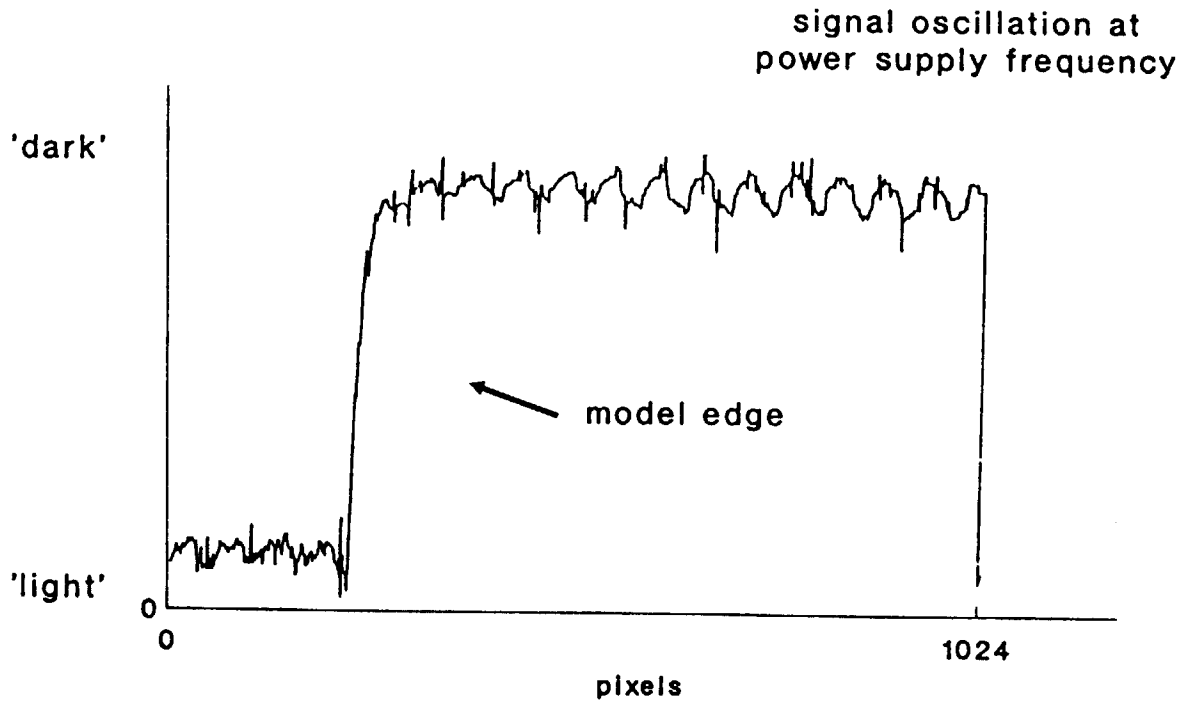

Figure 7.1: showing interference on
axial sensor (no.5) from electromagnets
video output - model in suspension

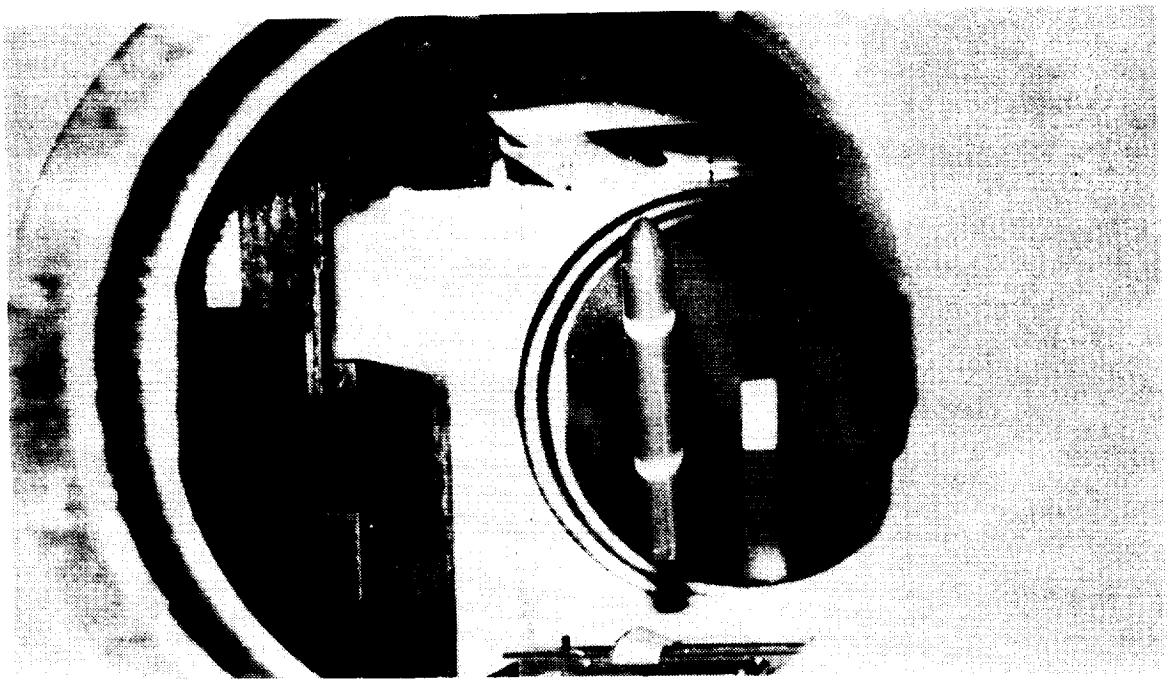

Figure 7.2a: an early test showing model at 70 degrees angle of attack: view down-stream

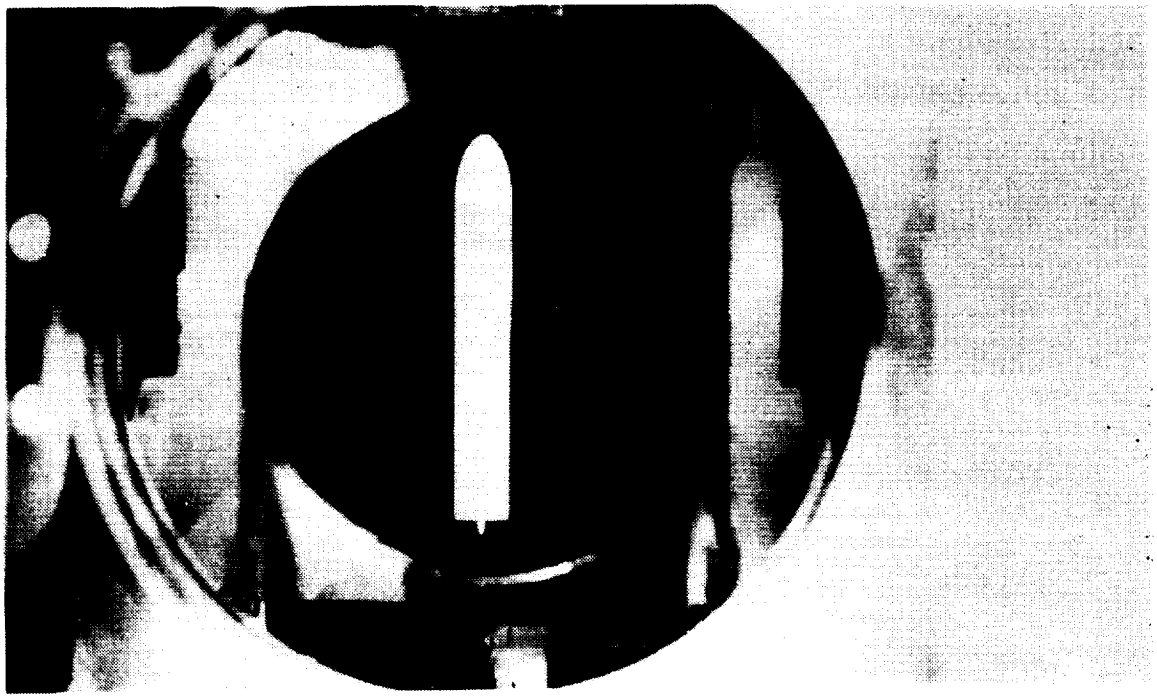

Figure 7.2b: a model at ninety degrees angle of attack showing high-lighted sensing system laser beams

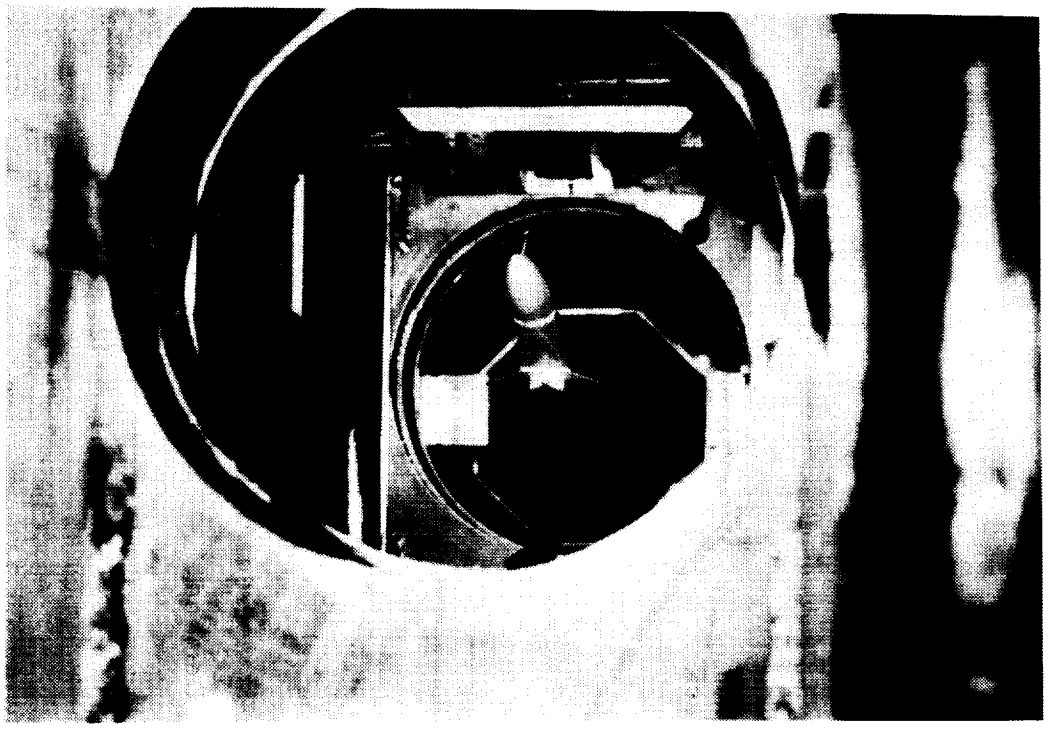

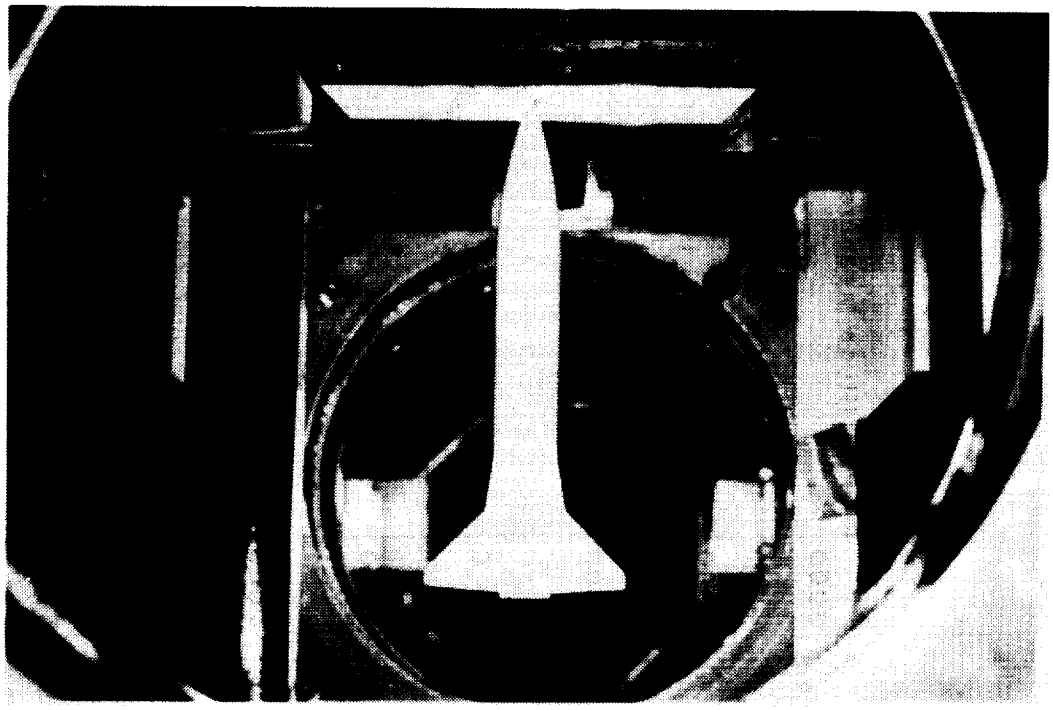

Figure 7.3: a demonstration model at 20 degrees and seventy degrees angle of attack

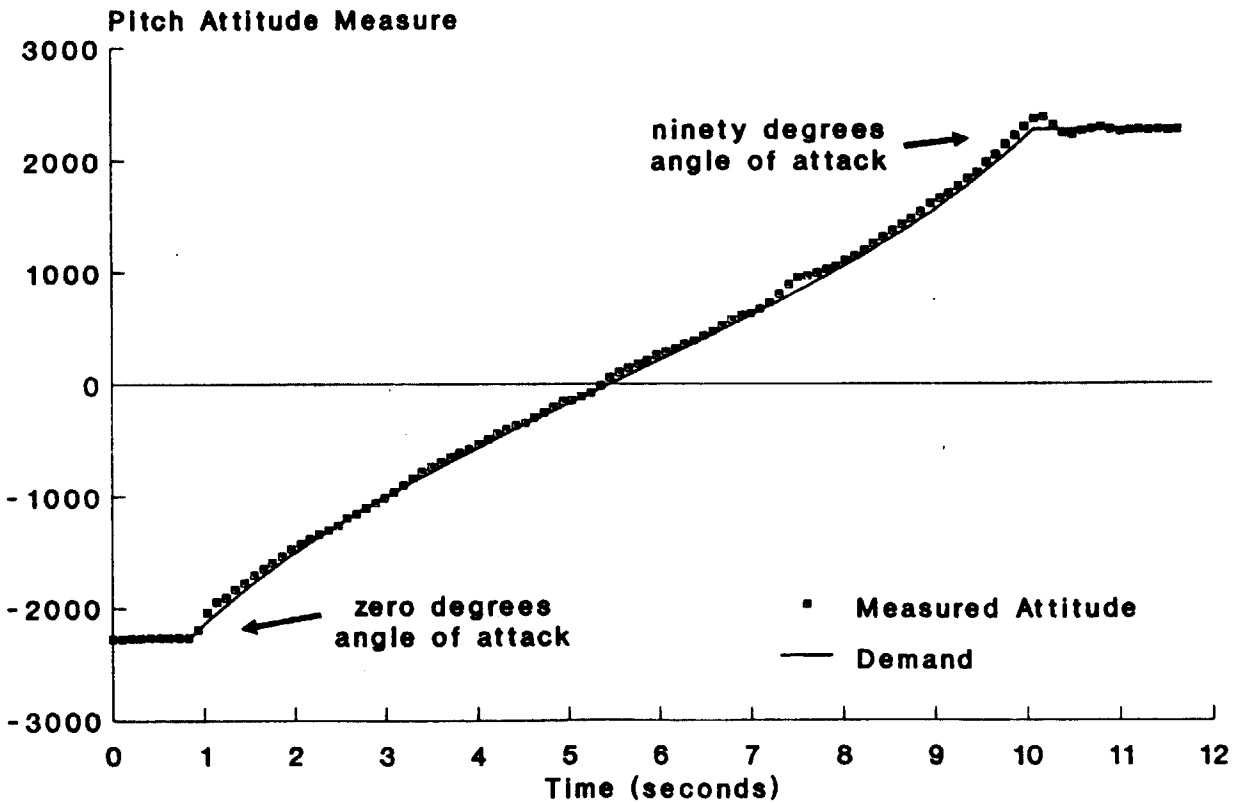

Figure 7.4: attitude-demand following
for a nought to ninety degree
model rotation

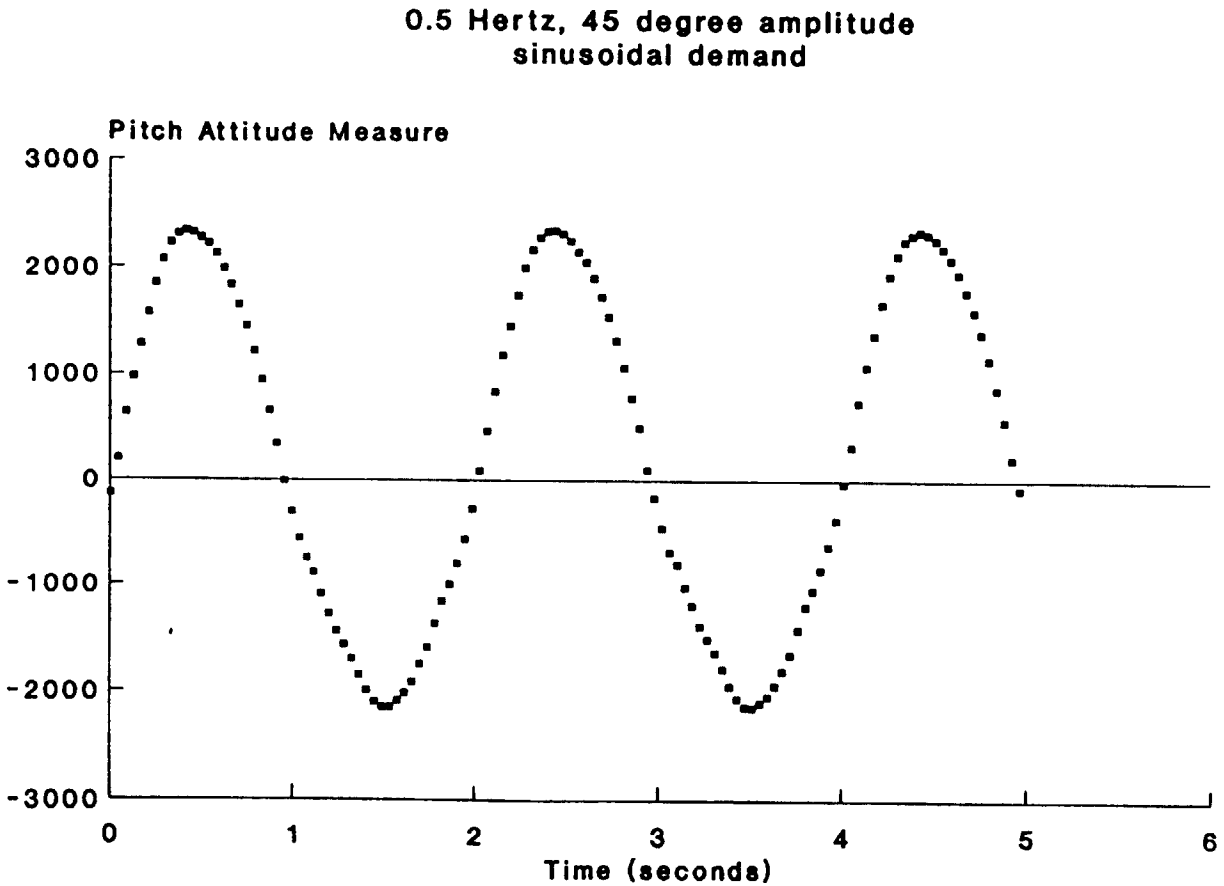

Figure 7.7: large amplitude oscillation in angle of attack

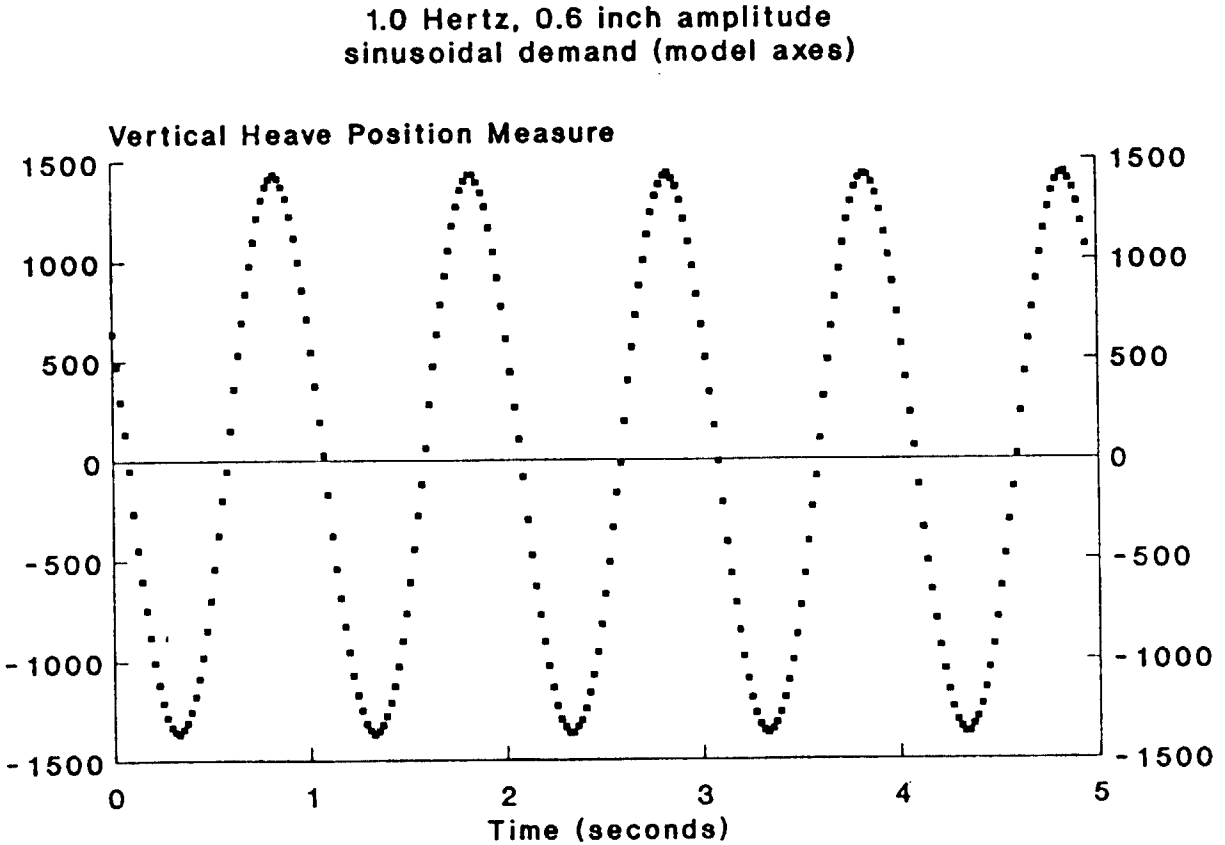

Figure 7.8: large amplitude heave oscillation at 45 degrees angle of attack

25 degrees to 45 degrees
angle of attack

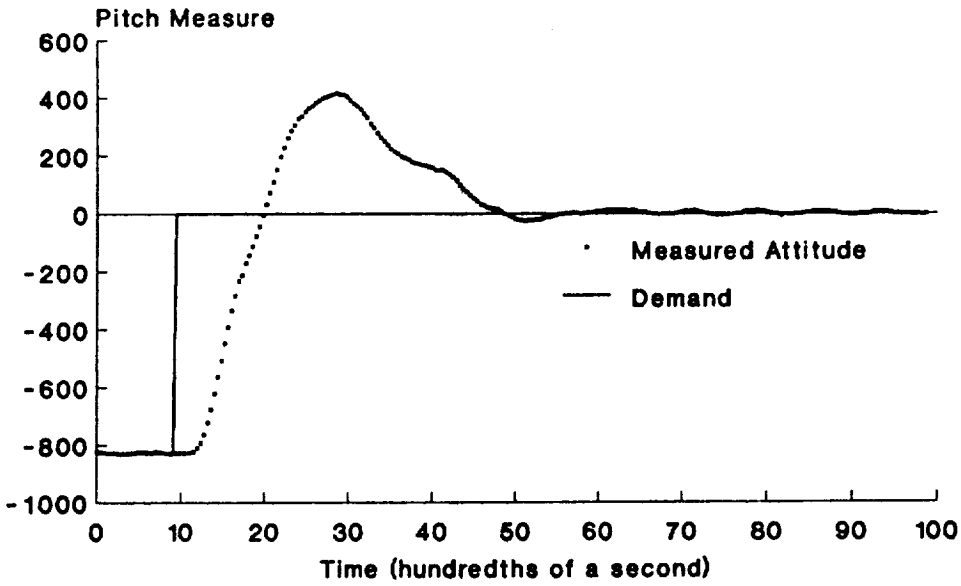

Figure 7.5: response of model to
step demand for change in attitude

25 to 65 degrees
angle of attack

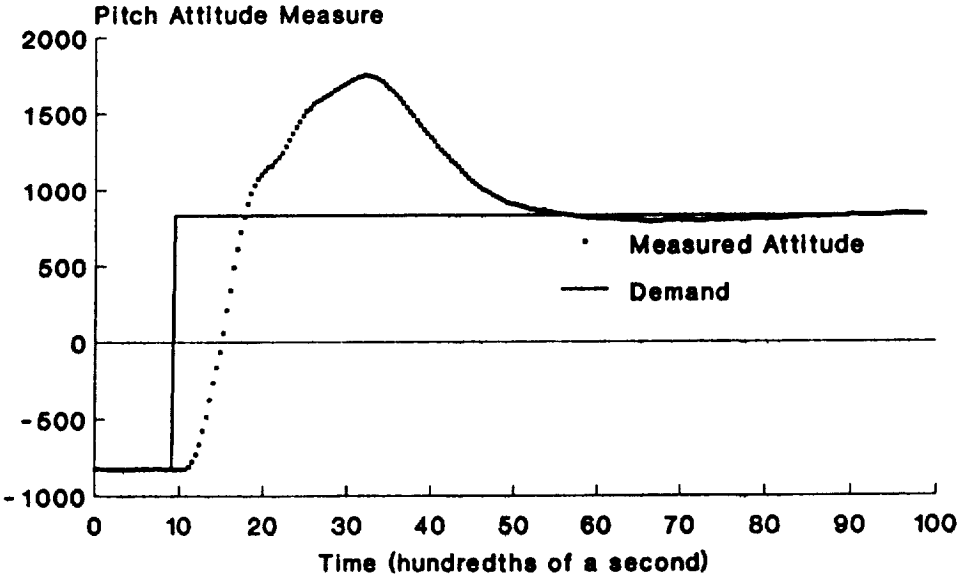

Figure 7.6: response of model to
step demand for change in attitude

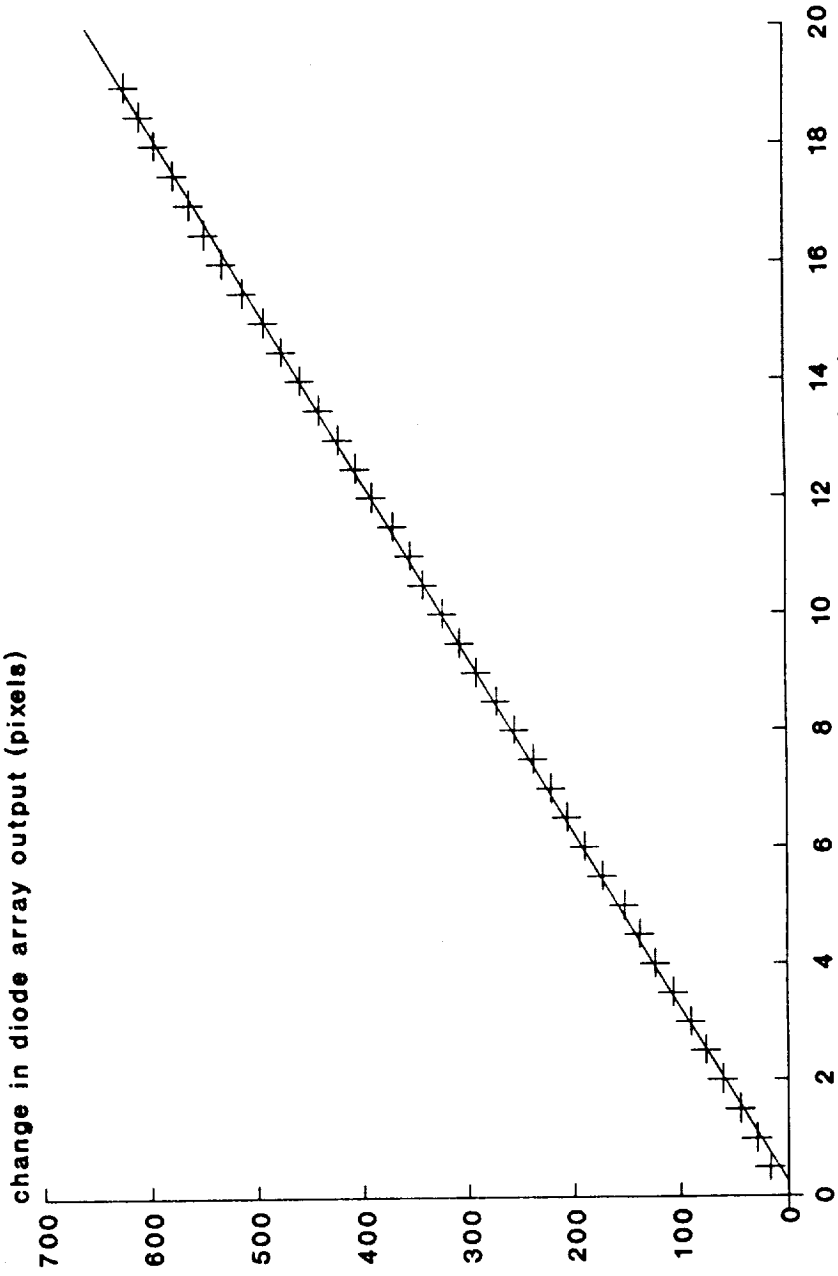

Figure 8.1: partial calibration of channel 1 photodiode array

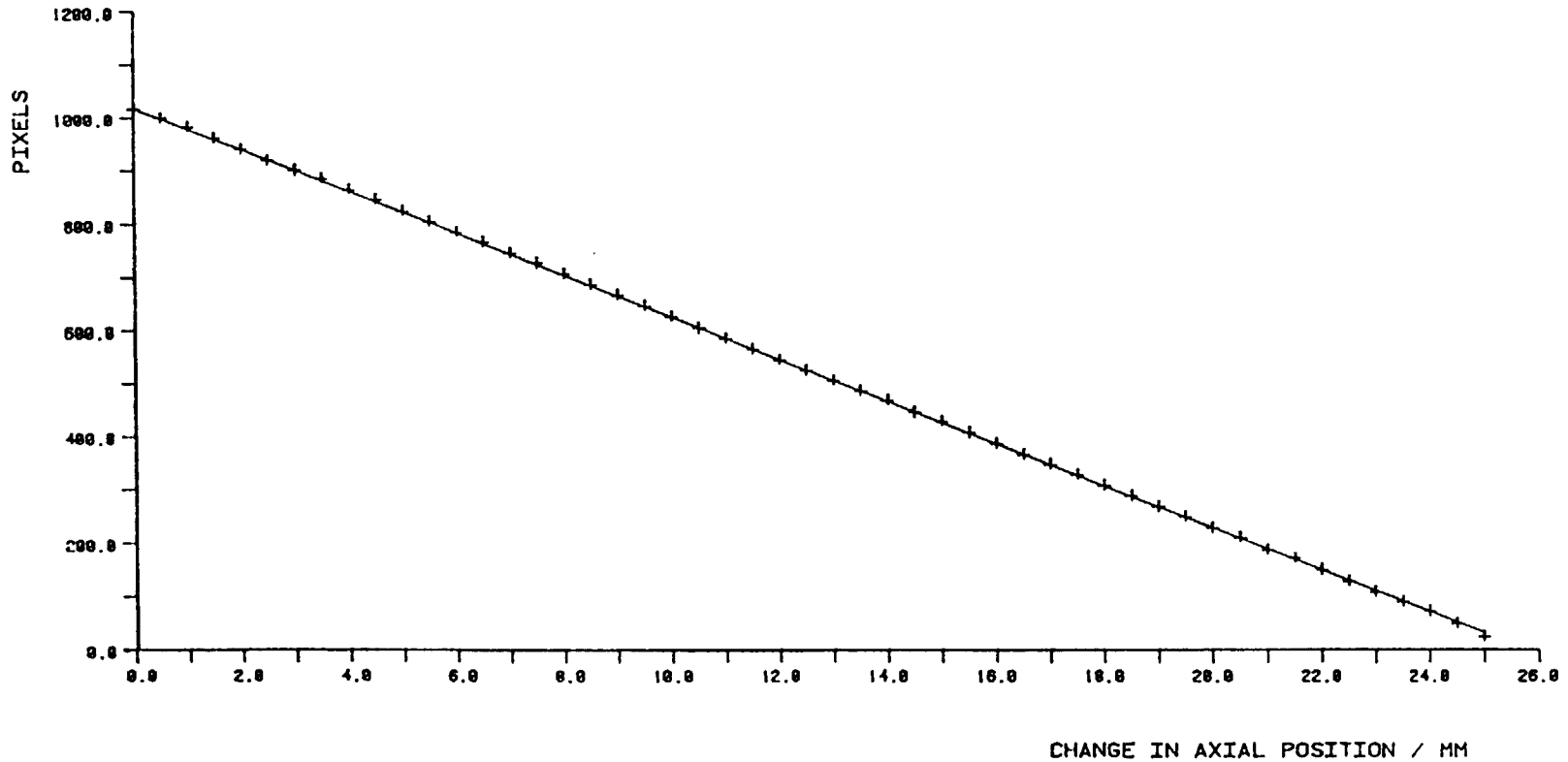

Figure 8.2: a calibration of the axial diode array sensor

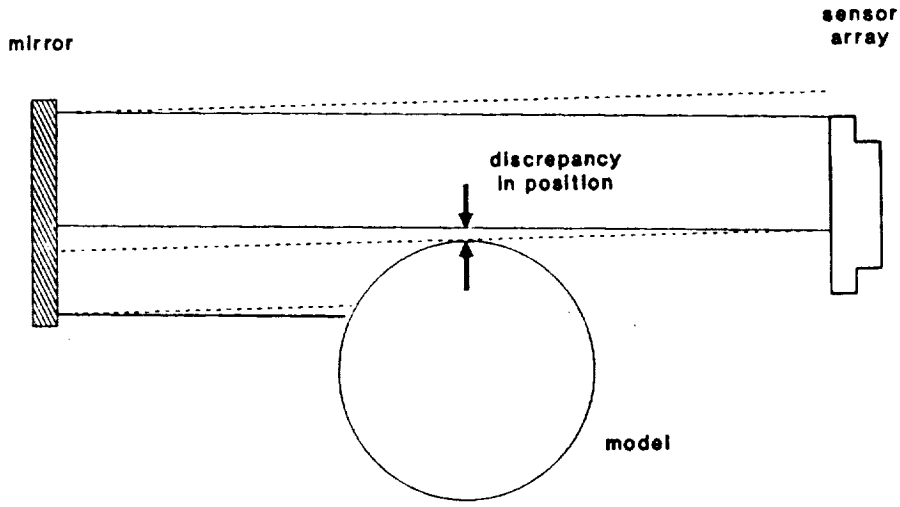

Figure 8.3: showing how an change in a mirror angle can result in an error in model position or attitude

Beams travelling from mirror at left to sensor at right
No change in array output is seen

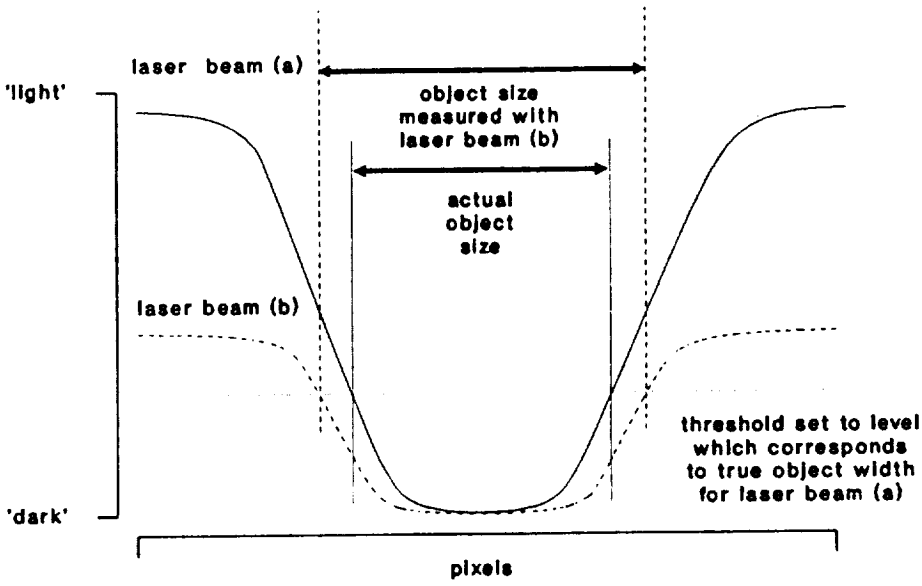

Figure 8.4: illustrating how the irradience level of an illuminating laser beam can affect the measured width of an object with a fixed transition detector threshold

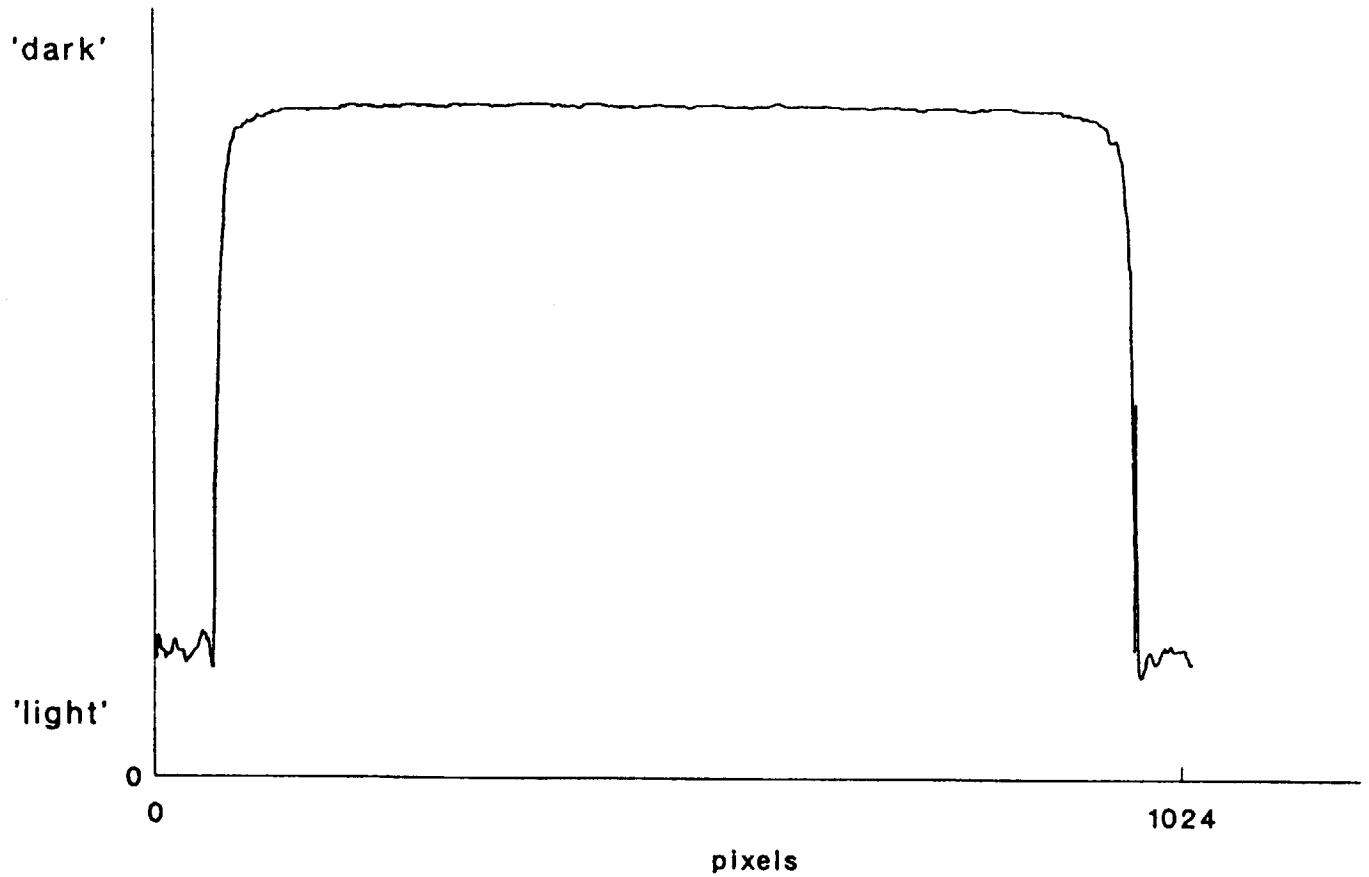

Figure 8.5a: video output on channel 1

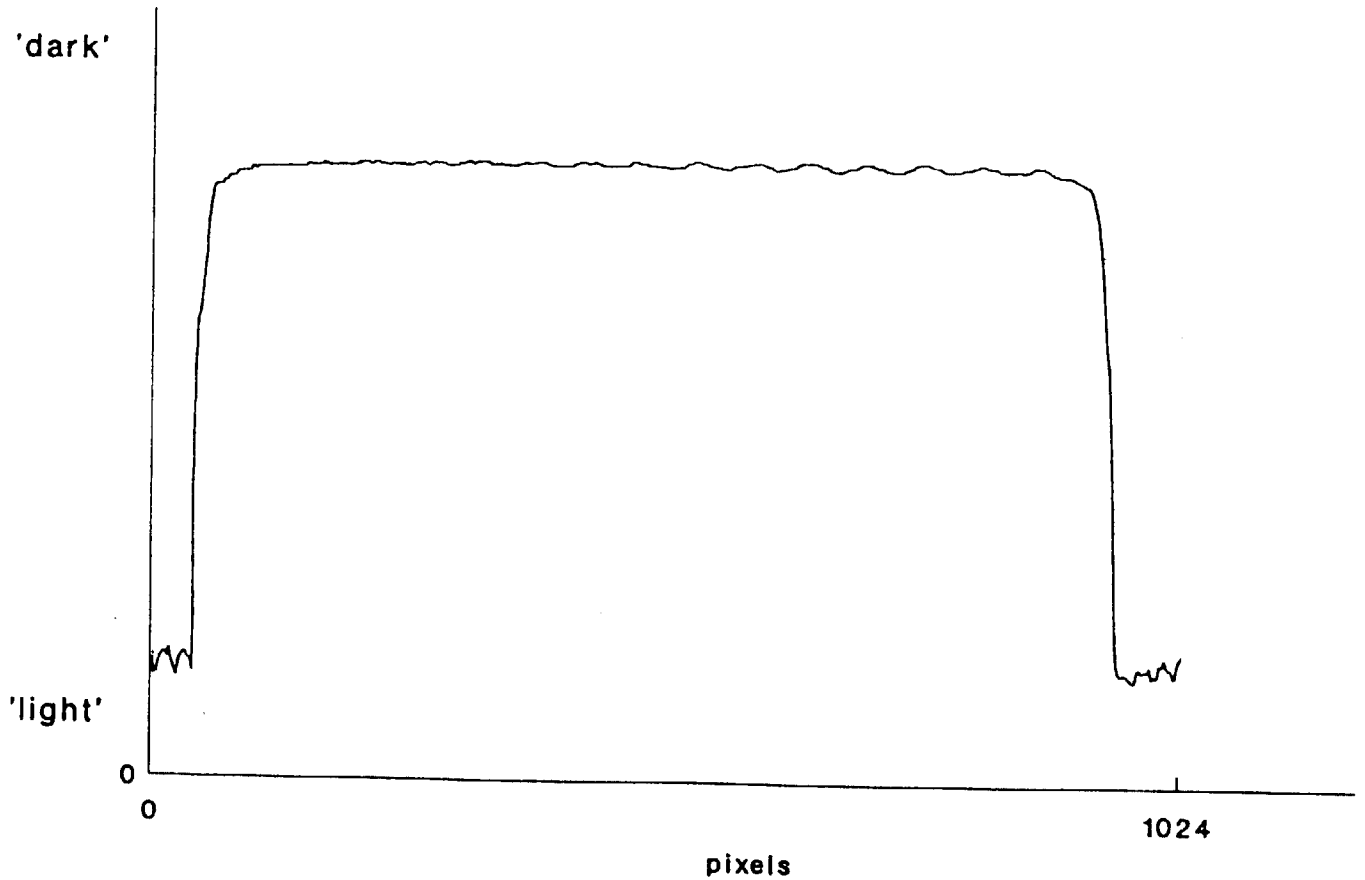

Figure 8.5b: video output on channel 2

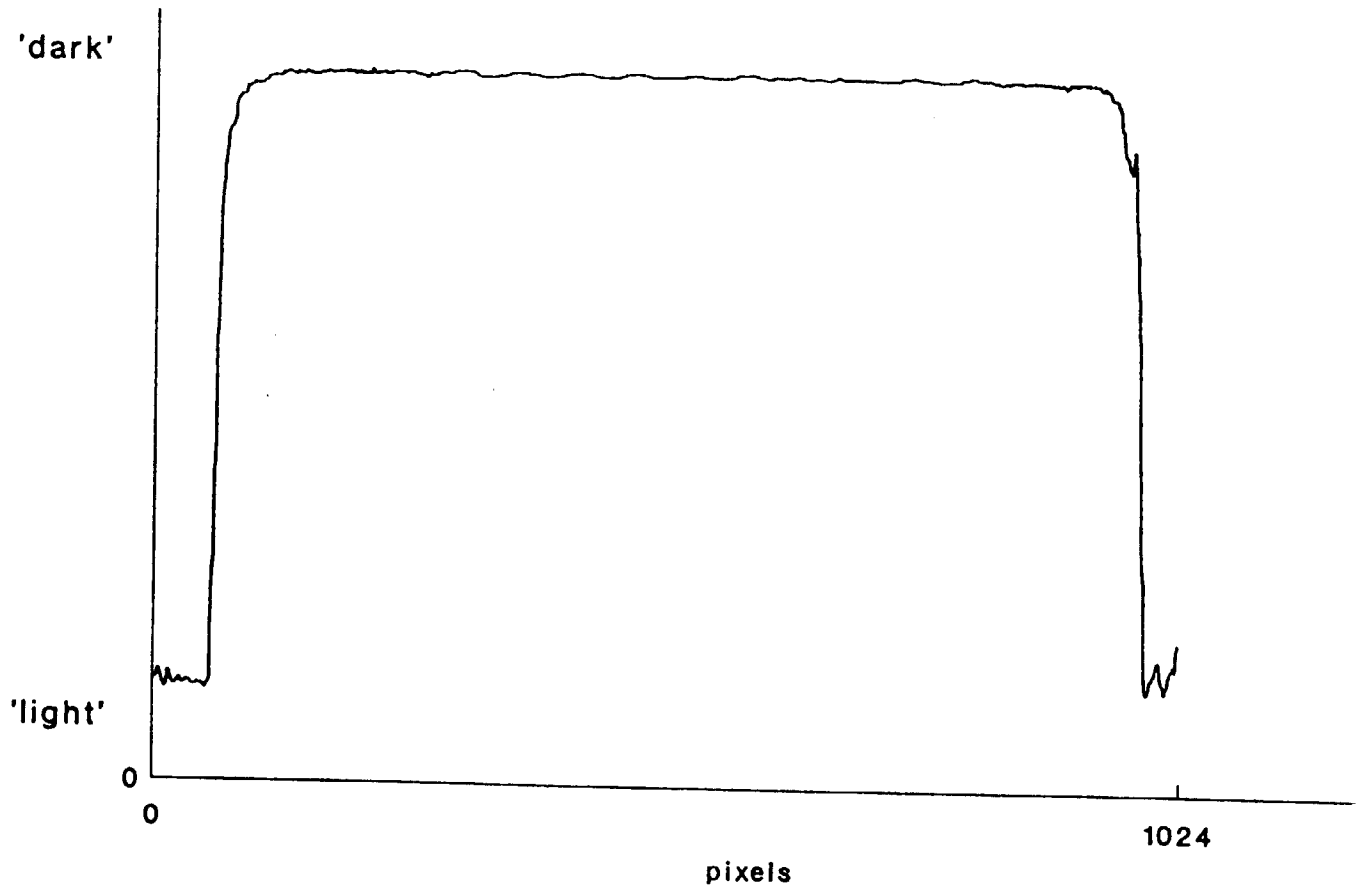

Figure 8.5c: video output on channel 3

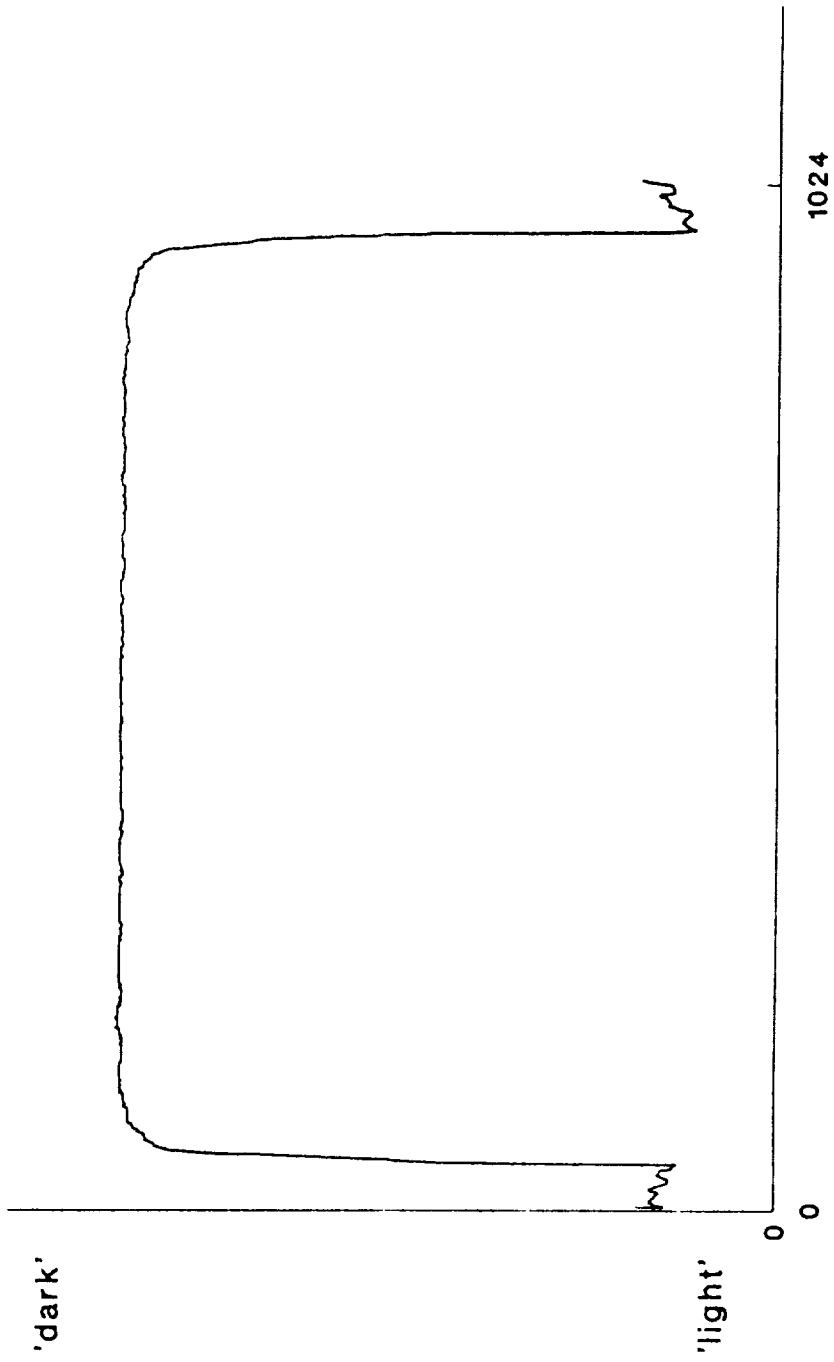

Figure 8.5d: video output on channel 4

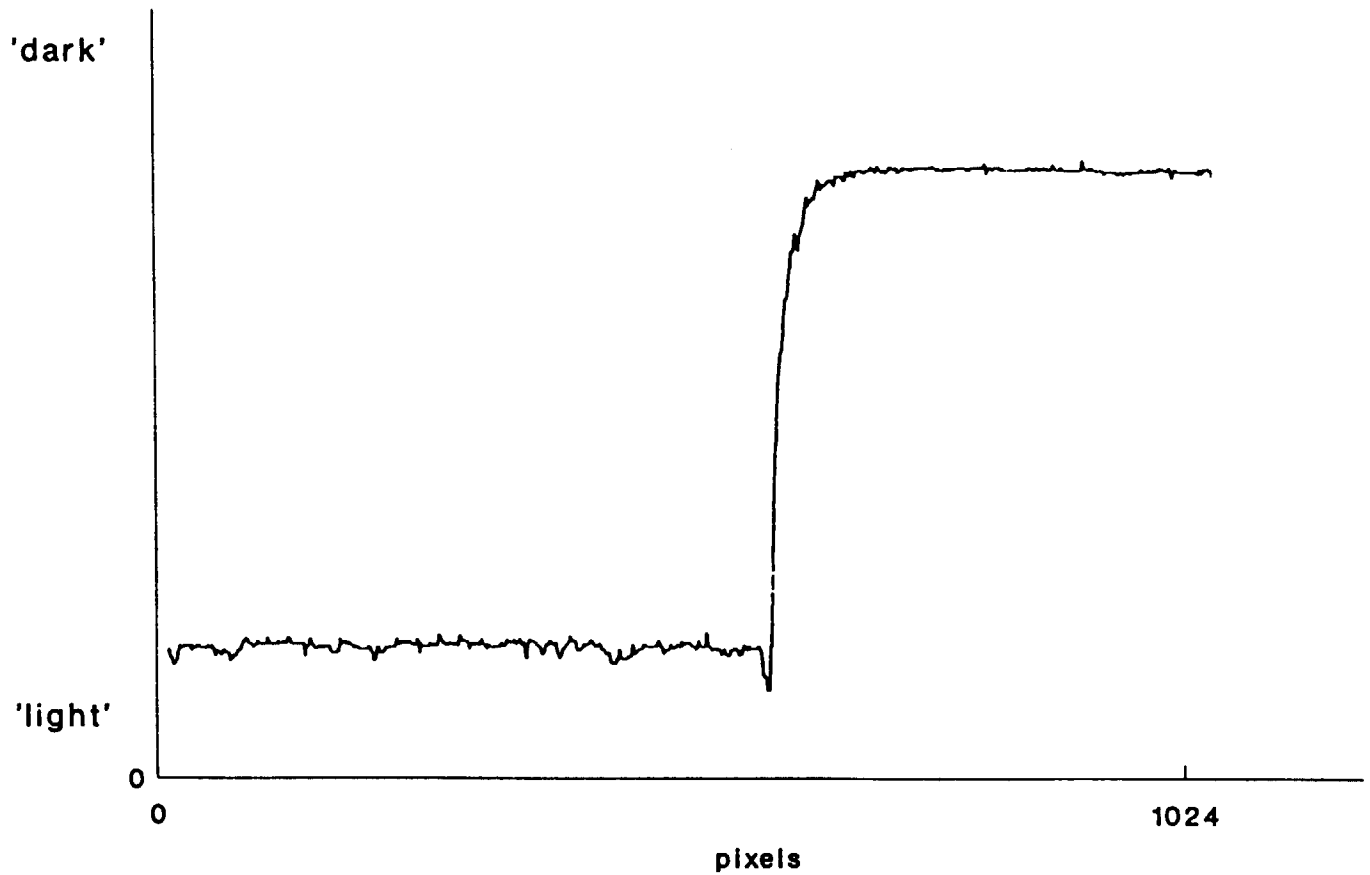

Figure 8.5e: video output on channel 5

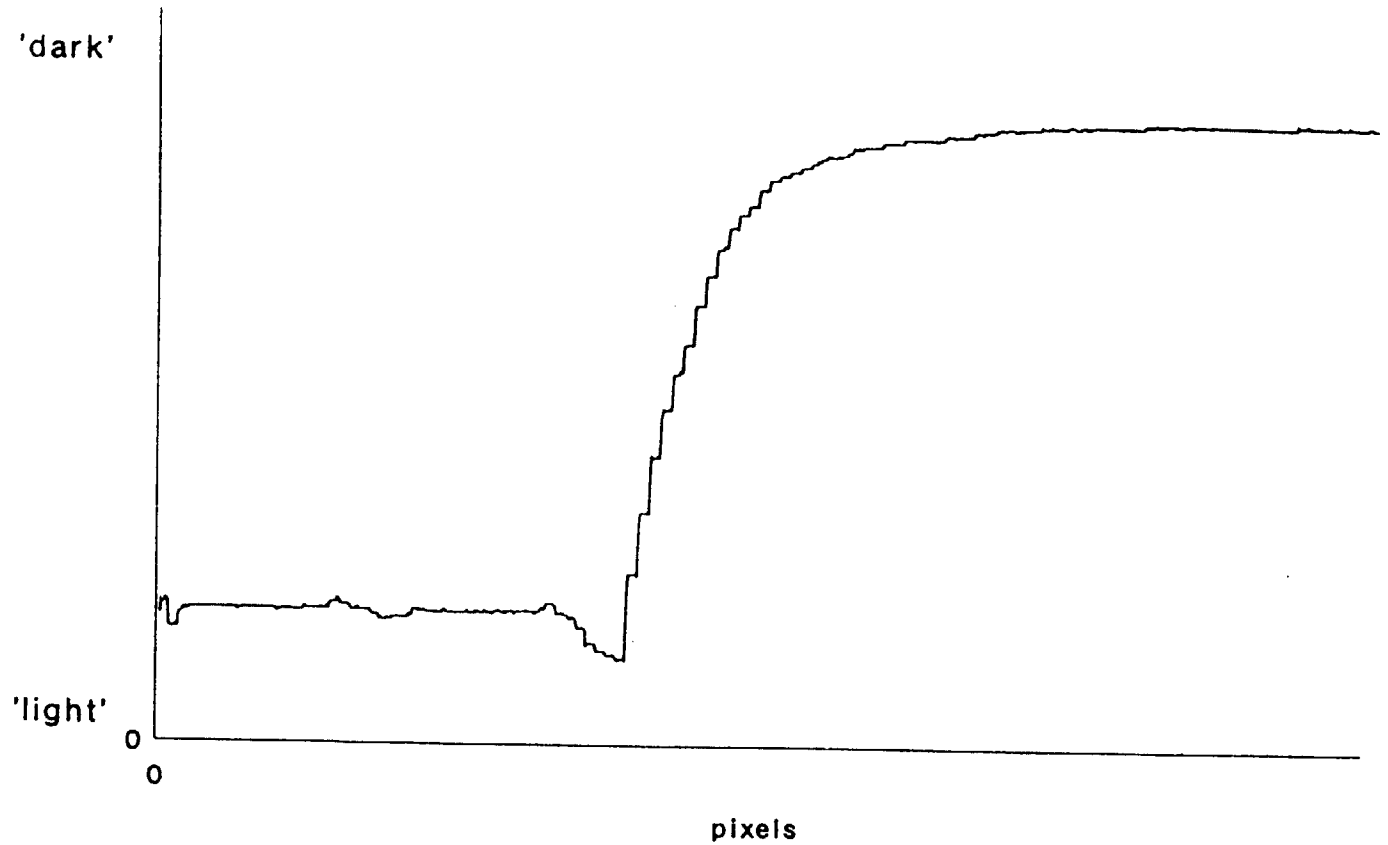

Figure 8.6: video output on channel 1
expanded to show one edge transition

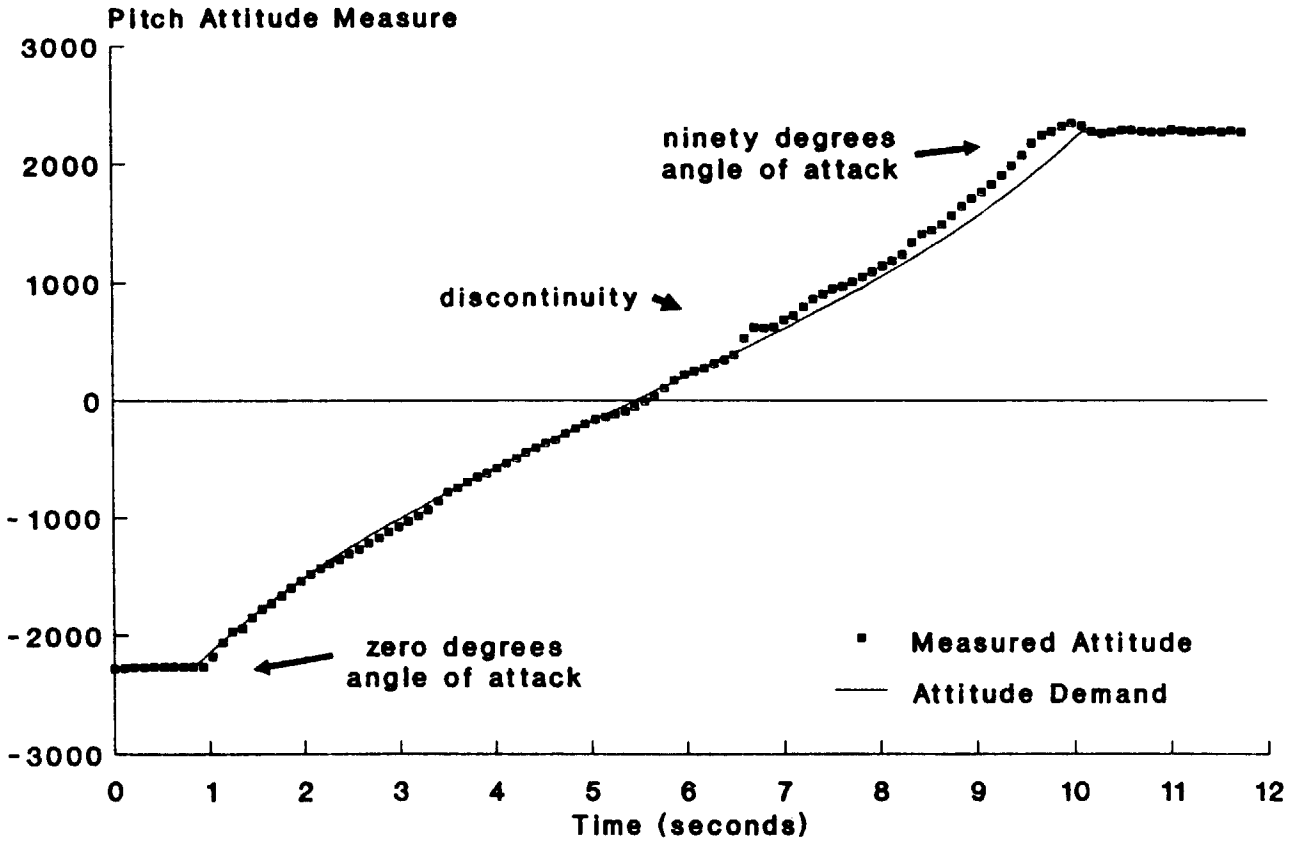

Figure 8.7: attitude demand-following for a 0 to 90 degree sweep showing a discontinuity caused by sensing system

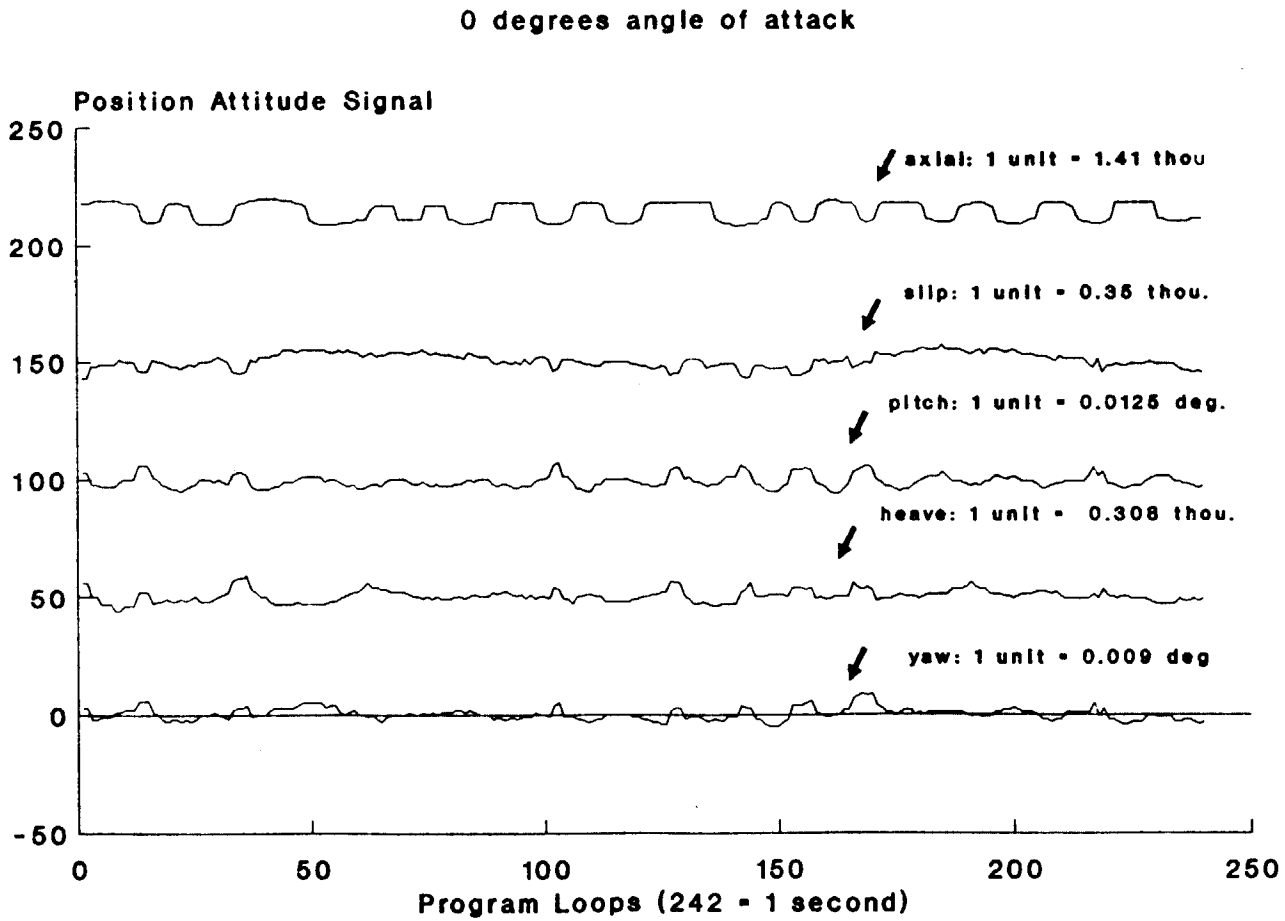

Figure 8.8a: position and attitude station keeping data

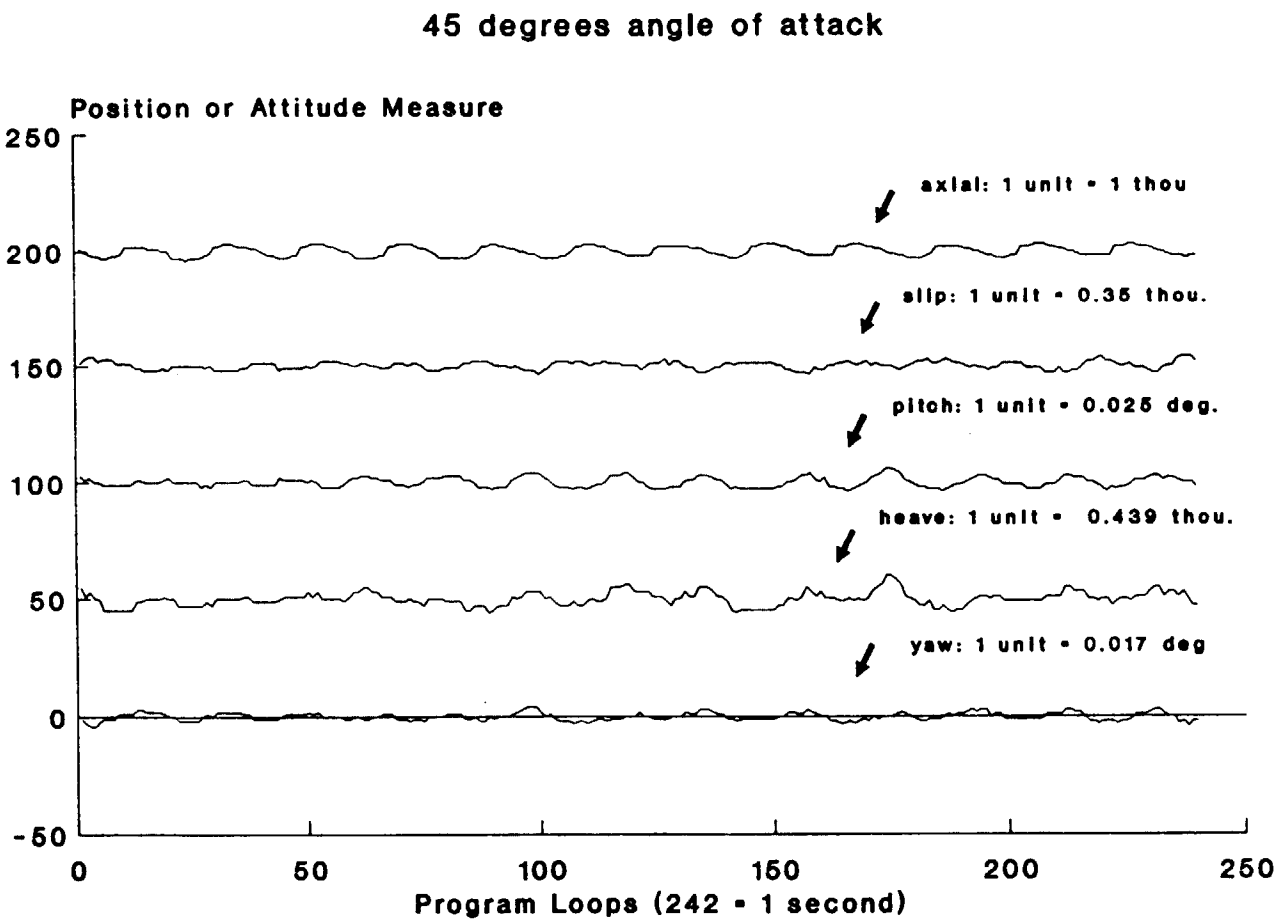

Figure 8.8b: position and attitude station keeping data

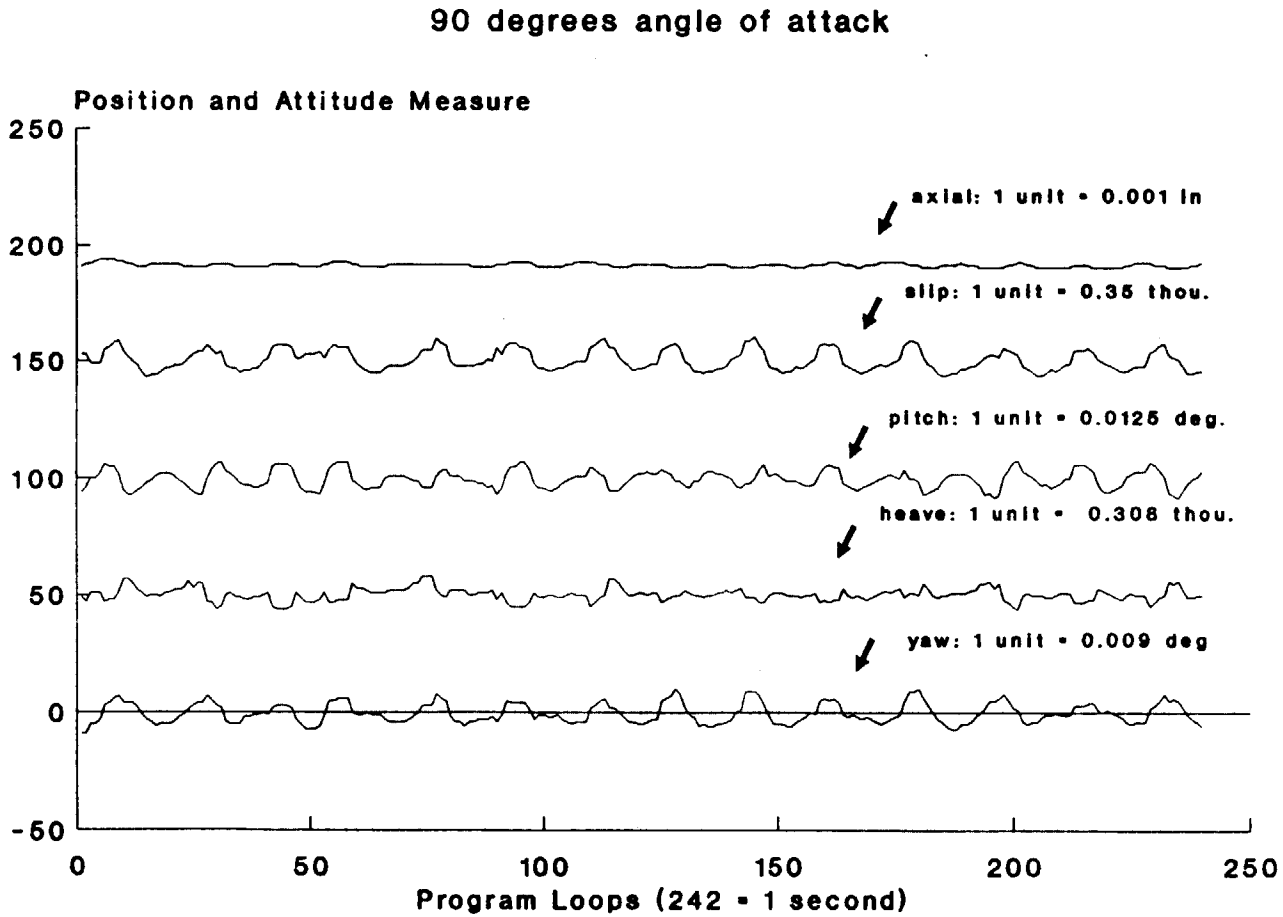

Figure 8.8c: position and attitude station keeping data

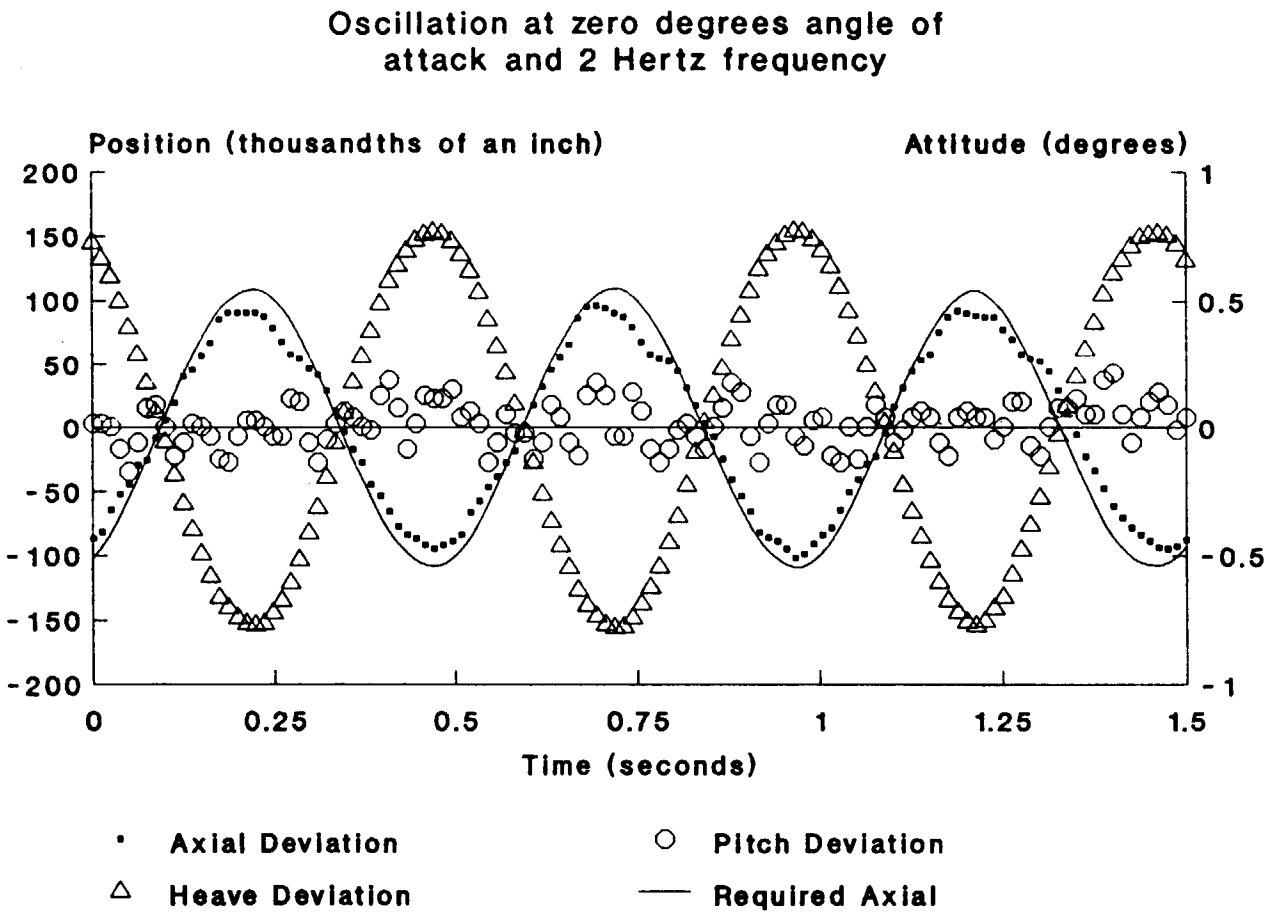

Figure 9.1: position and attitude in response to a demand for a vertical heave oscillation

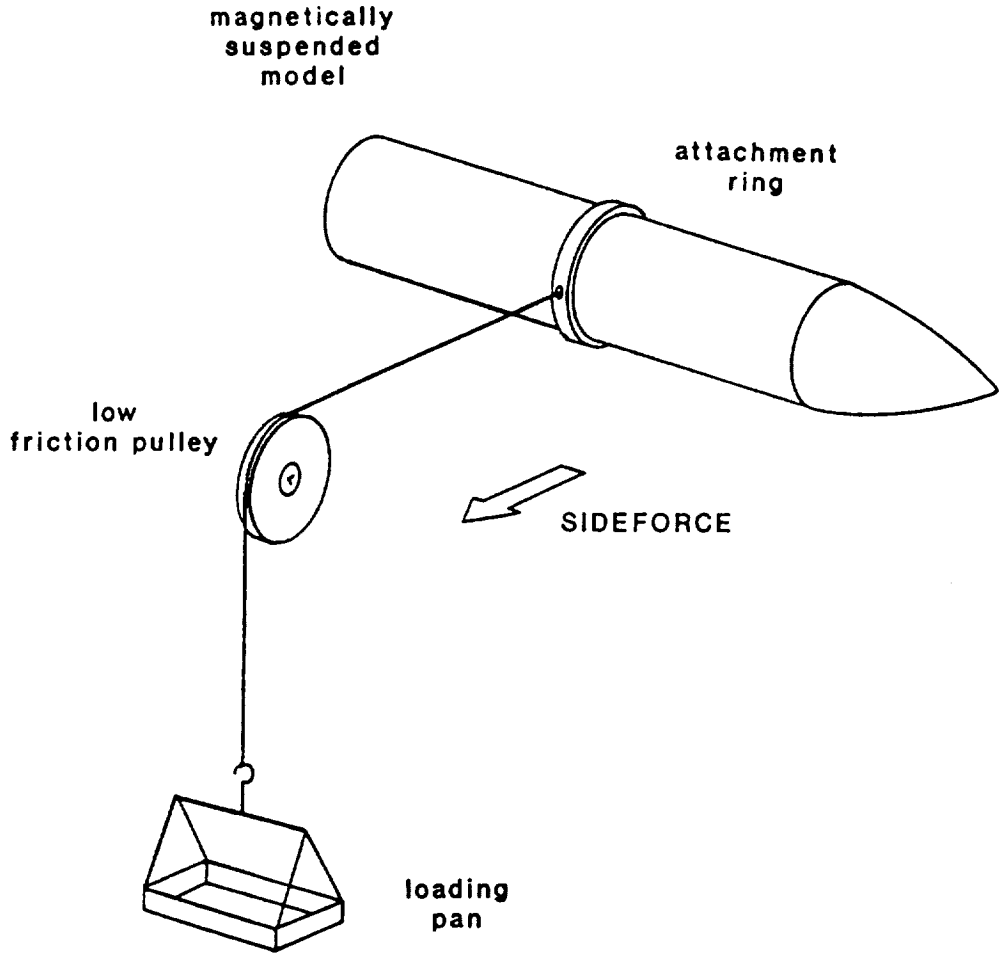

Figure 9.2: showing technique for applying sideforce loads to a magnetically suspended model

Gradient = 20.0 A/N

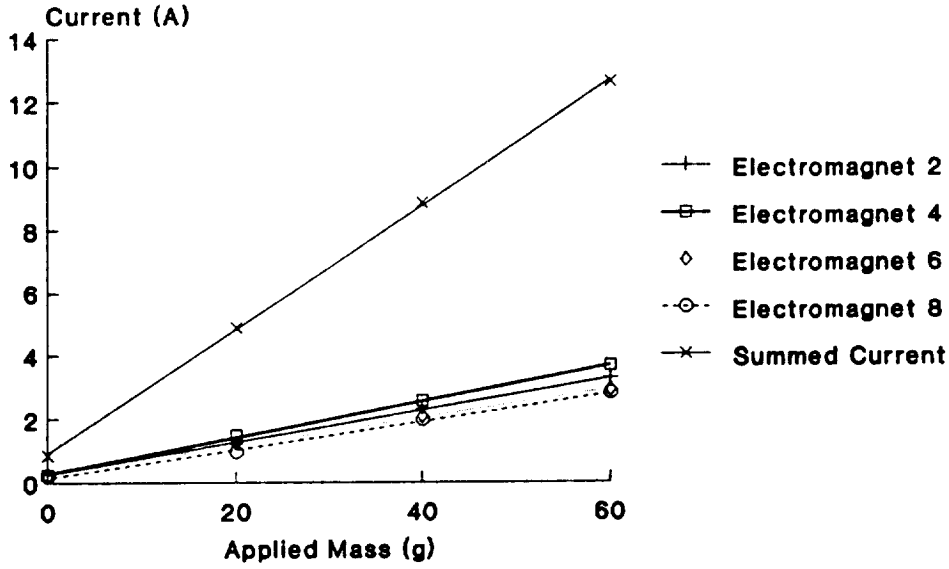

Figure 9.3a: sideforce calibration

Angle of Attack = 10 degrees

Gradient = 17.92 A/N

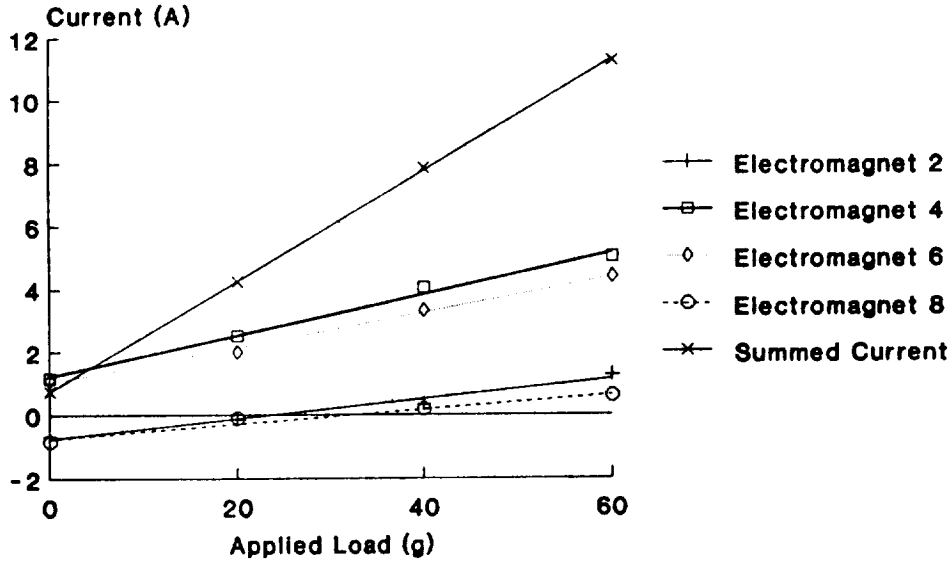

Figure 9.3b: sideforce calibration

Angle of Attack = 10 degrees

Gradient = 16.48 A/N

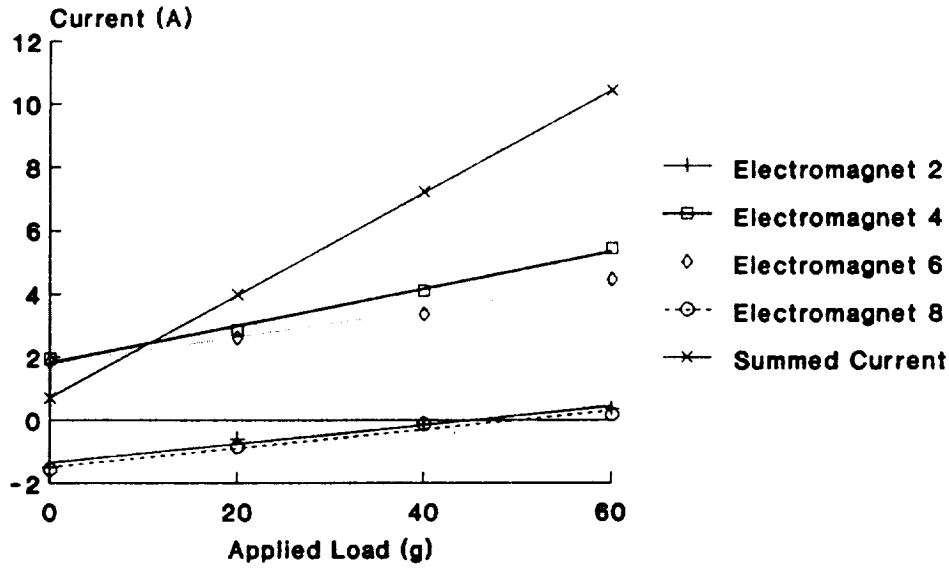

Figure 9.3c: sideforce calibration

Angle of Attack = 20 degrees

Gradient = 15.94 A/N

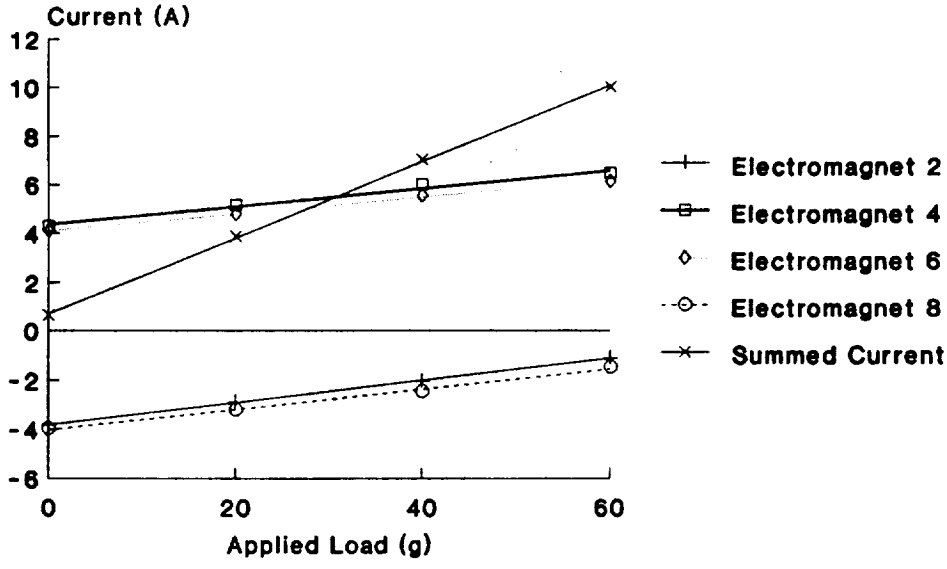

Figure 9.3d: sideforce calibration

Angle of Attack = 30 degrees

Gradient = 15.95 A/N

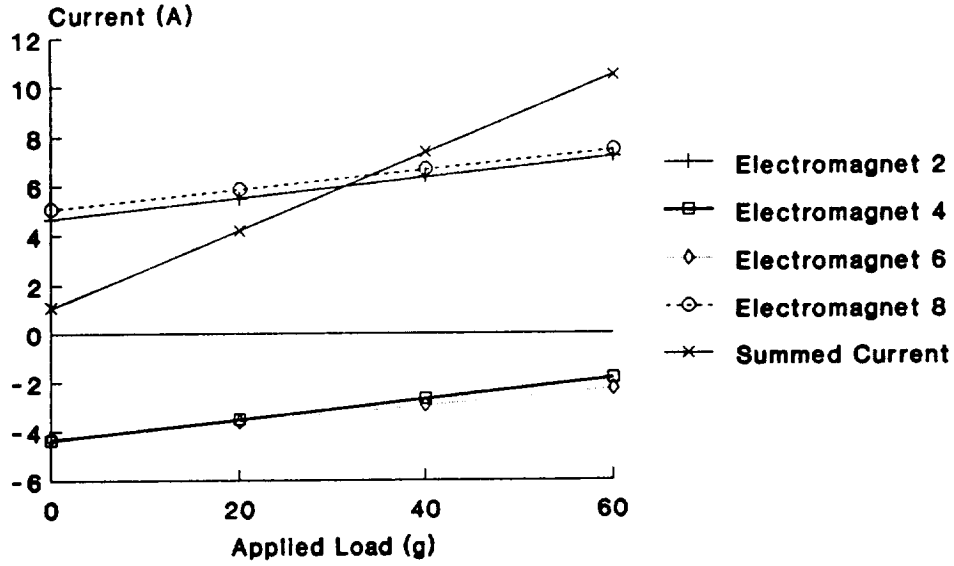

Figure 9.3e: sideforce calibration

Angle of Attack = 40 degrees

Gradient = 16.95 A/N

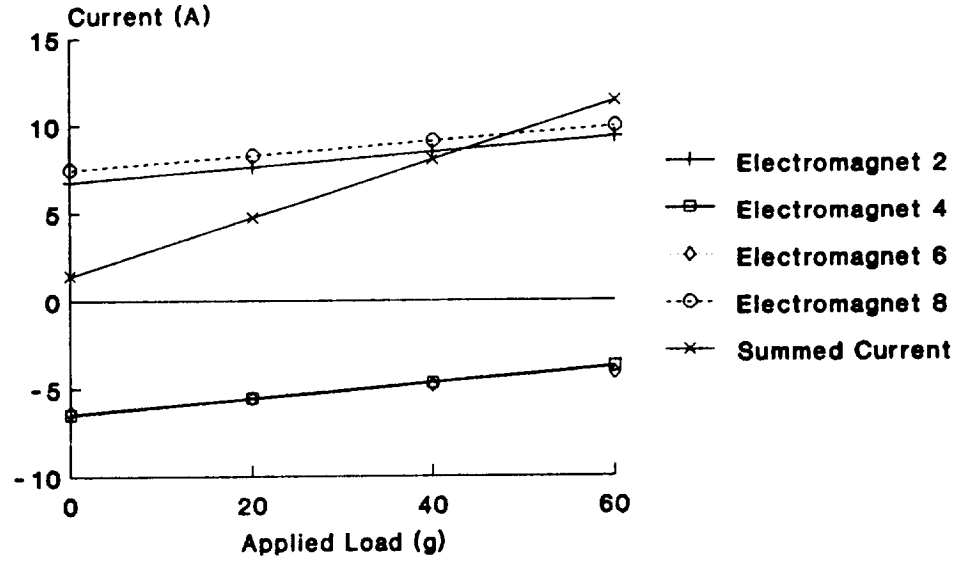

Figure 9.3f: sideforce calibration

Angle of Attack = 50 degrees

Gradient = 17.86 A/N

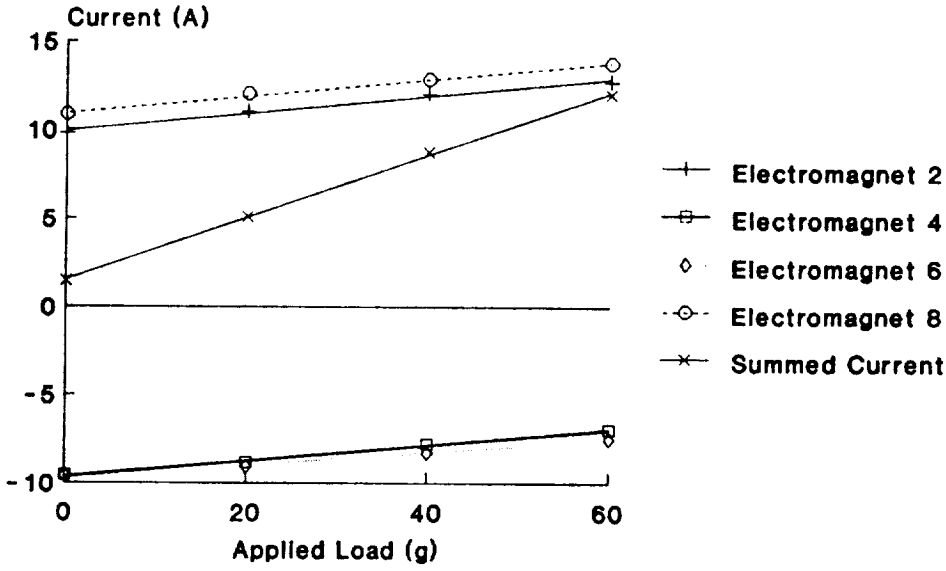

Figure 9.3g: sideforce calibration

Angle of Attack = 60 degrees

Gradient = 21.22 A/N

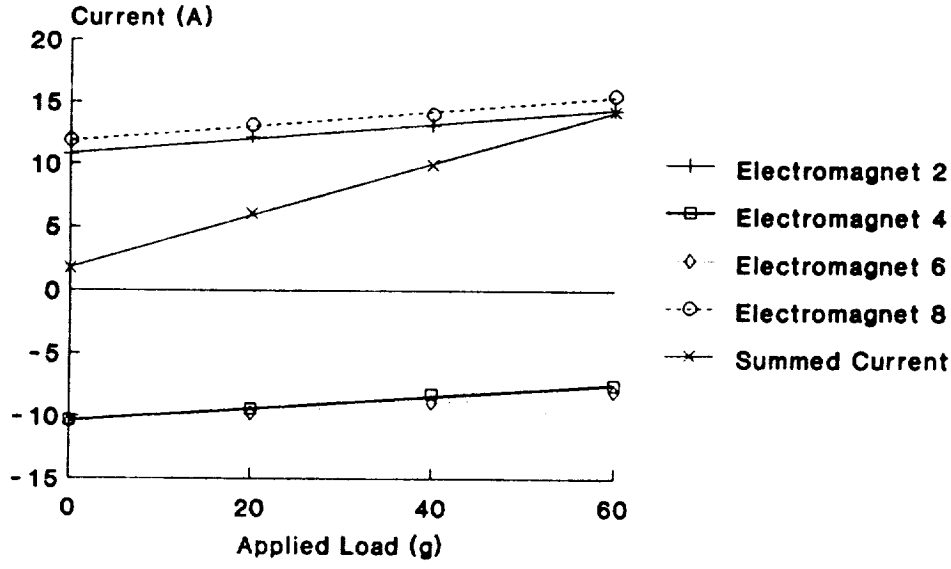

Figure 9.3h: sideforce calibration

Angle of Attack = 70 degrees

Gradient = 25.50 A/N

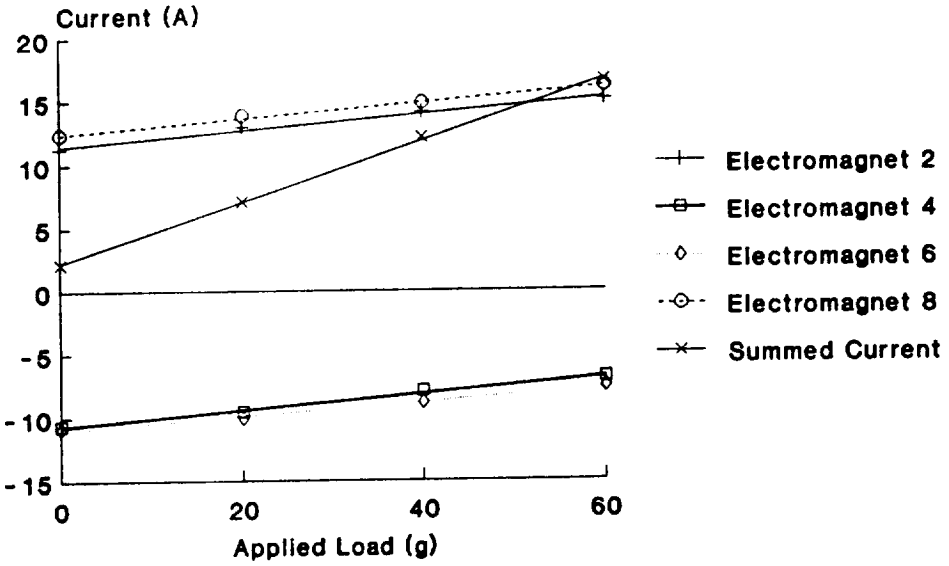

Figure 9.3i: sideforce calibration

Angle of Attack = 80 degrees

Gradient = 31.86 A/N

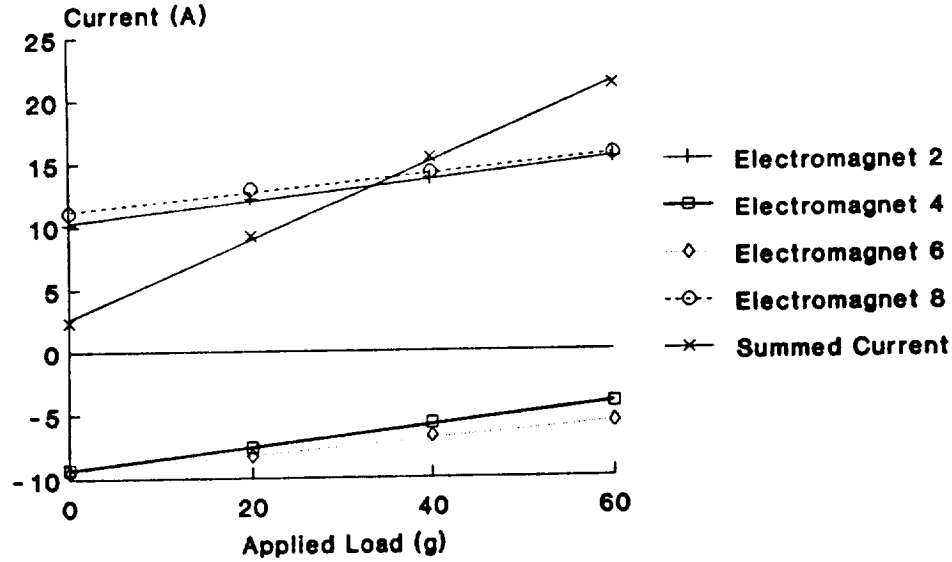

Figure 9.3j: sideforce calibration

Angle of Attack = 90 degrees

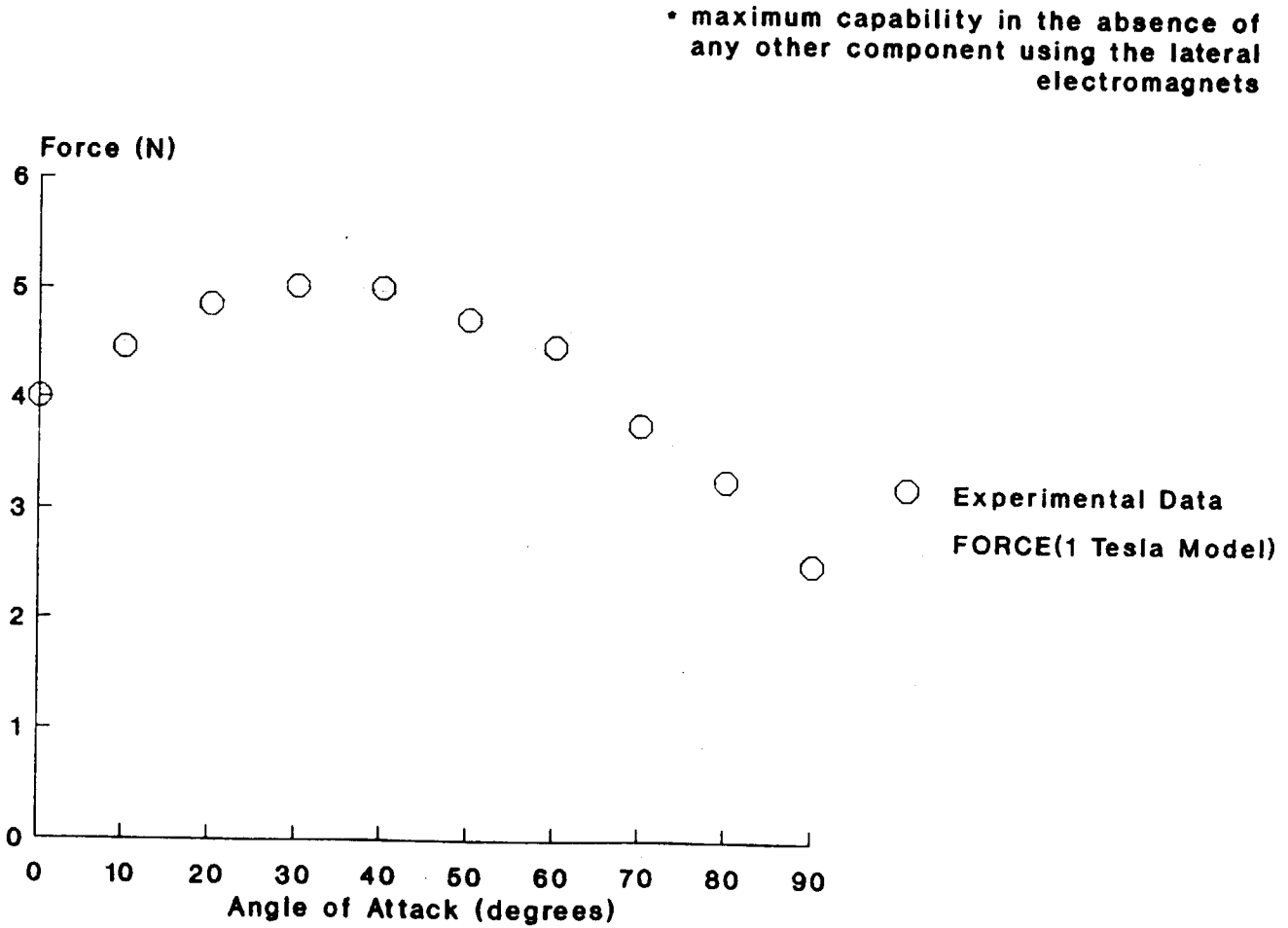

Figure 9.4: a comparison of predicted and measured amounts of sideforce from the lateral E/Ms

Gradient of Summed Current = 1.54 A/N

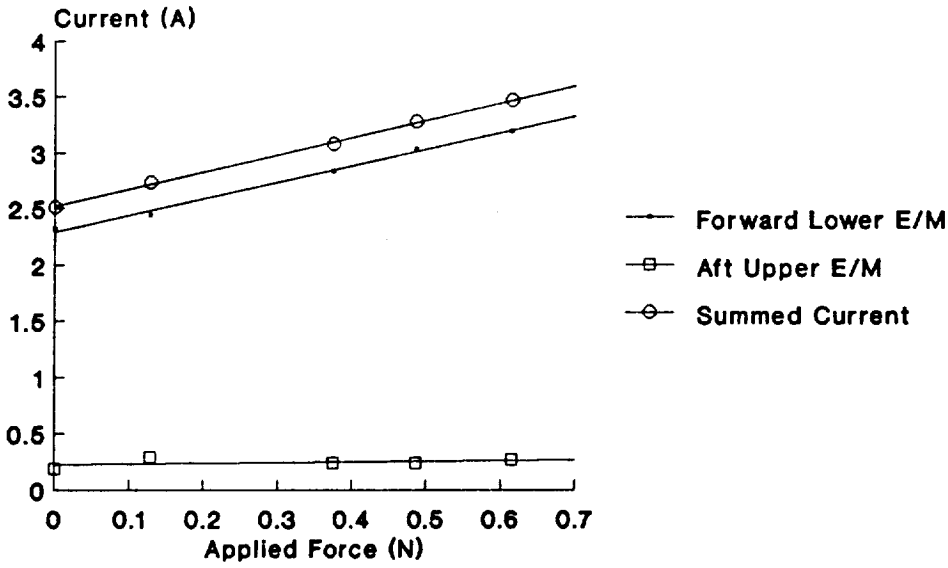

Figure 9.5a : vertical force calibration for electromagnet group 1 Angle of Attack = 90 degrees

Summed Current Gradient = 8.78 A/N

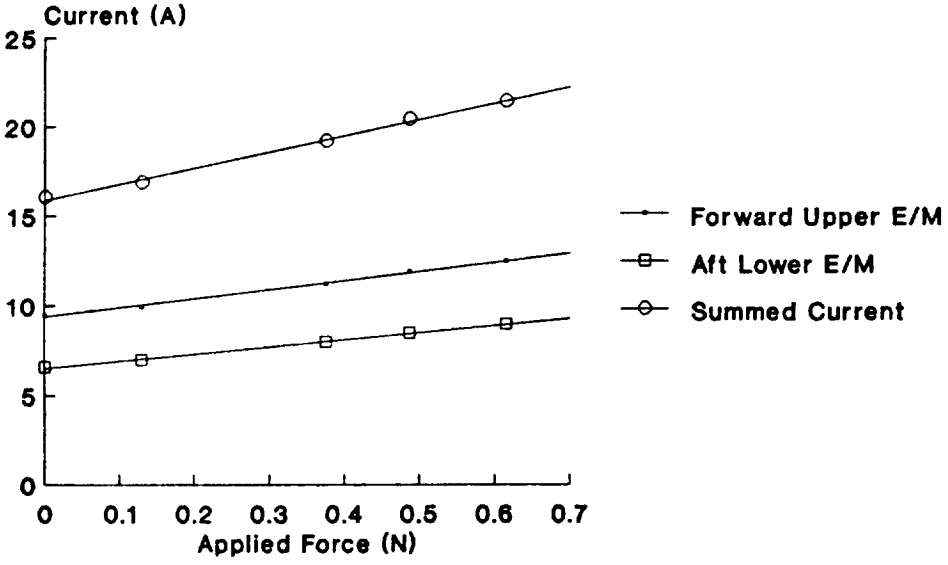

Figure 9.5b : vertical force calibration for electromagnet group 2 Angle of Attack = 90 degrees

(summed current data omitted for clarity
Gradient of Summed Current = 20.6 A/N

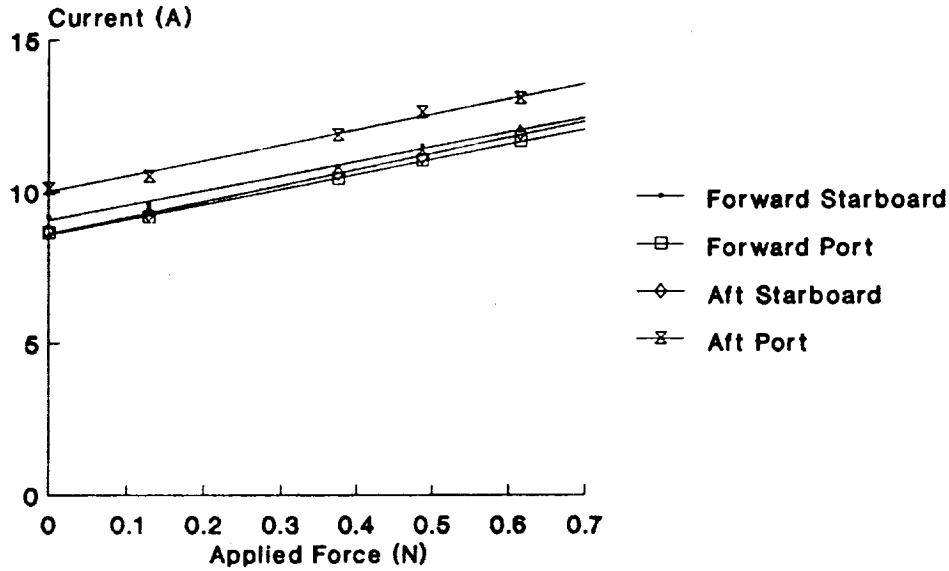

Figure 9.5c: vertical force calibration
for Electromagnet Group 3
Angle of Attack = 90 degrees

Summed Current Gradient = 1.61 A/N

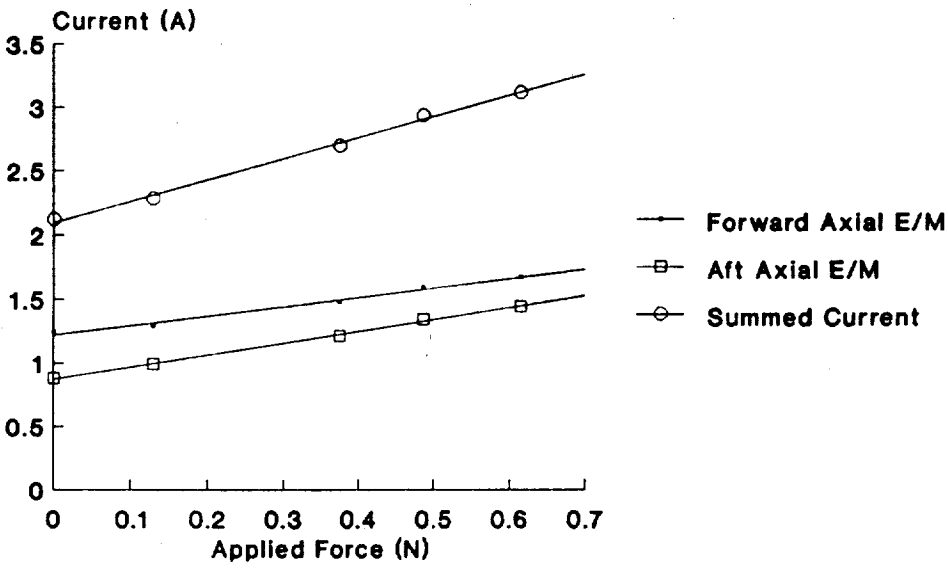

Figure 9.5d: vertical force calibration
for electromagnet group 4
Angle of Attack = 90 degrees

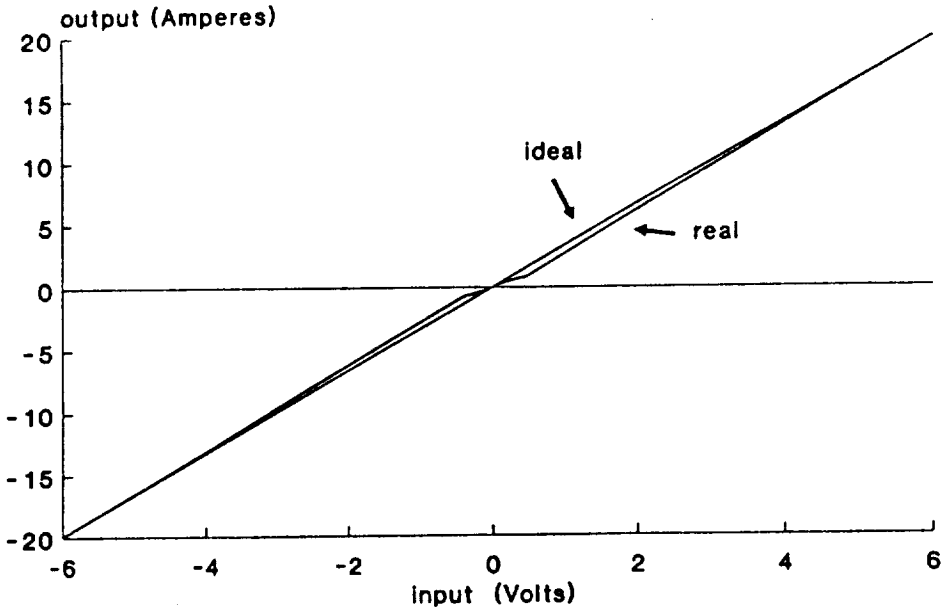

typical input/output characteristics
of power supplies

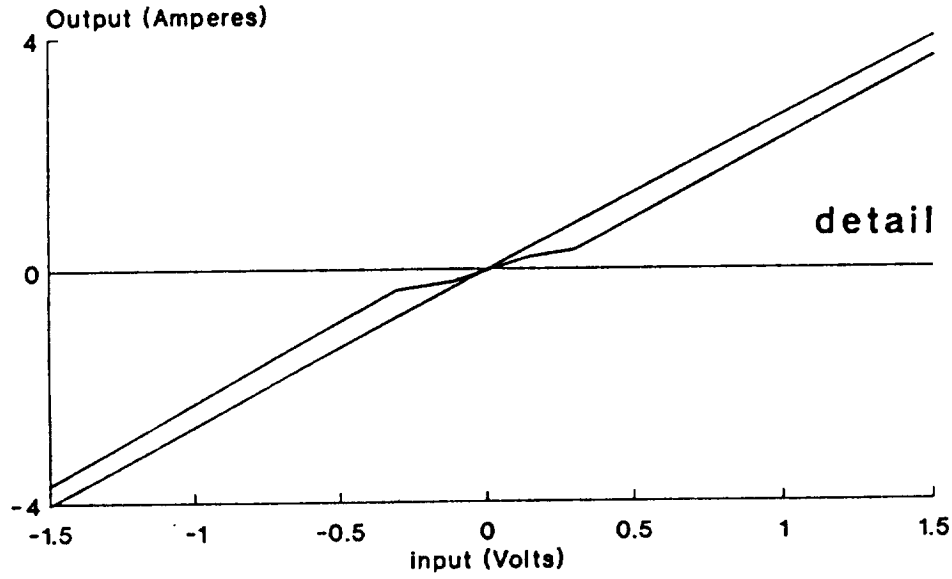

Figure 9.6: non-linearity of
power supply response

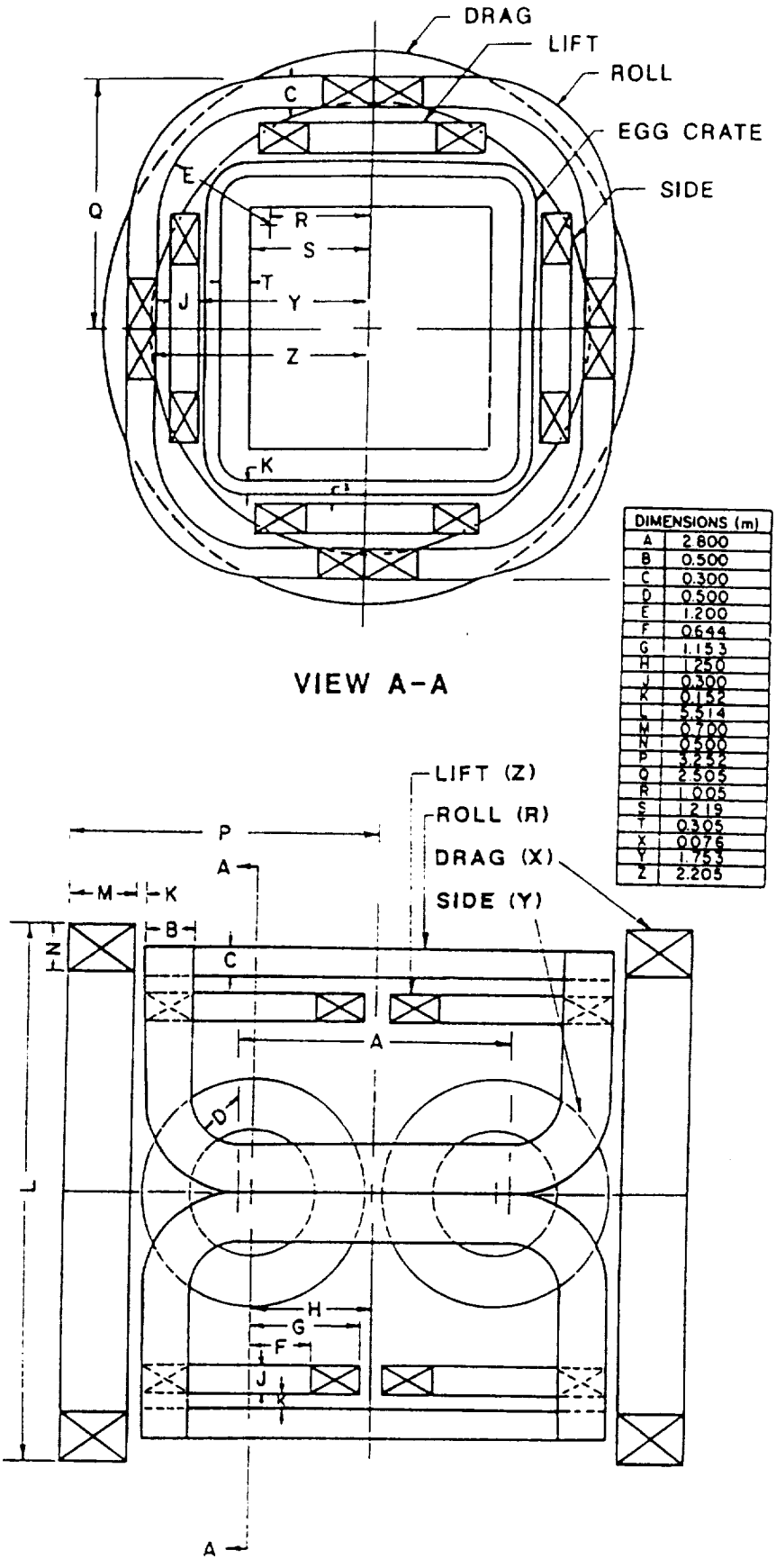

DIMENSIONS (m)	
A	2.800
B	0.500
C	0.300
D	0.500
E	1.200
F	0.644
G	1.153
H	1.250
J	0.300
K	0.152
L	5.514
M	0.700
N	0.500
P	3.333
Q	2.505
R	1.005
S	1.219
T	0.305
X	0.076
Y	1.753
Z	2.205

Figure 10.1: Madison Magnetics Inc.
Large MSBS design

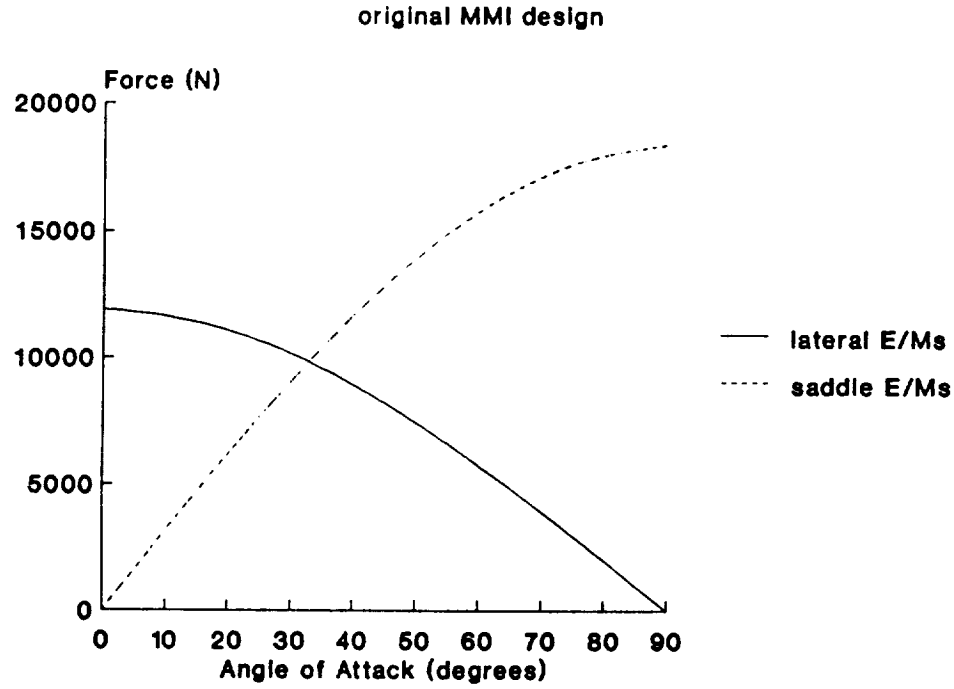

Figure 10.2a: sideforce from lateral and saddle electromagnets

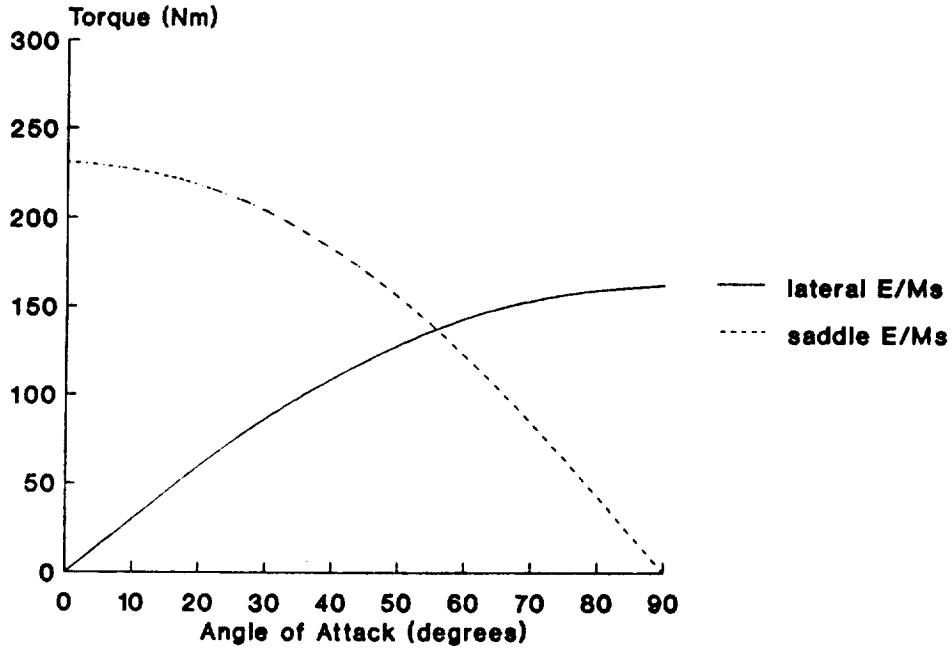

Figure 10.2b: roll torque from lateral and saddle electromagnets

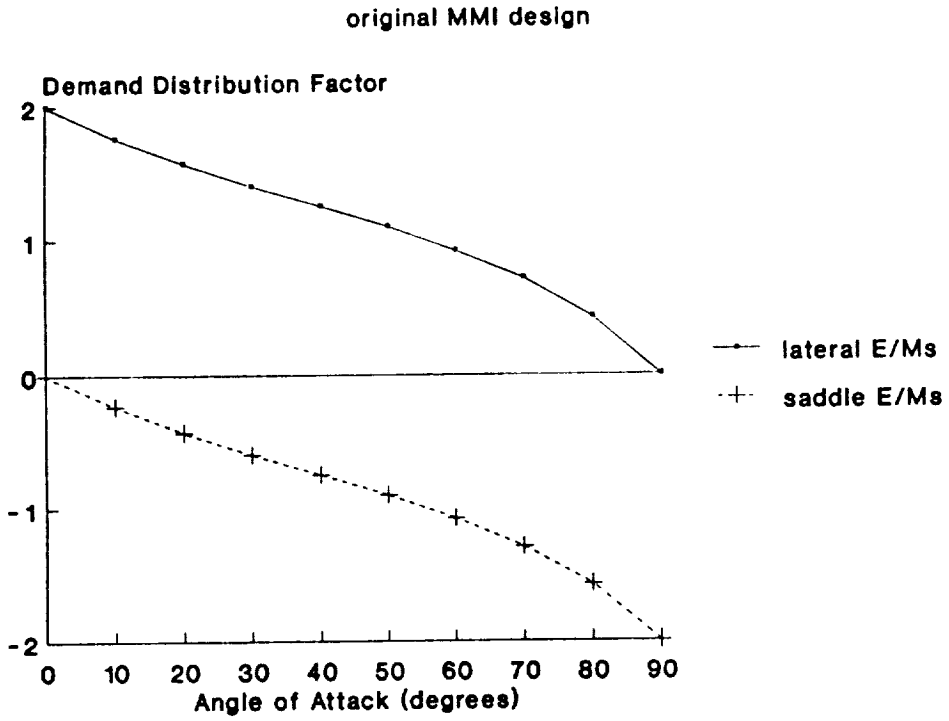

Figure 10.3a: demand distribution for sideforce generation

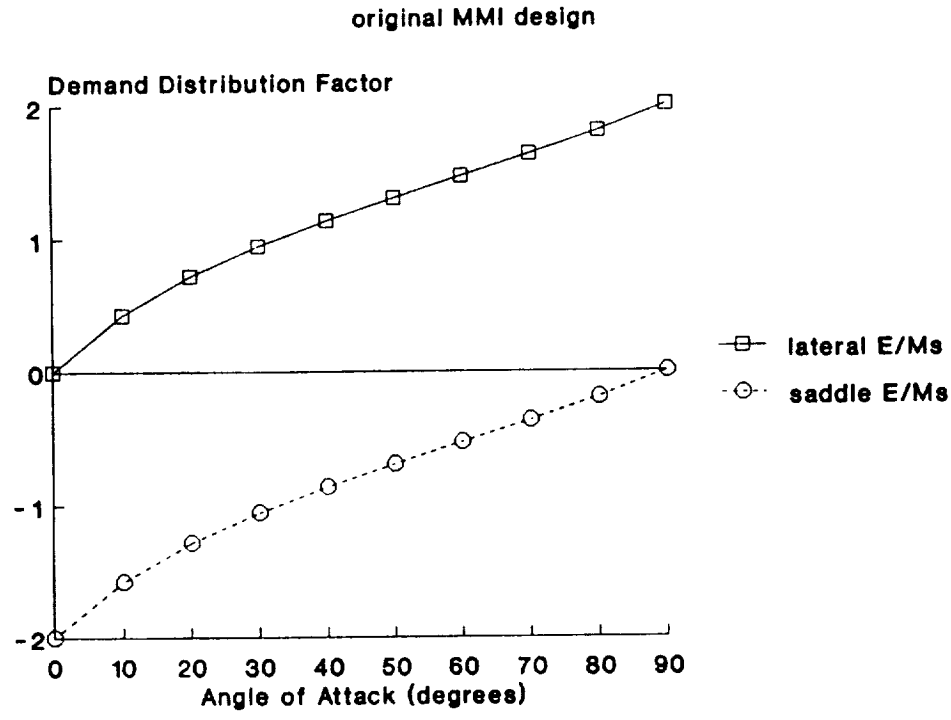

Figure 10.3b: demand distribution for roll torque generation

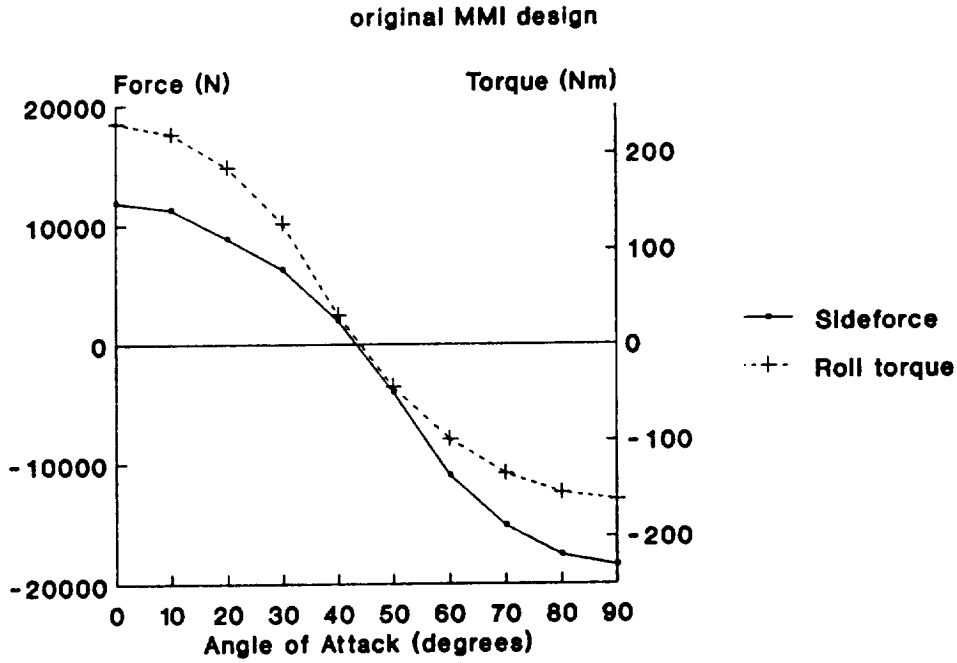

Figure 10.3c: sideforce and roll torque capability of MMI large MSBS design with demand distribution

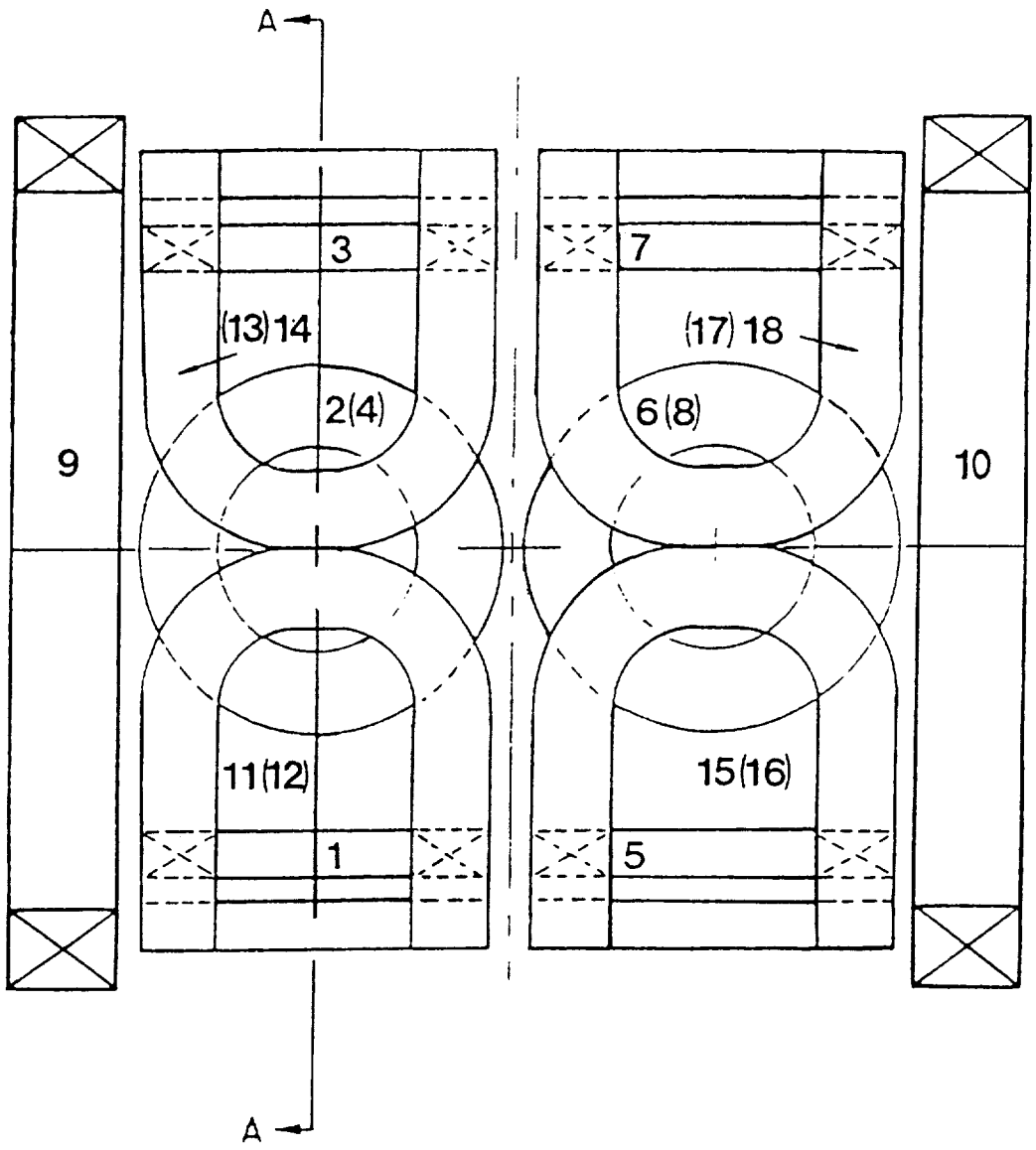

Figure 10.4: suggested modification to MMI large MSBS design

View on A-A is unchanged from Figure 10.1

E/M numbering scheme is indicated. Values in brackets are for E/Ms on opposite side of system.

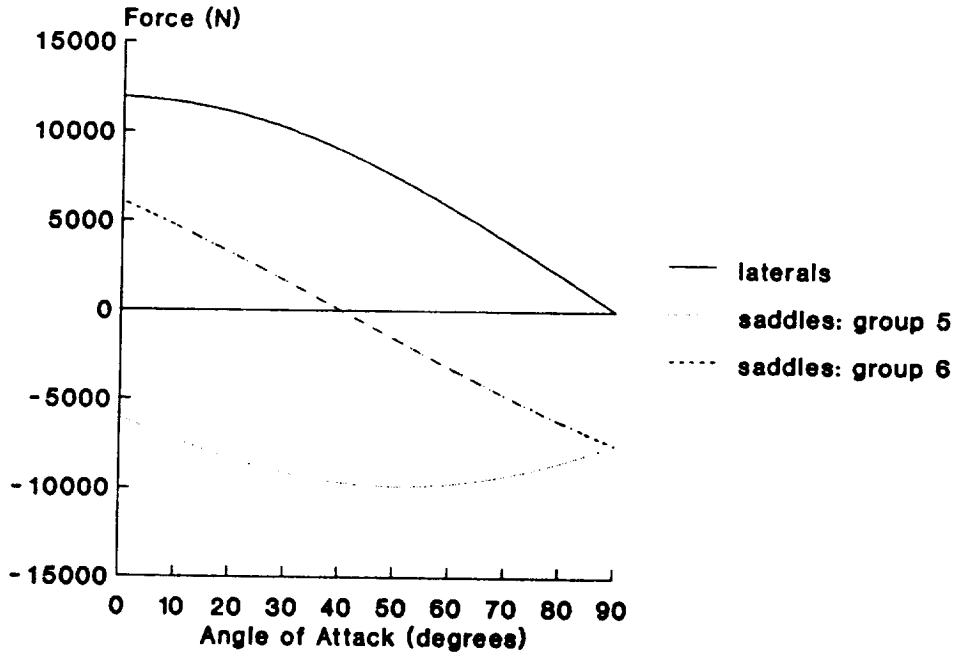

Figure 10.5a: sources of sideforce from improved MMI design

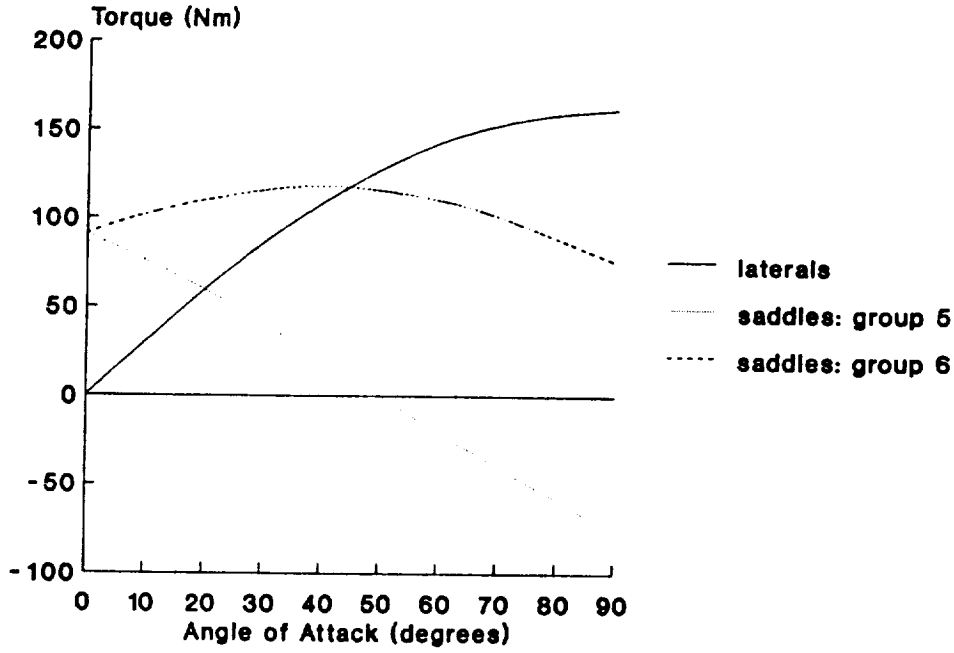

Figure 10.5b: sources of roll torque from improved MMI design

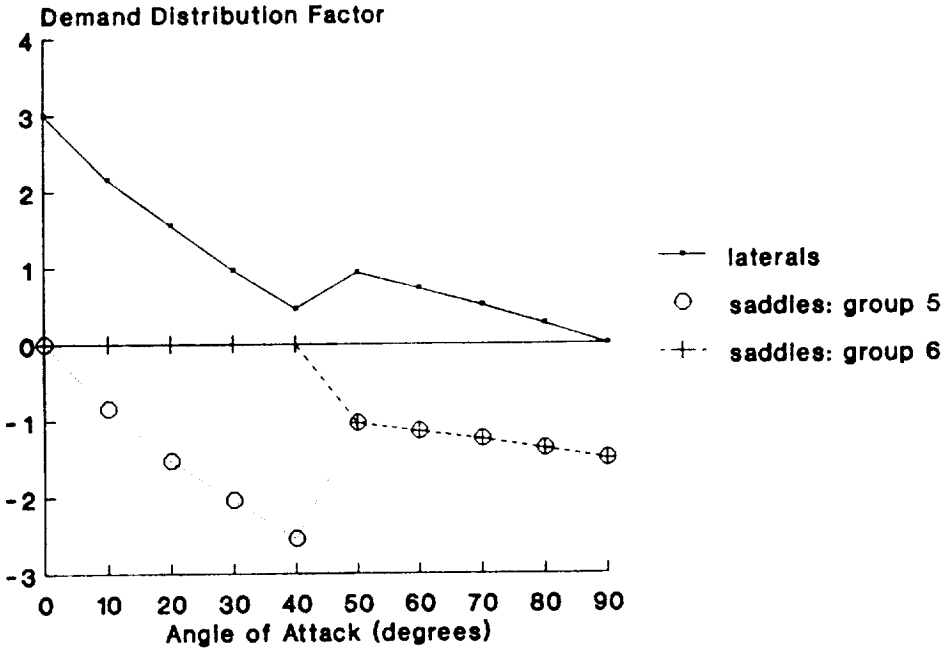

Figure 10.6a: demand distribution for sideforce generation

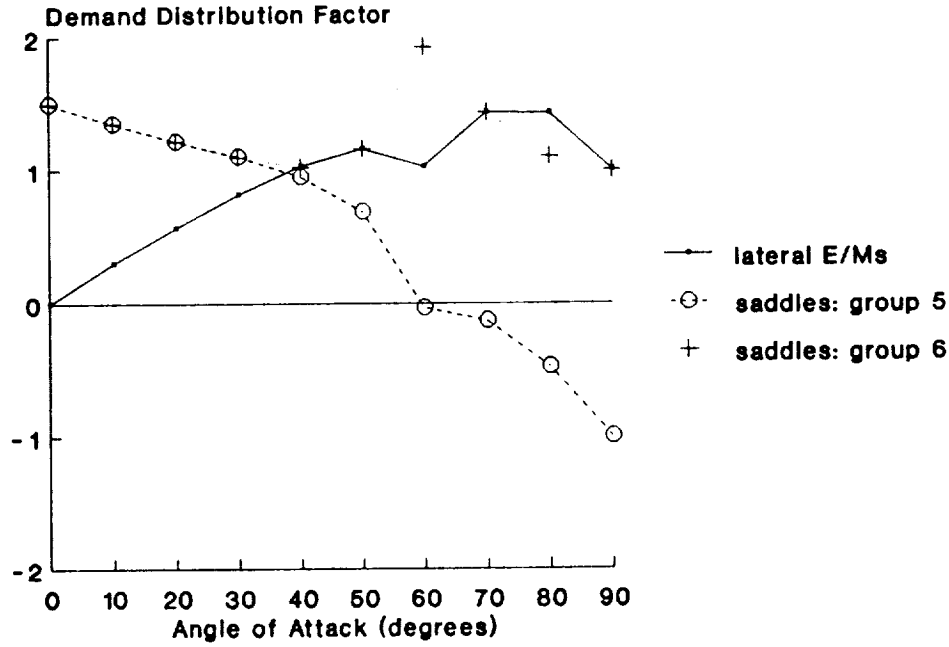

Figure 10.6b: demand distribution for roll torque generation

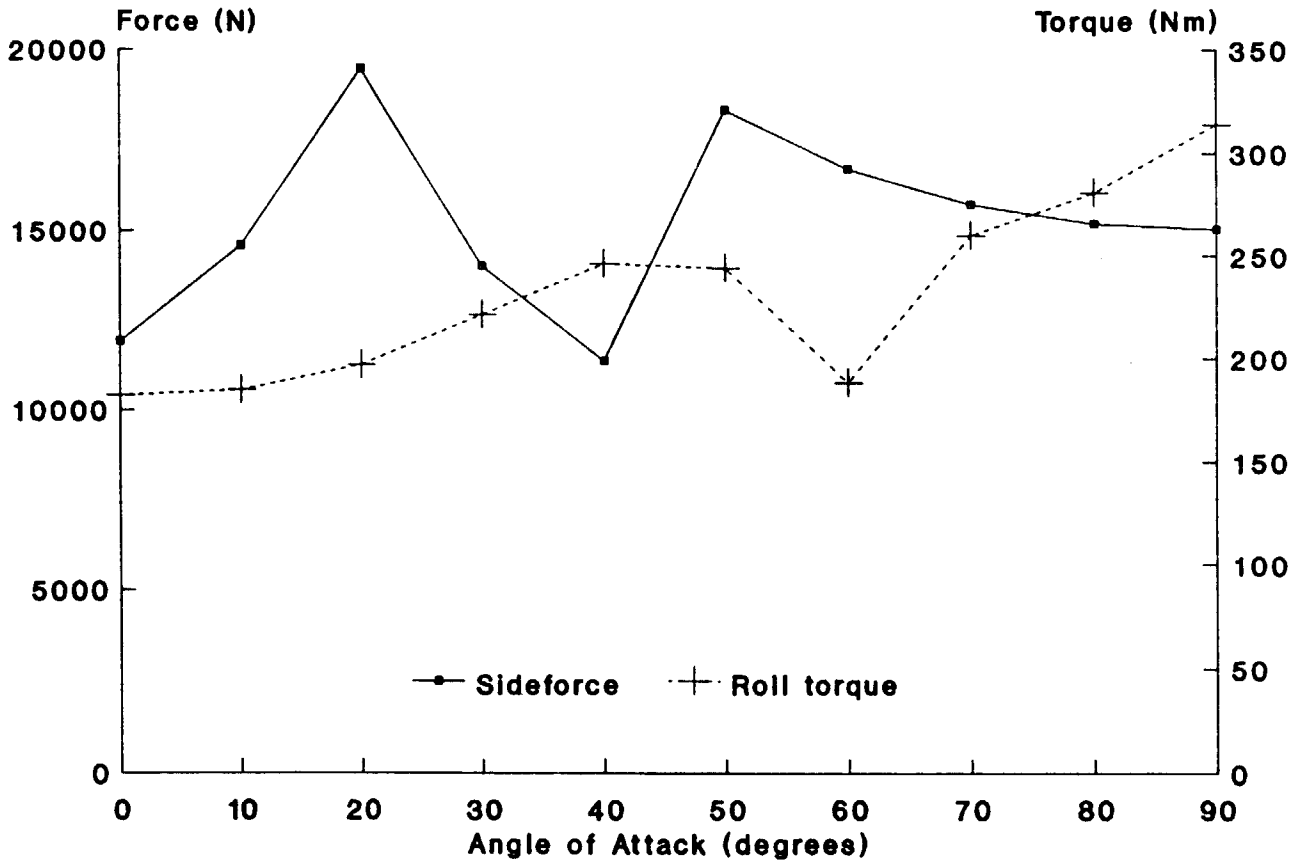

Figure 10.7: sideforce and roll torque capability of improved MMI design for a large MSBS

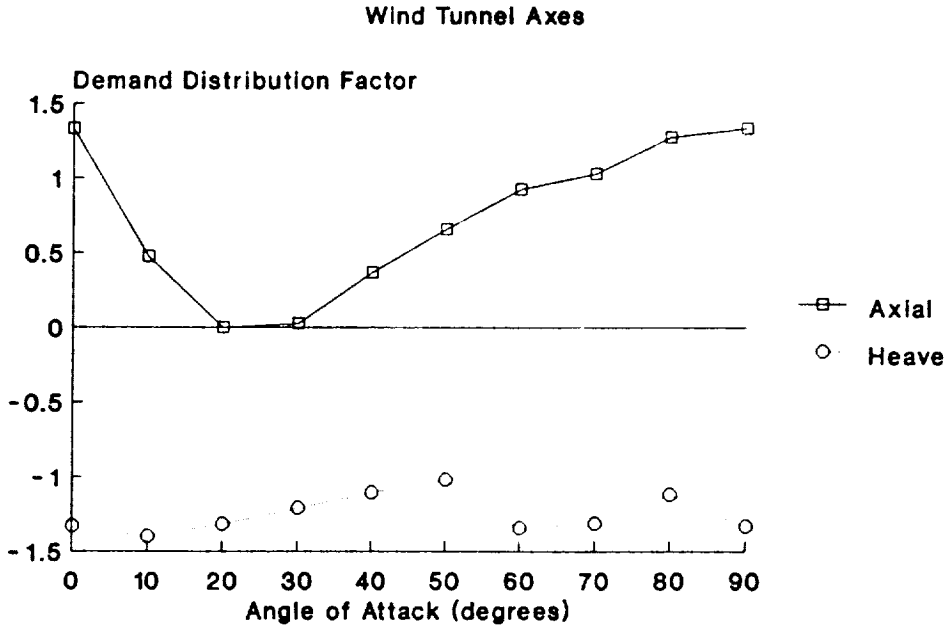

Figure 10.8a: demand distribution for forces in vertical plane. Electromagnet Group 1

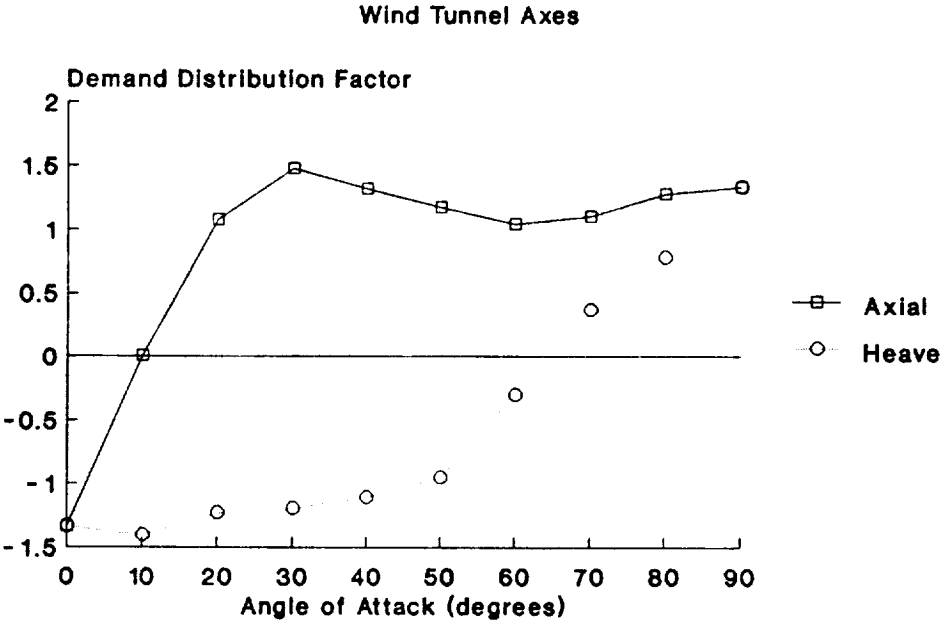

Figure 10.8b: demand distribution for forces in vertical plane. Electromagnet Group 2

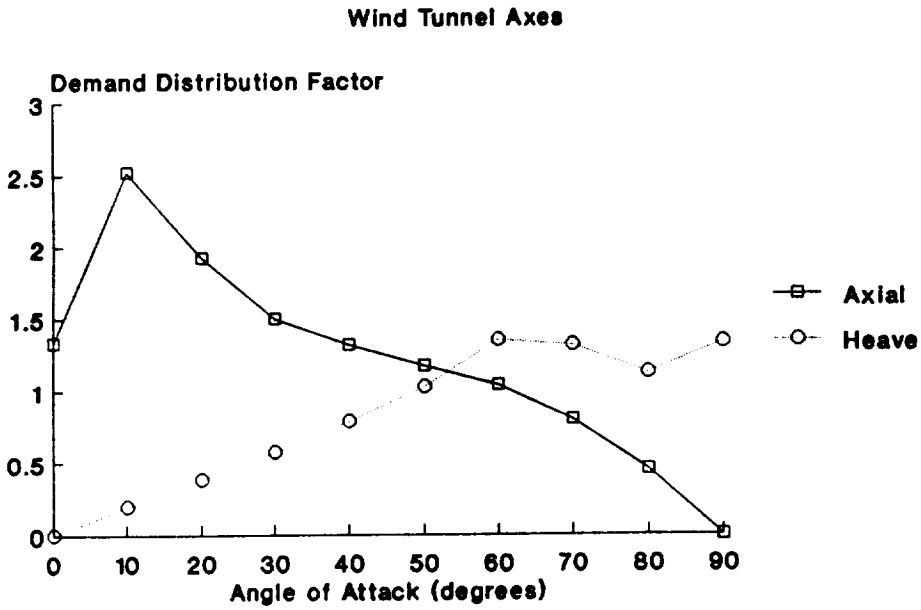

Figure 10.8c: demand distribution for vertical forces.
Electromagnet Group 4

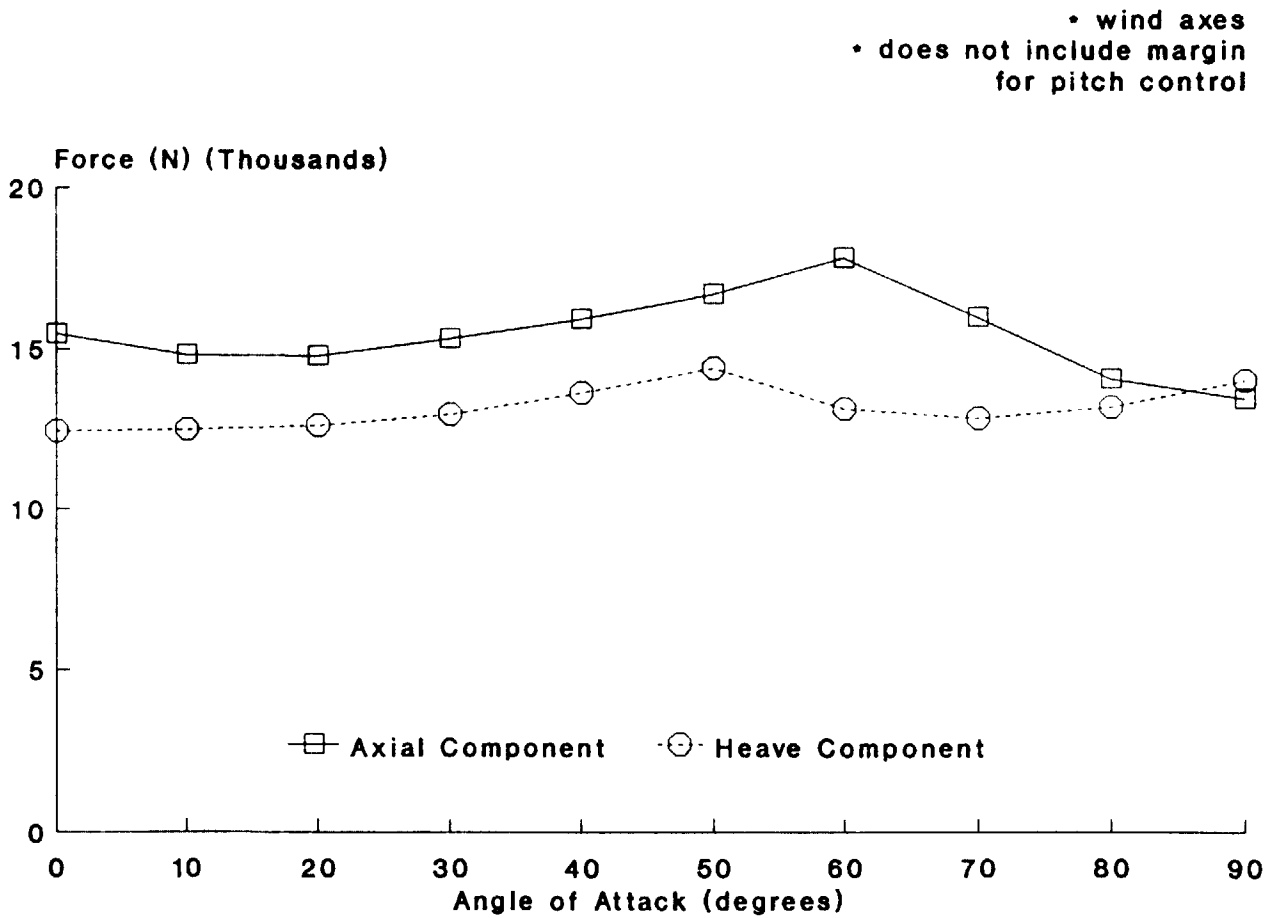

Figure 10.9: predicted vertical and axial force capability of modified MMI design for a large MSBS

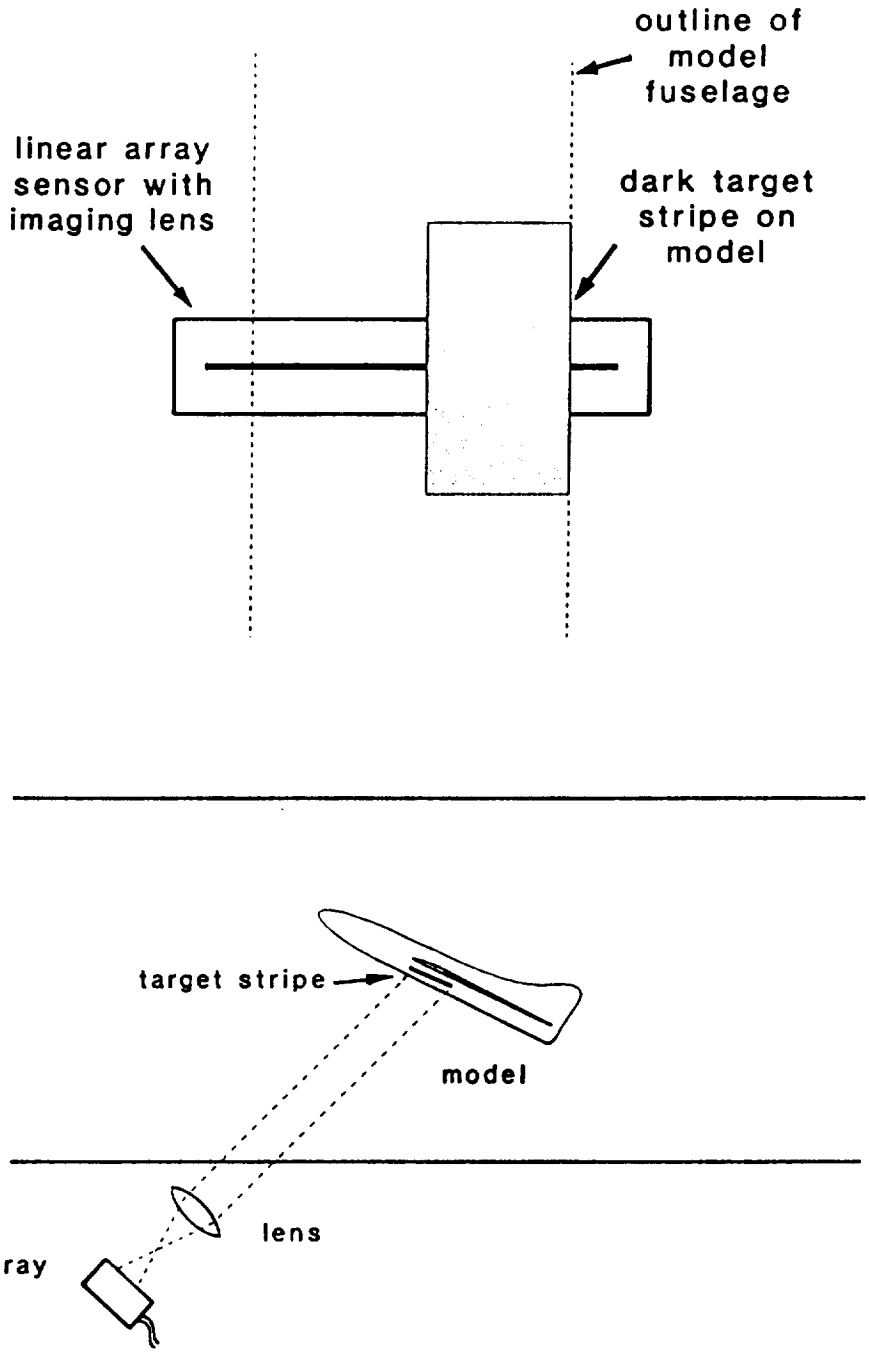

Figure 11.1: a possible roll motion sensor
for the Southampton MSBS

APPENDIX A

DESIGN OF OPTICAL SENSING SYSTEM

This appendix covers the design of the components of the optical model position sensing system used for extreme attitude suspension. This includes an estimate of the light transmission properties of the various optical components.

Four Main Sensors

The four main photodiode arrays are illuminated by laser light sheets produced by an Aerotech 8mW Helium-Neon laser with the following characteristics:

beam diameter	1.4 mm
beam divergence	4.1 milli-radians
polarisation	random
spatial mode	high order multimode

The comparitively large beam divergence (four times greater than many Gaussian distribution lasers) is a considerable disadvantage, in that the beam spreads to around 7mm over the system path length. This results in a large reduction in the light entering the photodiode arrays. However, after expansion and collimation, the resulting beam is seen to have a more even distribution along the length of the sensor than that which results from the Gaussian distribution beam used for the axial sensing channel.

The main beam is expanded by a cylindrical rod lens of 4mm diameter, mounted in a custom-made holder screwed to the laser safety shutter. The lens has a single-layer antireflection coating. The beam is collimated by a single layer coated 100mm focal length plano-convex cylindrical lens, mounted in a holder with fine rotational control. Adjustment of focussing is provided through use of a screw controlled translating stage.

The collimated beam enters a light box consisting of three 40mm coated cube beam splitters and three 38mm coated right angle prisms. These

produce four beams which leave the light box in two pairs travelling outwards at 180^{o} to each other and at 90^{o} to the incoming collimated beam. Micrometer controlled transverse stages with .01 mm resolution and half inch travel support four of the elements permitting independent positional control in a sense normal to the beam plane. The laser, collimation lens and light box are supported by a standard triangular section optical bench 3 feet in length and bolted to the MSBS lower frame.

The four main beams each strike a 2 inch diameter silver coated mirror, flat to 2 wavelengths and mounted in gimbals adjustable by 10^{o} in two axes to a resolution of .14 arc seconds. The gimbals are bolted to angled adapters which give the light beam a nominal deflection of 57^{o}, so that they travel up towards the wind tunnel test section. The adapters are attached to screw thread translating stages, which permit motions of the beams transverse to their length to resolutions better than 0.001 inch. The stages are in turn bolted to the side supports of the MSBS frame.

The four beams then strike 63mm by 31.5mm mirrors attached to fixed mirror mounts. The mirrors are multilayer coated and flat to two wavelengths. The mounts project from the cross members which also carry the lateral electromagnets. The angle of these mounts is such as to deflect the beams across the wind tunnel test section according to the geometry explained in the main text and Appendix C. Similar mounts and mirrors return each of the beams to the vertical plane before they strike the photodiode array sensors.

The sensors, carried on 2 by 3 inch electronic cards, are screwed to mounts consisting of a custom made brass rotating stage, operated by a thumb screw acting against a spring loaded lever, and two x-y stacked transverse stages, of the type described above. The rotating stage also permits the sensors to be crudely adjusted (to about the nearest degree) about an axis perpendicular to the sensor length. This setting is used through examination of the weak reflected beam produced by the sensor glass window to ensure that the incident beam strikes the sensor normally.

All the other adjustable mount settings are used in the beam alignment process outlined in the main text.

Estimation of Irradiance Requirement for Main Channel

Information supplied by the manufacturers of the RL1024G sensor may be used to calculate the light intensity required to ensure saturation of the arrays.

The responsivity of the device is defined as the product of the absolute diode sensitivity and the pixel area:

$$R = S.a \text{ in } A/W/cm^2$$

The absolute sensitivity S is dependent on the wavelength of the incident light and on the characteristics of the array window, whilst the pixel area a is known for the particular array.

The saturation exposure is the saturation charge divided by the responsivity;

$$EXP_{sat} = Q/R \text{ in } J/cm^2$$

Now the energy required per to saturate one diode is;

$$\begin{aligned} E &= EXP_{sat} \cdot a \\ &= Q/S \text{ Joules} \end{aligned}$$

The power for a scan time of t is;

$$\begin{aligned} P &= E/t \\ &= E.f/n \end{aligned}$$

where f is the scanning frequency and n is the number of diodes in the array. The power input in one scan of the array is thus:

$$\begin{aligned} P_{tot} &= nP \\ &= Q.f/S \end{aligned}$$

The arrays are intended to receive only the laser light with negligible background light. From the manufacturer's data (52), for the 632.8 nm frequency range, the sensitivity is 0.4 A/W.

With a 242 Hz loop rate, and 1024 elements per array, plus the equivalent of 9 diodes of processing time at the end of scan, the scanning frequency is

$$f = 250000 \text{ Hz}$$

The saturation charge is specified as 4 picocoulombs, giving:

$$P_{tot} = 2.5 \text{ micro Watts}$$

This power is spread over an area of 0.001 inch by 1.024 inches, or 0.0066 cm^2.

The multimode laser is assumed to have an idealised 'top hat' irradiance distribution, which permits an estimate of the amount of light actually entering the sensor to be made.

With a 4mm diameter, 2.9mm focal length rod lens, the laser beam divergence angle is 13.6^{o} (ignoring the initial beam divergence). With a 100mm focal length collimation lens, the width of the resulting beam is 48mm. The lateral thickness of the beams by the time they reach the sensors is 7mm. Thus the effective beam area is 3.36 square centimetres. To produce the required power as above, each beam must be 1.27 mW in power, implying that the laser power is 5.08 mW. However, a large proportion of the beam energy is lost in reflections at each of the optical components. For the worst case, this may be estimated as follows:

expansion lens	0.99
collimation lens	0.99
beam splitter 1	0.95
right angle prism	0.98
beam splitter 2	0.95
gimballed mirror	0.90
fixed mirror 1	0.94
test section window (entering)	0.95 (when fitted)
test section window (leaving)	0.95 (when fitted)
fixed mirror 2	0.94
Total Transmission	0.62
Transmission times input power	4.96mW

Thus the laser power is not excessive. However, the specified power of the laser is a minimum value, and according to the manufacturers, is in fact significantly exceeded by the true value. Also, the transmission of the other beams is slightly better, owing to the fewer number of optical components used.

Axial Channel Optical System

The axial channel light originates in the 1mw Gaussian distribution laser previously used with the analogue axial sensor. It is mounted on a framework bolted to the aft axial electromagnet supports. The laser beam is expanded by an anti-reflection coated 2.9mm focal length rod lens and collimated by a 250mm coated cylindrical lens held in a rotatable mount with focussing adjustment. The collimated beam is reflected by a 100mm by 31.5mm enhanced reflectivity mirror into the rear of the wind tunnel test section from beneath. The mirror mount tilt angle is adjustable via a spring loaded thumb screw. Coarse longitudinal adjustments of the mount are also possible by having it built onto a pair of brass rails, with locking screws to fix the position.

The collimated beam then strikes a similar 100mm by 31.5mm mirror which is attached to a mount screwed to the underside of the aft upper electromagnet. This mount permits the beam to be tilted about an axis along the length of the mirror. The beam is reflected so that it travels back across the test section at an angle of 45^{o} to the vertical.

As originally configured, the beam then struck the axial position sensor, which was fitted to a mount which could be adjusted in one rotational and one translational sense. However, for the reasons explained in the text, the axial sensor was subsequently removed from the test section, and supported on a rotating and translating mount bolted to the aluminium plate table already fitted to the port side of the MSBS for other uses. The laser beam is reflected to the new sensor location by a 40mm by 25mm mirror attached to a rotating and translating mount in the location previously occupied by the axial sensor mount.

APPENDIX B

DIFFRACTION OF SHADOW EDGE IN A COLLIMATED BEAM OF LIGHT

The theory presented here is adapted from Reference 53.

The magnetically suspended model may be regarded as a semi infinite screen placed in a bem of collimated light. At the model to sensor distances of relevance here, near field or Fresnel diffraction theory may be used to predict the form of the shadow edge produced. The situation is illustrated below.

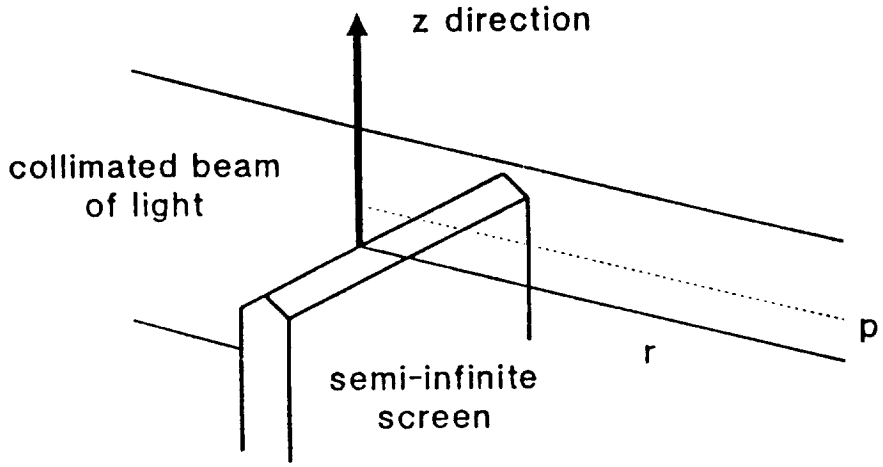

A non-dimensional parameter v may be used to describe the point of observation p perpendicular to the beam direction. It is defined thus:

$$v = z(2/\lambda\, r)^{\frac{1}{2}}$$

where z and r are the distances shown and λ is the wave-length of the light. For the helium-neon lasers, this is 632.8 nm. If the uniformly distributed light has an irradiance value I_o, the theory gives the value of the irradiance at P to be:

$$I = I_o/2[(\tfrac{1}{2} - C(v)^2 + S(v))]^2$$

C(v) and S(v) are the Fresnel integrals, whose values are tabulated in the Reference. At z = 0, that is, in line with the model's edge, the two functions are both zero, giving $I = I_o/4$. The irradiance distribution plotted in terms of non-dimensional parameters is:

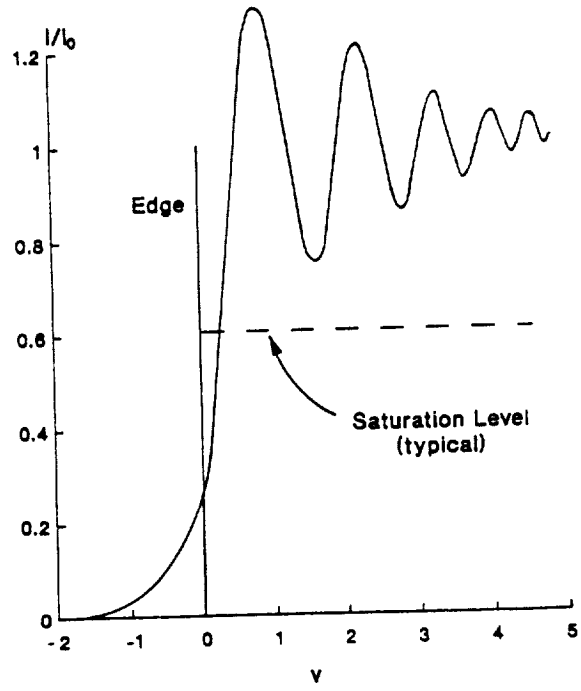

However with the MSBS sensing system, the value of I_o has been chosen such that the oscillatory fringes shown are not seen. Thus it is not possible to determine directly from the sensor signal where the true model edge lies. Using the technique of comparing the sensing system estimation of the width of a reference object with the true value, the MSBS control program avoids this problem.

To determine the expected number of pixels for a transition as viewed by the sensing system arrays, we assume that the majority of the transition occurs between v = 1 and v = -1.5. The distances between the model and all the arrays is similar for the final version of the sensing system;

that is, with the axial sensor removed to the outside of the test section. The distance is 0.3m.

Thus:	for v = –1.5	z = 0.462 mm
and	for v = 1.0	z = 0.308 mm

Thus the complete transition occurs over 0.77 mm, or about 30 pixels. Because of the setting of the threshold level, the visible part of the transition shown by the array video outputs will be slightly less than this: 20 to 25 pixels is likely, with some variation being caused by the differing illumination levels on each of the channels.

APPENDIX C

DETAIL GEOMETRY OF SENSING SYSTEM AND THE PROGRAM PIXEL

Introduction

The Fortran program PIXEL calculates the information used in the main control program MSHI in the position sensing and user demand offset algorithms. The program assumes the geometry of the sensing system light beams which is described here.

The program permits the user to input the dimensions of the model to be suspended in the extreme attitude MSBS, although it must be of uniform circular cross-section. The assumed sensing system consists of two pairs of light beams intersecting symmetrically along with a single axial beam at the tail end of the model. The user selects the range of pitch and yaw attitudes for which position sensor data is required. The information calculated is output to a data file, which may then be accessed and used by the extreme attitude control program.

The information required by the control program consists of the following items:

1) the model centreline location as viewed by the four main sensors,

2) the apparent model radius as viewed by four main sensors,

3) the offset of axial sensor output to account for change in apparent length with changes of angle of attack,

4) the value of the decoupling factors for the axial to heave or heave to axial channels, depending on the axis system in use.

Because of symmetry considerations, the first two pieces of information need only be calculated for one pair of crossed beams; the program MSHI replicates the data for the second pair.

Fundamental Geometry used in PIXEL

The following information relates to the specific arrangement and dimensions used with the Southampton MSBS, but may be easily extended to alternative configurations.

The two pairs of beams which illuminate the four main sensors are intended to form two 90 degree crosses in the sense of being viewed from upstream or downstream of the test section. From this the crossing angle in the plane of the beams may be deduced to be 70.53°. The intersecton area of each pair has the dimensions shown.

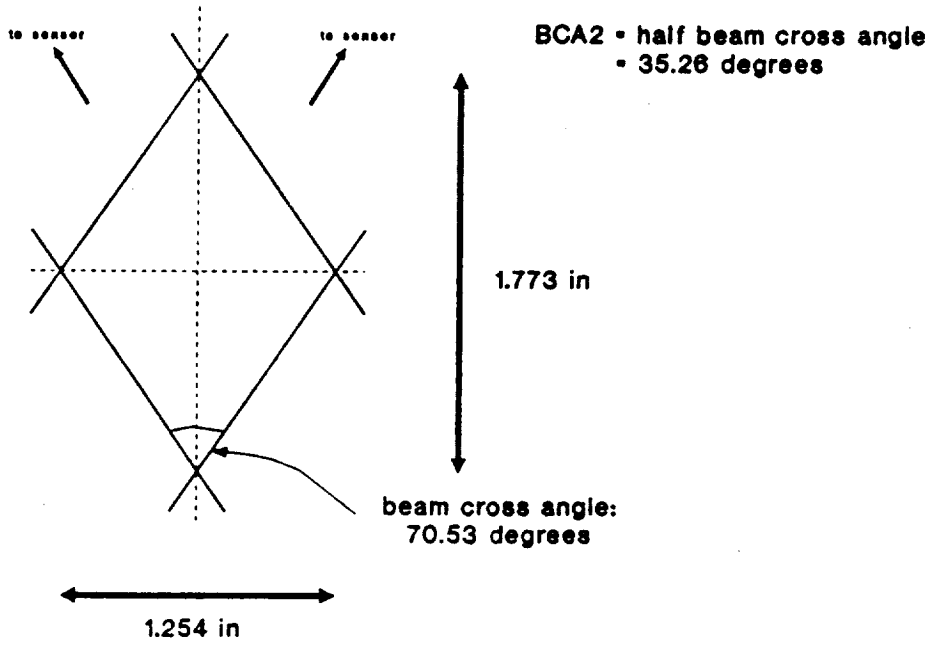

Each pair is separated by a distance of 2 inches in the perpendicular sense (the beam separation,BS):

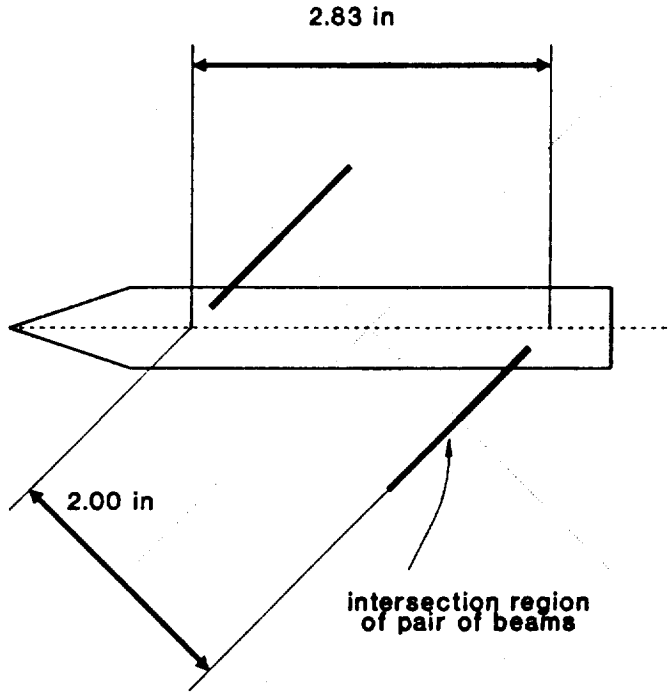

To calculate the movement of the model centreline as 'seen' by the two arrays, the following geometry is used.

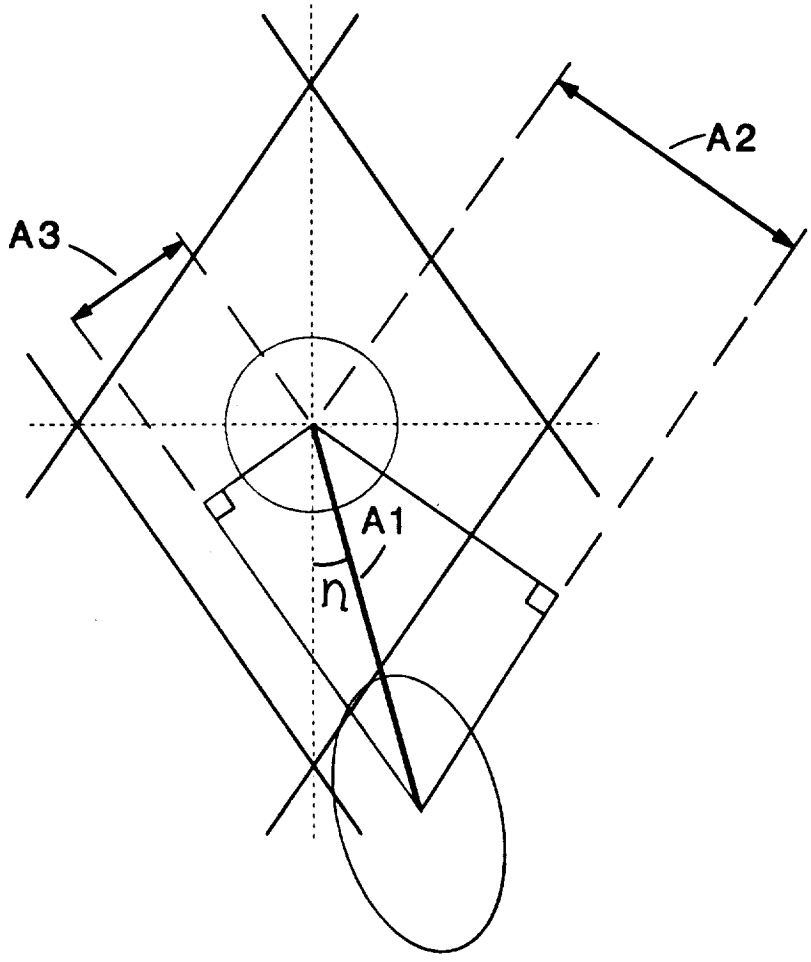

Using elementary geometry it can be deduced that the scalar motion of the centreline of the model in the plane of the beams is given by:

$$A1 = \tfrac{1}{2}.BS.\tan\theta / \cos\eta$$

where $$\eta = \tan^{-1}(\tan\psi / \tan\theta)$$

and θ and ψ are the pitch and yaw attitude relative to the datum.

The projected components of A1 seen by the two sensors are given by

$$A2 = A1 \cos p \quad \text{where} \quad p = 90 - (\eta + BCA2)$$

$$A3 = A1 \sin q \quad \text{where} \quad q = \eta - BCA2$$

The program adds minus signs to the calculated values in order to take account of the sense of motion relative to the datum attitude, which is with the model centreline laying half-way along the length of each of the four main sensors.

Increase of Apparent Radius of Model Through Pitching and Yawing

As the model rotates in the two rotational degrees of freedom away from the datum, the apparent model radius changes according to the following geometry. At any angle the elliptical intersection wiht the beam cross area is given has a major axis AXMAJ and a minor axis AXMIN, equal to the model diameter.

Now $$AXMAJ = AXMI/\cos d$$

where $$\tan d = 2\,A1/BS$$

Transforming the ellipse from the plane of the beams to model axes thus:

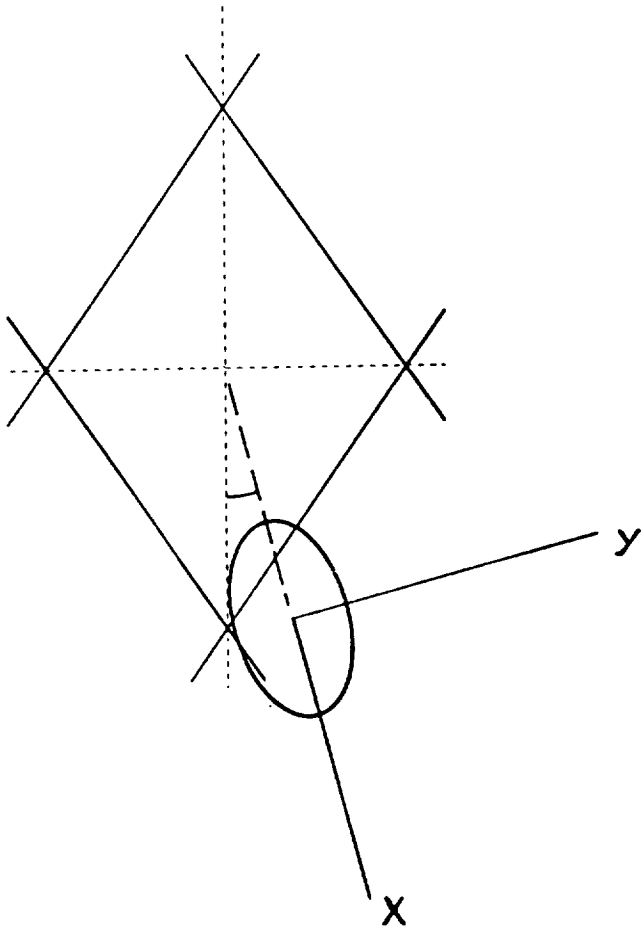
y
X

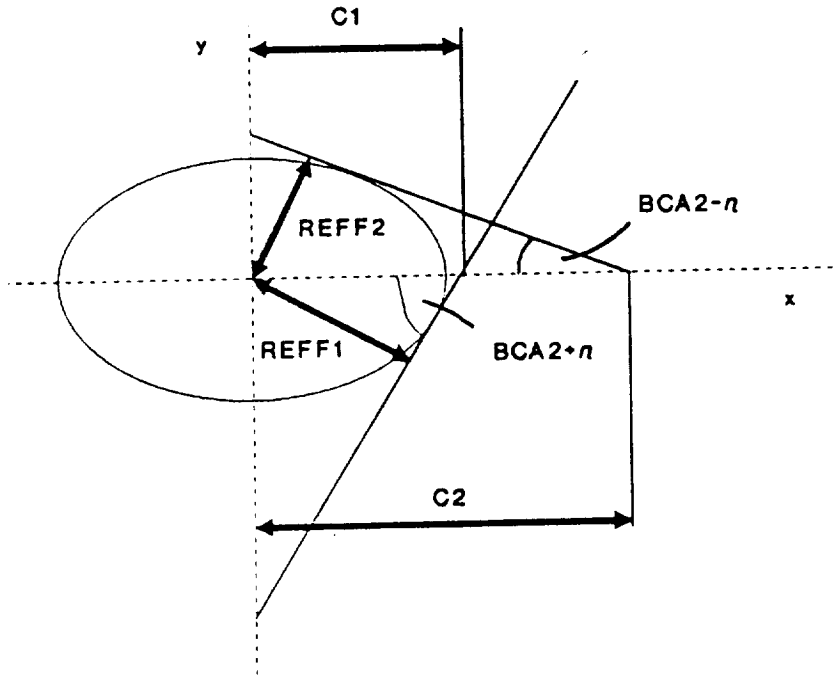
C1
y
REFF2
BCA2-n
x
REFF1
BCA2+n
C2

The shadow edges are two tangents to the ellipse. The expression for a tangent with gradient m is:

$$y - mx = \sqrt{m^2 AXMI^2 + AXMAJ^2}$$

The distances required and shown on the diagram above are C1 and C2.

For C1, m = -tan (BCA2 + η)

and for C2, m = tan (BCA2 - η)

Substituting these into the expression above, C1 and C2 may be calculated for y = 0.

From these, the effective model radii can be calculated:

REFF1	=	C1 sin (BCA2 + η)	for all η
REFF2	=	C2 sin (BCA2 - η)	for $\eta \neq$ BCA2
REFF2	=	AXMI	for η = BCA2

Change in Model Apparent Length with Change in Pitch Attitude

The formula for calculating the apparent change in model length with angle of attack is given in Section 5.5. As all the models suspended in SUMSBS have approximately the same length, this value is fixed in the program to be 4.2 inches. Simple editing allows it to be altered if desired.

Sections 5.4 and 5.5 outline the need to remove portions of the feedback signal in certain degrees of freedom from the signal in others in order to ensure the decoupled nature of the feedback data. Three decoupling quantities are involved. A description of the calculation of the pitch to axial decoupling quantity is given in the main text. The remaining two are based on the present angle of attack and are obtained via PIXEL.

In the sensing system axes controller, the heave to axial decoupling component is required. As explained in the main text, this is given by:

$$AX - HE = C_1 \tan \theta . e_5$$

The tangent of the angle of attack relative to the datum (45 degrees) is calculated by the original version of PIXEL. The decoupling constant C_1 is determined by the sensing system geometry and it takes account of the relative sensitivity of the position measures of the two channels.

From above, a vertical heave motion in the plane of the intersection region of the crossed pairs of beams, which is seen by each of the four main sensors as a change of 1024 pixels (a total of 4096), will correspond to an actual translation of 1773 thousandths of an inch. The gain of the heave channel is thus 2.309 per thou. The sensitivity of the axial sensor, with the improved axial sensor location (Section 7.5), is 1 per thou. The decoupling constant C_1 is thus given by the ratio of these; that is 2.309.

With the model axes based controller in use the cosine and sine of the angle of attack relative to the datum of 45° degrees is calculated and stored by a different version of the program PIXEL. In calculating the vertical heave position signal, a second quantity C_2 is introduced in the main text. This ensures that the heave signal is in a consistent scale with the axial signal, and is simply the reciprocal of C_1: 0.433.

APPENDIX D

INPUT OPTIONS TO PROGRAM FORCE USED TO SIMULATE MADISON MAGNETICS LARGE MSBS DESIGN

The following dimensions and input options correspond to the terminology used in NASA CR-172154 (Reference 28).

Original MMI Design

Eight Main Solenoidal Electromagnets

input option INOPT 3 (lateral pseudo-circular)

symmetry option 10

Dimensions (m)

DX	DY	RAD1	RAD2	DX1	DX2	NDIVR	NDIVY	NSEG	ANGLE
1.25	0	0.644	1.153	1.753	2.053	1	1	12	0

Two Axial Solenoidal Electromagnets

input option INOPT 4 (axial pseudo-circular)

symmetry option 7

Dimensions (m)

X1	X2	RAD1	RAD2	NDIVR	NDIVX	NSEG
2.552	3.252	2.257	2.757	1	1	12

Four Saddle Roll Electromagnets

input option INOPT	1 (single loop)
symmetry option ISYMM	4
no. of elements	8

Element Co-ordinates (m)

X	2.15	2.15	2.15	-2.15	-2.15	-2.15	-2.15	-2.15
Y	0.5	1.1	2.505	2.505	2.505	2.505	1.1	0.5
Z	2.505	2.505	1.1	0.5	0.5	1.1	2.505	2.505

Modified MMI design with Eight Saddle Electromagnets

Input Option	1 (single loop)
Symmetry Option	10
no. of Elements	8

x	2.15	2.15	2.15	2.15	0.25	0.25	0.25	0.25
y	0.5	1.1	2.505	2.505	2.505	2.505	1.1	0.5
z	2.505	2.505	1.1	0.5	0.5	1.1	2.505	2.505

NASA
National Aeronautics and Space Administration

Report Documentation Page

1. Report No.	2. Government Accession No.	3. Recipient's Catalog No.
NASA CR-181895		

4. Title and Subtitle
Techniques for Extreme Attitude Suspension of a Wind Tunnel Model in a Magnetic Suspension and Balance System

5. Report Date
October 1989

6. Performing Organization Code

7. Author(s)
David Huw Parker

8. Performing Organization Report No.

10. Work Unit No.
505-61-01-02

9. Performing Organization Name and Address
University of Southampton
Department of Aeronautics and Astronautics
Southampton, Hants, SO9 5NH
ENGLAND

11. Contract or Grant No.
NSG-7523

13. Type of Report and Period Covered
Contractor Report

12. Sponsoring Agency Name and Address
National Aeronautics and Space Administration
Langley Research Center
Hampton, VA 23665-5225

14. Sponsoring Agency Code

15. Supplementary Notes
NASA Langley Research Center Technical Monitor: Richmond P. Boyden
Alternate: Robert A. Kilgore
This report is the thesis submitted by Dr. Parker for the Degree of Doctor of Philosophy, April 1989.

16. Abstract

Although small scale magnetic suspension and balance systems (MSBSs) for wind tunnel use have been in existence for many years, they have not found general application in the production testing of flight vehicles. One reason for this is thought to lie in the relatively limited range of attitudes over which a wind tunnel model may be suspended. This paper reports on modifications to a small MSBS at Southampton University to permit the suspension and control of axisymmetric models over angles of attack from less than zero to over ninety degrees. Previous work had shown the existing arrangement of ten electromagnets was unable to generate one of the force components needed for control at extreme attitudes. Examination of possible solutions resulted in a simple alteration to rectify this deficiency. To generate the feedback signals to control the suspended model, an optical position sensing sensing system using collimated laser beams and photodiode arrays was installed and tested. An analytical basis was developed for distributing the demands for force and moment needed for model stabilisation amongst the electromagnets over the full attitude range. This was implemented by an MSBS control program able to continually adjust the distribution for the instantaneous incidence in accordance with pre-scheduled data. Results presented demonstrate rotations of models from zero to ninety degrees at rates up to ninety degrees per second, with pitching rates rising to several hundred degrees per second in response to step-change demands. A study of a design for a large MSBS suggests that such a system could be given the capability to control a model in six degrees of freedom over an unlimited angle of attack range.

17. Key Words (Suggested by Author(s))	18. Distribution Statement
Magnetic Suspension Position Sensing	Unclassified - Unlimited Subject Category - 09, 35

19. Security Classif. (of this report)	20. Security Classif. (of this page)	21. No. of pages	22. Price
Unclassified	Unclassified	269	A12